F

N73-21410

NASA CR-121098
MTI 72TR34

DESIGN AND FABRICATION OF GAS BEARINGS FOR BRAYTON CYCLE ROTATING UNIT

by A. Frost, J. M. Tessarzik, and E. B. Arwas

MECHANICAL TECHNOLOGY INCORPORATED

prepared for

NATIONAL AERONAUTICS AND SPACE ADMINISTRATION

NASA Lewis Research Center
Contract NAS 3-10951

1. Report No.	2. Government Accession No.	3. Recipient's Catalog No.
NASA CR-121098		

4. Title and Subtitle	5. Report Date
DESIGN AND FABRICATION OF GAS BEARINGS FOR BRAYTON CYCLE ROTATING UNIT	March 1973
	6. Performing Organization Code

7. Author(s)	8. Performing Organization Report No.
A. Frost, J. M. Tessarzik, and E. B. Arwas	MTI 72TR34
	10. Work Unit No.

9. Performing Organization Name and Address	11. Contract or Grant No.
Mechanical Technology Incorporated 968 Albany-Shaker Road Latham, New York 12110	NAS 3-10951
	13. Type of Report and Period Covered
12. Sponsoring Agency Name and Address	Contractor Report
National Aeronautics and Space Administration Washington, D.C. 20546	14. Sponsoring Agency Code

15. Supplementary Notes

Editor, W. D. Waldron, Mechanical Technology Incorporated; Project Manager, Lloyd W. Ream, Power Systems Division, NASA Lewis Research Center, Cleveland, Ohio

16. Abstract

Analysis, design, and testing of two types of pivoted pad journal bearings and a spiral-grooved thrust bearing suitable for direct installation into the NASA 2 to 15 KW Brayton Cycle Rotating Unit (BRU) have been accomplished. Both types of tilting pad bearing assemblies are of the preloaded type, consisting of three pads with one pad flexibly mounted. One type utilizes a non-conforming pivot,while the other replaces the conventional spherical pivot with a cruciform flexible member. The thrust bearing is flexure mounted to accommodate static machine mis-linement. Test results indicate that both types of journal bearings should satisfy the require-ments imposed by the BRU. Hydrostatic tests of the spiral-grooved thrust bearing showed it to be free of pneumatic hammer with as many as 24 orifices over the BRU pressure and load range.

17. Key Words (Suggested by Author(s))	18. Distribution Statement
Brayton cycle Gas bearings Nonconforming pivots Cruciform support	Unclassified - unlimited

19. Security Classif. (of this report)	20. Security Classif. (of this page)	21. No. of Pages	22. Price*
Unclassified	Unclassified	161	$3.00

* For sale by the National Technical Information Service, Springfield, Virginia 22151

TABLE OF CONTENTS

TABLE OF CONTENTS (Cont'd)

LIST OF ILLUSTRATIONS

LIST OF ILLUSTRATIONS (Cont'd)

LIST OF ILLUSTRATIONS (Cont'd)

LIST OF ILLUSTRATIONS (Cont'd)

LIST OF ILLUSTRATIONS (Cont'd)

LIST OF ILLUSTRATIONS (Cont'd)

LIST OF ILLUSTRATIONS (Cont'd)

LIST OF TABLES

SUMMARY

Journal and thrust bearings suitable for direct incorporation into the NASA's 2 KW to 15 KW Brayton Cycle Rotating Unit (BRU) have been designed, tested, and delivered to the NASA. The bearing assemblies were designed to be incorporated into the BRU without modification to the existing BRU bearing mounting flanges.

Two different types of three pad tilting pad journal bearings were tested. One utilized a conventional spherical nonconforming pivot where the relative motion at the pivot joint is accommodated by rolling motion and elastic deformation within the Hertzian contact zone. The other type circumvented the potential problems associated with relative motion within the pivot by replacing the pivot with a flexible member called a "cruciform". The "cruciform" accommodates the necessary pad pitch, roll, and yaw motions by elastic bending of the "cruciform" beams.

A flexible mounted (to accommodate static misalignment) spiral-groove thrust bearing was selected for the BRU application primarily because of its high ultimate load capacity - especially at low ambient pressures. Both journal and thrust bearings incorporated hydrostatic jacking for start-up. The test results of the journal bearing compoents indicated that, from a hydrodynamic load capacity standpoint, both had near identical performance. Also, introduction of hydrostatic recesses and orifices for jacking degraded hydrodynamic performance and hydrostatic performance for both bearing types was adequate for the BRU application.

The single nonconforming pivoted pad tested experienced roll type instabilities in the overspeed region of the BRU operating range. From the test results, it was not possible to determine whether similar instabilities would be encountered in the BRU. Only actual experimentation in the BRU will be able to answer this question. No instabilities were experienced during the tests with the "cruciform" mounted journal bearing pad.

The spiral-grooved thrust bearing was tested under nonrotating hydrostatic conditions over the BRU supply and ambient pressure range. Six, 12 and 24 orifices configurations were tested. The spiral-grooved bearing was found to be free of pneumatic hammer under all conditions tested. Increased numbers of orifices, however, did increase the load that could be applied before hydrostatic lock-up occurred.

Pneumatic hammer was prevalent in the NASA supplied BRU step-sector thrust bearing at all sub-atmospheric ambient pressures and for all supply pressures between 90 psia and 150 psia. The load vs. eccentricity ratio* characteristics of the step-sector thrust bearing was similar to those of the six orifice spiral groove bearing although film thicknesses were smaller because of the smaller total clearance.

* Eccenticity ratio = displacement divided by one-half total clearance.

INTRODUCTION

This report describes the analytical, design, and experimental efforts conducted for the NASA Lewis Research Center under contract NAS 3-10951. The primary purpose of the work was to provide back-up bearing components to the NASA for the 2 to 15 KW Brayton Rotating Unit (BRU) which has been developed by another contractor under contract NAS 3-9427. The back-up bearing components are designed such that they can be installed directly into the BRU without modification to the BRU bearing mounting flanges or other components.

The design of the back-up bearings was based upon the present state-of-the-art of gas bearing technology and made use of the experience gained in the prior, successful development of Brayton Cycle turbomachinery under NASA Contracts NAS 3-4179 and NAS 3-6013. Under these contracts, a gas bearing supported dynamic simulator for an axial flow turbocompressor, as well as the complete, gas bearing supported alternator were fully developed and successfully operated. The design of the back-up bearings also made use of the technology generated under other work, specifically including the analytical and test program under NASA Contract NAS 3-7629 on pivots of high temperature gas bearings for Brayton Cycle application, as well as other technology programs.

Two back-up journal bearing designs and one back-up thrust bearing design were evolved on the program. As specified by the NASA, both journal bearing designs were of the basic preloaded tilting pad type incorporating three pads, one of which is flexibly mounted to accommodate differential radial circumferential and thermal growths between rotor and stator elements.

One journal design featured pads supported on pivots designed in such a manner that the oscillatory motions of the pads are accommodated by elastic deflections and rolling motions in the Hertzian contact zone of the pivot, instead of by relative sliding between the mating pivot elements. This type of pivot design is referred to as "nonconforming" i.e., the radius of curvature of the female member is slightly larger than the male member such that rolling motion can be achieved. This is the type of pivot utilized in the aforementioned machinery developed under NASA contracts NAS 3-4179 and NAS 3-6013 and tested extensively on NAS 3-7629. With the pivot configuration utilized in the prototype BRU bearing developed under NAS 3-9427, the male and female members are lapped together resulting in pure sliding motion. This type of pivot is termed "conforming".

The other journal design featured pads supported on a "cruciform" flexure. The "cruciform" accommodates the pad roll, pitch, and yaw motions of the pad by elastic bending of the "cruciform" beams. Thus, the questions of pivot fretting and wear inherent with the conventional spherical (or cylindrical) pivot are circumvented with the "cruciform" pivot.

Unlike the journal bearing, the type of thrust bearing to be designed and tested was not specified by the NASA. Both step-type and spiral-groove type thrust bearings were considered as they both have been successfully

applied to previous gas bearing machinery. Following a comprehensive design study, the spiral-groove type was selected, primarily because of its superior load capacity under low ambient (low BRU power level) conditions.

Single pads of journal bearings incorporating both the nonconforming pivot and prototype cruciform flexure were extensively tested under simulated BRU operating conditions. In addition, a pad incorporating a modified cruciform flexure design was subjected to hydrostatic testing. All were concluded to be suitable for the BRU application. Also, the spiral-grooved thrust bearing assembly along with a NASA supplied step-sector thrust bearing assembly were tested under nonrotating conditions to explore the limits of hydrostatic pneumatic instability. The spiral-groove thrust bearing was found to be free of pneumatic instability under all BRU pressure and load conditions. The step-sector thrust bearing experienced pneumatic hammer under all sub-atmospheric ambient pressures and with supply pressures between 90 psia and 150 psia.

The main body of this report is divided into four major sections. The first section entitled "Bearing Analysis and Design", summarizes the details of the design of the thrust and journal bearing elements.

The second major section entitled "Experimental Performance of Spiral-Groove and Step-Sector Thrust Bearings" describes the hydrostatic testing and test results of the spiral-groove bearing assembly designed and fabricated on the subject contract and the step-sector thrust bearing designed and fabricated on NAS 3-9427.

The final three major sections describe the testing of single pivoted journal pads; one supported on a "nonconforming pivot", one supported on a "prototype cruciform" flexure, and one supported on a "modified cruciform" flexure. All three designs were fabricated on the subject contract.

In addition to the testing of the back-up bearing components reported herein, the complete bearing assemblies are currently being tested in the BRU dynamic simulator at the NASA Lewis Research Center.

BEARING ANALYSIS AND DESIGN

This section of the report covers the results of the analytical, conceptual design and optimization phases of the program.

The data presented describes the results of detailed investigations of:

(a) the performance characteristics for a range of sizes of two types of thrust bearings,

(b) three types of thrust bearing cooling techniques,

(c) two types of journal bearings, and

(d) rotor dynamic characteristics.

Conclusions are drawn concerning the most suitable thrust and journal bearings for use in the Brayton-cycle rotating unit. Additionally, recommendations are made for bearing coating materials and bearing instrumentation.

THRUST BEARING ANALYSIS

Hydrodynamic Thrust Bearing

The performance requirements for the BRU hydrodynamic thrust bearing were defined as follows:

The thrust bearing shall be double acting and suitable for operation at 36,000 rpm in a gaseous mixture of helium and xenon (molecular weight - 83.8) under the load and ambient pressure conditions given in Table I shown below.

TABLE I - THRUST BEARING OPERATING REQUIREMENTS

Alternator Power Level KW	Ambient Pressure, psia	Design Load, lb.* Turbine End Up Rotor Vertical	Design Load, lb.* Rotor Horizaontal (or in space)
10.5	42.6	9	31
6.0	25.1	-4	18
2.5	12.6	-9	13

* Positive values of thrust load denote thrust directed toward the turbine. Negative values denote thrust directed toward the compressor.

Three types of hydrodynamic, thrust bearing face geometries were considered for this application:

1) Spiral Groove

2) Plain Step

3) Shrouded Step.

The spiral-groove geometry uses shallow, helical pumping grooves to pressurize the lubricant and is widely used in self-acting, gas-lubrication applications. It has high capacity down to much lower levels of ambient pressure than do other hydrodynamic bearing types. Spiral groove thrust bearings were used, for example, in both the 12,000 rpm turboalternator and the 50,000 rpm turbocompressor simulator, of the NASA's "A" engine.

The plain "Rayleigh" step geometry relies on shallow, inscribed steps for its hydrodynamic pressure generation. This type of thrust bearing was used in the NASA's "A" engine radial-flow turbocompressor and, also, in the prototype BRU.

The shrouded step bearing uses a geometry similar to the plain step bearing, except that it has sealing lands at the sides of the recessed regions, in order to reduce side-leakage flow and thereby raise load capacity.

A preliminary analysis was made with the above three bearings to:

1. Establish the bearing size required, and
2. Select the preferred geometry on the basis of load capacity and power loss comparisons for the three bearing types.

Preliminary Bearing Size Calculations

The bearing size was selected to provide an operating film thickness of about 1 mil at design speed and under the maximum steady-state load, assuming fully flat and parallel faces. To establish the bearing size for this condition, initial calculations were made assuming a spiral grooved thrust bearing. These were made for a range of bearing outer diameters from 3.5 inches to 5.25 inches and the computed values of film thickness and power loss versus bearing outer diameter are plotted in Figure 1. The other geometrical parameters used for these calculations were:

- Double acting bearing (equal thrust faces), with 4 mils axial play
- Bearing I.D. = 2.1"*
- In-flow design with 18 grooves
- Groove helix angle = 72^{o}
- Ratio of groove to land width = 1.6
- Ratio of grooved to total radial length = 0.6

* This is the true value of the inside diameter, which is determined by the existing rotor geometry. In the data of Figure 1, this value was used for the power loss calculations. However, for the film thickness calculations, the effective bearing area was assumed to end at the pitch diameter of the row of orifices through which the jacking gas is admitted during starts

and stops. In the data of Figure 1, this "effective" inside diameter was assumed to range from 2.42 inches for the 3.5 inch O.D. thrust plate, to 2.53 inches for the 5.25 inch O.D. thrust plate. This assumption was later deemed to be unduly conservative and the 2.1 inch I.D. value was used in all subsequent calculations.

The conditions of operation corresponding to the data of Figure 1 are:

- Speed = 36,000 rpm
- Lubricant viscosity = 5.1×10^{-9} lb-sec/in.^{2}
- Ambient pressure = 12.6 psia.

The above noted value of ambient pressure, which corresponds to 2.25 KW(e) operating point, is the minimum in the BRU application. The data of Figure 1 is, however, equally applicable to the other, higher values of ambient pressure corresponding to the 6.0 and 10.5 KW(e) power levels, because the film thickness and power loss of the spiral grooved thrust bearing are essentially independent of ambient pressure, within the range of compressibility numbers encountered in the BRU application.

From the data of Figure 1, a 4.25 inch O.D. thrust plate was selected. This has a film thickness of about 0.97 mils under 31 pounds load and the power loss for the double-acting bearing ranges from about 200 watts under 4 pounds load to about 245 watts under 31 pounds load.

Comparison of Plain and Shrouded-Step Bearings

Unlike the spiral-grooved bearing, the performance characteristics of the plain and shrouded-step bearings are affected by the ambient pressure level. The optimum values of the geometrical parameters of these bearings vary with compressibility number. For the purpose of this preliminary analysis, the bearings were optimized (from maximum load capacity standpoint) for the following conditions:

- Bearing size = 4.25" O.D. x 2.1" I.D.
- Speed = 36,000 rpm
- Ambient Pressure = 25.1 psia
- Lubricant viscosity = 5.1×10^{-9} lb-sec/in.^{2}
- Film thickness = 0.6 mils

The optimization was made for a film thickness of 0.6 mils (instead of the design value of about 1 mil), to insure highest tolerance to thrust overloads.

The optimization analysis that was conducted was an approximate one, in which the geometrical parameters were varied, one at a time, and the load capacities calculated in each case using a finite-difference computer program

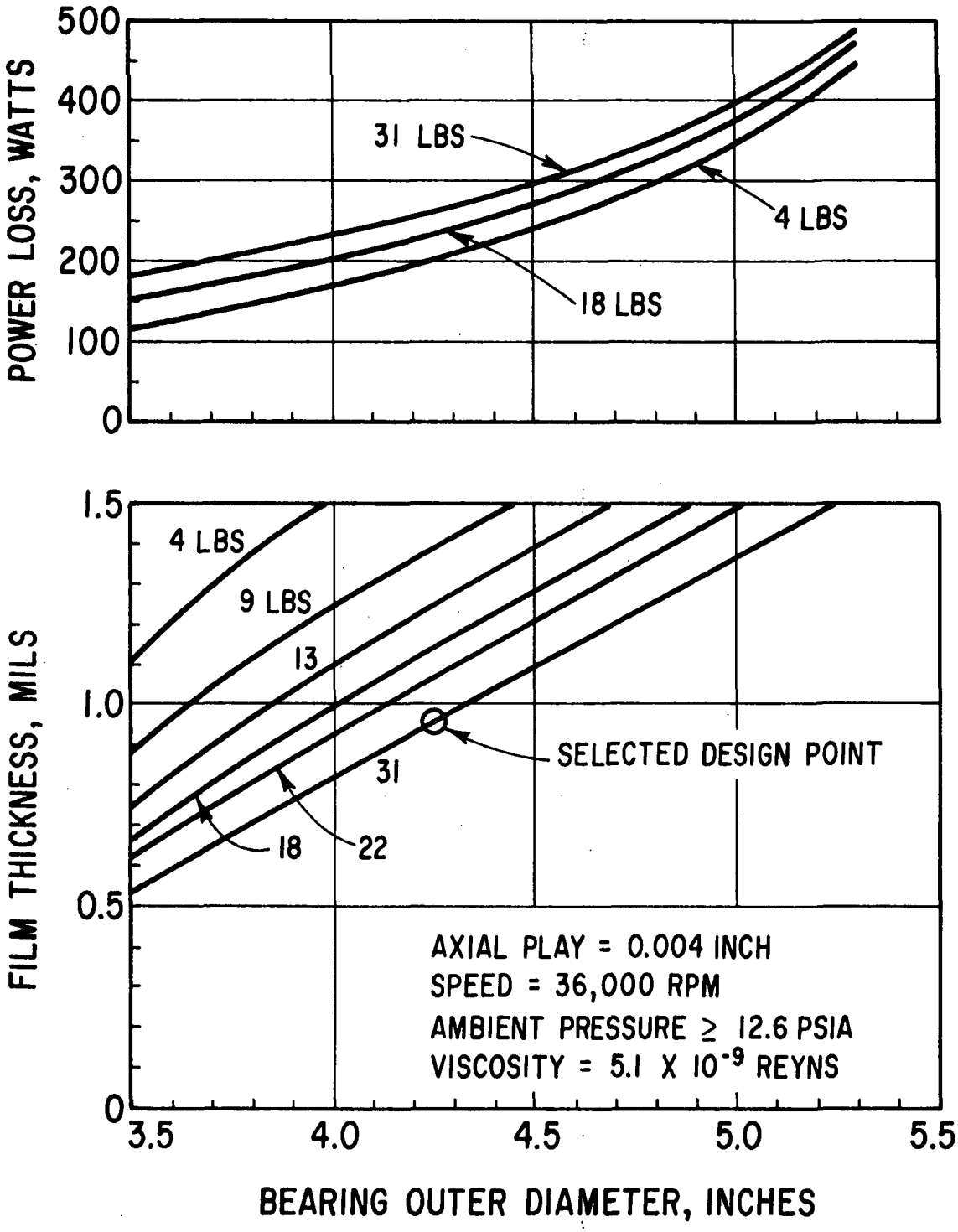

Fig. 1 Effect of Diameter on Film Thickness and Power Loss for Spiral-Groove Thrust Bearing

for plain and shrouded-step bearings with annular geometry and compressible-flow lubrication. These calculations led to the selection of the following parameters for the shrouded-step bearing, as illustrated in Figure 2:

- Ratio of recessed circumferential length to total circumferential length

$$\left(\frac{\theta_g}{\theta_{tot}}\right) = 0.6$$

- Ratio of radial seal length to total radial length $\left(\frac{W}{R_o - R_1}\right) = 0.186$.

Table II shows the effects of varying the number of pads. As shown in Table II, the highest load capacity is achievable if the annulus is divided into three segments. Because of the concern that this minimum number of segments would make the bearing unduly sensitive to distortions, it was decided to use a five segment design instead, although this has about 5 percent less load capacity under ideal conditions (i.e., with fully flat and parallel mating faces).

TABLE II - EFFECT OF VARYING NUMBER OF PADS

O.D. = 4.25 Inches, I.D. = 2.10 Inches, Speed = 36,000 RPM, Film Thickness = 0.0006 Inches, Viscosity = 5.1×10^{-9} Reyns

Number of Pads	Pad Arc Length (θ_{tot})	Load
3	114.0^o	100 lb.
5	68.4^o	95 lb.
7	$48\ 9^o$	84 lb.
9	38.0^o	72 lb.

A five segment design was also used for the plain step bearing, but here the calculations showed that the recessed regions in each segment should be smaller ($\theta_g/\theta_{tot} \approx 0.6$).

Figure 3 compares the calculated load capacities of the optimized plain and shrouded-step bearings, as a function of step depth. At a film thickness of 0.6 mils, the plain-step bearing has a maximum load capacity of 70 pounds corresponding to a step depth of about 0.7 mils. For the same 0.6 mils film thickness, the shrouded-step bearing has a peak load capacity of 94 pounds at a step depth of about 1.3 mils.

From load capacity standpoint therefore, the shrouded-step bearing is seen to be significantly superior to the plain-step bearing. The subsequent analysis was then limited to consideration of spiral-grooved and shrouded step bearings.

BEARING O.D. = 4.25 INCHES
BEARING I.D. = 2.1 INCHES
SPEED = 36,000 RPM
FILM THICKNESS = 0.0006 INCH
STEP DEPTH = 0.0015 INCH
VISCOSITY = 5.1 X 10^{-9} REYNS

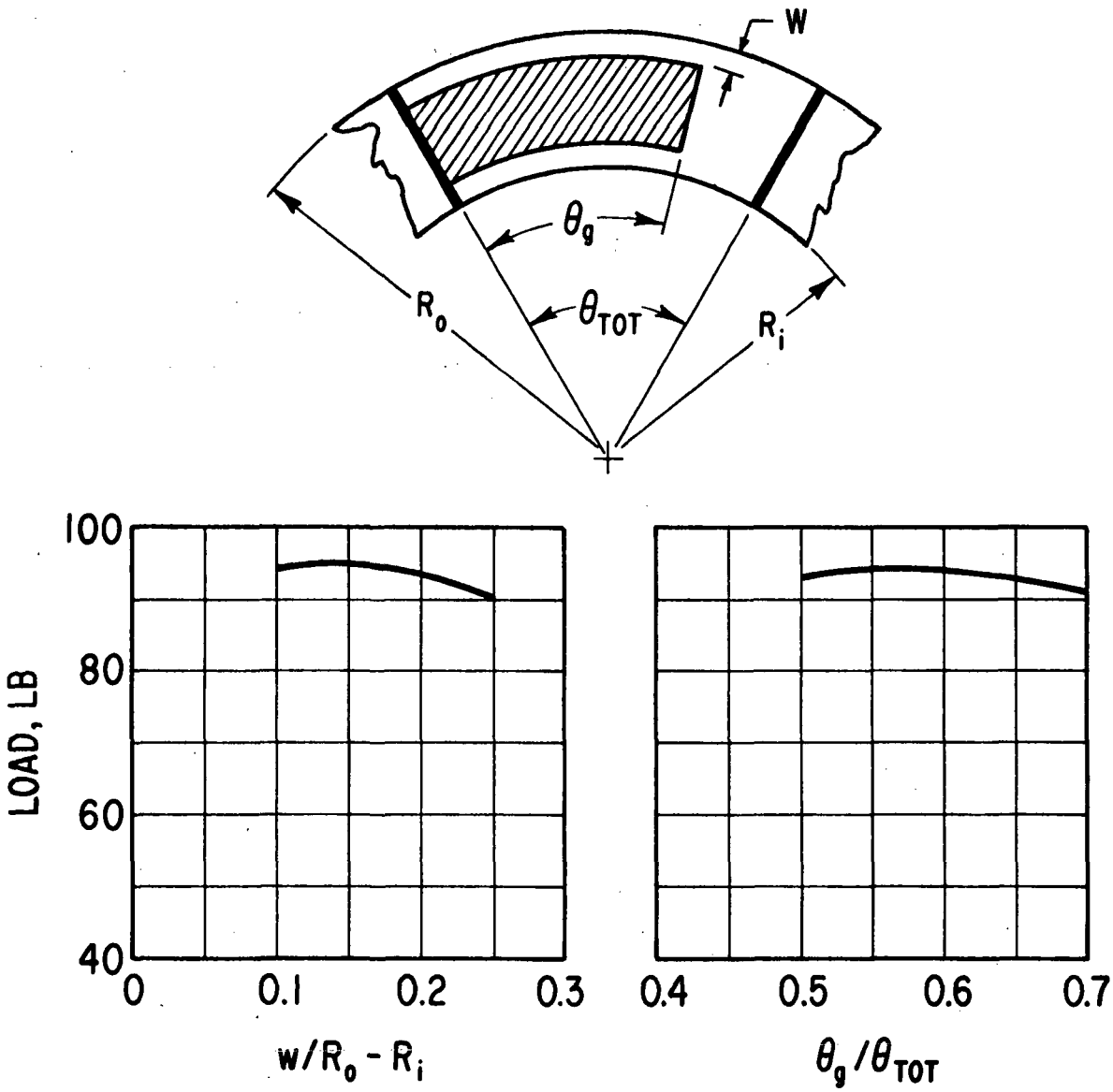

Fig. 2 Effect of Step Geometry on Shrouded-Step Thrust Bearing Load Capacity

Fig. 2

BEARING O.D. = 4.25 INCHES
BEARING I.D. = 2.1 INCHES
SPEED = 36,000 RPM
THRUST PLATE HAS 5 EQUAL SEGMENTS
OPTIMIZATION MADE FOR h = 0.0006 INCH
VISCOSITY = 5.1 X 10^{-9} REYNS

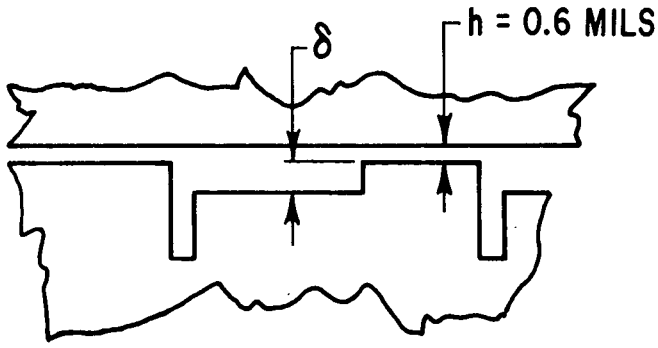

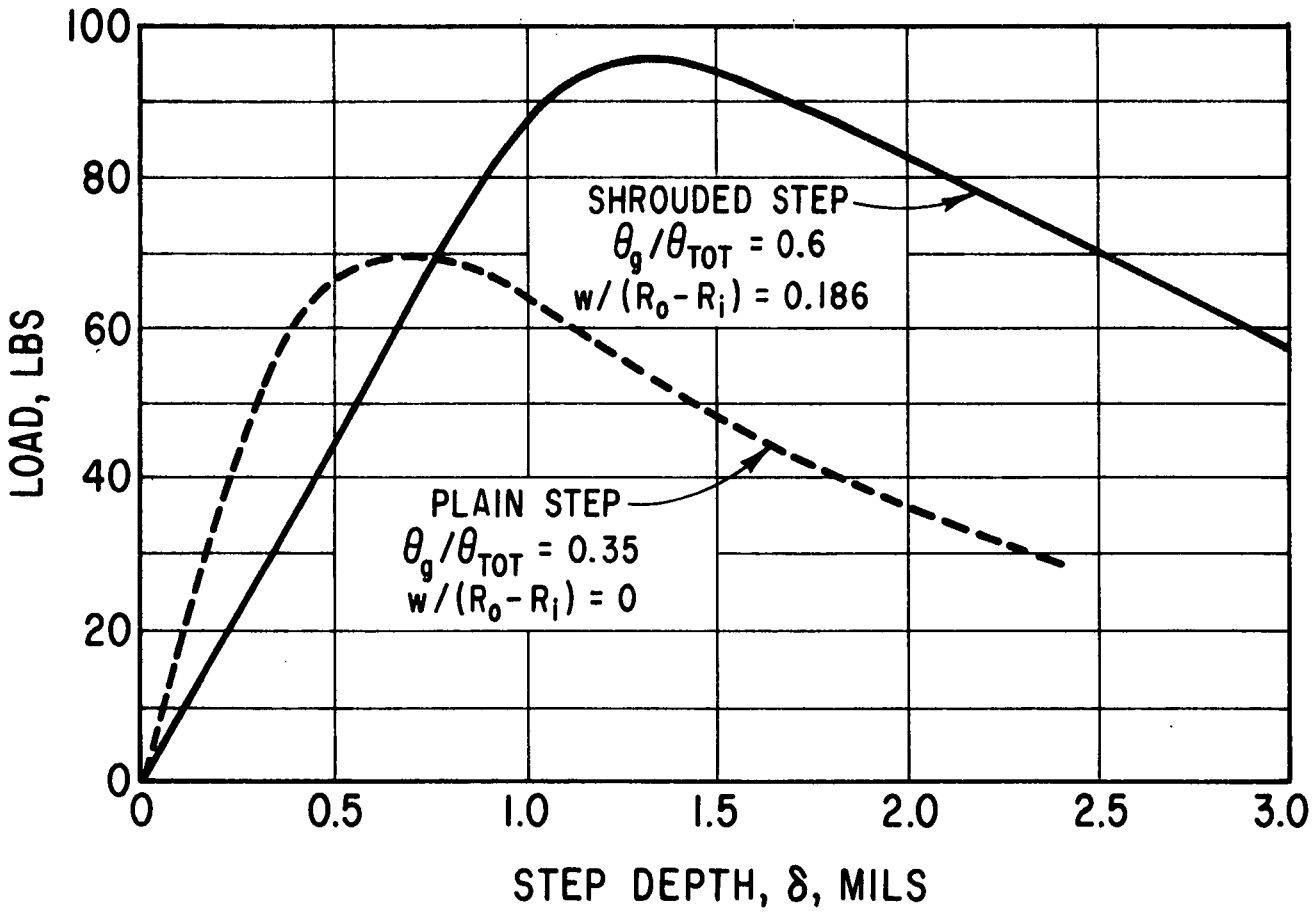

Fig. 3 Effect of Step Depth on Step-Type Thrust Bearing Load Capacity

Comparison of Shrouded-Step and Spiral-Grooved Bearings

Calculations based on a diameter of 4.25 inches showed that the load carrying capacity of the double-acting, spiral grovved bearing was independent of ambient pressure in the range of pressures under consideration. The load carrying capacity of the shrouded-step bearing, however, was found to be somewhat sensitive to ambient pressure. Figure 4 shows a plot of load versus film thickness for both types of double-acting bearings. From this curve it is seen that the load carrying capacity of the spiral-grooved bearing is slightly better than that of the shrouded-step bearing at film thicknesses of 0.001 inches and above. Below this film thickness the load carrying capacity of the spiral-grooved bearing is noticeably higher than that of the shrouded-step bearing. Data describing the performance of the shrouded-step bearing at an ambient pressure of 42.6 psia (10.5 KW condition) is not shown on Figure 4. Preliminary calculations showed, however, that the performance at film thicknesses above 0.001 inch is essentially constant at ambient pressures of 25.1 and 42.6 psia. Below film thicknesses of 0.001 inch the load capacity of the shrouded-step bearing increases with increasing ambient pressure. This increase in load capacity at 42.6 psia is small and does not surpass the load carrying capacity of the spiral-grooved bearing.

A plot of friction loss versus film thickness for the 4.25 inch diameter double-acting thrust bearing with 0.004 inch total axial clearance is shown on Figure 5 for the spiral-groove and shrouded-step types of bearing. From this figure it is seen that the spiral-groove bearing has a friction loss of 5 to 10 watts more than the shrouded-step bearing in the film thickness range between 1.0 and 2.0 mils, this being the film thickness range in which the bearing will normally operate.

An important feature of thrust bearing design, particularly when the bearing is provided with self-aligning capabilities, is the angular or tilt stiffness of the gas film. To achieve good alignment between the thrust runner and the thrust stator, the tilt stiffness of the self-aligning machanism should be considerably less than that of the gas film.

Angular stiffness for both the shrouded-step and spiral-groove double-acting thrust bearings is shown on Figure 6. This figure shows that the spiral-groove bearing has angular stiffness characteristics which are independent of ambient pressure in the range of interest and which are considerably higher than the stiffness characteristics of the shrouded-step bearing.

The analyses used to determine the performance characteristics shown in Figure 4, 5 and 6 assumed the surfaces of the thrust runner and thrust stator to be flat and parallel. In practice, of course, the surface deviate from these ideal conditions. Analysis of the effects of the "dish" type distortion ; i.e., minimum film thickness at the bearing O.D. with one or both bearing surfaces concave, showed that the load carrying capacity of both bearing types was similarly affected by distortion. The results of this analysis, shown in Figure 7, indicate the spiral-grooved thrust bearing to be the most suitable for operation under conditions involving distortion,

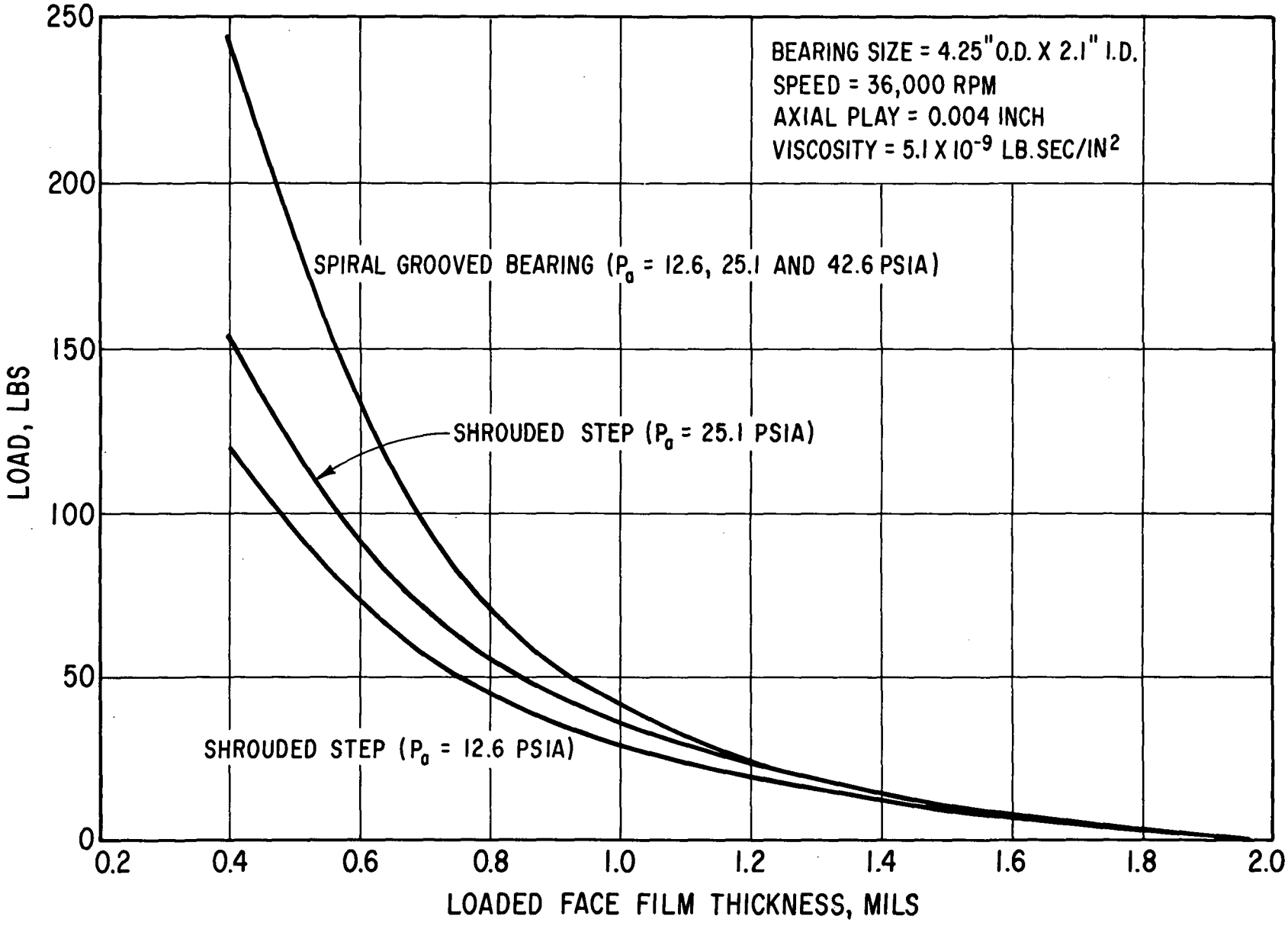

Fig. 4 Load Capacity of Double-Acting Thrust Bearings

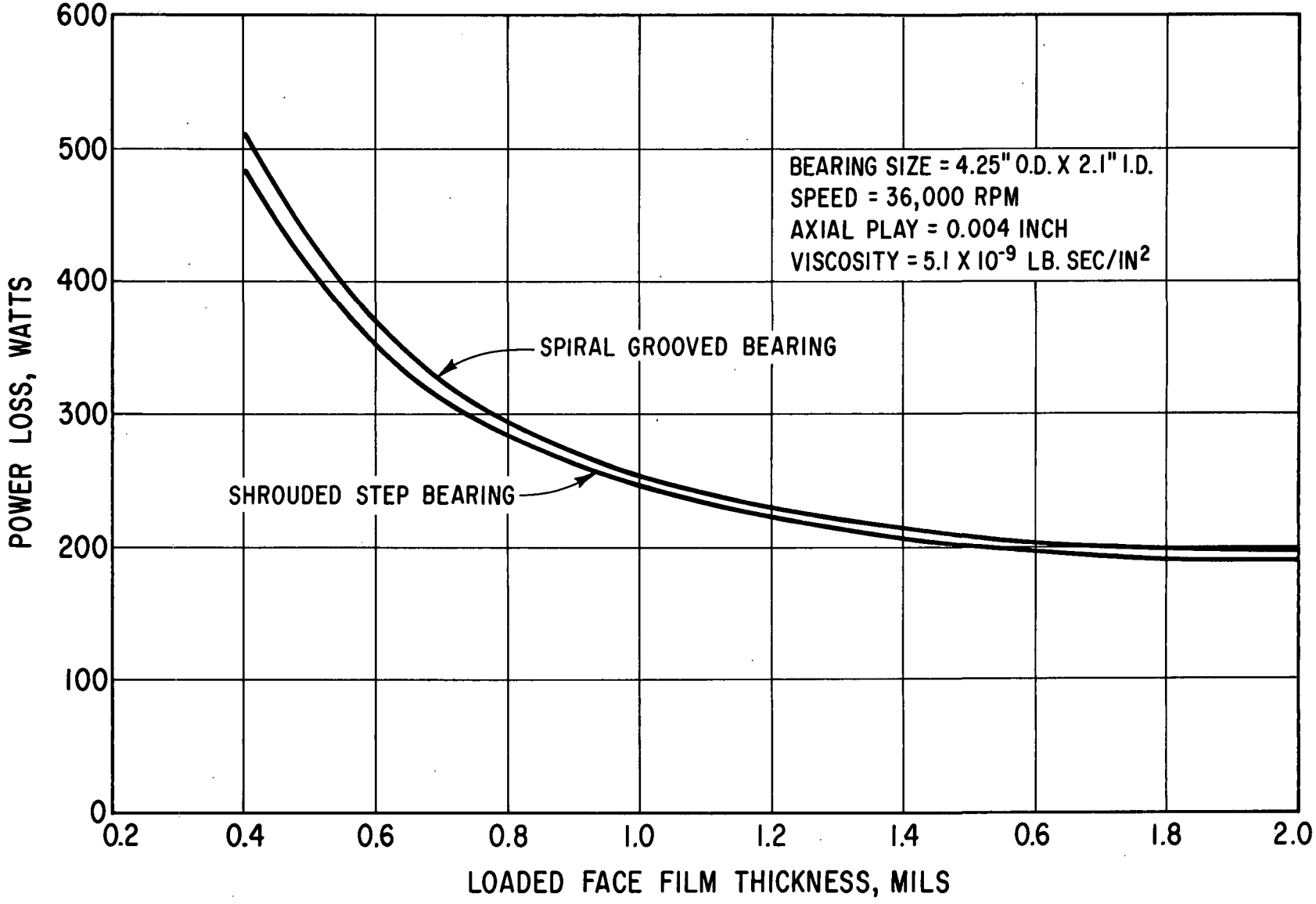

Fig. 5 Power Loss of Double-Acting Thrust Bearings

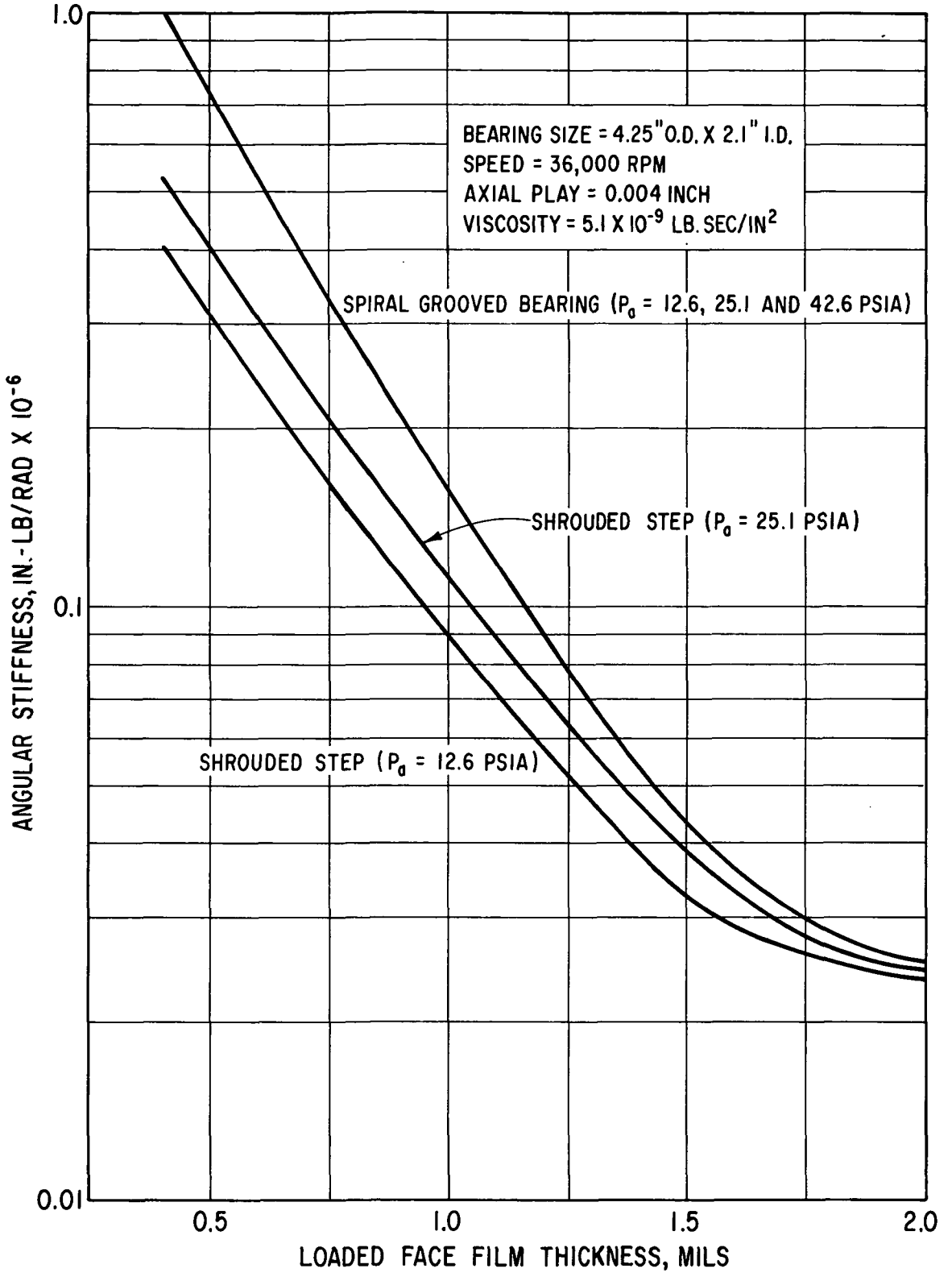

Fig. 6 Angular Stiffness of Double-Acting Thrust Bearings

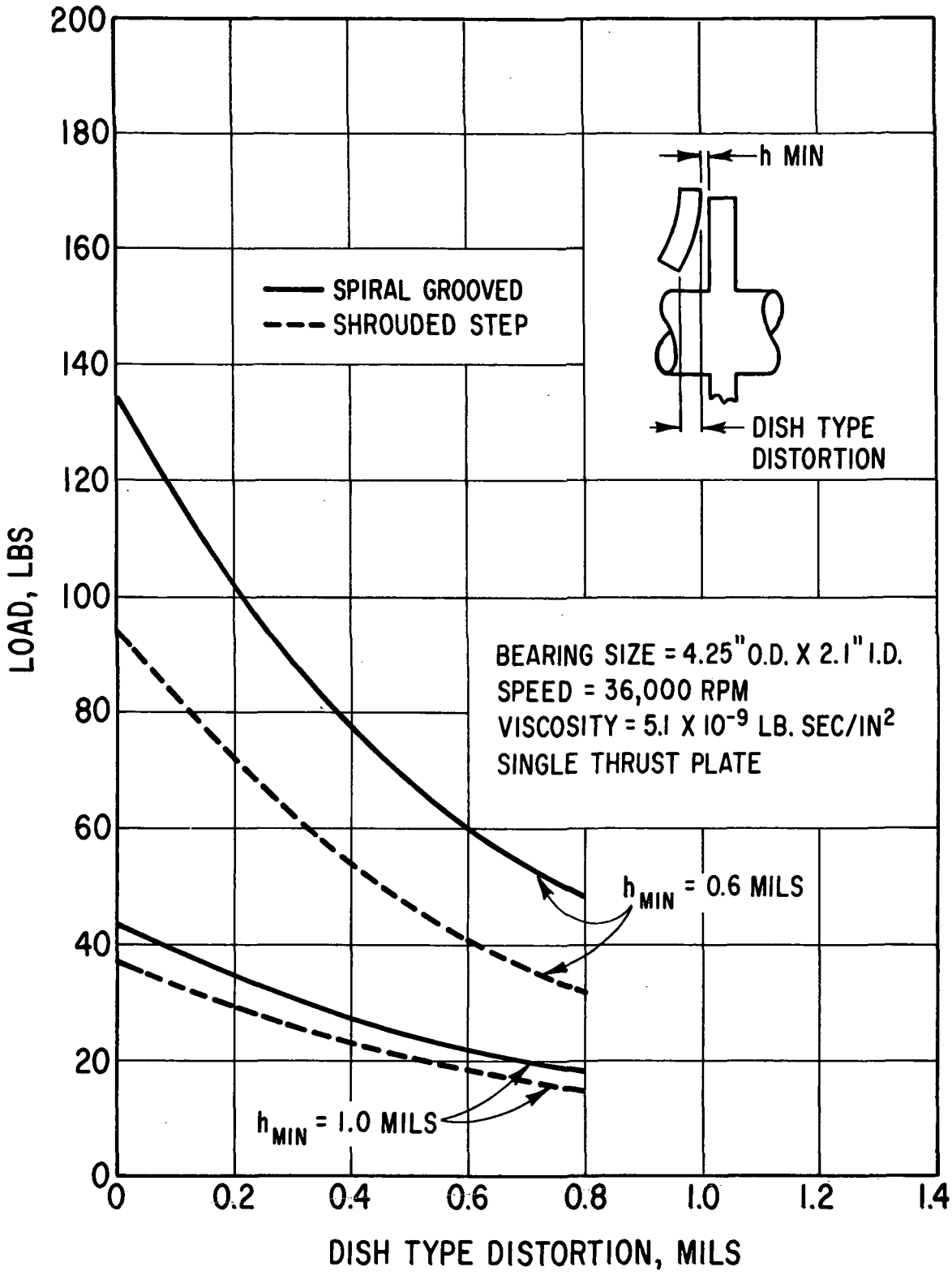

Fig. 7 Effect of Thermal Distortion on Thrust Bearing Load Capacity

largely because of the inherently higher load carrying capability of this type of bearing.

Hydrostatic Operation

The design objective load capacity of the thrust bearing under start-up conditions where it is operated hydrostatically was 100 pounds. A supply of helium-xenon gas at a pressure of 140 psia is available for hydrostatic operation of the bearing.

Analyses were performed to determine the load carrying capacity of the two types of hydrodynamic bearings into which are built the orifices necessary for hydrostatic operation. In these analyses the effects of rotation were neglected. In both cases the hydrostatic orifices have been built into the bearings which were optimized for hydrodynamic operation at a film thickness of 0.0006 inches. The geometry of both the spiral-groove and shrouded-step thrust bearings, including the hydrostatic orifices, is shown in Figure 8. The calculated hydrostatic load carrying capacity of both bearing types was found to be almost identical at film thicknesses in excess of 0.001 inches. At film thicknesses less than 0.001 inches, however, the spiral groove bearing exhibited better hydrostatic load carrying characteristics than the stepped-sector bearing. Figure 9 shows a plot of the calculated hydrostatic load versus film thickness for the double-acting spiral-groove bearing. From this curve it is seen that the bearing should be capable of carrying a load of 100 pounds at the design point ambient pressure of 25.1 psia a film thickness of 0.0004 inches. The curves of load versus film thickness for ambient pressures of 12.6 and 42.6 psia, also shown on Figure 9, indicate that the load carrying capacity decreases with increasing ambient pressure.

A film thickness in excess of 0.0008 inches at a load of 100 pounds would normally be recommended for all values of ambient pressure. Film thicknesses of this magnitude can be obtained by increasing the number of feeding orifices. Unfortunately the possibility of encountering pneumatic hammer increases with an increased number of orifices. In addition, tests of other thrust bearings have indicated that pneumatic hammer can be induced in a normally stable hydrostatic thrust bearing by the application of periodic external vibration as specified in NASA specification P 1224-1.

While the phenomenon of pneumatic hammer is well documented and fundamentally understood, analyses for predicting threshold of hammer in hybrid bearings have not been developed. Thus, it is necessary to experimentally establish the maximum permissible number of orifices. Based upon past experience, it was felt that the six-orifice design would be free of pneumatic hammer, at least under "static" environmental conditions, and that the smaller film thicknesses resulting from the small number of orifices would be tolerable under start-up conditions. (As the speed is increased from zero to design speed, the hydrodynamic portion of the bearing will pick up a part of the load, causing the film thickness to increase above the minimum at zero speed, where only the hydrostatic portion is carrying the load.) Thus, the six-orifice design was initially chosen realizing that, as a result of subsequent

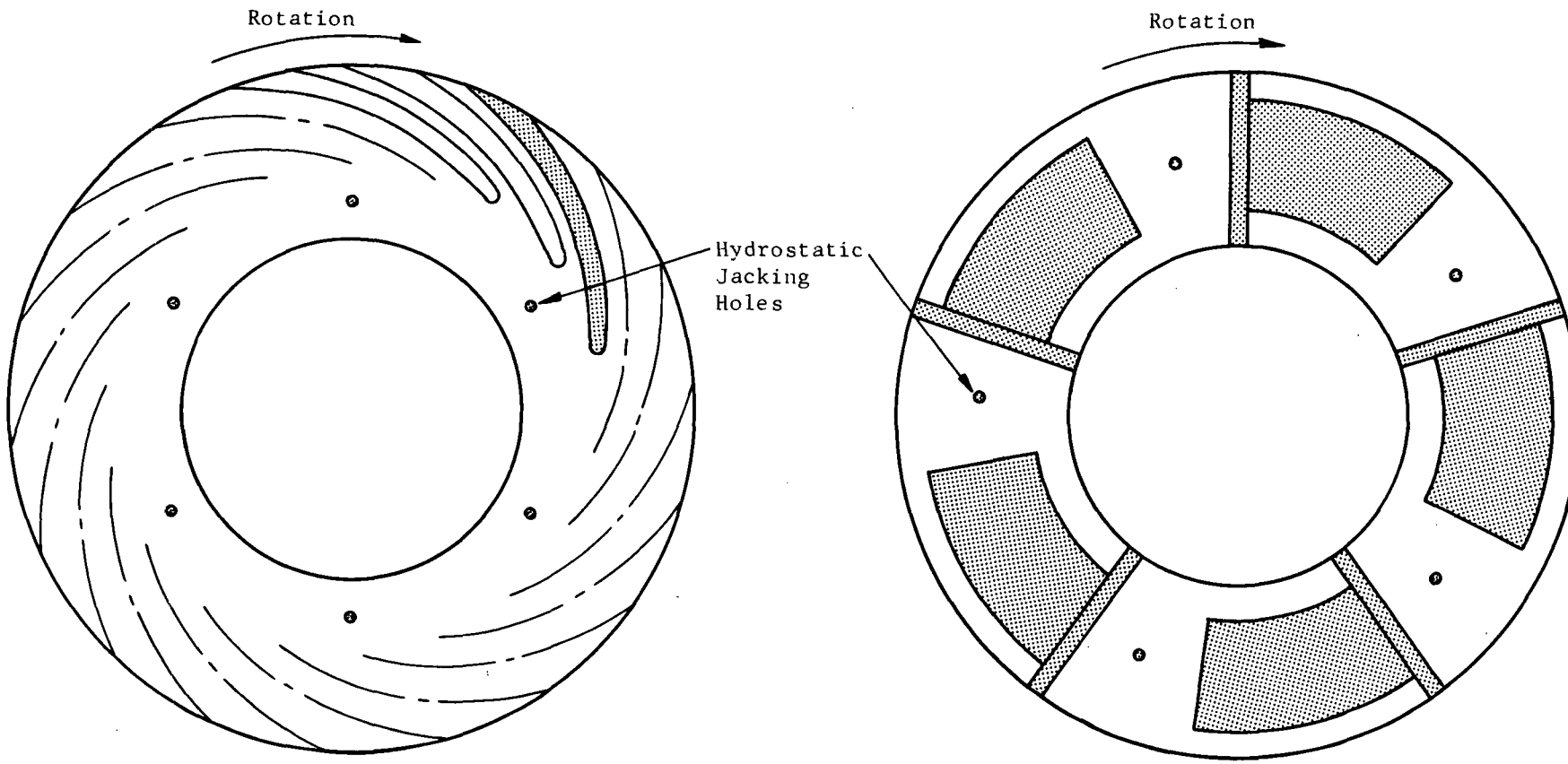

4.25" O.D. x 2.1" I.D.
18 Grooves, 72.9° Helix Angle, 1.8 mils deep
Inner Radius of Grooved Annulus = 3.06 inches
Groove width to land width ratio = 1.6

HELICAL GROOVED THRUST PLATE

4.25" O.D. x 2.1" I.D.
5 Segments, each 68.4° subtended angle
Pocket subtended angle = 41°
Pocket depth = 1.5 mils
Radial seal width = 0.2"

SHROUDED STEP THRUST PLATE

Fig. 8 Schematics of Spiral-Grooved and Shrouded-Step Thrust Bearings

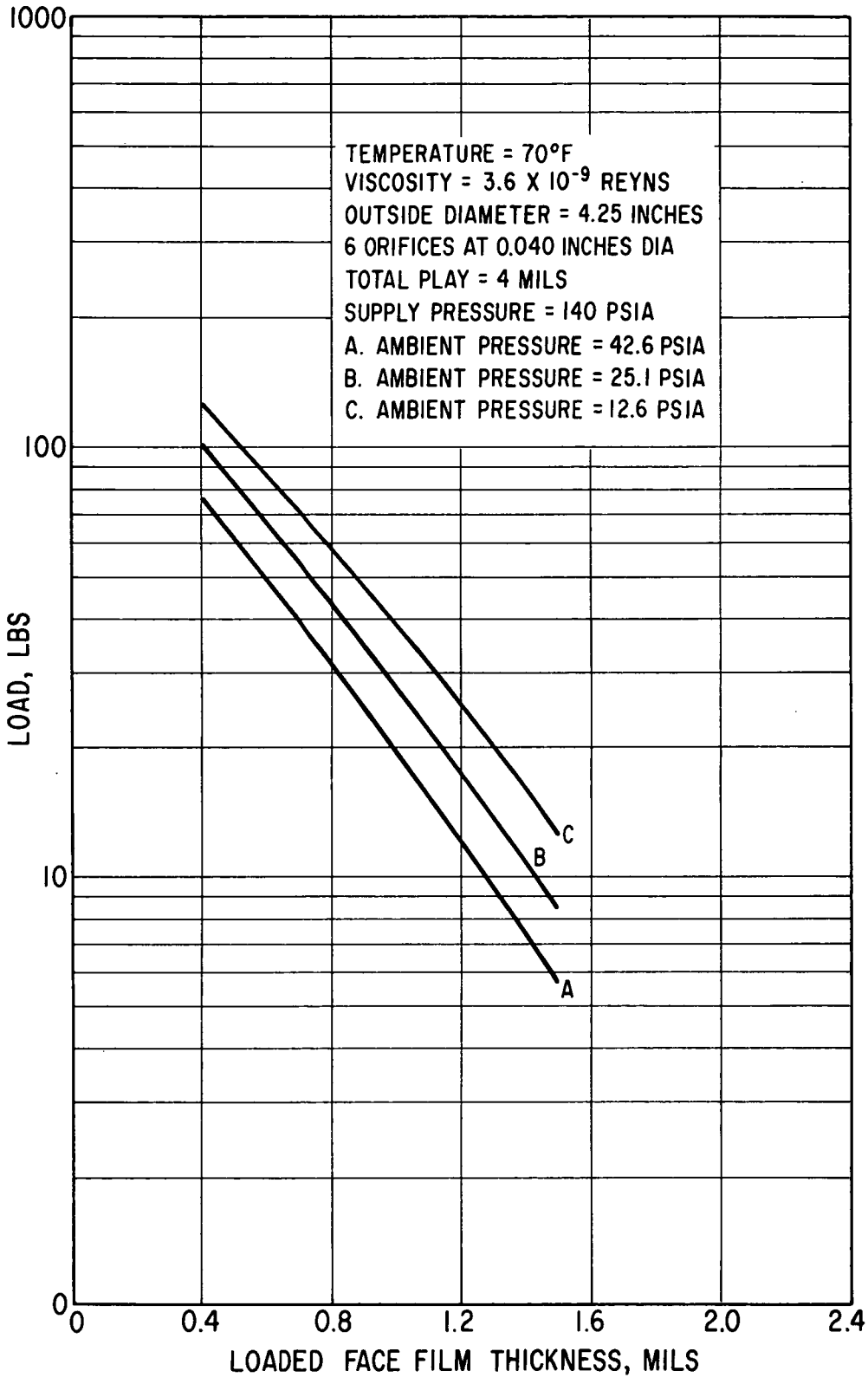

Fig. 9 Calculated Hydrostatic Load Capacity of Double-Acting Spiral-Groove Thrust Bearing

experimentation, it might be possible to increase the number of orifices to improve the hydrostatic load capacity.*

THRUST BEARING THERMAL ANALYSES

Preliminary thermal analyses were performed on three different concepts for removing the heat generated by friction loss in the thrust bearing. The three concepts examined were:

(a) the design as it exists in the BRU, i.e., the heat flows radially inward through the thrust runner into the copper shunt, then axially along the copper shunt into the compressor wheel which dissipates the heat to the system process fluid;

(b) dissipation of the heat to liquid-cooled, thrust-bearing stators (in this concept the alternator coolant system was considered as the source of the required liquid); and

(c) dissipation of the heat to helium-xenon-cooled, thrust-bearing stators (this concept required a gas bleed from compressor discharge).

The primary requirements of the thrust-bearing cooling system are (1) attainment of an essentially isothermal condition in the thrust-bearing and adjacent journal bearing, (2) the attainment of a reliable system, and (3) a system which does not impose undue penalties on overall BRU conversion efficiency.

Preliminary calculations indicated that concept (c) would require in excess of eight percent bleed flow before this technique offered any opportunity of maintaining isothermal conditions. A flow rate of this magnitude would significantly impair overall BRU efficiency, thus, the concept was abandoned as being impractical.

Evaluation of concept (b) showed that the thrust bearing and adjacent journal bearing could be maintained at essentially isothermal conditions if the coolant supply temperature to the bearing was maintained at about 200°F. This concept, while resulting in the most uniform temperature distribution of the concepts examined, requires the introduction of liquid coolant into the bearing cavity, a feature which leads to complexity and the attendant uncertainties concerning reliability. Since the shunt-cooled approach discussed below resulted in acceptable bearing temperature gradients, the liquid-cooled approach was also abandoned.

The boundary conditions, heat transfer coefficients and heat generation rates used in performing the thermal analysis were as follows:

* Subsequent testing discussed later in this report demonstrated that the spiral-groove thrust bearing was free of pneumatic hammer with as many as 24 orifices, and that the 100-pound load could be carried at a minimum film thickness of 0.0008 inches under all ambient pressure conditions with 12 orifices.

Heat Transfer Coefficients:

Impeller:	$h = 110$ Btu/hr-ft^2-F Based on mean impeller Reynolds number
Stationary surfaces:	$h = 10$ Btu/hr-ft^2-F (assumed)
Curvic coupling:	$k = 6.75$ Btu/hr-ft-F Based on contact area of 0.234 in.^{2} (i.e., 1/4 annulus area) $k = k_{steel} \times \frac{\text{area of contact}}{\text{annular area}}$
Alternator flux gap:	$K_{equiv} = 0.782$ Btu/hr-ft-F Based on Taylor number and Reynolds number for 0.020 inch radial gap.

Heat Generation Rates:

Thrust bearing loaded face	- 170 watts
Thrust bearing unloaded face	- 70 watts
Journal bearing	- 50 watts

Fluid Properties:

Xe-He mixture:	$C_p = 0.0593$ Btu/lb-F $k = 0.0168$ Btu/hr-ft-F at 180 F $\mu = 19.45$ lb/ft-sec at 180 F
Dow Corning 200 fluid:	$C_p = 0.460$ Btu/lb-F

One percent of the cycle fluid was assumed to enter the bearing cavity at 280 F. This gas leaves the cavity via the labyrinth seal.

Unless otherwise stated, the interface thermal contact resistance between the copper shunts and journal, thrust runner, and impeller was taken to be negligible.

The results of the nodal point thermal analysis of the thrust bearing and adjacent journal bearing area are shown in Figure 10. This analysis was made for the condition when the maximum deviation from isothermal would be expected. As can be seen in Figure 10 the thrust runner is essentially isothermal in the axial direction. The radial temperature gradient in the runner is approximately 44 F over the radial distance between the I.D. of the stator and the O.D. of the runner. This gradient leads to the surfaces of the runner becoming concave by approximately 50 microinches. (The effects of concave surfaces on the load carrying capacity of the thrust bearing were previously shown in Figure 7.)

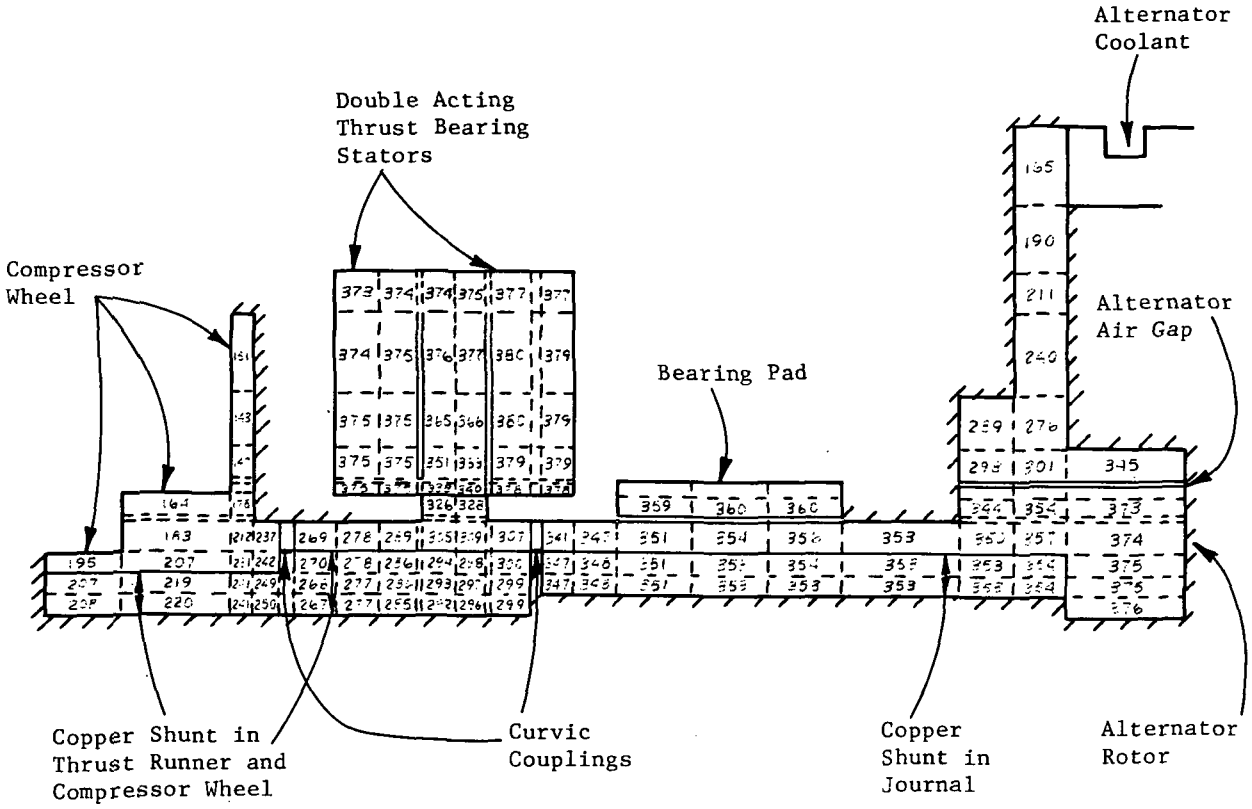

All Temperatures in °F

Surface Considered to be Insulated

Fig. 10 Temperature Distribution in the BRU Thrust Bearing and in the Adjacent Journal Bearing at the 10.5 KW Power Level Condition

During the preliminary analysis stages, the primary feature of concern about the reliability of concept (a) as a mechanism for the removal of heat from the thrust bearing, was related to the effects of a loss of thermal contact between the copper shunt and the compressor wheel. An analysis was, therefore, performed which assumed total loss of thermal contact in this region. The results are shown in Figure 11, and as can be seen, this worst case condition only results in an increase of the absolute temperature of the thrust and journal bearing region. Both bearings remain essentially isothermal in the regions of importance and it was concluded, therefore, that this concept of heat removal should prove to be reliable.

THRUST BEARING MECHANICAL DESIGN

Design studies were performed which allow the incorporation of a 4.25 inch diameter double-acting thrust bearing into the BRU envelope. The envelope and interface dimensions used in these studies were those provided by the NASA (NASA drawing SKP 18408). Basically, the recommended design utilizes the existing surface, location and bolt holes to mount the thrust bearing assembly. The assembly fits within the envelope formed by the BRU compressor back shroud and the journal bearing carrier.

The thrust bearing design consists of two flat plates bolted together at the periphery and separated by a spacer which is 0.004 inch thicker than the thrust runner. The bearing surface of each plate contains the helical groove pattern, also the orifices required for hydrostatic operation. The bearing assembly is flexibly supported, by four spokes, from an outer member which locates and attaches the bearing assembly to the BRU interface. The four-spoke flexible support member is a furnace brazed subassembly consisting of an inner ring joined to an outer ring by means of the spokes which are brazed to the rings. To prevent buckling of the spokes due to differential thermal expansion, they have been positioned tangentially to the inner and outer rings. With this configuration, differential expansion causes the inner ring to rotate relative to the outer ring, a motion which is acceptable to the design.*

The calculated angular or tilt stiffness of the spoked flexure assembly is 3.89×10^4 in-lb/rad. This is approximately one third of the tilt stiffness of the gas film at the maximum load condition of 31 pounds. Thus, the flexure will accomodate 75 percent of any misalignment which may exist between the thrust runner and stator. The remaining misalignment will be accomodated by the gas film. At zero load conditions, the tilt stiffness of the gas film is two thirds of the tilt stiffness of the flexure. In this case 60 percent of the misalignment will be accommodated by the gas film. This situation is acceptable because, under zero load conditions, the film thickness would normally be 0.002 inch, of which 0.001 inch could be used to accommodate misalignment before the design criteria of 0.001 minimum film

* Photographs of the thrust bearing components are shown in Figure 26. These components which were used for hydrostatic performance experimentation, were identical to the BRU back-up bearing design.

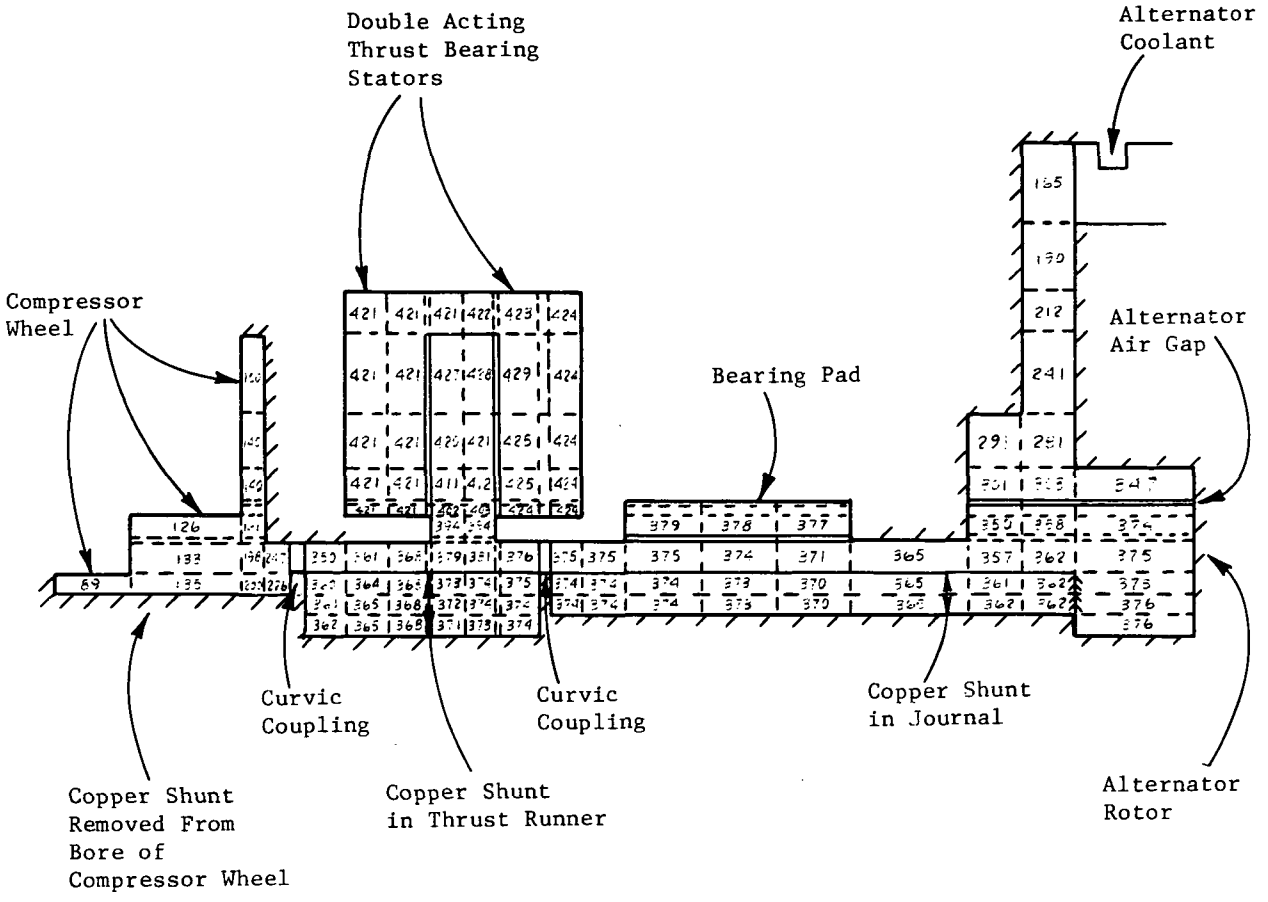

All Temperatures in °F

////// Surface Considered to be Insulated

Fig. 11 Temperature Distribution in the BRU Thrust Bearing and in the Adjacent Journal Bearing When Thermal Contact Between the Copper Shunt and the Compressor Wheel is Removed (10.5 KW Power Level Condition)

thickness was isolated. The design of the BRU and the set-up procedures available for the initial alignment of the thrust bearing during assembly are such that it is considered most unlikely that the thrust bearing assembly will ever be required to accommodate as much as 0.002 inch misalignment under any of the specified conditions of operation.

The introduction of flexibility in the tilt direction also results in flexibility in the axial direction. Axial flexibility is not desirable from the standpoint of retention of axial clearances around the compressor and turbine wheels under all conditions of BRU operation. The flexure design has, therefore, been optimized, as far as is possible within the available space envelope, to give the highest axial stiffness that can be obtained in association with the desired tilt stiffness. The calculated axial stiffness of the thrust bearing flexure assembly is 2.63×10^4 lb/in. The total axial movement of the thrust runner during BRU operation was calculated to be as follows:

Horizontal or Space Operation - Hydrodynamic

Power Level (kw)	Direction of Thrust Runner Movement	Amount of Movement Accommodated by Bearing Film (inches)	Amount of Movement Accommodated by Thrust Flexure (inches)	Total Movement of Thrust Runner (i.e., of the shaft) (inches)
10.5	Toward Turbine	0.0009	0.0012	0.0021
6.0	Toward Turbine	0.0007	0.0007	0.0014
2.25	Toward Turbine	0.0005	0.0005	0.0010

Vertical Operation - Hydrodynamic (Terrestrial)

Power Level (kw)	Direction of Thrust Runner Movement	Amount of Movement Accommodated by Bearing Film (inches)	Amount of Movement Accommodated by Thrust Flexure (inches)	Total Movement of Runner (inches)
10.0	Toward Turbine	0.0004	0.0004	0.0008
6.0	Toward Compresor	0.0002	0.0002	0.0004
2.25	Toward Compressor	0.0004	0.0004	0.0008

Vertical Operation - Hydrodynamic (Terrestrial) (continued)

Operation Under a 6-g Acceleration - Hydrodynamic

6.0	Either Direction	0.0014	0.005	0.0064

Operation Under 100-Pound Load - Hydrostatic

6.0	Either Direction	0.0016	0.0038	0.0054

Features were introduced into the design that allow for the adjustment the thrust stator to obtain alignment with the runner. The same adjustment feature may be used to position the rotor axially. The capacitance type instrumentation inserted into the bearing for the purposes of measuring film thickness during operation may also be used during assembly to ensure that the thrust stator and thrust runner are accurately aligned.

SUMMARY OF THRUST BEARING DESIGN

The following summarizes the design parameters and features of the selected back-up thrust bearing.

Bearing Type:	Spiral Grooved
Bearing O.D.:	4.25 inches
Bearing I.D.:	2.10 inches
Number of Groves:	18
Groove Depth:	0.0015/0.0020 inches
Groove Width to Land Width Ratio:	1.6
Inner Radius of Groove Annulus:	1.80 inches
Groove Helix Angle:	72.9 Degrees
Number of Jacking Gas Orifices:	6*
Diameter of Orifices:	0.035/0.045 inches
Orifice Location Diameter:	2.50 inches
Type of Self-Aligning Support:	Tangential Flexure
Number of Flexures:	4
Flexure Assembly Angular Stiffness:	3.89×10^4 in-lb/rad.
Flexure Assembly Axial Stiffness:	2.63×10^4 lb/in
Runner Substrate Material:	AlSl 4340 (RC 26-32)
Stator Substrate Material:	AlSl 416 (RC 26-32)
Flexure Material:	Carpenter Custom 455
Runner and Stator Surface Coating:	Chrome Oxide
Coating Thickness:	0.0015/0.0020 inches

* Based Upon Test Results Described Later in this Report.

CONCLUSIONS DRAWN FROM THRUST BEARING DESIGN ANALYSIS

To ensure reliable operation of the BRU over the specified range of operating conditions, the following conclusions relating to the thrust bearing have been drawn.

1. The spiral-grooved thrust plate design is preferable to the step-sector designs principally because of the higher "ultimate" load carrying capacity which is attainable from the spiral-grooved design.

2. The thrust bearing should be increased in size from the current 3.5 inches O.D. to 4.25 inches O.D.. The present inside diameter of 2.1 inches should be retained. The principal benefits to be derived from this increase in size are:

   a) approximately 0.0005 inch increase in film thickness at the maximum load condition,

   b) approximately three-fold increase in "ultimate" load carrying capacity, and

   c) approximately three-fold increase in angular stiffness of the gas film.

   The principal penalty resulting from this change will be an increase in the friction power losses as follows:

   Horizontal or Space Hydrodynamic

Alternator Power Level (KW)	Friction Loss For Original 3.5 Inch Diameter Double-Acting Bearing (watts)	Friction Loss Recommended 4.25" Diameter Double-Acting Bearing (watts)	Increase In Friction Loss (watts)
10.5	182	240	58
6 0	148	220	72
2.25	130	215	85

   Vertical Operation - Hydrodynamic (Terrestrial)

10.5	127	205	78
6.0	110	197	87
2.25	140	205	65

3. Increase the axial play between the thrust runner and thrust stators from 0.003 inch to 0.004 inch for the purpose of minimizing the power loss.

4. Retain the method presently used for the dissipation of thrust-bearing friction-generated heat. That is, the radial inflow of heat through the thrust-runner into a shrunk-fit copper shunt, then axial heat flow throught the copper followed by radially outward heat flow, across a further shrink fit, to the compressor wheel and into the system process fluid.

5. Utilize a flexure-type, self-aligning mechanism to support the thrust bearing assembly.

JOURNAL BEARING ANALYSIS

The performance requirement for the BRU journal bearing were defined as follows:

The journal bearings shall be suitable for operation at 36,000 rpm in a gaseous mixture of helium and xenon (molecular weight - 83.3) under the loads resulting from either horizontal or vertical operation. The ambient pressure range shall be 12.6 to 42.6 psia. The bearings shall be of the pivoted-pad type with non-conforming pivots. Each pad shall be provided with features which allow for hydrostatic operation of the bearings during start-up and shut-down of the BRU.

Hydrodynamic Journal Bearings

Analyses and optimization studies were performed to determine the configuration and geometry of hydrodynamic journal bearings best suited to meet the operational requirements of the BRU. The analyses and studies were performed using the 6.0 KW design-point values of ambient pressure and bearing temperature for two values of bearing load, namely, 11.25 pounds which is the static load on the turbine-end bearing during horizontal operation in a one "g" environment, and zero pounds which is the static load on both bearings during vertical or space operation.

The primary features of bearing performance which have been taken into consideration are:

(1) load carrying capacity,

(2) friction loss,

(3) pivot-point film thickness,

(4) pad-film natural frequencies of vibration in the pitch and roll directions of pad motion,

(5) stiffness and damping,

(6) tolerance to variations in radial temperature distribution in journal, pads and bearing support structure, and

(7) bearing set-up characteristics.

Analyses were performed to determine the effects on these bearing performance features of machined bearing clearance (C_p), operating clearance (C_p'), the number of pads comprising a bearing (three or four-pad configurations) and the stiffness of the flexures used to support each pad. (Definition of the parameters C_p and C_p' are given in Figure 12.)

Preliminary calculations indicated that either three- or four-pad bearing configurations with a nominal diameter of 1.75 inches and an L/D = 0.75 (i.e., the proportions of the present BRU bearings), were capable of carrying the required load of 11.25 pounds at acceptable values of pivot film thickness. The decision was made, therefore, to retain the present values of bearing diameter and length for all further analyses and optimization studies. This approach, of course, minimizes the problems associated with interfacing the back-up bearings with the BRU.

The first stage of the optimization procedure was the determination of the machined clearance (C_p) and the operating clearance (C_p').

For operation at the specified design-point conditions the most significant of these parameters is C_p' as this quantity largely determines the performance of the bearing. To permit the widest possible variation in the values of C_p' during operation without the bearing losing preload and, hence, becoming unstable, it becomes necessary to select a relatively large value of machined clearance C_p. The values of C_p and C_p' selected for the back-up bearings have been optimized to give good performance at design-point conditions while retaining the ability to accommodate variations in operating clearance.

A comparison showing the performance of three-pad and four-pad journal bearing configurations using the optimized values of C_p and C_p' is given in Table III.

From Table III it is seen that performances of the three-pad and four-pad bearing configurations are so nearly equal that selection of the preferred configuration, on the basis of design-point performance, becomes a marginal decision. Consideration of other factors such as the ease of fabrication, use of the existing bearing support structures, and ultimate load carrying capacity, however, leads to the selection of the three-pad bearing configuration for use in the BRU. Figure 13 shows a plot of calculated pad load versus pivot film thickness for the recommended three-pad bearing.

Probably the most important feature of bearing design is a characteristic of the flexures used to support the individual pads which comprise a bearing. While the flexures do not influence static bearing performance at the selected design point conditions, they significantly affect dynamic performance at these conditions. The primary value of the flexure lies in its ability to accommodate the differential thermal expansion and journal centrifugal growth within the bearing components, which are associated with start-up, shut-down or off-design operation of the BRU. Without the use of a flexure or flexures, the gas film would have to accommodate both the differential thermal expansion and the journal centifugal growth associated with the operational range under consideration. It can be readily shown that operational feasibility

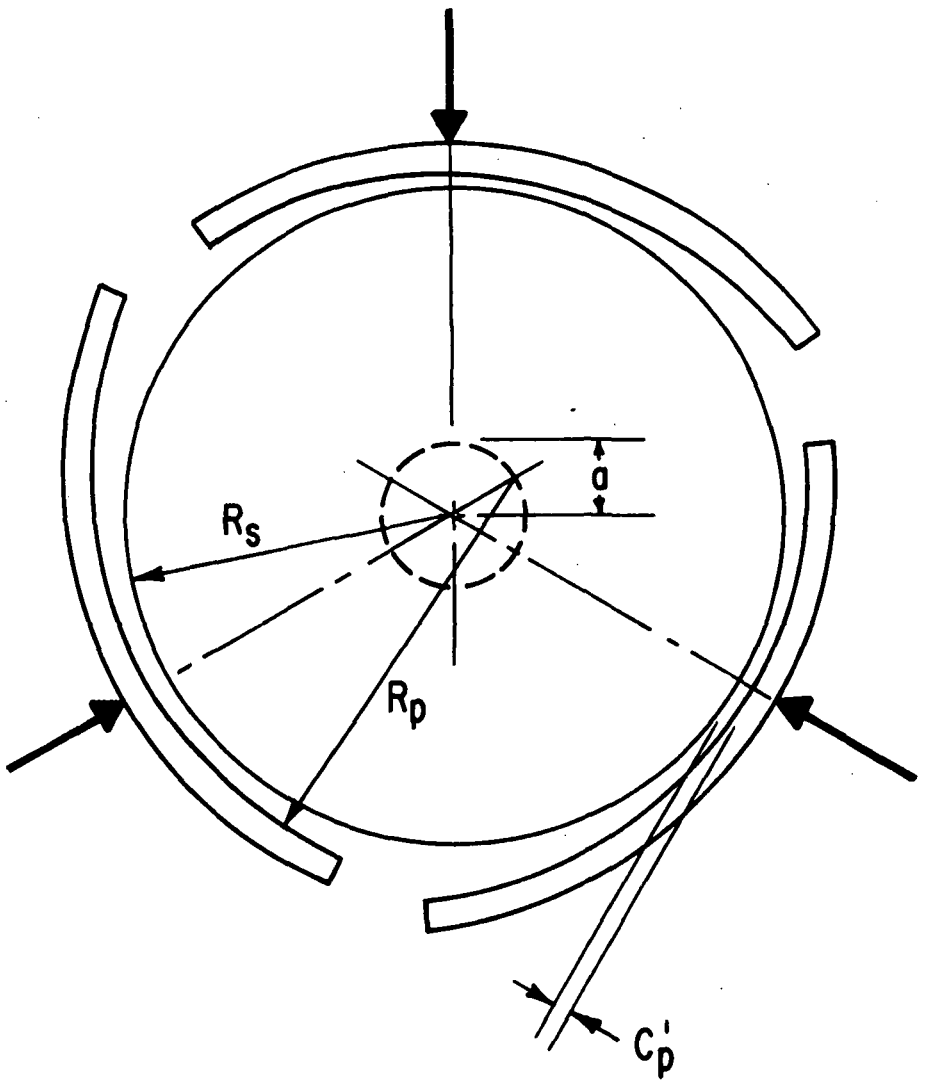

PAD TO SHAFT (OR "MACHINED") CLEARANCE: $C_p = R_p - R_s$

OPERATING CLEARANCE: $C_p' = R_p - a - R_s$

GEOMETRICAL PRELOAD FACTOR: $m = 1 - \frac{C_p'}{C_p}$

Fig. 12 Geometry of Preloaded Tilting Pad Bearing

TABLE III COMPARISON OF "THREE-PAD AND "FOUR-PAD" JOURNAL BEARING DESIGNS

	Three-Pad Brg.	Four-Pad Brg.
Minimum Pivot Film Thickness (mils)	0.48	0.45
Total Bearing Power Loss (watts)	59	62
Frequency Ratios*		
Lower Pads - pitch	>2	>2
roll	>2	>2
yaw	0.82	0.84
Frequency Ratios*		
Upper Pads - pitch	1.83	1.88
roll	1.60	2.10
yaw	0.49	0.51

Bearing Load = 11.25 lb

Speed = 36,000 rpm

Ambinet Pressure = 25.1 psia

C_p = 2.1875 mils (at 6.0 kw design point)

C_p' = 0.6 mils (at 6.0 kw design point)

* Ratio of pad-film natural frequency to rotational frequency.

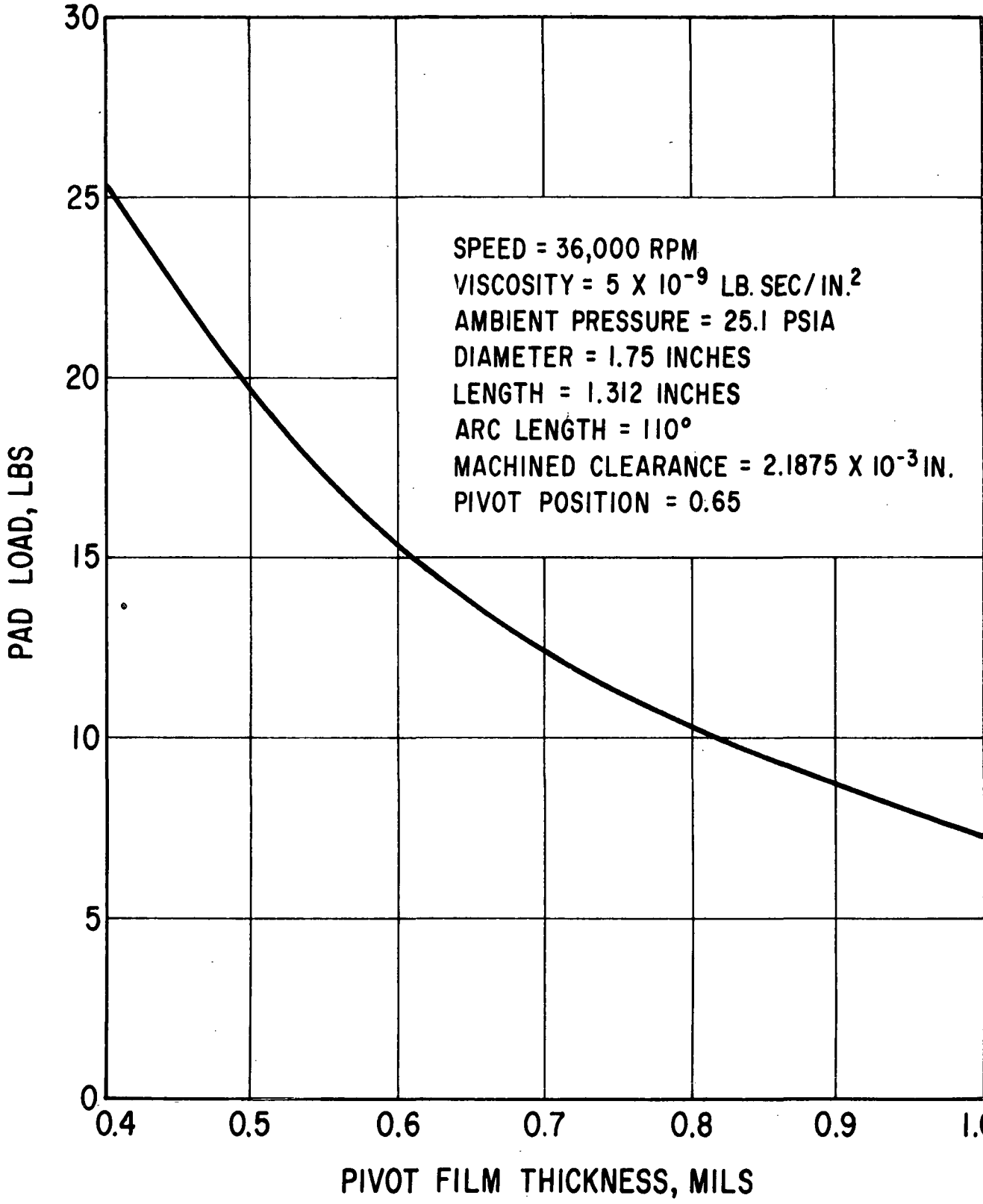

Fig. 13 Pad Load Versus Pivot Film Thickness for 3-Pad Bearing at 6.0 KW Power Level Design Conditions

of the machine without flexures could only be achieved if the temperatures within the bearing area were controlled within fairly narrow limits. The introduction of flexures with properly slected values of stiffness widens significantly the limits of temperature variation within which the bearing will perform adequately, because the flexure, rather than the gas film, accommodates dimensional variations.

The selection of the most appropriate flexure stiffness for the BRU application requires a compromise between three desirable features as follows:

(1) Accommodation of the widest possible range of radial temperature gradients within the bearing components.

(2) Attainment of the maximum amount of damping available from the gas film, thereby reducing the amplitude of vibration at the bearings resulting from rotor unbalance.

(3) Freedom from clamping of the journals by the pads at setup, thereby opening up the possibility of start-up and shutdown without the use of hydrostatic jacking of the journal bearings.

Accommodation of a wide range of radial temperature gradients can be accomplished by the use of a very soft flexure system. Such a system, however, results in the pads being clamped (preloaded) against the journal at zero speed set-up conditions. Figure 14 shows a plot of flexure stiffness versus diametral bearing clearance at setup for three values of design operation clearance (C_p'). From this figure it is seen that the amount of negative diametral bearing clearance at setup, i.e., clamping, increases as the value of flexure stiffness decreases. It is also seen that the larger design values of operating clearance C_p' permit the use of softer flexures. The softest flexure system that can be used for the BRU without clamping the rotor shaft at setup consists of three flexures, each having a stiffness of 18,750 lb/in. Such a flexure system would permit a diametral clearance at setup of 0.25 mils, this being the minimum clearance considered feasible from practical considerations.

An increase in the amount of gas film damping, relative to that which can be obtained with the three equal-stiffness flexure system, can be obtained by using a statically equivalent system consisting of two very stiff flexures in conjunction with one very soft flexure. In this case, the stiffness of the soft flexure would be 6250 lb/in. With a flexure of this stiffness, the setup clearance would remain at 0.25 mils, i.e., no clamping.

The use of a flexure system consisting of two very stiff flexures and one flexure with a stiffness of 2000 lb/in. would give the bearing the widest practical tolerance to radial temperature gradients. The pads in this case would be preloaded against the shaft at zero speed set-up conditions. Flexures with significantly lower stiffnesses would be subject to very large deflections and the resulting stress levels would be unacceptable.

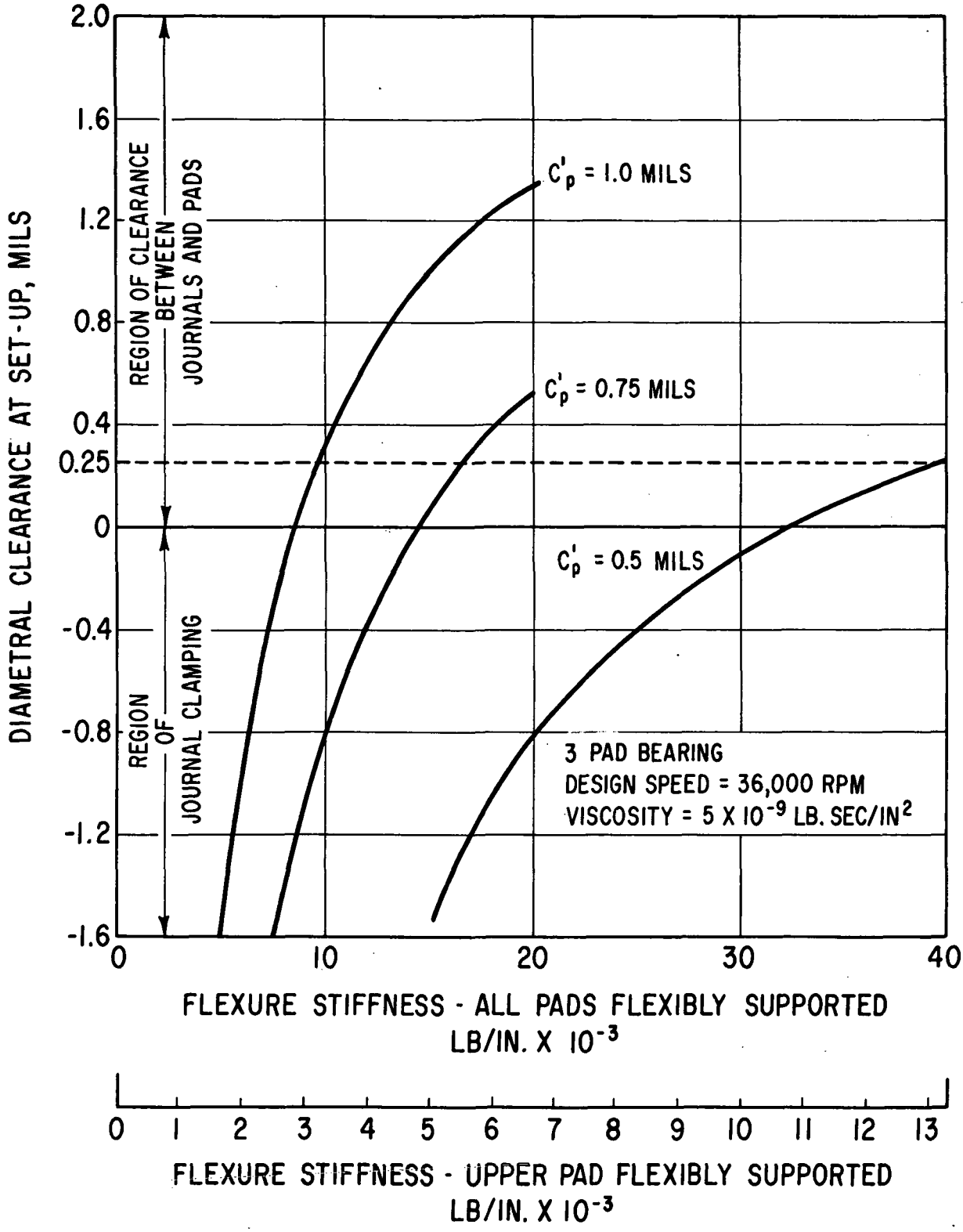

Fig. 14 Effect of Design Point Operating Clearance and Flexure Stiffness on Diametral Setup Clearance

Figure 15 shows the effect on pad load of variations in the radial temperature distribution within the bearing components. Negative values of ΔT indicate temperature changes from design point values that result in a reduction in bearing clearance. Positive values of ΔT indicate temperature changes resulting in an increase in clearance. These plots are for two different values of flexure stiffness, both of which use two stiff flexures in conjunction with a soft flexure. In one case, the soft flexure has a stiffness of 2000 lb/in. (the value used in the present BRU design) which results in a wide tolerance to radial temperature gradients but involves pad-to-shaft clamping at set-up. In the other case the soft flexure or preferably, the intermediate flexure, has a stiffness of 6250 lb/in., i.e., a reduced tolerance to radial temperature gradients but without pad-to-shaft clamping at setup.

Hydrostatic Operation

Hydrostatic lift off is required as a feature of each pad of a journal bearing. The inclusion of this feature reduces significantly the torque required to start the BRU, particularly in the case where the flexure characteristics result in the bearing pad clamping the journal when hydrostatic jacking is not in use. Additionally, this feature removes the possibility of damage to the bearing surfaces by rubbing during the start-stop periods of BRU operation.

Basically the hydrostatic journal bearing involves a supply of helium-xenon (at a pressure of 140 PSIA) which passes throught the pivot, but avoids the high-stress pivot/seat contact zone, through a check valve and an orifice into a pocket cut into the surface of the pad. Each pad in both journal bearings are similarly equipped.

The hydrostatic bearing has been designed to operate at 0.3 to 0.4 mils film thickness under conditions of maximum static load and at the maximum ambient pressure of 42.6 PSIA. Maximum static load occurs with the machine in a horizontal attitude in a 1g environment and with a 2000 lb/in. flexure exerting a clamping force of eleven pounds. The total force on each of the loaded pads under these conditions at a film thickness of 0.5 mils will be approximately 25 pounds. The flow requirements for each bearing (three pads) under maximum load conditions will be 4.5×10^{-4} lb/sec.

Calculations have not been performed to determine bearing film thicknesses and flows for operation in the vertical attitude, with stiffer flexures or with lower ambient pressures. Generally, however, the tendency will be toward slightly larger film thicknesses and flow rates.

The hydrostatic gas supply system (see Figure 16) to each pad is provided with two valves, each of which is located within the bearing pad. The primary vlave is located under the pivot seat and operates as a preloaded check valve which permits jacking gas to flow to the bearing when hydrostatic operation is required. When the bearing is operating hydrodynamically this valve closes and prevents back flow of the gas in the bearing film. The secondary valve, which is located around the pivot, is open when the bearing is oper-

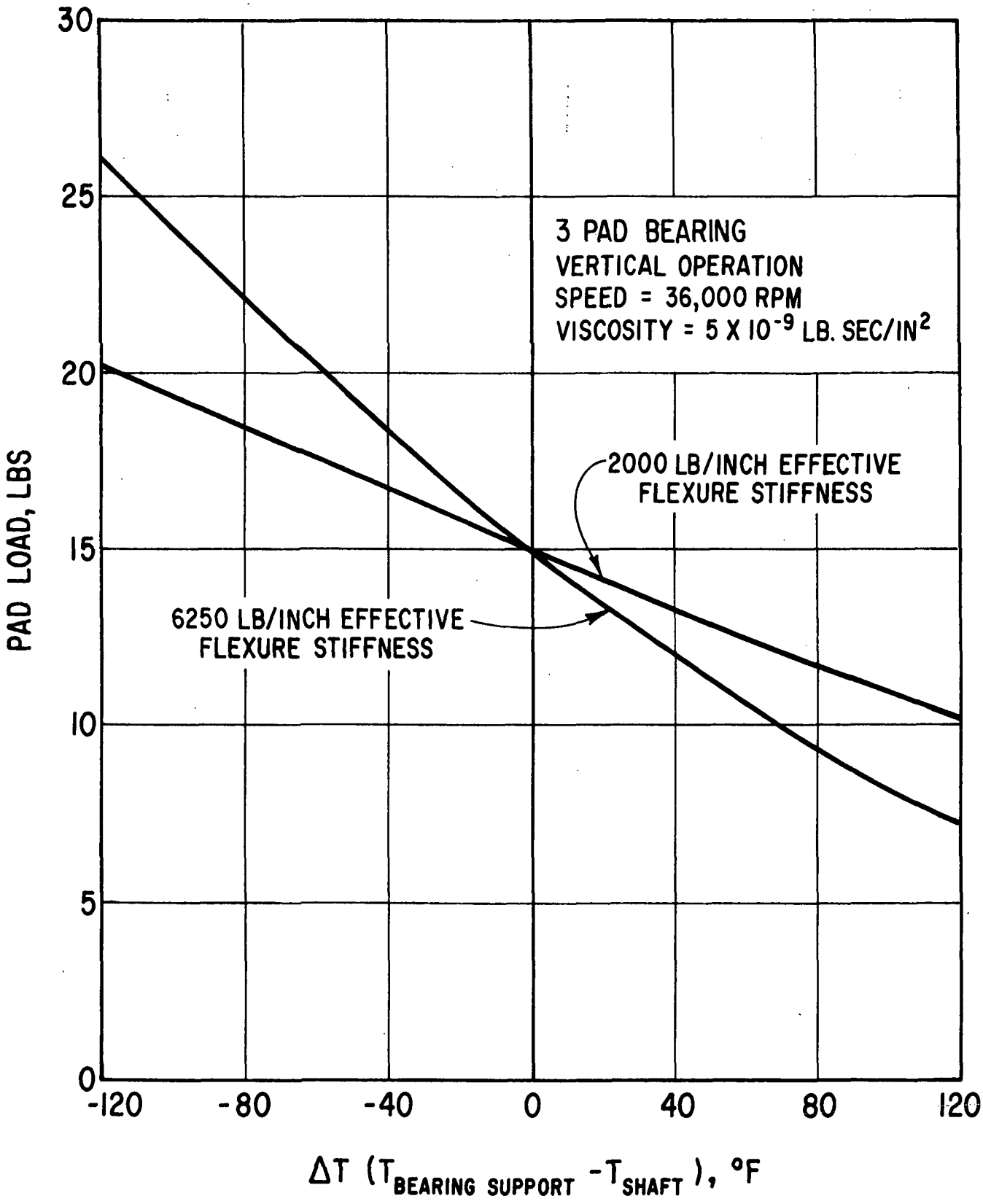

Fig. 15 Effect of Radial Temperature Gradients on Pad Load for Two Values of Flexure Stiffness

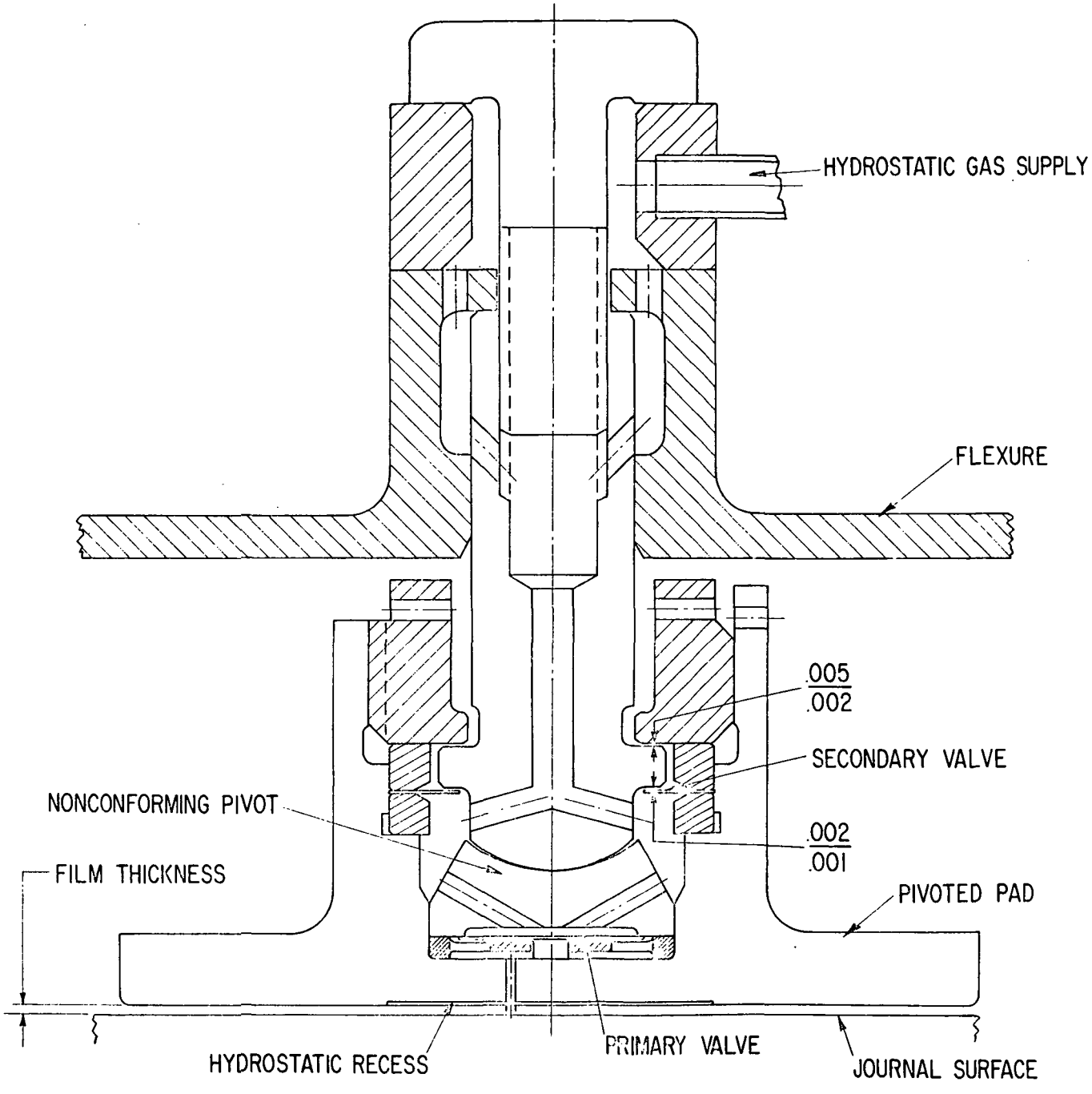

Fig. 16 Cross Section of Nonconforming Pivoted Pad Bearing Showing Hydrostatic Jacking System

ating hydrodynamically. The introduction of high pressure gas for jacking purposes causes this valve to deflect and seal against the pivot rod, thereby preventing the loss of jacking gas to the bearing cavity.

JOURNAL BEARING THERMAL ANALYSIS

Thermal analyses were performed to determine the temperature distribution in the compressor-end and turbine-end journal bearing regions. The thermal analysis of the compressor-end bearing was performed in conjunction with the thermal analysis of the thrust bearing which was discussed earlier. The boundary conditions used in the thermal analysis of the turbine-end journal bearing were as follows:

Heat Transfer Coefficients:

Stationary Surfaces:	$k = 10$ Btu/hr-ft^2-F (assumed)
Curvic Coupling:	$k = 6.75$ Btu/hr-ft-F Based on contact area 0.234 in^2 (i.e., 1/4 annulus area) $k = k_{steel} \times \frac{\text{area of contact}}{\text{annulus area}}$
Alternator Flux Gap:	$k_{eq} = 0.782$ Btu/hr-ft-F Based on Taylor number and Reynolds number for 0.020 inch radial gap
Radiation Shield Flux Gap:	$k = 178$ Btu/hr-ft^2-F Based on Taylor number and Reynolds number for 0.005 inch radial gap

Temperature boundary conditions were assumed at locations 2,3,5,7,9, and 10, as indicated in the thermal analysis model.

The analyses took into consideration the introduction of one percent of system gas flow into each bearing cavity at a temperature of 280°F. This gas is assumed to leave the bearing cavities via the labyrinth seals located at the back of the compressor and turbine wheels. Because the journal bearing supports are thermally decoupled from the alternator end plates, these supports are not included in the analysis. The temperature of the supports is assumed to reach that of the journals to which the supports are thermally coupled by reason of the extended portion of each support that closely conforms to the journals.

The calculated temperature distributions at the 10.5 KW power level condition are shown in Figure 10 for the compressor-end journal bearing and Figure 17 for the turbine-end journal bearing. From these figures it is seen that the temperature distribution is very uniform in both the journals and bearings. The mean bearing temperature at the turbine-end bearing is shown to

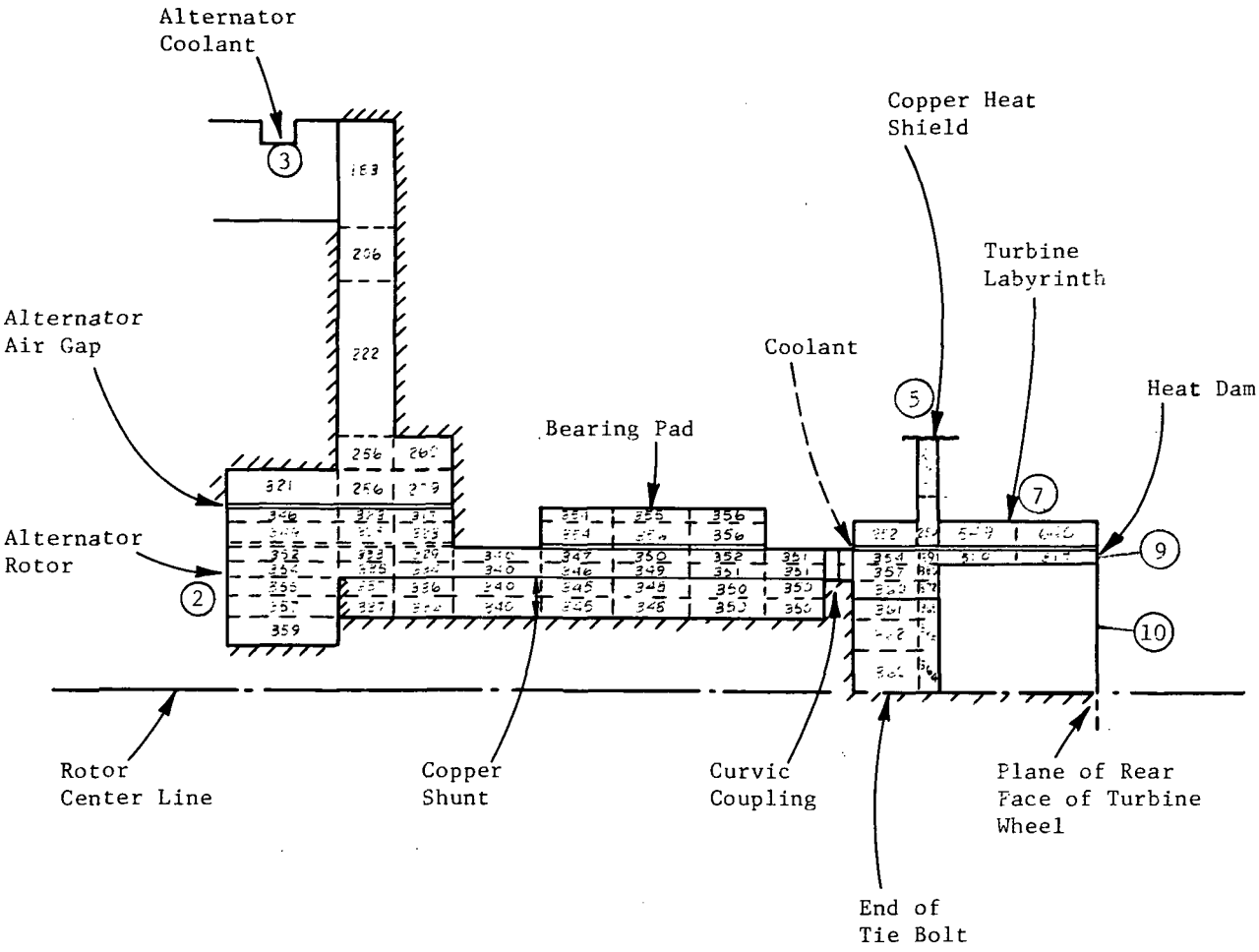

Fig. 17 Temperature Distribution in the BRU Turbine End Journal Bearing Area at the 10.5 KW Power Level

be 355°F while the mean temperature at the compressor end is shown to be 378°F. These temperature levels and distributions should be acceptable for satisfactory operation of the journal bearings.

JOURNAL BEARING MECHANICAL DESIGN

The mechanical design of the recommended three-pad journal bearings is identical for both the compressor-end and turbine-end of the BRU The interface between the bearing components and the BRU occurs at the three flat surfaces on each of the existing bearing support structures and, of course, at the journals which will retain the existing diameter and tolerance.

The design of the journal bearings, shown in Figures 16 and 18 consists of flexure-mounted, nonconforming pivoted-pad journal bearings with provisions for hydrostatic jacking. The flexures are of two different stiffnesses, the lower pair being designed for 2×10^6 lb/in. while the upper flexure will be 2×10^3 lb/in., or alternately 6.25×10^3 lb/in. (see the discussion on flexure stiffness on pages 24 and 25). The flexure shown in Figure 18 has a stiffness of 2×10^3 lb/in. Both the upper and lower journal bearing flexures are of Carpenter Custom 455. This material is a martensitic age-hardenable stainless steel with a 0.2 percent yield strength of 237,000 psi. The endurance limit of this material is in excess of 100,000 psi at 2×10^7 cycles. The pivot seat and pivot rod are of M1 tool steel heat treated to the RC 60-62 condition.

The mechanical design of the jacking gas supply and pivot systems was evolved from consideration of the design criteria shown in Table IV.

Three conceptual designs were studied in detail before the design shown in Figures 16 and 18 was selected for use in the BRU. This design closely conforms to the aforementioned design criteria with, however, one possible exception. This exception concerns criteria number 19 which requires that the shut-off flow through the primary and secondary valves should be zero after 1000 cycles of operation or 50,000 hours use. When considered from a design point of view, the valves should be capable of meeting the criteria. There is, however, the possibility that dirt or debris may prevent the valve from seating properly and therefore, permitting a leak. During the design stage considerable emphasis was placed on features that allowed access for visual inspection and cleaning of the components used for the internal distribution of hydrostatic gas. It is concluded that the valves will perform satisfactorily when assembled and used in a clean environment.

ROTOR DYNAMICS

Analyses have been performed to determine the rotor critical speeds and the response of the rotor to unbalance located in the planes of the compressor and turbine wheels.

The model of the rotor upon which the critical speed and unbalance response analyses were based, was determined by scaling the drawings provided by the NASA. The analyses were performed using the mass of the 4.25 inches diameter thrust runner. While the mass of the copper shunts was included in the analyses it was assumed that this copper does not contribute to rotor stiffness.

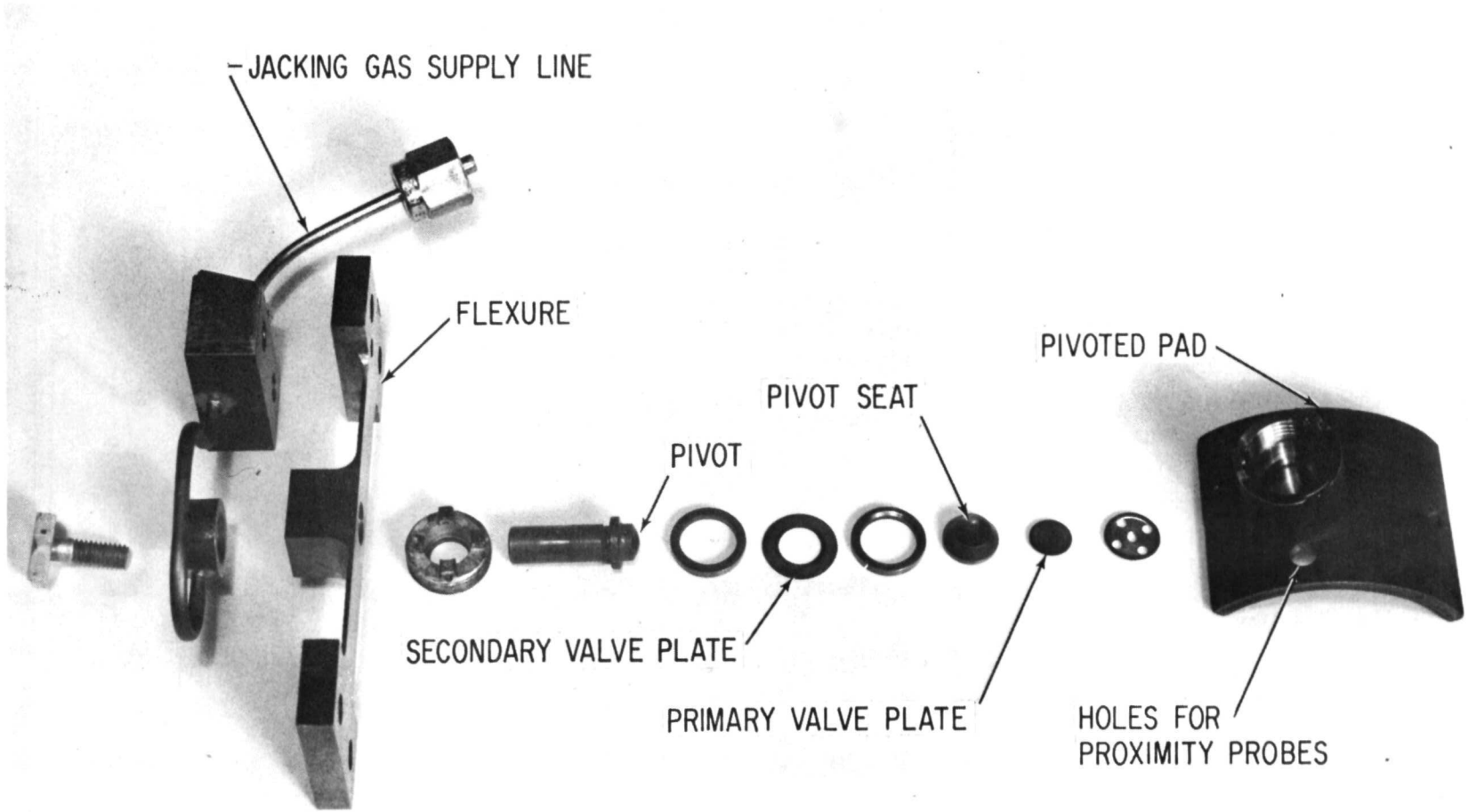

Fig. 18 Nonconforming Pivoted-Pad Journal Bearing Components

TABLE IV DESIGN CRITERIA FOR TILTING PAD BEARING WITH NONCONFORMING PIVOT AND PROVISIONS FOR HYDROSTATIC JACKING

1. Operational Capacity to $500^{o}F$
2. Nonconforming Spherical Pivot
3. No Jacking Gas Holes In Hertzian Contact Zone of Pivot
4. Minimum Pad Mass and Inertia
5. Maximum Metal Thickness Under High Stress Contact Zone(> 0.08 in.)
6. Pivot Hertzian Stress < 100,000 PSI
7. Pivot Conformity To Be Selected to Give Best Rolling Characteristics, i.e., R_2/R_1 To Be A Maximum Consisten With Acceptable Stress Levels
8. Dimension From Pivot Contact Surface To Bearing Pad To Be A Minimum
9. Pivot and Sperical Socket Material - M1 Tool Steel
10. Pad ToPivot Retaining Device (For Assembly Only)
11. No Restraint To Pad Motion
12. No Fatigue Limited Members (Pipes or Bellows)
13. Avoid Use of Materials With Questionable Life Characteristics
14. Valve Elements (Metallics) Stressed < 100,000 PSI
15. Secondary Valve To Be Noncontacting Except During Application Of Jacking Gas
16. Primary Valve Natural Frequency > 4000 CPS
17. Sencondary Valve Natural Frequency > 4000 CPS
18. Primary Valve To Open When Supplied With 150 PSIA Jacking Gas
19. Primary And Secondary Valve Flow At Shut-Off To Be Zero After 1000 Cycles of Operation Or 50,000 Hours Use
20. Flow Area Through Primary Valve To Be > 5 Times Jacking Gas Orifice Area

Rotor critical speed versus bearing stiffness is shown plotted in Figure 19. For the range of bearing stiffnesses applicable to the BRU bearings the rotor will pass through the first two critical speeds in the speed range between 5000 - 15,000 RPM. At design speed the rotor will be operating well below the third critical which occurs at approximately 55,000 RPM. Figure 20 shows the mode shapes at the first and second criticals. The first critical is seen to be conical with, as indicated by the straight line, a rigid rotor. The second critical is translatory with only a slight amount of bending occuring in the rotor.

Calculations of the rotor response to unbalance have been performed using the stiffness and damping characteristics possessed by the bearing configuration that utilizes three flexures, each having a stiffness of 18,750 lb/in. Calculations have also been performed for the statically equivalent flexure system which uses two very stiff flexures in conjunction with an intermediate flexure with a stiffness of 6,250 lb/in. The calculations were performed for 0.0172 ounce-inches of unbalance in the planes of the compressor and turbine wheels. This amount of unbalance respresents a total rotor mass eccentricity of 0.0001 inches, half of which was considered to act in the plane of each wheel.

A comparison of the results of the rotor response calculations for the two flexure systems showed the amplitudes of vibration of the rotor at the rigid body critical speeds to be reduced by a factor of four when the two stiff flexures were used in conjunction with one intermediate flexure. Amplitudes of vibration at design speed were found to be almost identical for both flexure systems.

Figures 21,22 and 23 show the unbalance response amplitudes of rotor vibration in the planes of the compressor bearing, rotor center of gravity, and turbine bearing respectively, for "in-phase" and "out-of-phase" unbalance located in the compressor and turbine wheels. It should be noted that the bearing system is not isoelastic and as a result the amplitudes of vibration will be different in the X and Y directions, i.e., the orbit of journal motion will be elliptical. At design speed the minor axis of the orbit ellipse will be in the order of 80 percent of the major axis. When the rotor passes through the rigid body critical speeds, however, the degree of ellipticity will increase significantly. The values of unbalance amplitudes shown in Figure 21, 22 and 23 represent one half of the major axis of the orbit ellipse.

The magnitude of unbalance used for calculation purposes is significantly larger than would be expected in practice. For example, the BRU rotor can be readily balanced on a balancing machine to better than 1×10^{-3} oz-in. in the compressor and turbine planes, the major axis of the orbit as the machine passes through the rigid body critical speeds will be in the order of 50 microinches. At design speed the major axis of the orbit will be in the order of 30 microinches. It should be noted, however, that the exact size of the rotor orbit is also dependent on bearing performance which, ultimately, is dependent upon the temperature distribution between journals, pads and bearing support.

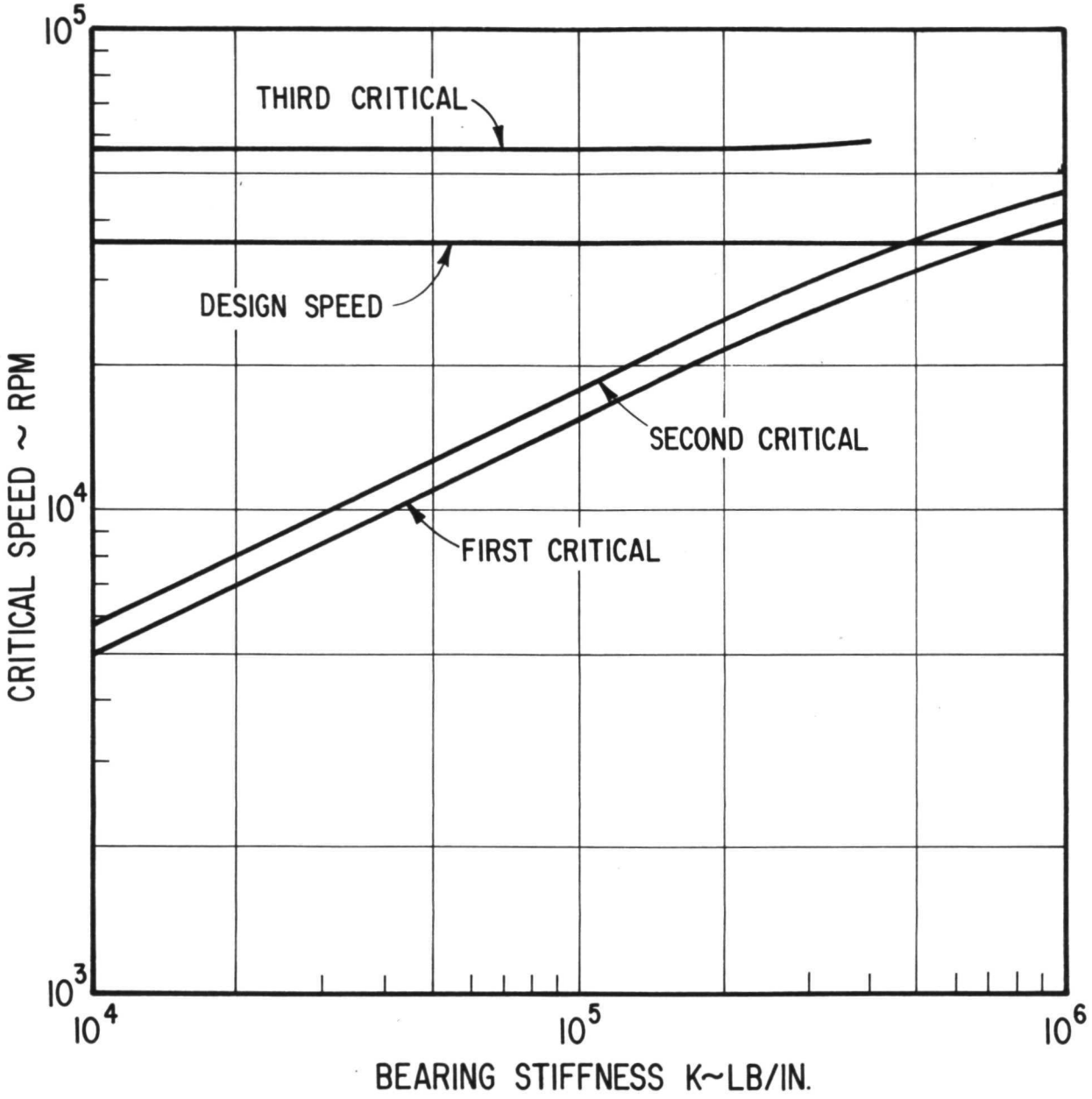

Fig. 19 BRU Rotor Critical Speed vs. Bearing Stiffness (Thrust Runner OD = 4.25 Inches)

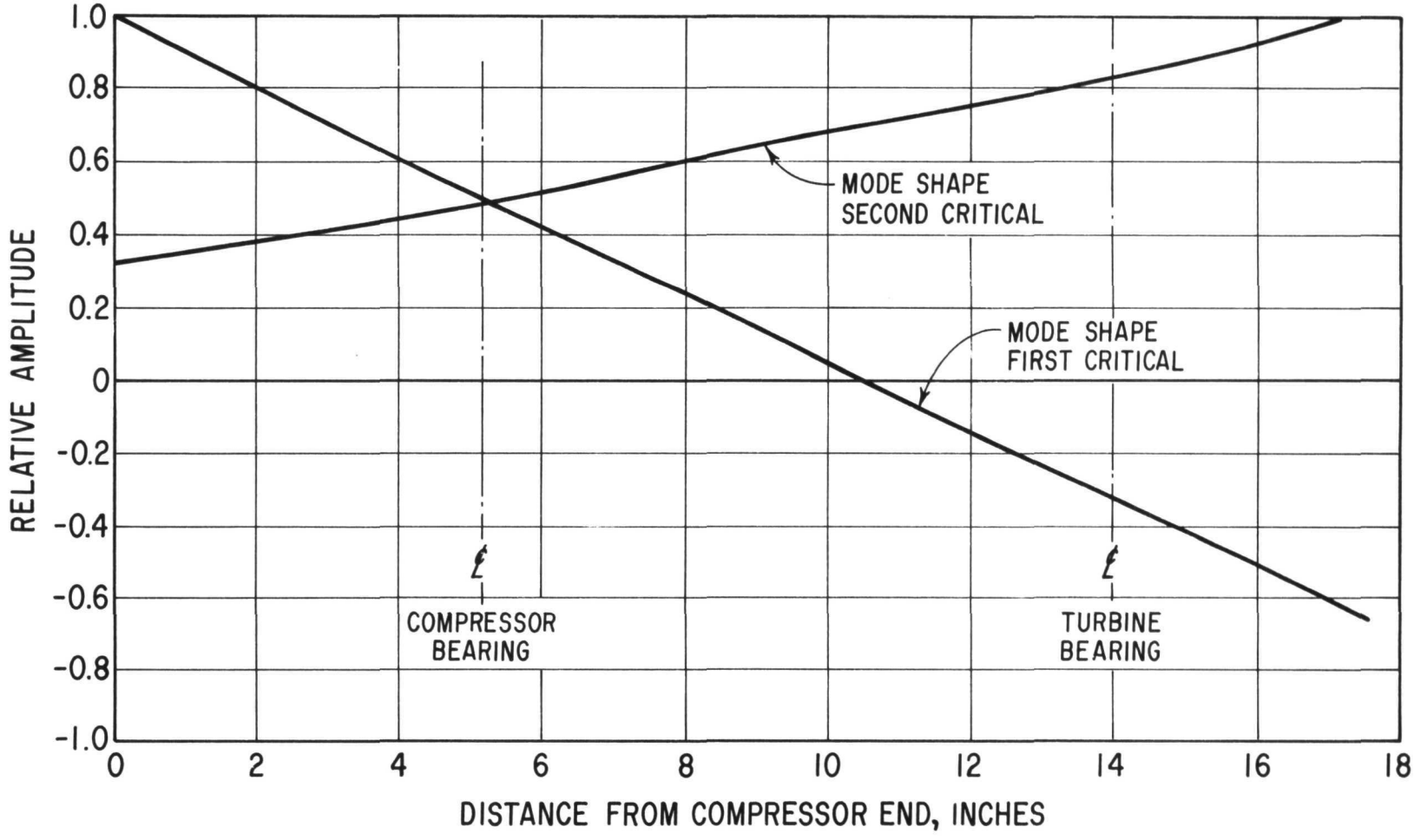

Fig. 20 BRU Rotor Mode Shapes - 1st and 2nd Criticals

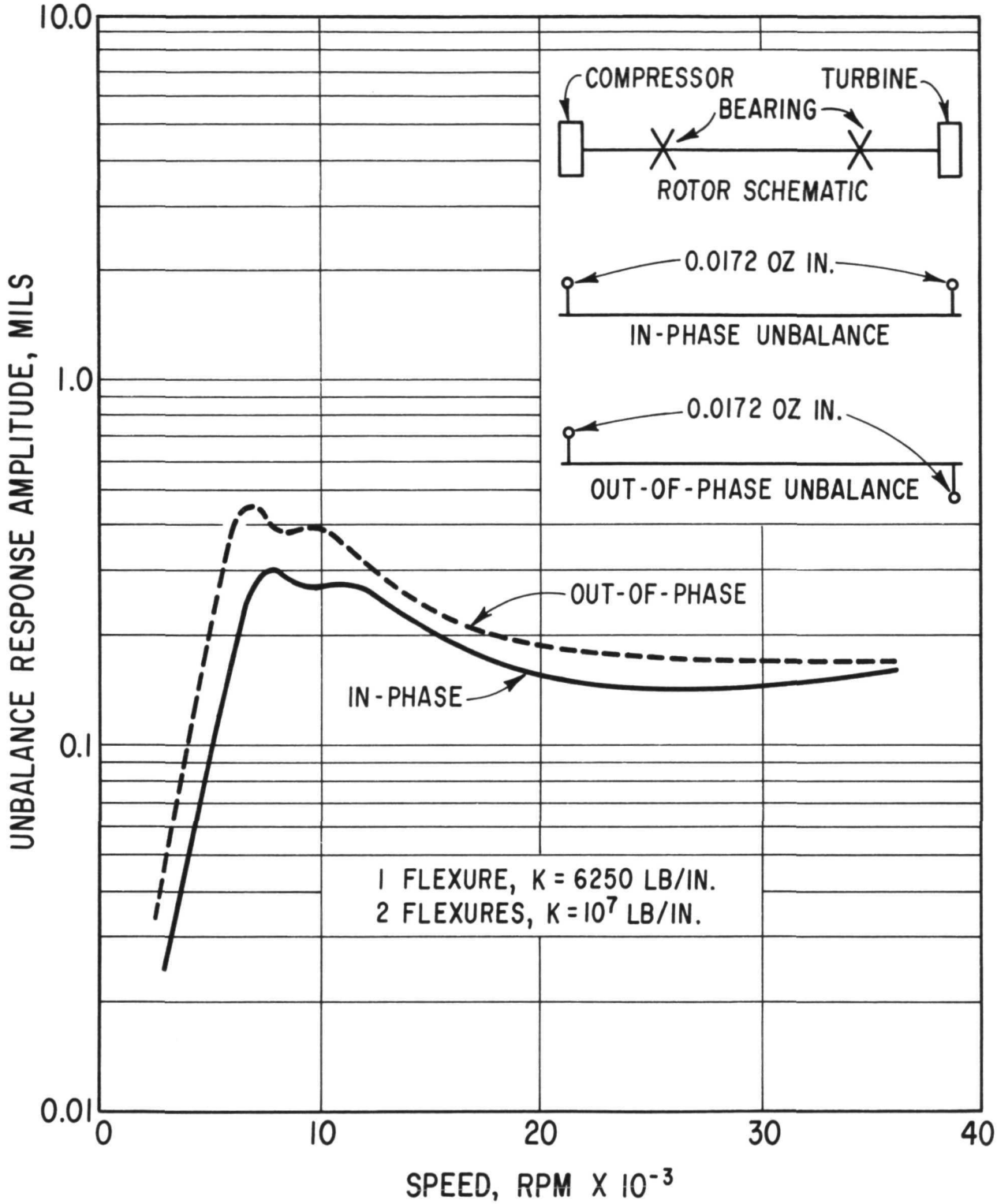

Fig. 21 Unbalance Response of BRU Rotor In Plane of Compressor Bearing

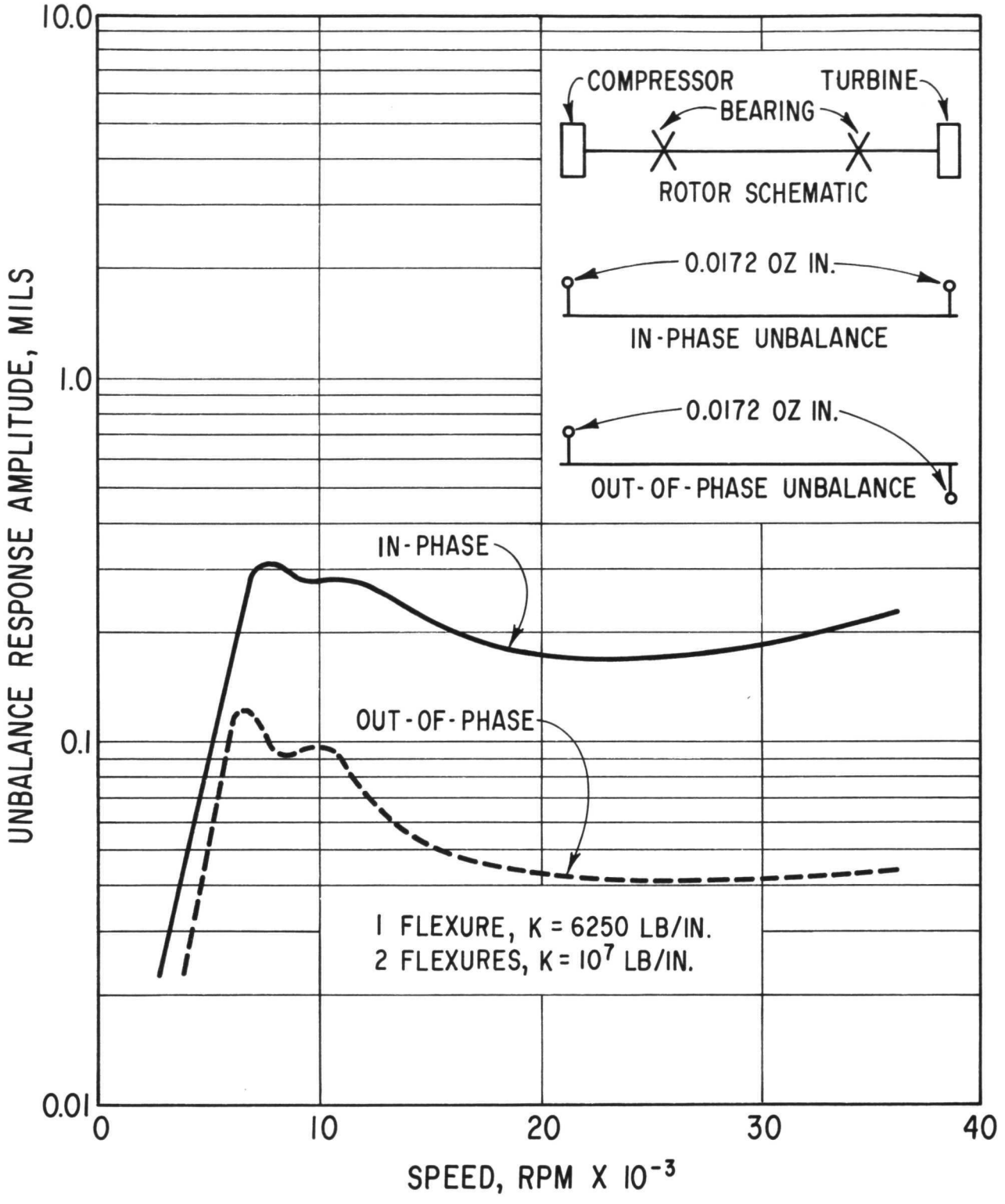

Fig. 22 Unbalance Response of BRU Rotor In Plane of Rotor Center of Gravity

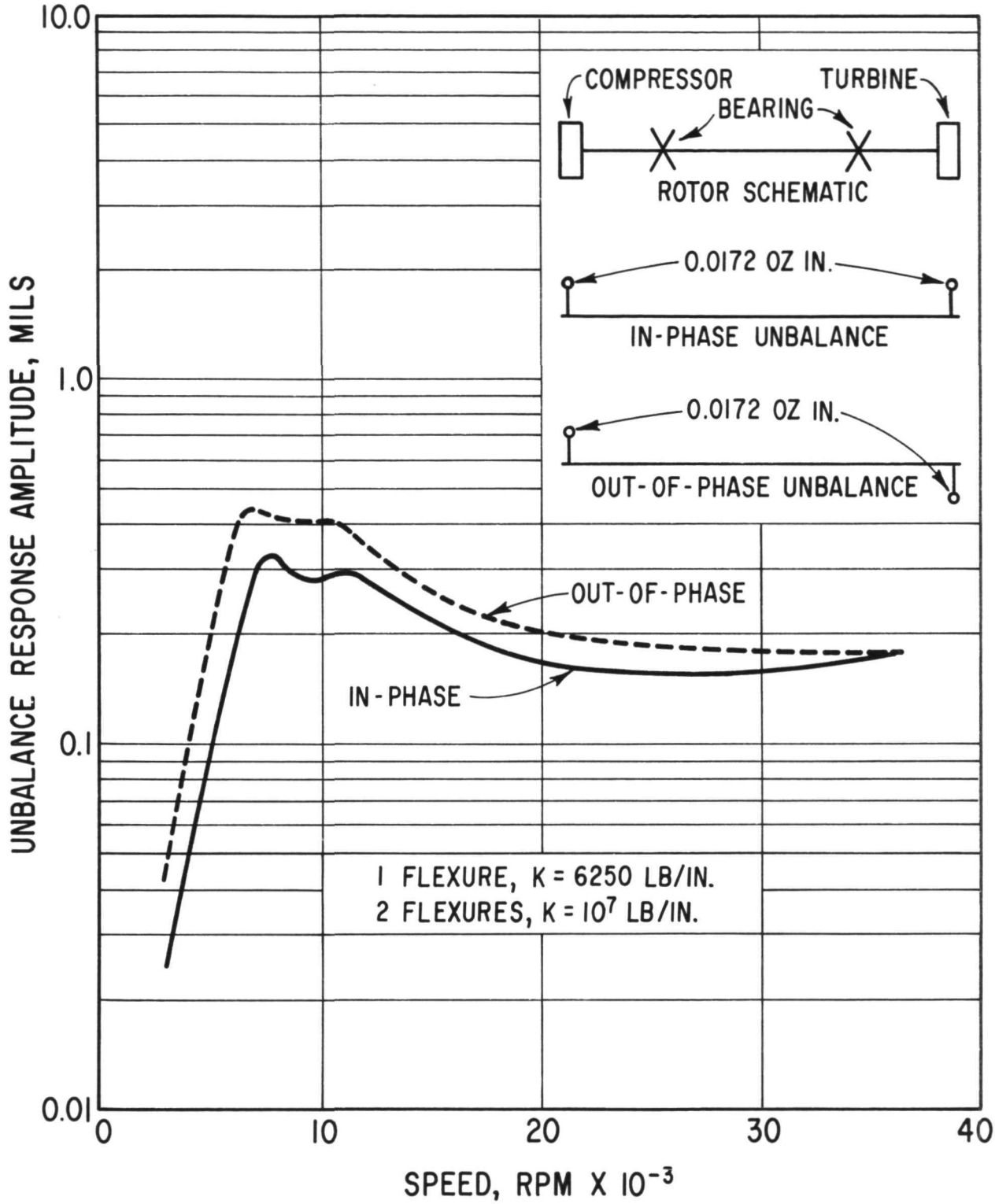

Fig. 23 Unbalance Response of BRU Rotor In Plane of Turbine Bearing

Consideration must also be given to the possibility of the occurance of mass shift within the rotor. Such shifts can occur as a result of relative motion between the elements located by means of curvic couplings, relaxation of the interference fits which locate the copper shunts or asymetric creep in the turbine wheel. Determination of the magnitude of the unbalance resulting from such shifts has not been attempted. However, it is considered that mass shifts resulting in changes of unbalance from 1×10^{-3} ounce inches should not prove hazardous to BRU operation.

SUMMARY OF NONCONFORMING PIVOTED PAD JOURNAL BEARING DESIGN

The following summarizes the design parameters and features of the selected back-up journal bearing.

Bearing Type:	Three Pad Tilting Pad
Pad Diameter:	1.7544 Inches
Journal Diameter:	1.7496 Inches
Pad Length:	1.312 Inches
Pad Arc Length:	110 Degrees
Pivot Position:	71.5 Degrees from Leading Edge
Pivot Diameter:	0.375 Inches
Pivot Seat Diameter:	0.3937 Inches
Number of Jacking Gas Orifices:	1
Diameter of Orifice:	0.0135 Inches
Orfice Location:	At Pivot Point
Number of Flexibly Mounted Pads:	1
Flexure Stiffness:	2000 lb/in or 6250 lb/in
Pad Substrate Material:	AISI 416 (RC26-32)
Pivot and Seat Material:	M1 Tool Steel (RC60-62)
Flexure Material:	Carpenter Custom 455
Journal and Pad Surface Coating:	Chrome Oxide
Coating Thickness:	0.002/0.004 Inches

CONCLUSIONS DRAWN FROM JOURNAL BEARING DESIGN ANALYSIS

To ensure reliable operation of the BRU over the specified range of operating conditions, the following conclusions relative to the journal bearings have been drawn.

1. The present three pad journal bearing configuration with one flexure mounted pad should be retained.

2. The present bearing size should be retained.

3. Primary and secondary valves need to be introduced into the non-conforming pivoted pad design to prevent loss of hydrodynamic film pressure and loss of hydrostatic supply gas to the bearing cavity.

4. The present 2000 lb/in flexure provides for a high tolerance of radial thermal gradients. However, it results in clamping of the shaft at start-up making hydrostatic jacking mandatory. Thus, a stiffer flexure (6,250 lb/in) should be tested in the BRU to assess its flexibility relative to elimination of jacking and to assess its limitations relative to actual radial thermal gradients.

The operating characteristics of the journal bearing at the 6.0 KW power level design point are as follows:

	Space Operation	Horizontal Operation in a 1g Environment
Clearance ratio C/R	2.5×10^{-3}	2.5×10^{-3}
Pivot point film thickness (inches)	0.66×10^{-3} (all pads)	0.54×10^{-3} (loaded pads)
Fiction loss/bearing (watts)	51.0	52.0
Pivot/seat contact zone stress (psi)	3.6×10^{4} (all pivots)	4.0×10^{4} (loaded pivots)

BEARING MATERIALS

Gas-lubricated bearings have no boundary lubrication safeguards. It is, therefore, extremely important that the bearing surfaces be of highly compatible materials, so that incidental high-speed contacts due to shock, vibration, passage of dirt through the bearing or improper use of the machine will not result in serious damage to the rotor-bearing system. Also, where the possibility remains that the use of hydrostatic jacking of the journal bearings may be dispensed with, the bearing surfaces must be capable of surviving sliding contact over an appreciable number of starts and stops without damage or significant wear.

It is known that the compatibility of the materials used to fabricate the rotor-bearing parts would not be acceptable for sliding or high speed contact conditions of operation. The coating material recommended for the BRU bearings is a flame-sprayed deposition of chrome oxide, a material which in previous tests and turbomachinery applications has been found suitable for the service conditions involved.

BEARING INSTRUMENTATION

The successful and rapid development of high speed, gas-bearing turbomachinery

requires that the static and dynamic behavior of the rotor-bearing system be monitored with precision during the test and evaluation phases. In particular, the rotor-bearing instrumentation must:

1. provide data for quantitative evaluation of overall performance,
2. provide data for detailed evaluation of component performance and for refinement of component design, and
3. indicate whether or not the equipment is in a safe mode of operation.

The parameters which must be measured in order to satisfy these three points are the static and dynamic film thicknesses in the thrust and journal bearings, the dynamic motion of the journals and certain of the nonrotating bearing components.

The measurement of static and dynamic film thicknesses and the measurement of dynamic motion of the journals and bearing components can be accomplished using a displacement measuring system. This system measures the capacitance of the gas film between the tip of a transducer and the surface under observation. Specifically a capacitance system based on the Wayne-Kerr Model DM-100 or equivalent is recommended.

Measurements of thrust bearing film thickness should be made using three equally spaced capacitance probes located in the thrust plate adjacent to the journal bearing. Two capacitance probes should be used to measure film thickness in the thrust bearing adjacent to the compressor wheel. These five probes can also be used for the purpose of aligning the thrust bearing components during assembly.

In addition to making measurements of the thrust bearing film thicknesses, measurements of the dynamic motion of the thrust bearing stator relative to the BRU casings should be made. The capacitance probe used for making these measurements can also be used for making displacement measurements when calibrating the stiffness of the thrust bearing flexure support system.

The measurement of journal bearing film thickness is best accomplished by mounting the capacitance probe in the bearing pad. The probe should be located as close to the pivot point as the mechanical design allows. This location is selected because it is at this point that contact would occur between pad and journal in the event of gross overload or loss of clearance resulting from adverse temperature gradients. Therefore, each pad should be equipped with one capacitance probe for the purpose of film thickness measurement.

Measurement of the dynamic motion of the journal bearing pads in the pitch and roll directions is also recommended. This measurement can be made on one pad in each bearing assembly. Preferably, the flexure mounted pad would be selected for this purpose. The capacitance probes should be mounted in the pad, therby detecting pitch and roll motions relative to the journal. The pitch probe should be located toward the leading edge of the pad and on the bearing center-line. The roll probe should be located

toward the end of the pad and in line with the pivot. It should be noted that the pitch and roll probes can also be used for measuring pad film thickness at their respective locations.

A capacitance probe should also be located on each of the journal bearing support structures to measure the radial dynamic motion of the end of the soft flexure mounted pivot rod. This probe could also be used to measure the initial deflection of the 2,000 pound per inch flexure which is required to preload the bearing assembly.

The restraint to pad motion from the capacitance probe leads has not, in previous similar applications, resulted in any detectable adverse effects in bearing performance.

The measurement of dynamic journal motion relative to the BRU casings can be accomplished with the existing capacitance probes.

Measurement of the temperature of the bearing parts should be made using thermocouples. The recommended location for these thermocouples is given as follows:

1) Journal bearings

   a) one thermocouple located adjacent to the pivot on each bearing pad,

   b) four thermocouples on one of the loaded pads in each bearing located at the leading edge, the trailing edge and one at each end,

   c) three thermocouples equally spaced around each journal bearing support.

2) Thrust bearings

   a) three thermocouples on the reverse or nonactive side of each thrust stator. The thermocouples to be equally spaced and located along a radial line extending from the inside diameter to the outside diameter of the bearing.

PERFORMANCE UNDER THE ANTICIPATED ENVIRONMENTAL CONDITIONS

The NASA Specification P1224-1 lists the anticipated environmental conditions for which the BRU shall be designed to operate without malfunction or perfance degradation. Primarily this specification defines the shock, vibration and acceleration to which the BRU will be subjected whether operating or not.

An investigation of the effects of vibration and shock on the performance of gas-bearing space-power Brayton cycle turbomachinery is the subject of a NASA contract (NASW-1713) with MTI. However, the experimental and analytical effort in this program has not as yet advanced to the stage where soundly based predictions can be made concerning operation of the BRU.

However, the performance of the BRU bearings under conditions involving constant acceleration can be predicted. Specification P1224-1 indicates that the maximum acceleration will be 6g for a period of five minutes along the longitudinal axis of the launch vehicle. Dependent on the orientation of the BRU to the axis of the vehicle, this acceleration can result in loads of 132 pounds on the thrust-bearing or 67.5 pounds on each of the journal bearings. The bearing components must be capable of withstanding these loads whether the BRU is operating or not.

The performance of the bearings under 6g acceleration with the BRU running at the 6.0 KW power level design conditions is given as follows.

a) Hydrodynamic Thrust Bearing

Load	(pounds)	132.0
Film thickness	(inches)	0.0006
Total friction loss	(watts)	370.0

b) Hydrodynamic Journal Bearing (load between pads)

Load	(pounds)	67.5
Loaded pad film thickness	(inches	0.00013
Unloaded pad film thickness	(inches)	0.00077
Bearing friction loss	(watts)	121.0
Loaded pad load	(pounds)	78.5
Unloaded pad load	(pounds)	11.1

The most highly stressed components in the bearing assemblies are the journal bearing pivots and the thrust bearing flexible mounting. Both of these elements have been designed to have satisfactory stress levels under the 6g condition. The stress levels are as follows.

Loaded pad pivot contact zone stress (psi)	6.49×10^4
Thrust bearing flexure stress (psi)	2.0×10^5

The pivot contact zone stress level is well within the design criteria of 1×10^5 psi which has been established for continuous service of nonconforming pivots. The stress in the thrust bearing flexure is 85 percent of the 0.2 percent yield stress of the maraging steel from which the flexure is fabricated. The axial displacement of the rotor under the 6g acceleration condition amounts to 0.0064 inches. This axial displacement must be accommodated by the axial clearances on either side of the compressor and turbine wheels. These clearances have been specified by the NASA as 0.010 inches

and 0.017 inches for the compressor and turbine respectively at the 6.0 KW steady-state design point. A minimum clearance of 0.0036 occurs between the compressor wheel and casing under the 6g operating condition. The thrust bearing flexure system has not been provided with stops to limit the axial motion of the stator under the 6g conditions. However, suitable stops could be added at a later date if the need arises.

The orientation of the BRU for horizontal operation is such that the load is directed between the pivots which are supported by the two stiff flexures (flexure stiffness 2×10^6 lb/in.). Under 6g acceleration the load must remain in the same direction. The stress in the stiff flexures resulting from the 6g acceleration loads is below 1000 psi. The stress in the soft flexure reduces from 32,500 psi at the zero g condition to 26,300 psi at the 6g condition.

EXPERIMENTAL HYDROSTATIC PERFORMANCE OF SPIRAL GROOVE AND STEP SECTOR THRUST BEARINGS

The calculated hydrodynamic and hydrostatic performance of the spiral-groove thrust bearing design under BRU operating conditions was discussed in the preceding section. As was previously indicated, it was not possible to analytically predict the threshold of dynamic instability (pneumatic hammer) or the threshold of static instability (lockup). These limitations are normally experimentally determined.

The spiral-groove thrust bearing described in the preceding section was designed with six hydrostatic jacking orifices, this being a number which past experience indicated should be free of pneumatic hammer. The calculated film thickness under a 100 pound load at the 25.1 psia design condition was 0.0004 inch. By increasing the number of orifices beyond six, a significant increase in this operating film thickness could be anticipated. However, because of the increasing possibility of pneumatic hammer with increasing numbers of supply orifices, it was not prudent to recommend more than six orifices without first experimentally determining the stability threshold.

Thus, tests were conducted to determine experimentally the maximum number of orifices and thrust load capacity which would maintain bearing operation below the threshold of pneumatic hammer and the threshold of lockup.

Spiral-groove thrust bearings with 6, 12 and 24 equally spaced orifice holes 0.043 inch in diameter were tested. For comparison purposes, a BRU step-sector prototype thrust bearing was also tested.

All of the thrust bearing tests were performed at room temperature to simulate normal BRU start-up conditions. Performance was measured at four ambient pressure levels; subatmospheric (9psia or less), 14.7, 25.1 and 42.6 psia.

Because of the high cost of the BRU helium-xenon gas mixture, most of the testing was done using nitrogen gas. Since the product of viscosity and the square root of the gas constant (R) is higher for nitrogen than for He-Xe, the measured gas film thickness values are slightly higher than would be expected in He-Xe. To simulate the operating conditions of He-Xe, some tests were conducted using krypton as a bearing supply gas because its viscosity and gas constant is the same as the BRU He-Xe mixture.

DESCRIPTION OF TEST BEARING

The double-acting spiral-groove thrust bearing consists of two flat cylindrical plates bolted together at the periphery and separated by a spacer 0.004 inch thicker than the thrust runner, providing the 0.004 inch total axial play. The bearing stator elements shown in Figure 24 were coated

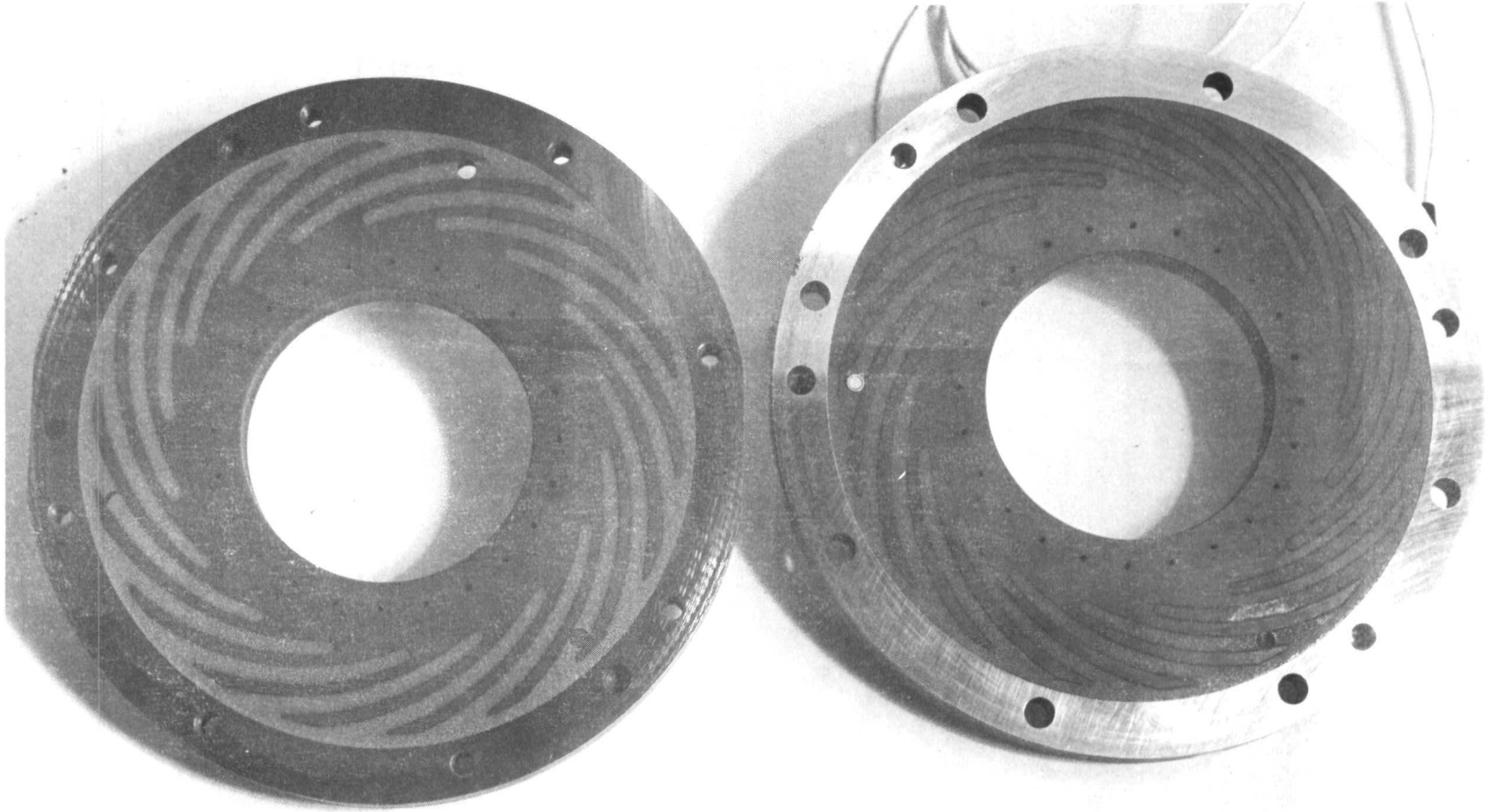

Fig. 24 Test Thrust Stators Showing Spiral Grooves and Hydrostatic Feeding Orifices

with chrome oxide and contained 24 orifices for hydrostatic operation. (For tests with fewer numbers of orifices, appropriate orifices were plugged with a epoxy.) The bearing assembly is attached to the inner ring of the flexure assembly shown in Figure 25. The outer member locates and attaches the bearing assembly to the test rig housing (or the BRU thrust bearing mounting flange). The thrust runner was attached to a mass which duplicated the mass of the BRU rotor such that the dynamic characteristics of an actual BRU rotor thrust bearing system under hydrostatic conditions could be simulated. The components comprising the spiral groove test bearing assembly are shown in Figure 26.

The NASA supplied BRU prototype step-sector thrust bearing assembly is shown in Figure 27.

DESCRIPTION OF TEST APPARATUS

The thrust bearing test rig is shown in Figure 28. The test bearing is located at the top of the test rig in the area above the large diameter flange seen in Figure 28. This flange forms the bottom of the pressure vessel in which the thrust bearing ambient conditions are maintained.

The simulated BRU rotor mass (20 pounds) attached to the thrust runner is located in the cylindrical section below the large diameter flange seen in Figure 28. This mass is centered radially by hydrostatic journal bearings so as to not impose any Coulomb friction forces on the rotor assembly which might impede the onset of pneumatic hammer. Thrust loads were imposed upon the test bearing by applying pressure to the chamber below the simulated BRU rotor mass. Noncontacting, close-clearance seals separated the thrust bearing cavity at one end and the thrust loader cavity at the other end of the rotor from the air journal bearing.

Since previous experience had indicated that pneumatic hammer could be induced in a hydrostatic gas thrust bearing by small axial vibrations, the whole test fixture was supported upon soft vibration mounts and attached to an electric shaker to facilitate inducing pneumatic hammer.

Figure 29 shows an overall view of the test apparatus with the pressure vessel removed and hanging from an overhead crane.

Gas Supply and Control System

The test thrust bearing was supplied with filtered nitrogen or krypton from storage tanks. Inlet control was obtained through a hand-operated pressure regulator and a test pressure gage. A flow meter and a thermometer downstream of the regulator were used for flow measurements.

Ambient pressure conditions around the test thrust bearing were controlled through appropriate setting of an exhaust regulator for above atmospheric pressures and through a different set of inlet-regulators to the pumped-out thrust bearing cavity for substmospheric pressures.

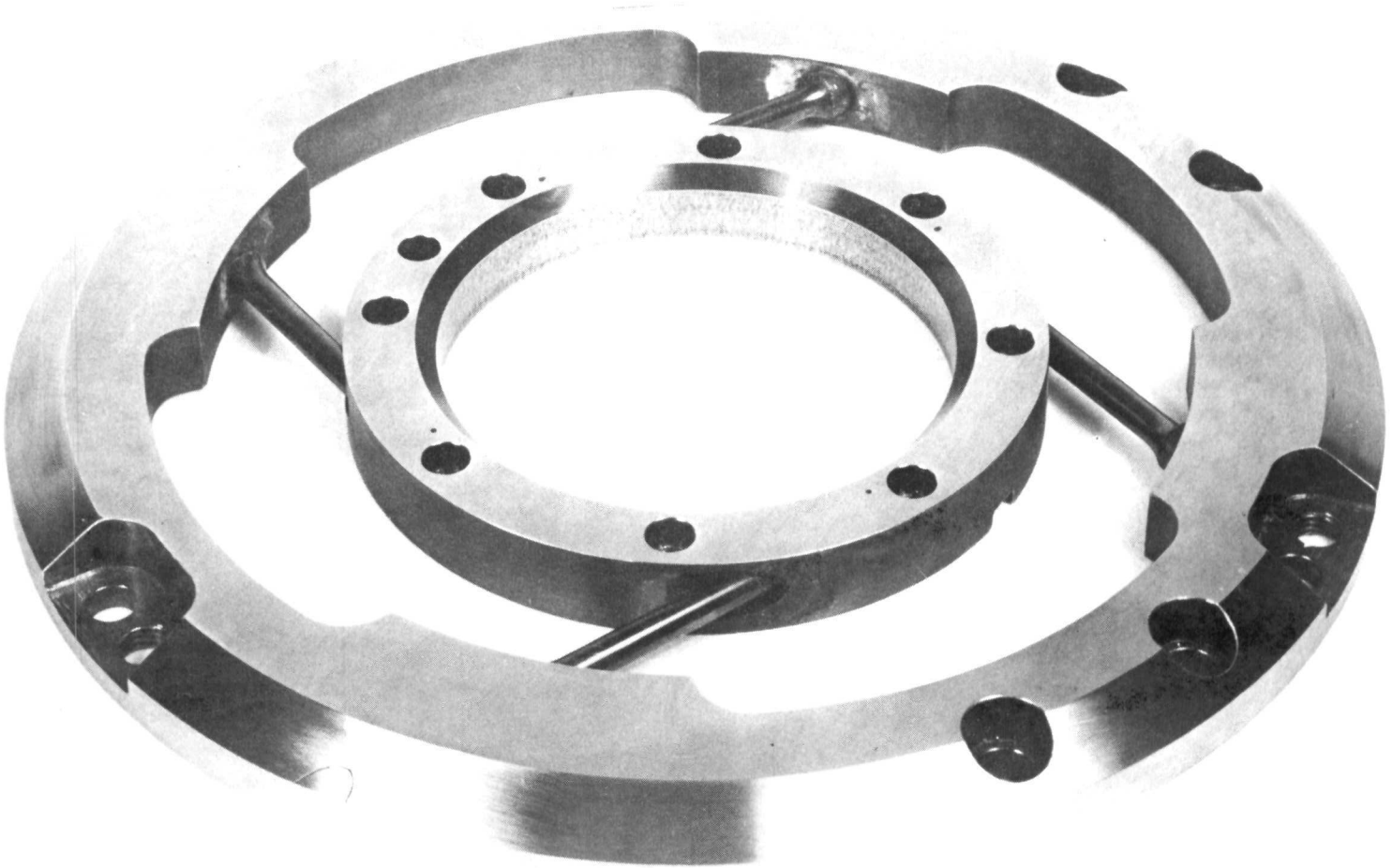

Fig. 25 Spiral-Groove Thrust Bearing Flexure Mount Showing Tangential Spokes

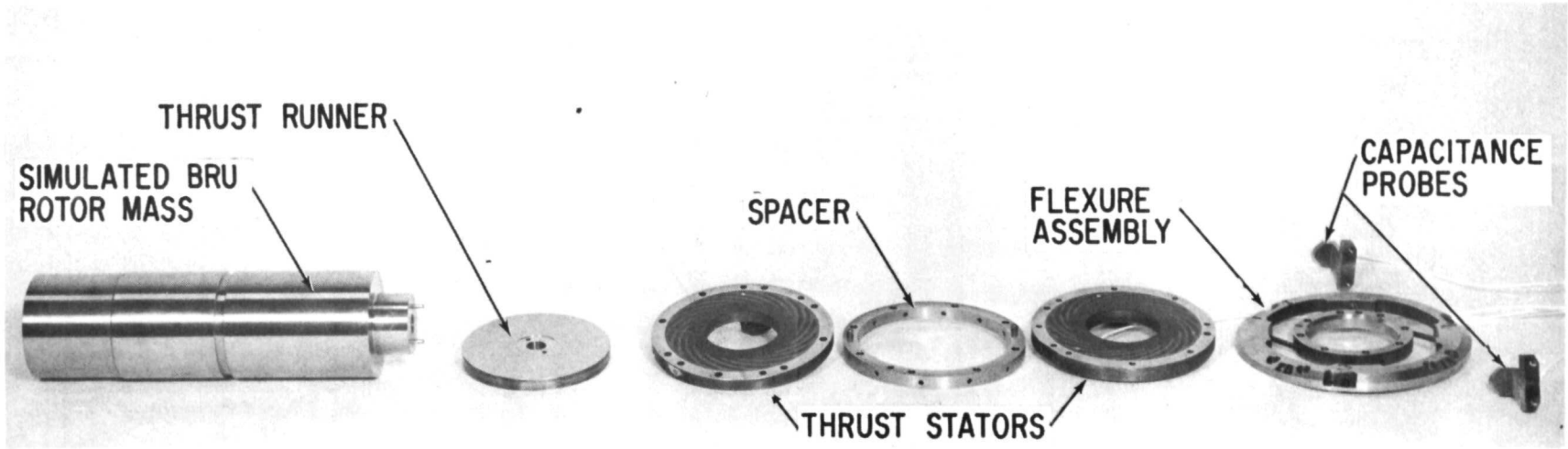

Fig. 26 Spiral-Groove Thrust Bearing Components

Fig. 27 Step-Sector Thrust Bearing Assembly

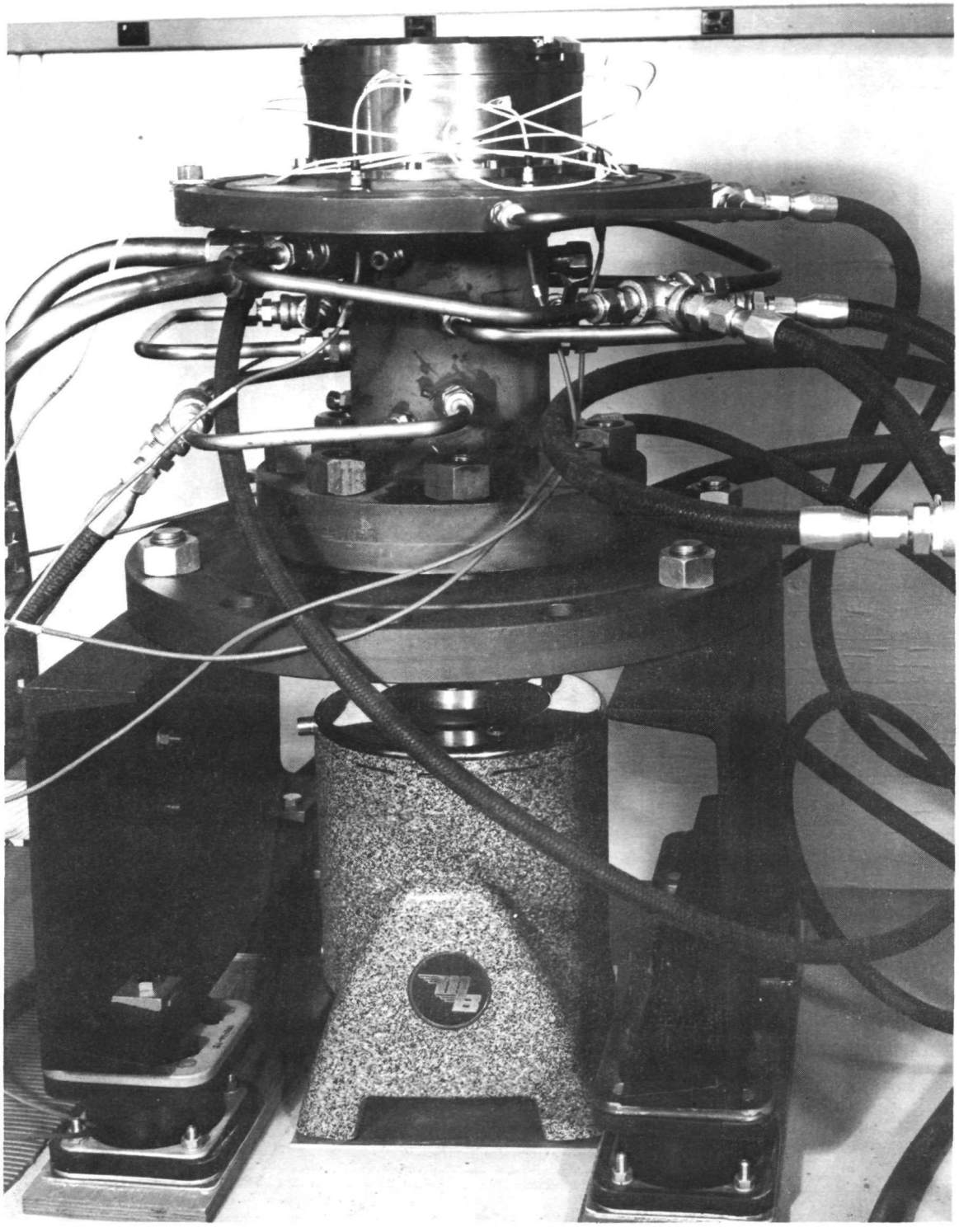

Fig. 28 Thrust Bearing Test Rig

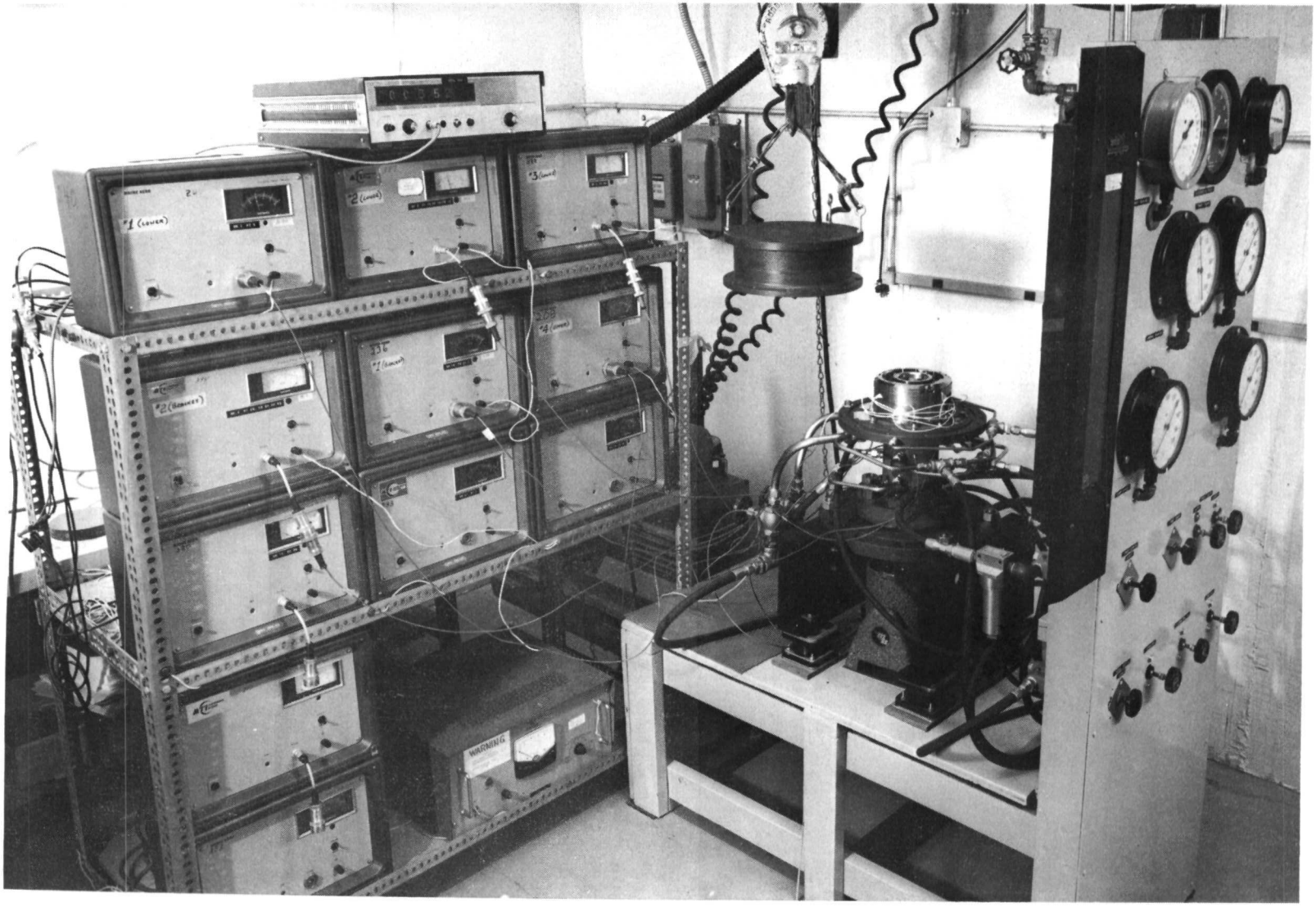

Fig. 29 Overall View of Thrust Bearing Test Apparatus

Subatmospheric pressures around the thrust bearings, which were held as low as the pumping capacity of the vacuum pump permitted, varied between 3 psia when the thrust bearing plates were equipped with six orifices and a high of 9 psia for thrust plates with 24 orifices and maximum thrust bearing gas supply pressure.

All subatmospheric test pressures were held as much as possible below the 12.5 psia BRU minimum operating pressure for maximum insurance that pneumatic bearing hammer would be detected in the broadest possible operating range.

Differential pressure between the test thrust bearing cavity and the cavity at the lower end of the rotor mass determined thrust bearing loading. For subatmospheric pressure conditions around the thrust bearing, the minimum thrust load was determined by the pressure difference between atmospheric pressure in the thrust loader and the subatmospheric pressure at the other end of the rotor mass in the thrust bearing cavity.

Electronic Instrumentation

Distance measurements (gas film thickness) between thrust plates and thrust runner were made with noncontacting capacitance sensors and Wayne Kerr amplifiers. The MTI-designed spiral-groove thrust bearing had three sensors spaced 120 degrees apart embedded in the lower (unloaded) thrust plate near the plate periphery in the grooved area. A fourth sensor was located opposite one of the three sensors in the upper thrust plate. All sensors were recessed below the bearing surface by approximately 0.001 to 0.002 inch. The gas film thickness measurement sensors had a nominal range of 0.005 inch. Individual calibration curves were used for all probes to translate voltage outputs as read off a digital voltmeter into distance measurements. Averages from all sensors have been plotted as film thickness, thereby eliminating the deviations due to misalignment between thrust plates and runner, which were typically around 0.000050 inch.

Thrust bearing flexure deflection under load was determined from two capacitance sensors spaced 90 degrees apart and mounted on the thrust bearing support structure (ground).

MEASURED HYDROSTATIC PERFORMANCE OF THE SPIRAL-GROOVE THRUST BEARING

Film Thickness Measurements with Nitrogen as Supply Gas

Three sets of curves depicting the relationship between gas film thickness, bearing load, bearing ambient gas pressure and bearing gas supply pressure are shown in Figures 30 through 44 for the spiral-groove back-up gas bearing with either 24, 12 or 6 orifices in each thrust plate.

With 150 psia bearing gas supply pressure, the 24 and the 12 orifice equipped bearings can support thrust loads up to 132 pounds at ambient pressures up to 42.6 psia (Figures 30 and 25). (The 132-lb load limit has been established from the stress limit on the flexure supporting the thrust bearing.) As the bearing gas supply pressure is decreased, the gas film

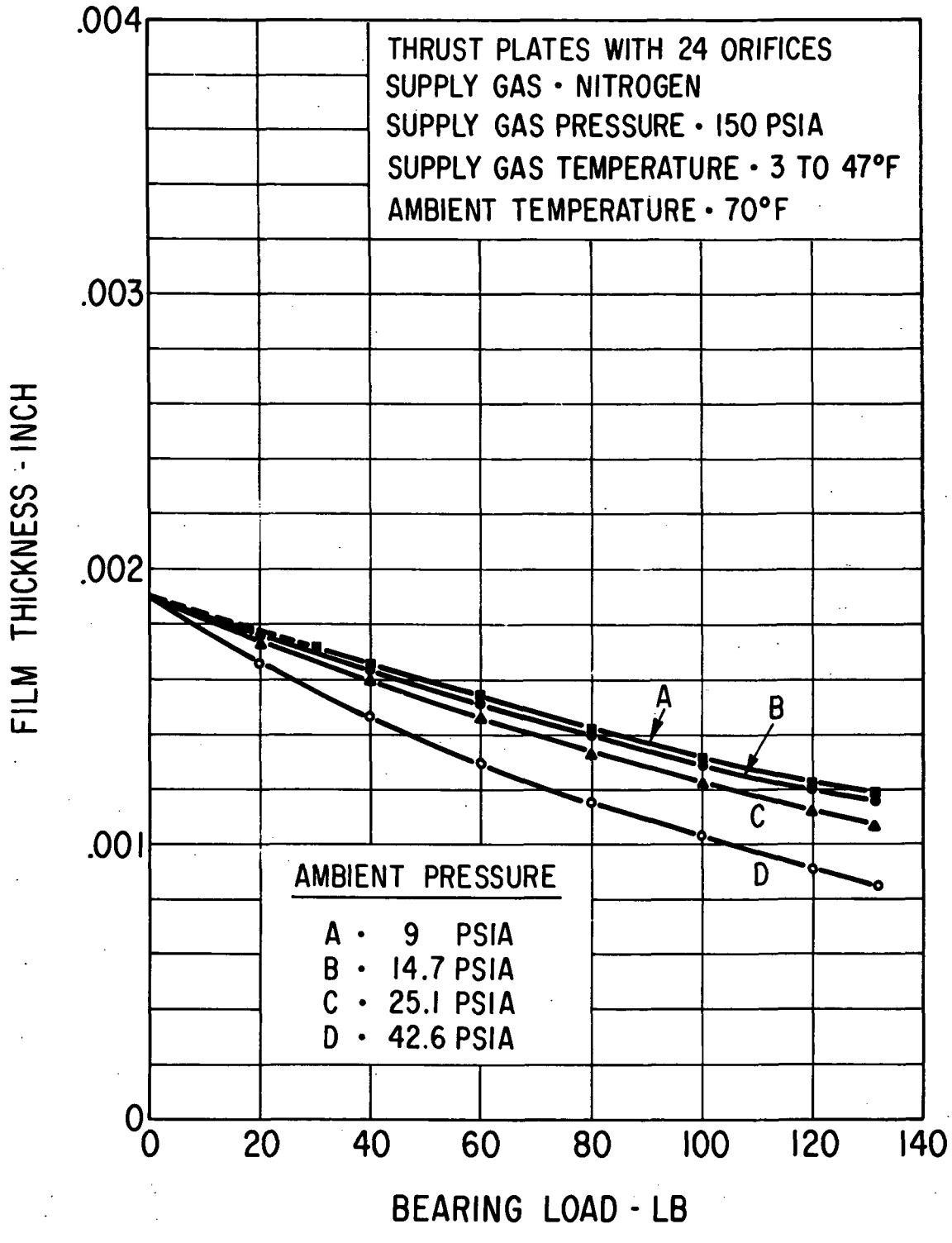

Fig. 30 Measured Hydrostatic Film Thickness for Double-Acting Spiral-Groove Thrust Bearing With 24 Orifices at 150 psia Supply Pressure in Nitrogen

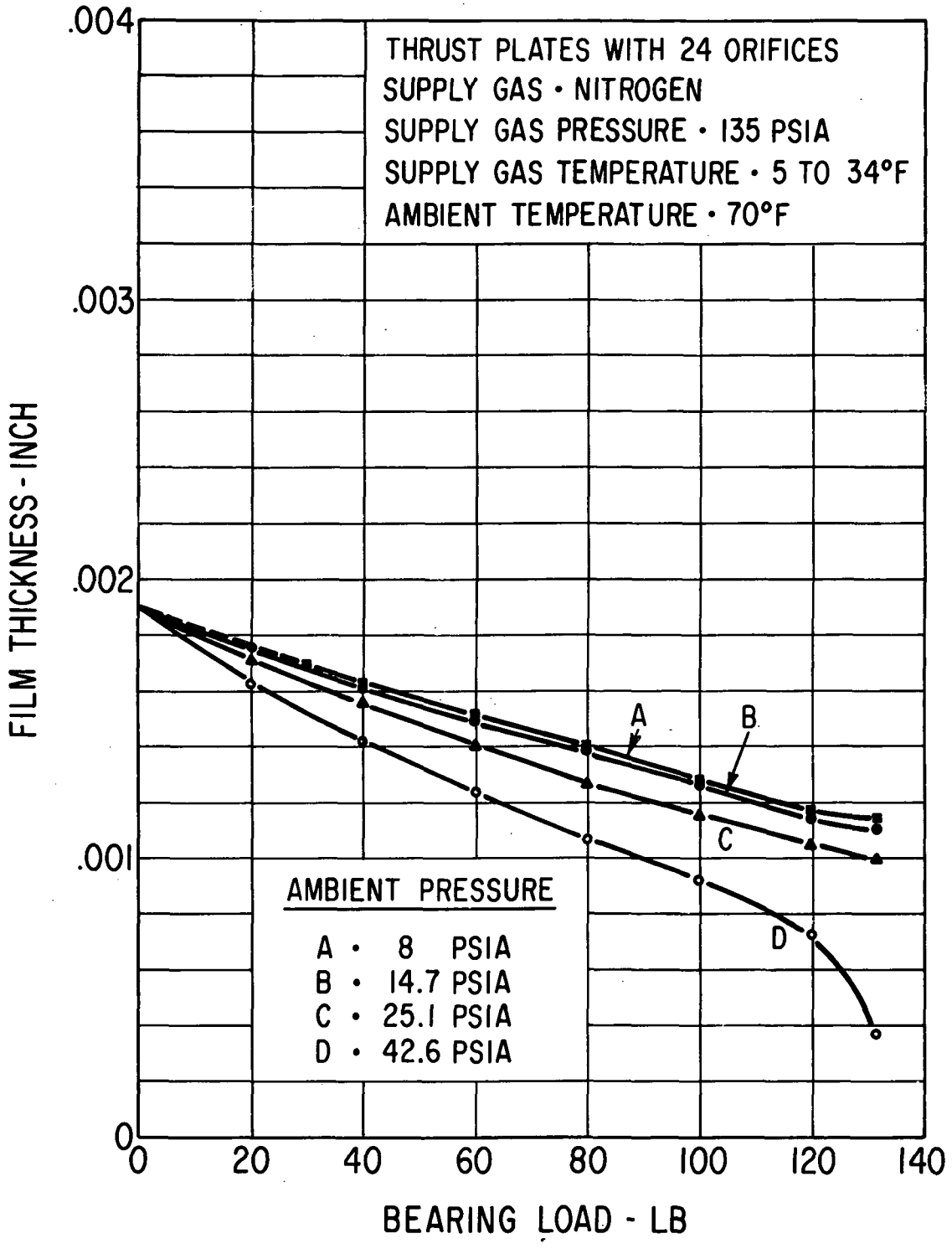

Fig. 31 Measured Hydrostatic Film Thickness for Double-Acting Spiral-Groove Thrust Bearing With 24 Orifices at 135 psia Supply Pressure in Nitrogen

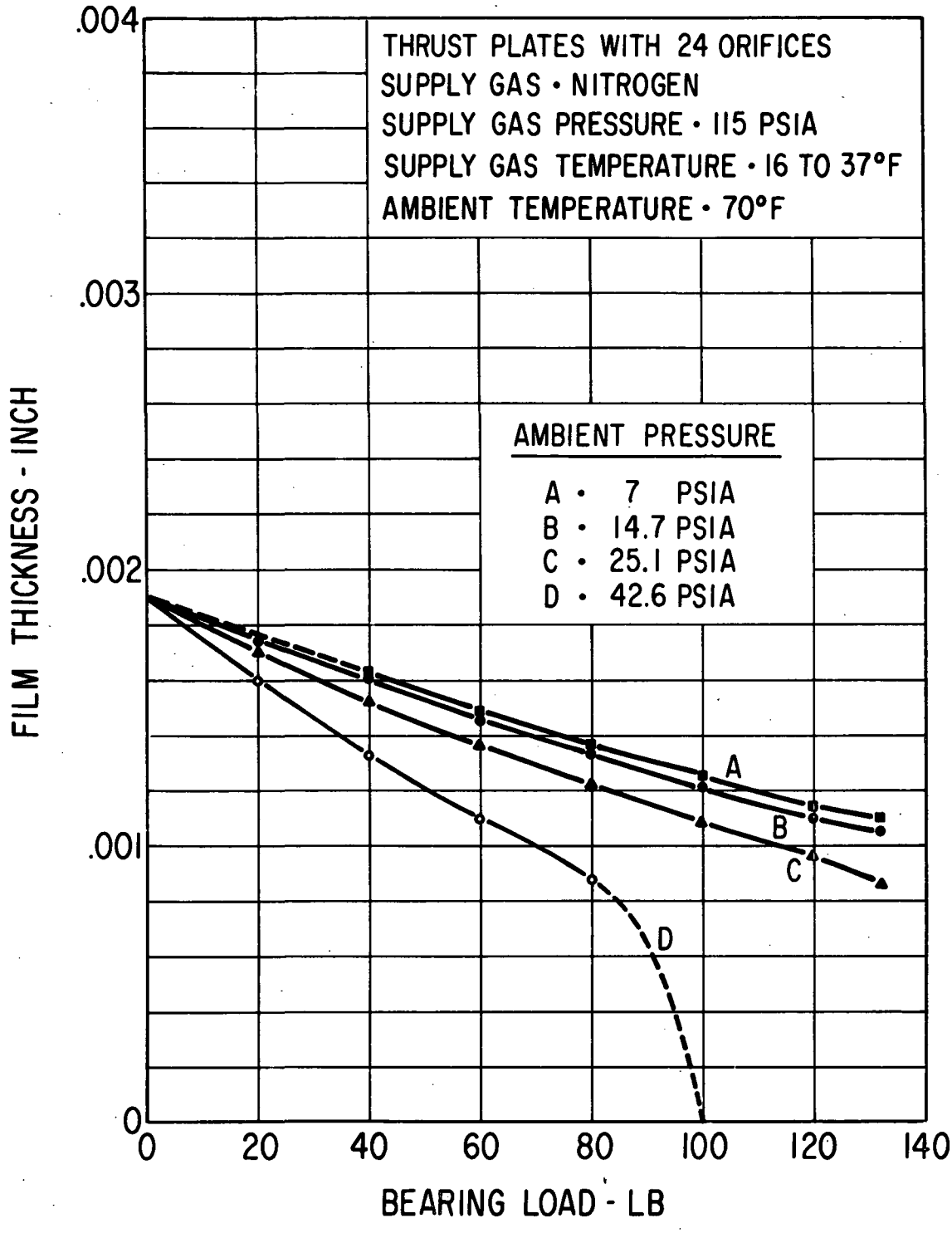

Fig. 32 Measured Hydrostatic Film Thickness for Double-Acting Spiral-Groove Thrust Bearing With 24 Orifices at 115 psia Supply Pressure in Nitrogen

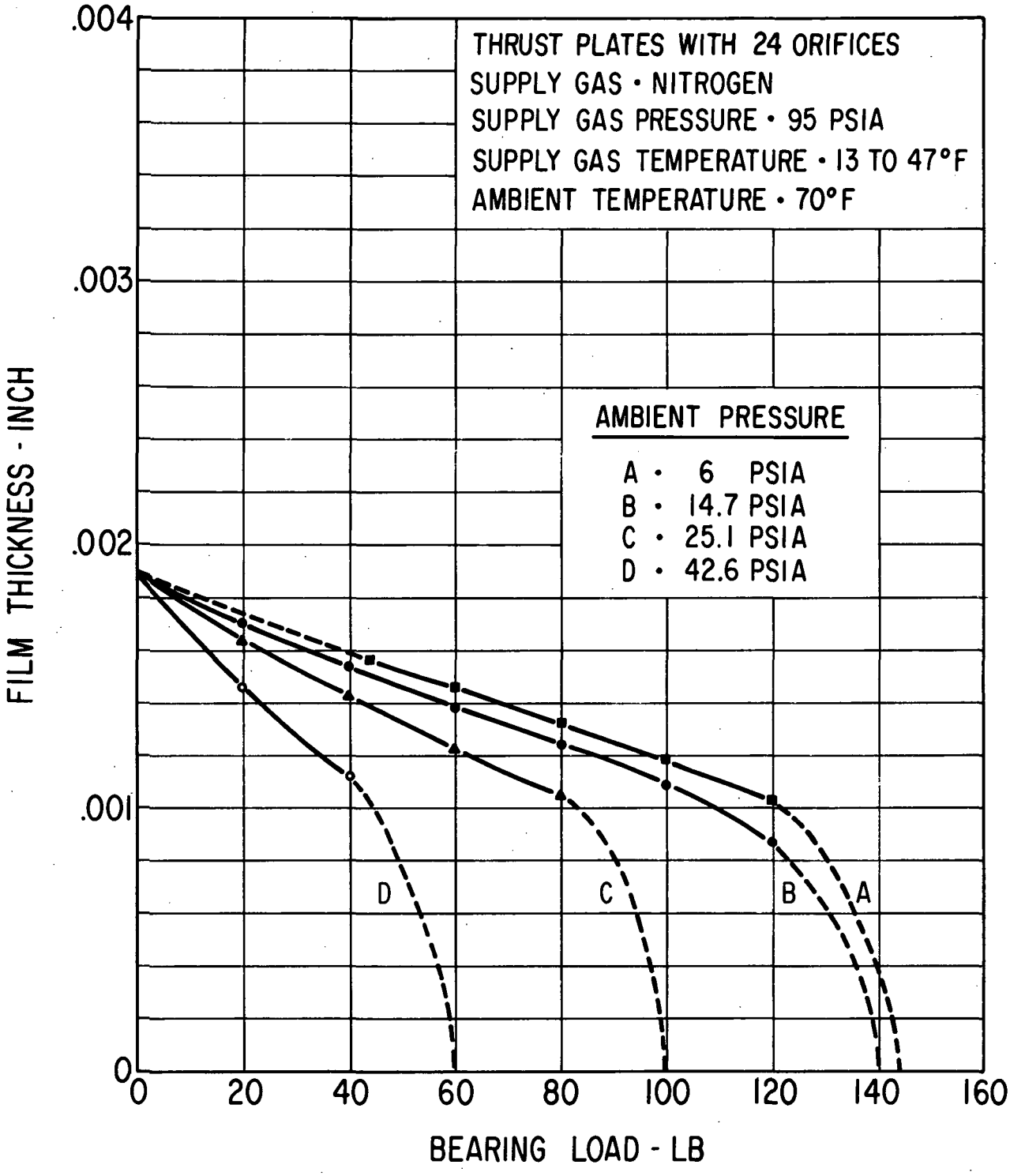

Fig. 33 Measured Hydrostatic Film Thickness for Double-Acting Spiral-Groove Thrust Bearing With 24 Orifices at 95 psia Supply Pressure in Nitrogen

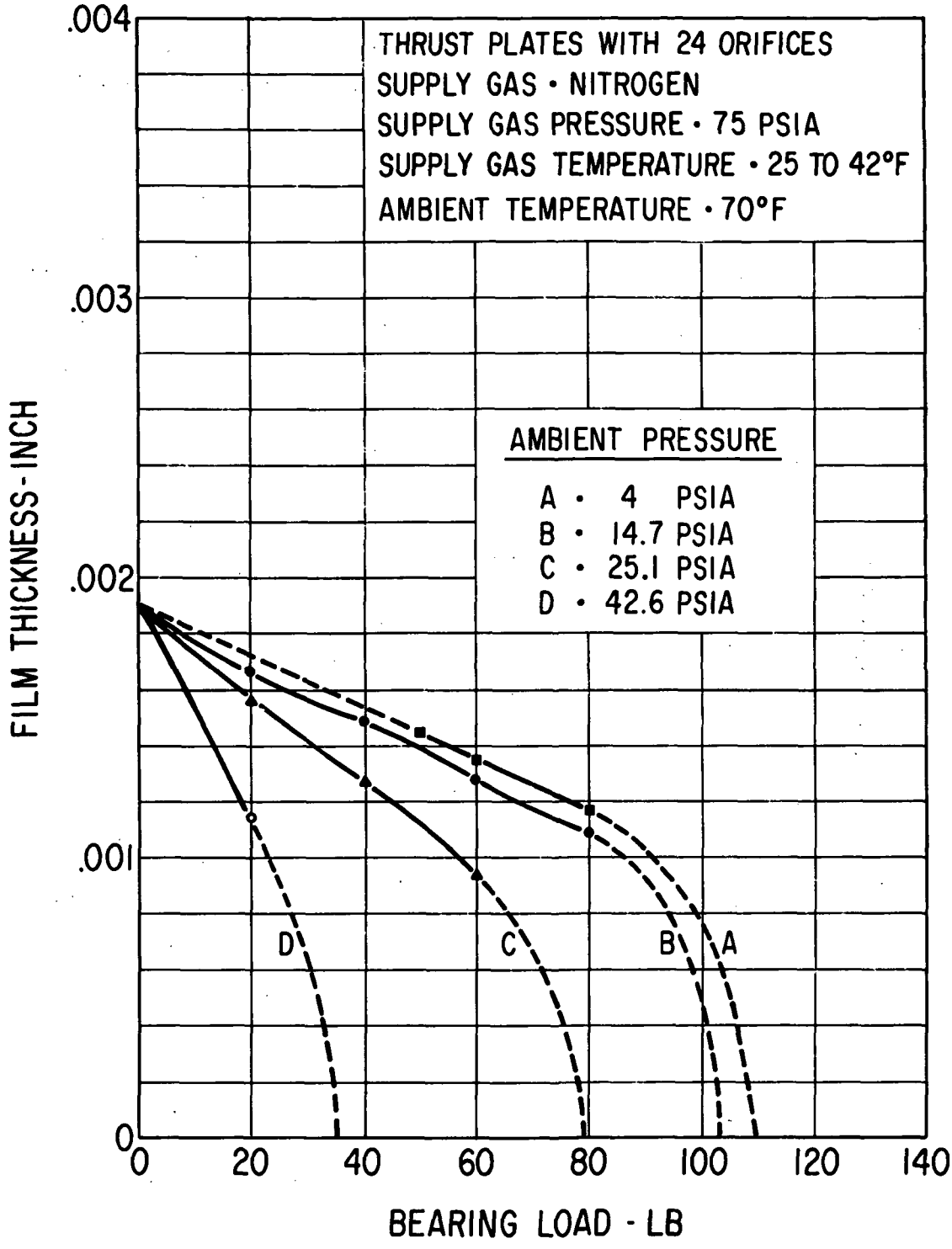

Fig. 34 Measured Hydrostatic Film Thickness for Double-Acting Spiral-Groove Thrust Bearing With 24 Orifices at 75 psia Supply Pressure In Nitrogen

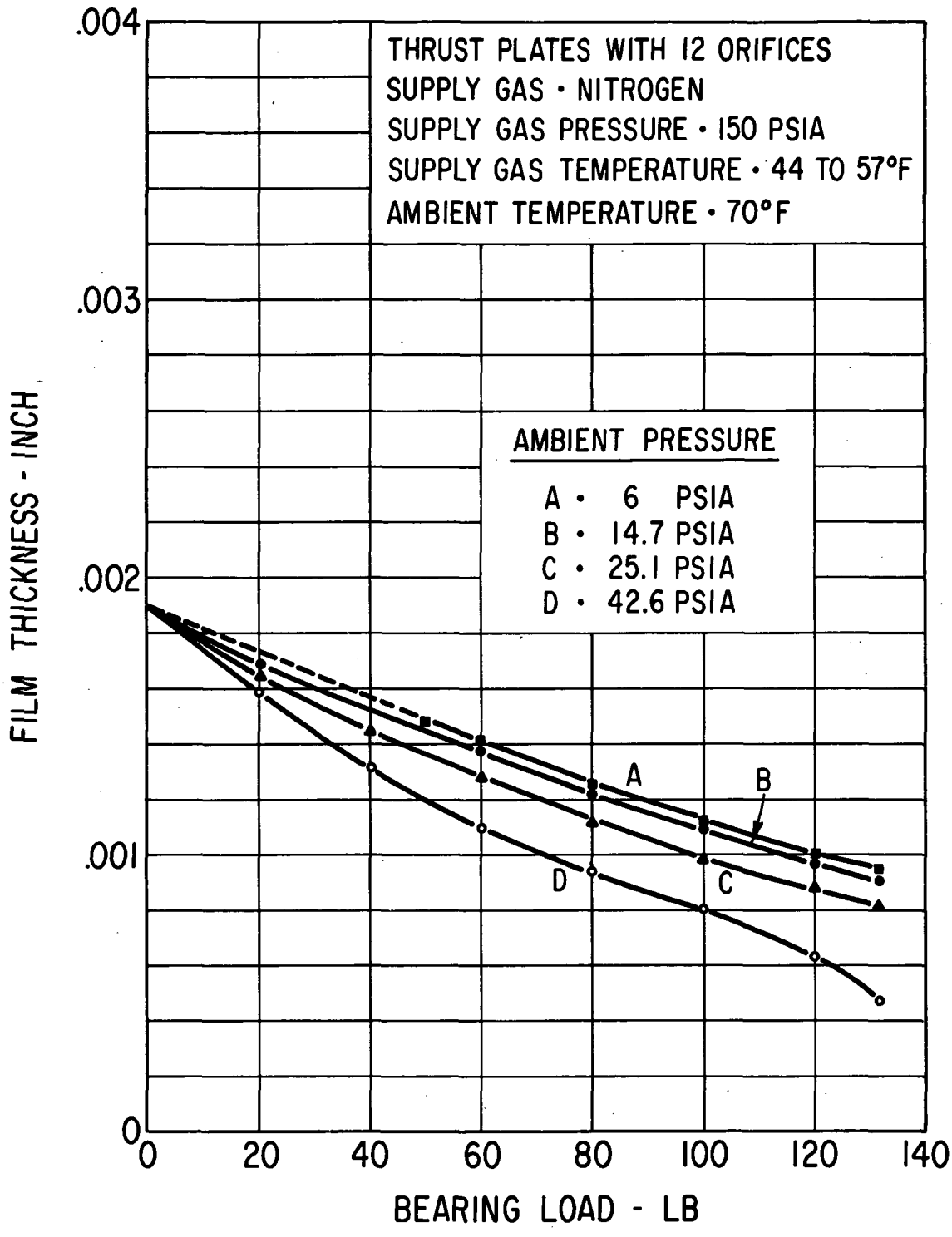

Fig. 35 Measured Hydrostatic Film Thickness for Double-Acting Spiral-Groove Thrust Bearing With 12 Orifices at 150 psia Supply Pressure in Nitrogen

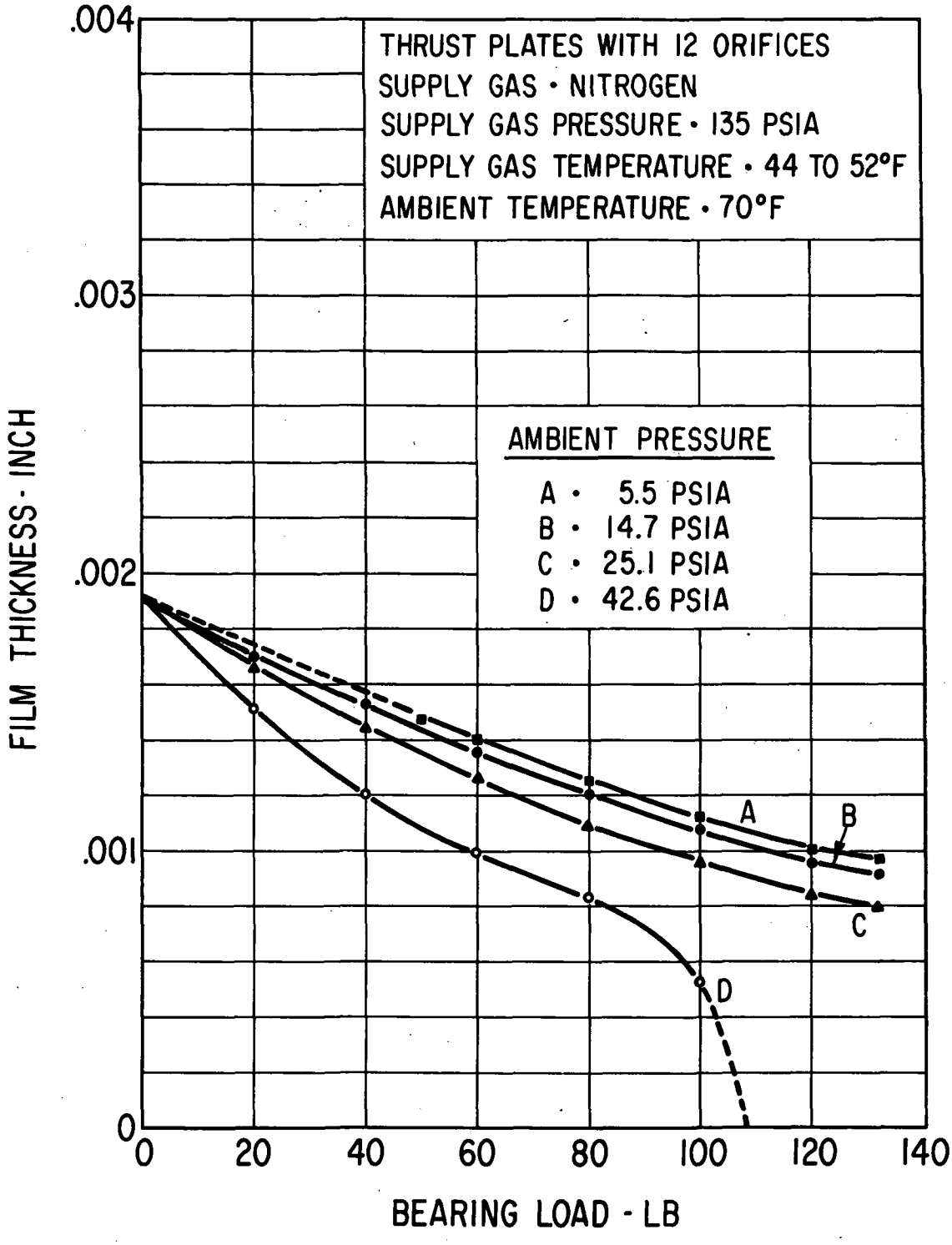

Fig. 36 Measured Hydrostatic Film Thickness for Double-Acting Spiral-Groove Thrust Bearing With 12 Orifices at 135 psia Supply Pressure In Nitrogen

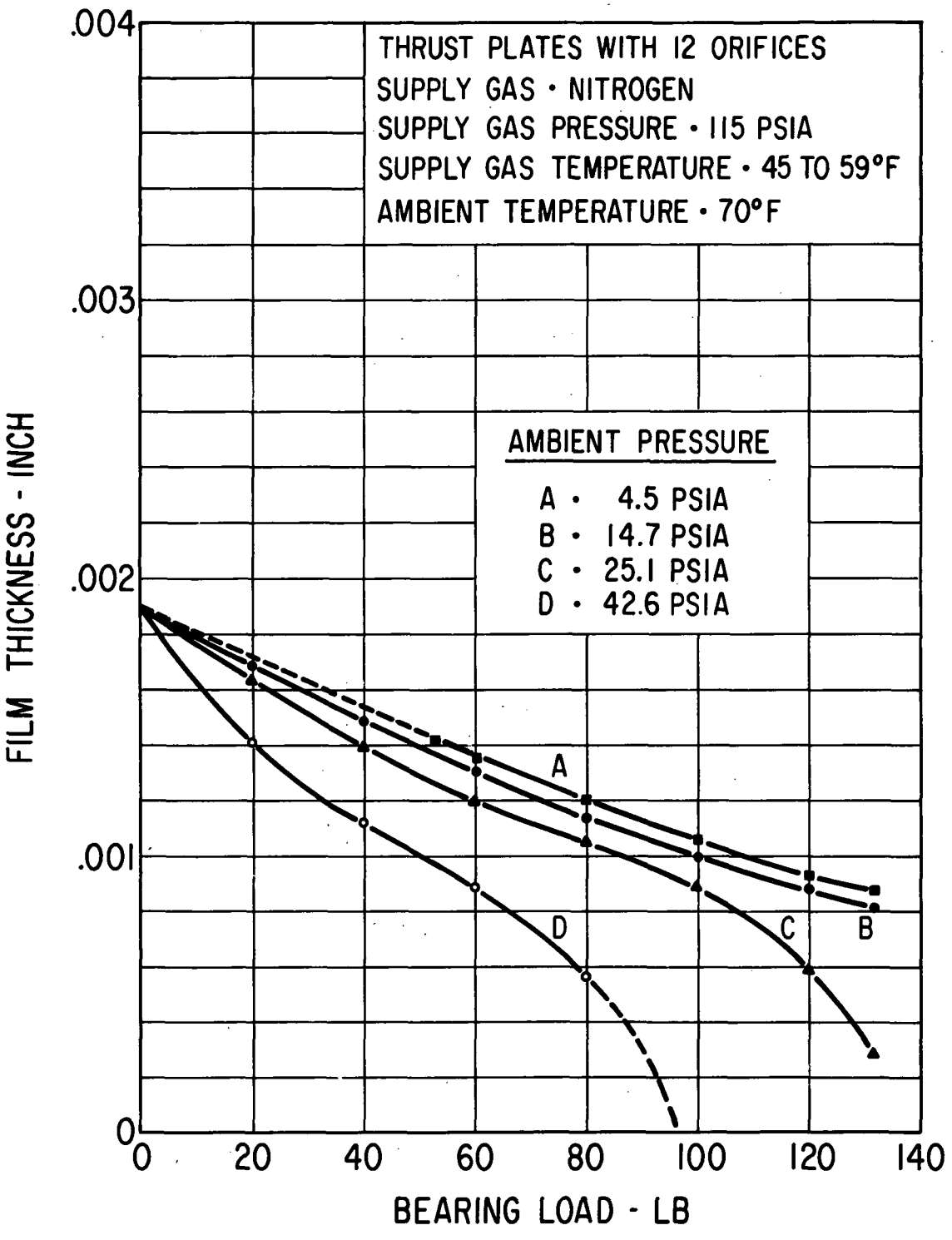

Fig. 37 Measured Hydrostatic Film Thickness for Double-Acting Spiral-Groove Thrust Bearing With 12 Orifices at 115 psia Supply Pressure in Nitrogen

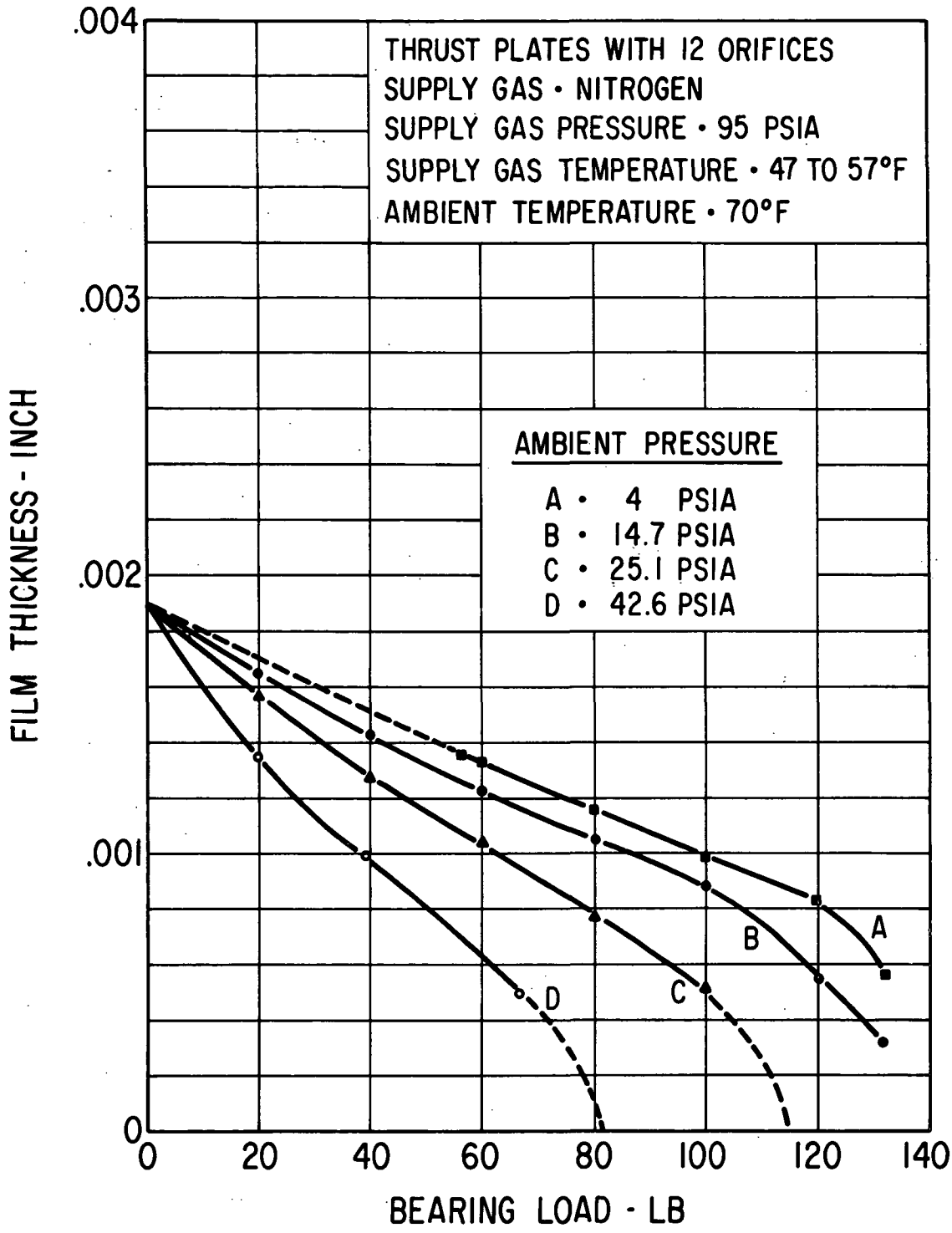

Fig. 38 Measured Hydrostatic Film Thickness for Double-Acting Spiral-Groove Thrust Bearing With 12 Orifices at 95 psia Supply Pressure in Nitrogen

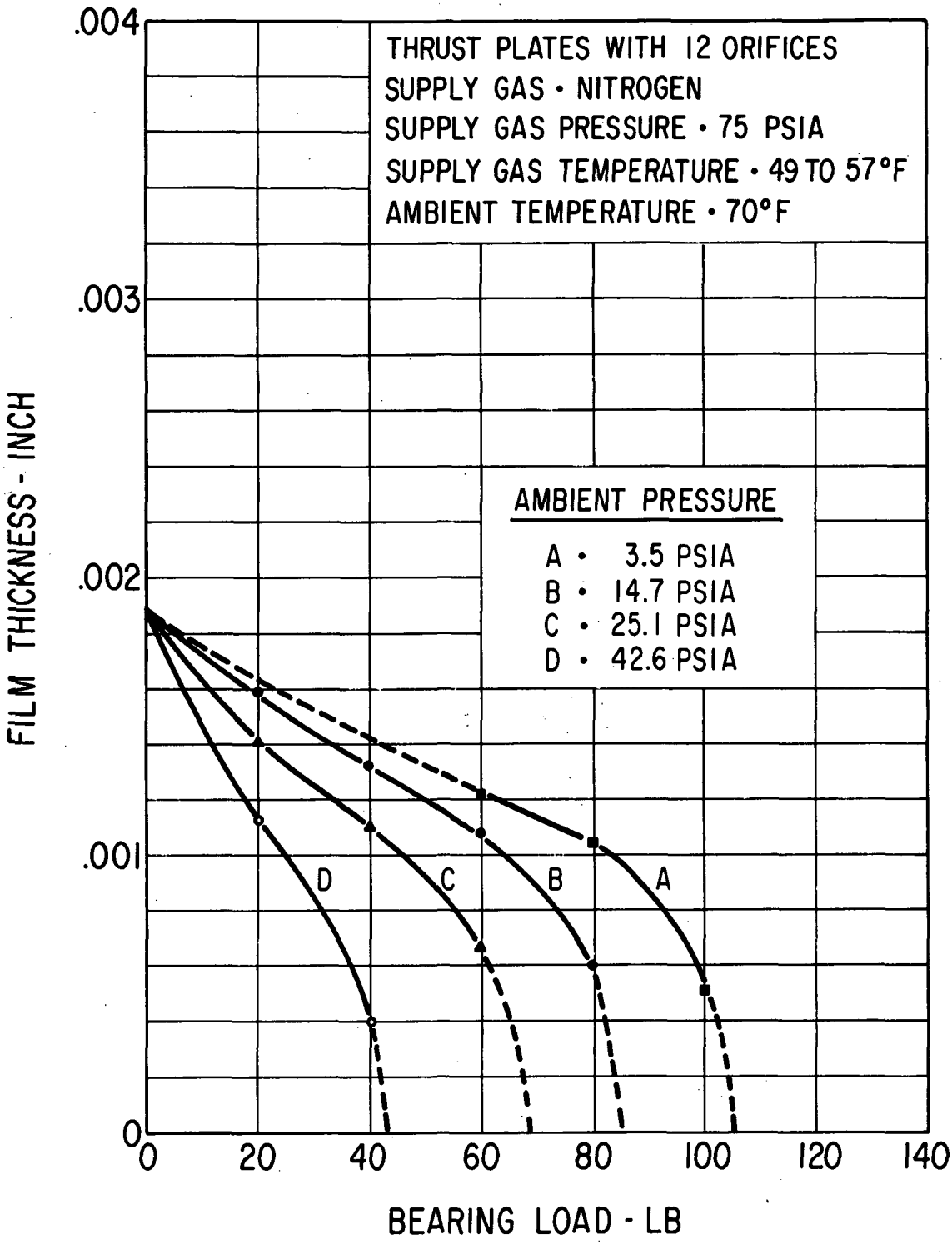

Fig. 39 Measured Hydrostatic Film Thickness for Double-Acting Spiral-Groove Thrust Bearing With 12 Orifices at 75 psia Supply Pressure in Nitrogen

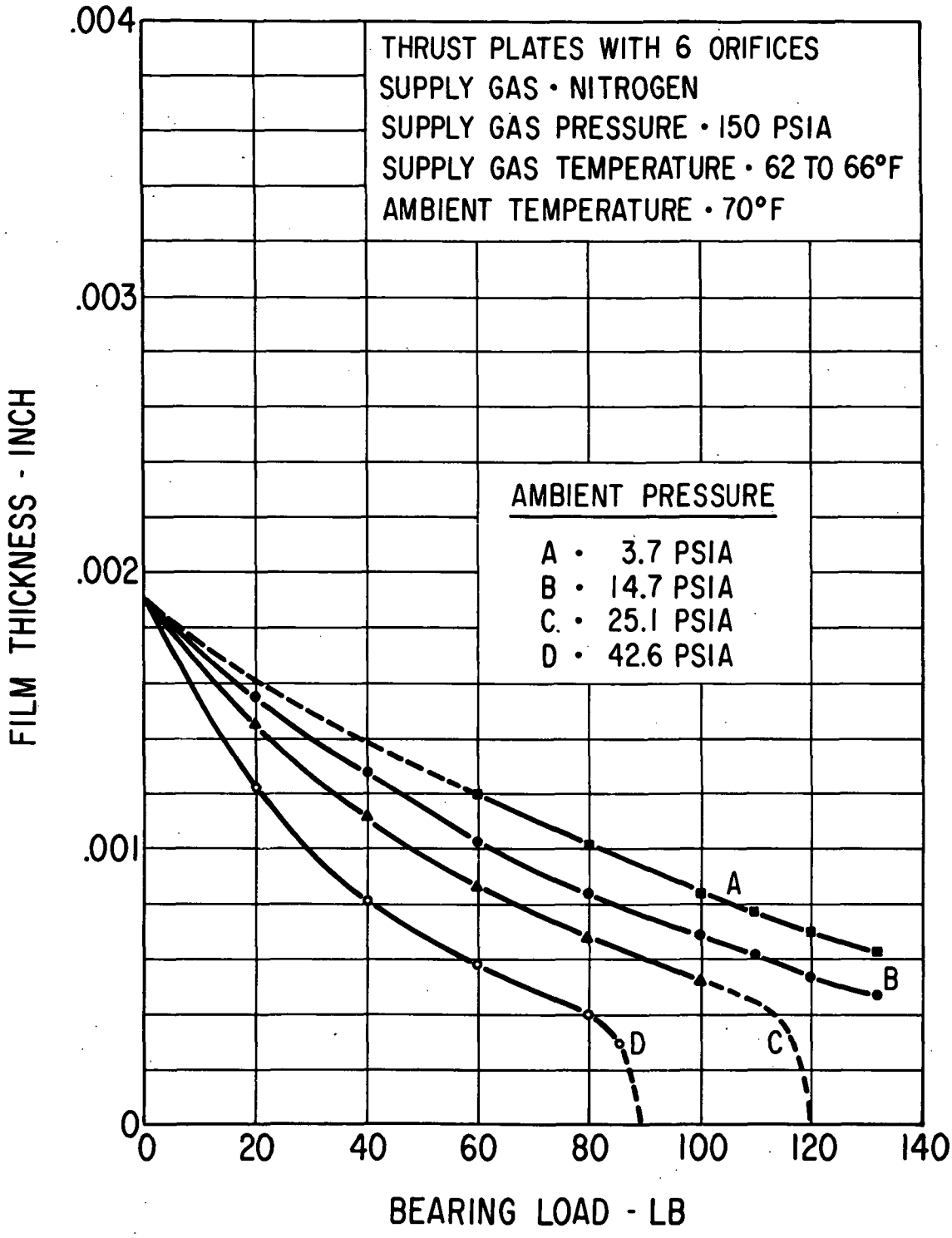

Fig. 40 Measured Hydrostatic Film Thickness for Double-Acting Spiral-Groove Thrust Bearing With 6 Orifices at 150 psia Supply Pressure in Nitrogen

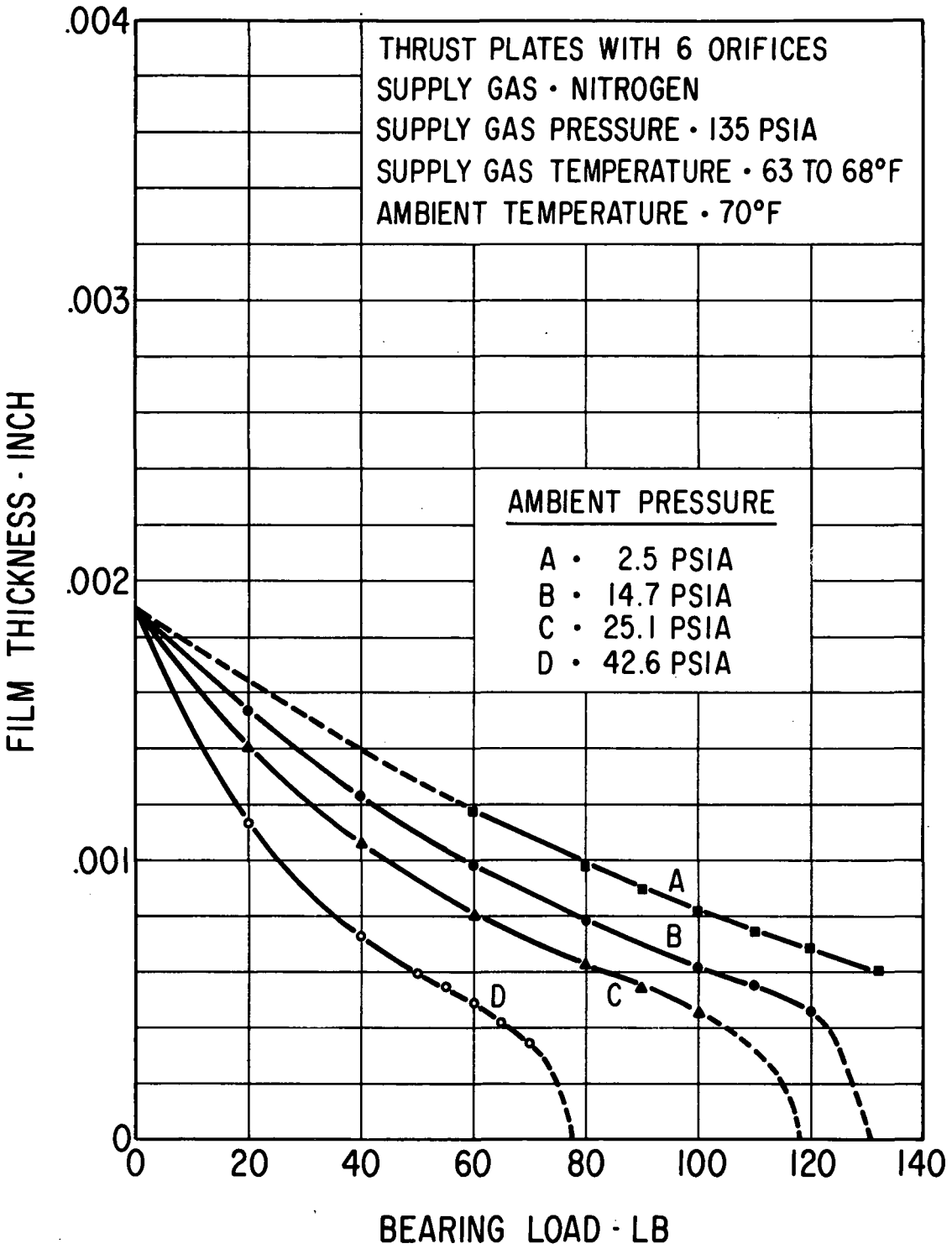

Fig. 41 Measured Hydrostatic Film Thickness for Double-Acting Spiral-Groove Thrust Bearing With 6 Orifices at 135 psia Supply Pressure in Nitrogen

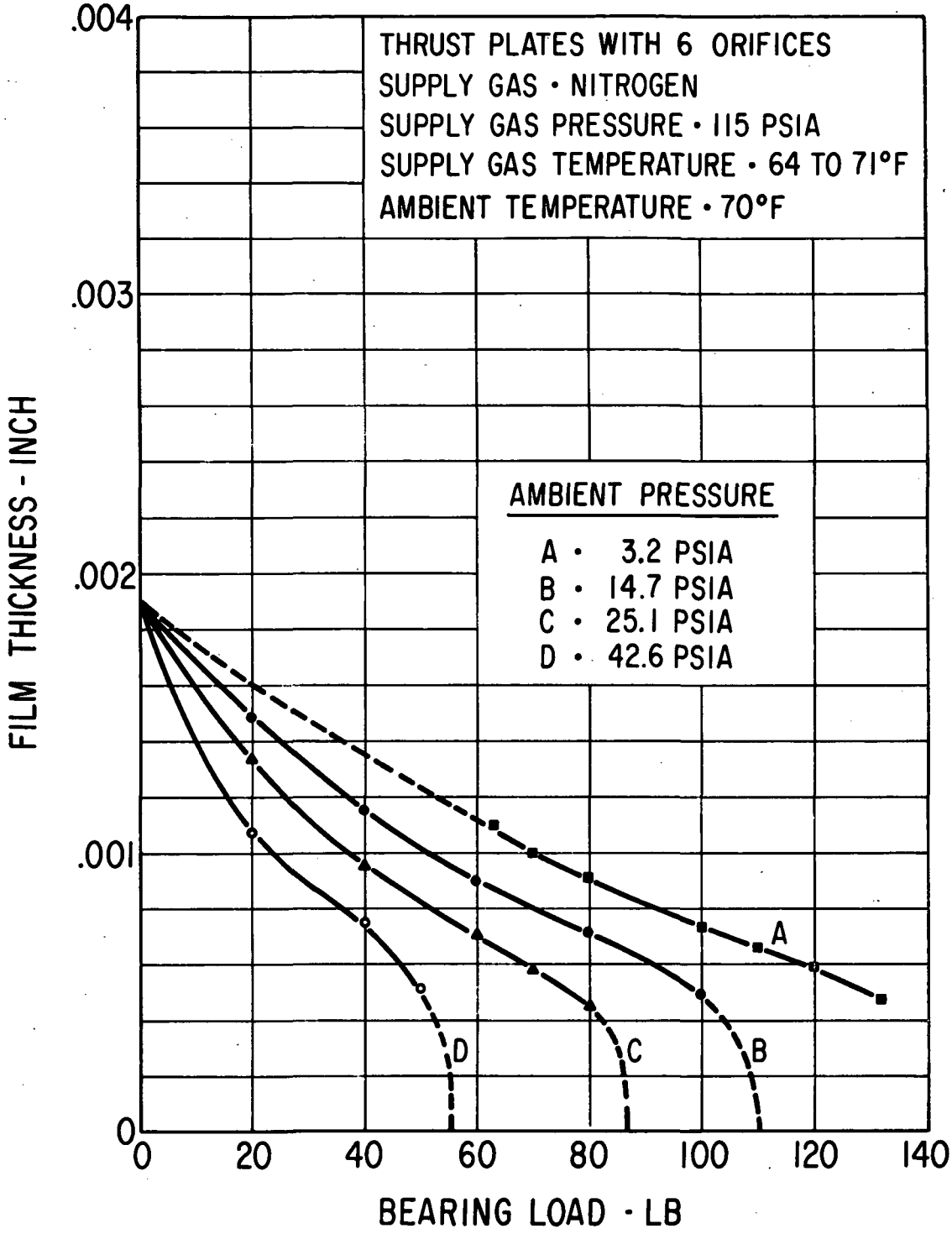

Fig. 42 Measured Hydrostatic Film Thickness for Double-Acting Spiral-Groove Thrust Bearing With 6 Orifices at 115 psia Supply Pressure in Nitrogen

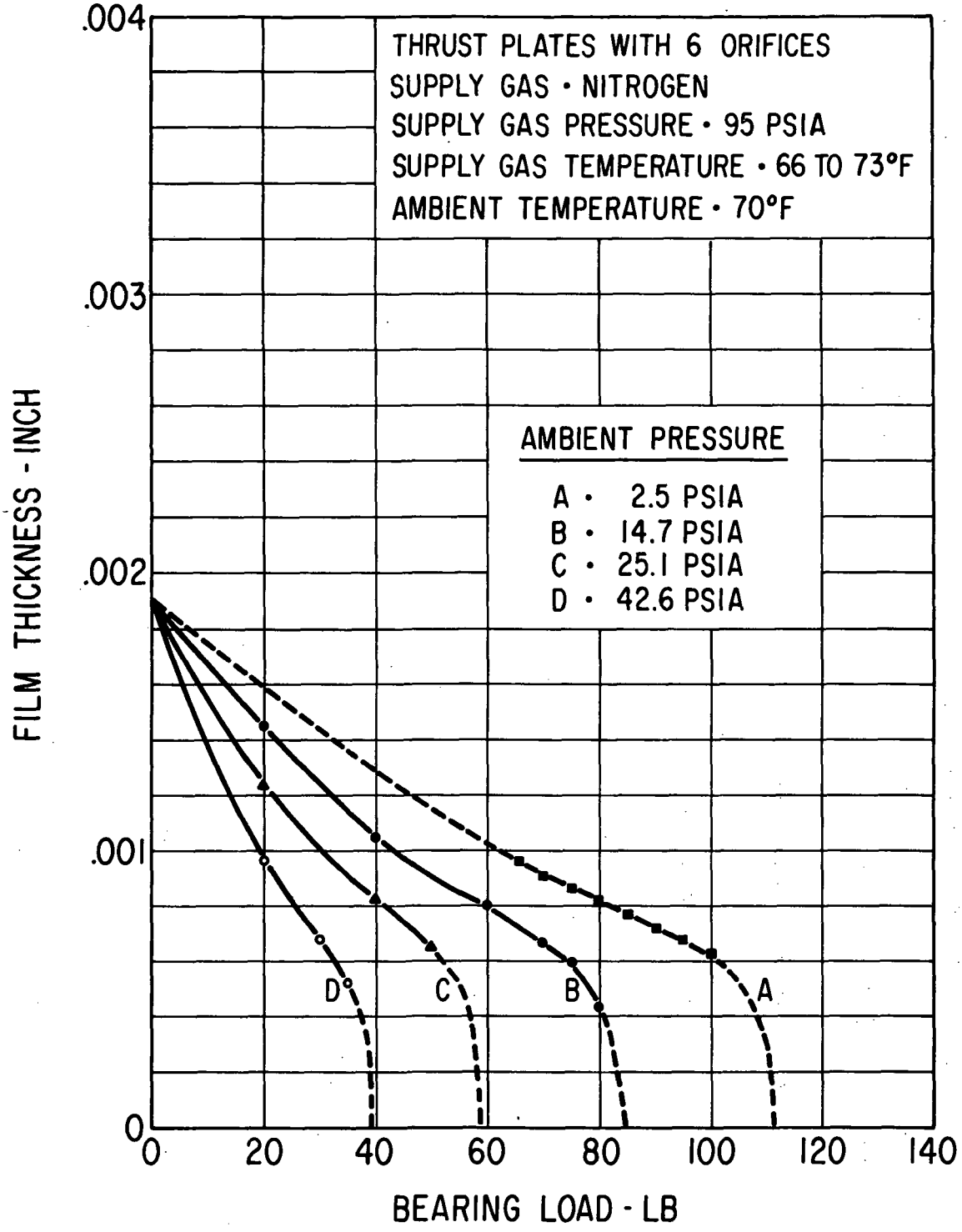

Fig. 43 Measured Hydrostatic Film Thickness for Double-Acting Spiral-Groove Thrust Bearing With 6 Orifices at 95 psia Supply Pressure in Nitrogen

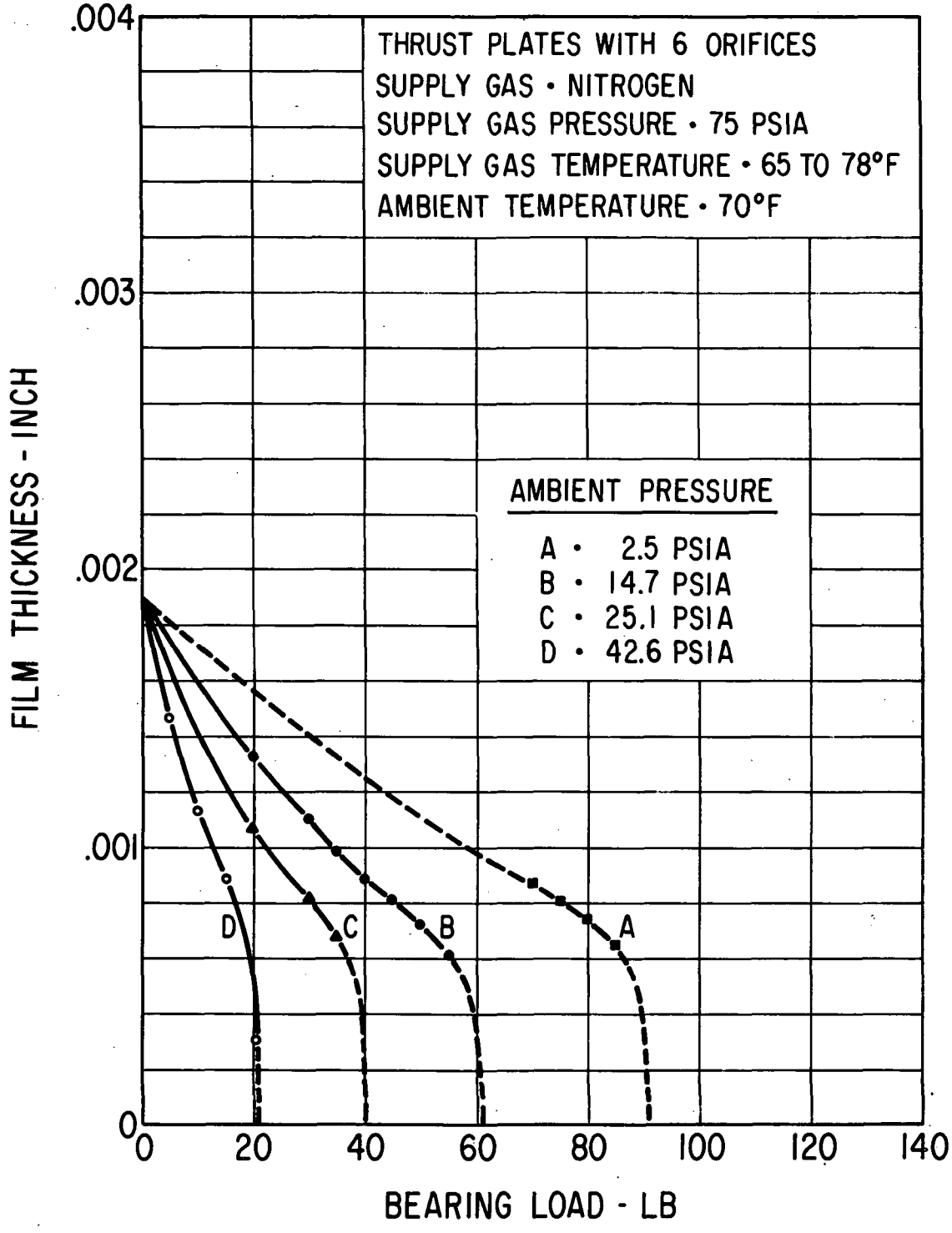

Fig. 44 Measured Hydrostatic Film Thickness for Double-Acting Spiral-Groove Thrust Bearing With 6 Orifices at 75 psia Supply Pressure in Nitrogen

thickness curves begin to exhibit a sudden drop-off at higher loads and ambient pressures. This sudden drop-off, which has been termed 'lockup' by previous investigators of the equivalent phenomenon in hydrostatic journal bearings, occurs at increasingly lower bearing eccentricities (film thickness) as the supply pressure is reduced, and the number of orifices is increased, as evident from inspection of Figures 34, 39 and 44.

However, the actual load carried by each bearing before lockup occurs, is largest for the 24 orifice bearing and smallest for the six orifice bearing. At the 25.1 and 42.6 psia ambient pressure condition and 150 psia supply pressure, the load carrying capacity of the six orifice bearing is limited to 100 and 60 pounds respectively.

The load carrying capacity data curves shown in Figures 30 through 44 were obtained with nitrogen as the bearing supply gas at room temperature ambient conditions. The supply gas temperature was dependent upon outside temperatures (storage tank) and the pressure expansion ratio between storage tank pressure and bearing ambient pressure. Hydrostatic bearing gas film values obtained with nitrogen approximate closely those anticipated for the He-Xe gas mixture, because the product of viscosity and square root of the gas constant, which affect the performance of a hydrostatic gas bearing, differs only by the ratio of 12.6/10.3 (N_2/He-Xe).

Film Thickness Measurements with Krypton as Supply Gas

Test data obtained for the six orifice bearing with krypton as the bearing supply gas confirms the theoretical prediction of nearly equal hydrostatic thrust bearing performance in nitrogen and krypton, and, for that matter, nitrogen and He-Xe, because the viscosity and the gas constant are equal for krypton and the He-Xe gas mixture used in the BRU.

The nonrotational hydrostatic thrust bearing film thickness measurements in krypton were conducted for 150, 115 and 72 psia bearing supply gas pressure and for bearing ambient pressures of 3, 14.7, 25.1 and 42.6 psia. The 3 psia ambient pressure condition is not representative of any BRU pressure operating level, but represents the lowest ambient pressure the test equipment was capable of producing under the given supply flow conditions.

The test data with krypton as supply gas is shown in Figures 45 through 47.

Supply Gas Flow for Hydrostatic Operation of the Spiral-Groove Thrust Bearing

The nitrogen supply gas flow, as it was determined in the course of all thrust bearing film thickness measurements, is shown in Figure 48. For each of the three bearing configurations of 24, 12 and 6 orifices a band of gas flow values is shown for each of the bearing gas supply pressures of 75, 95, 115, 135 and 150 psia. Each band contains all the test measurements that were made for all bearing loads between 0 and 132 lbs and for all ambient bearing pressures between 3 and 42.6 psia as recorded for the

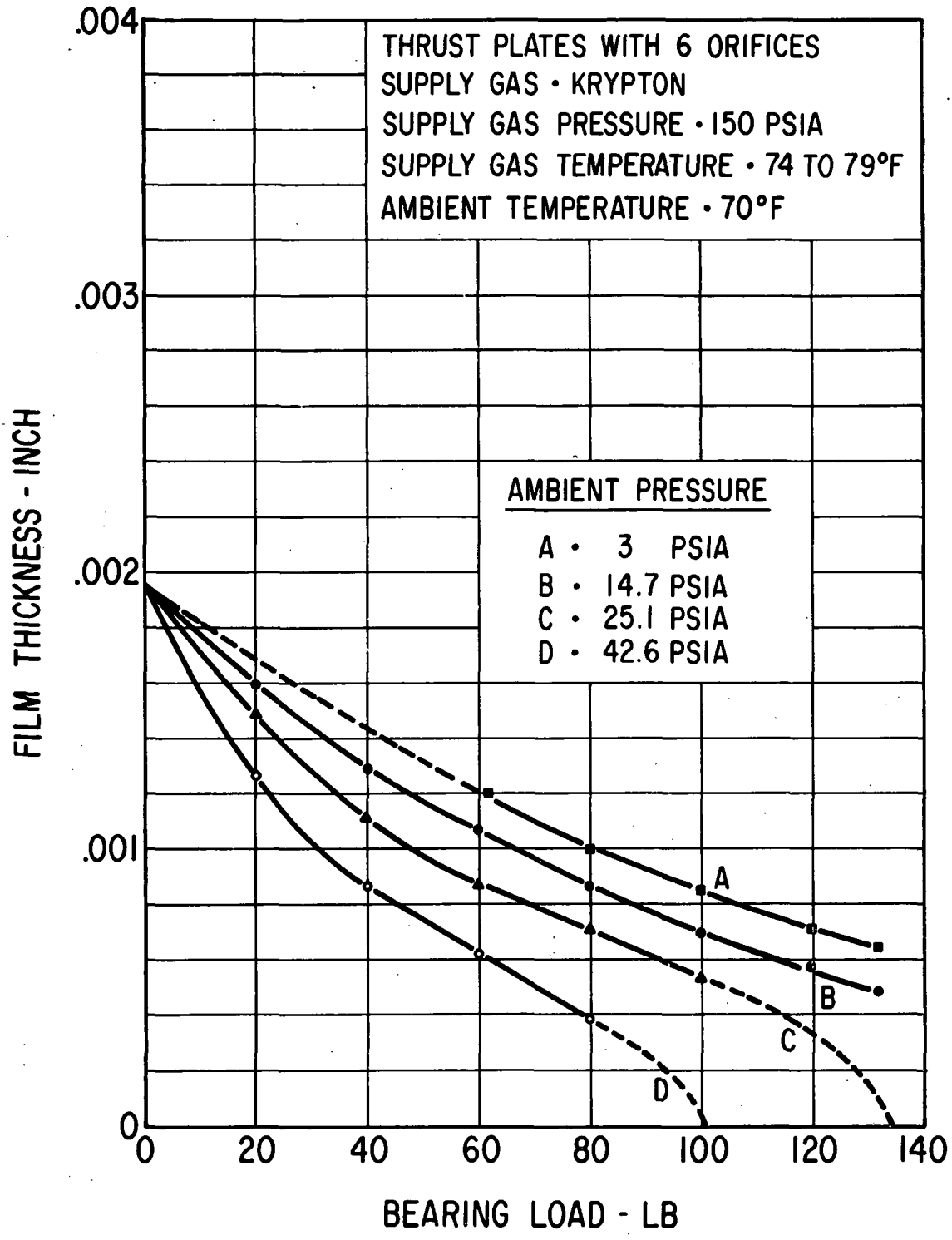

Fig. 45 Measured Hydrostatic Film Thickness for Double-Acting Spiral-Groove Thrust Bearing With 6 Orifices at 150 psia Supply Pressure in Krypton

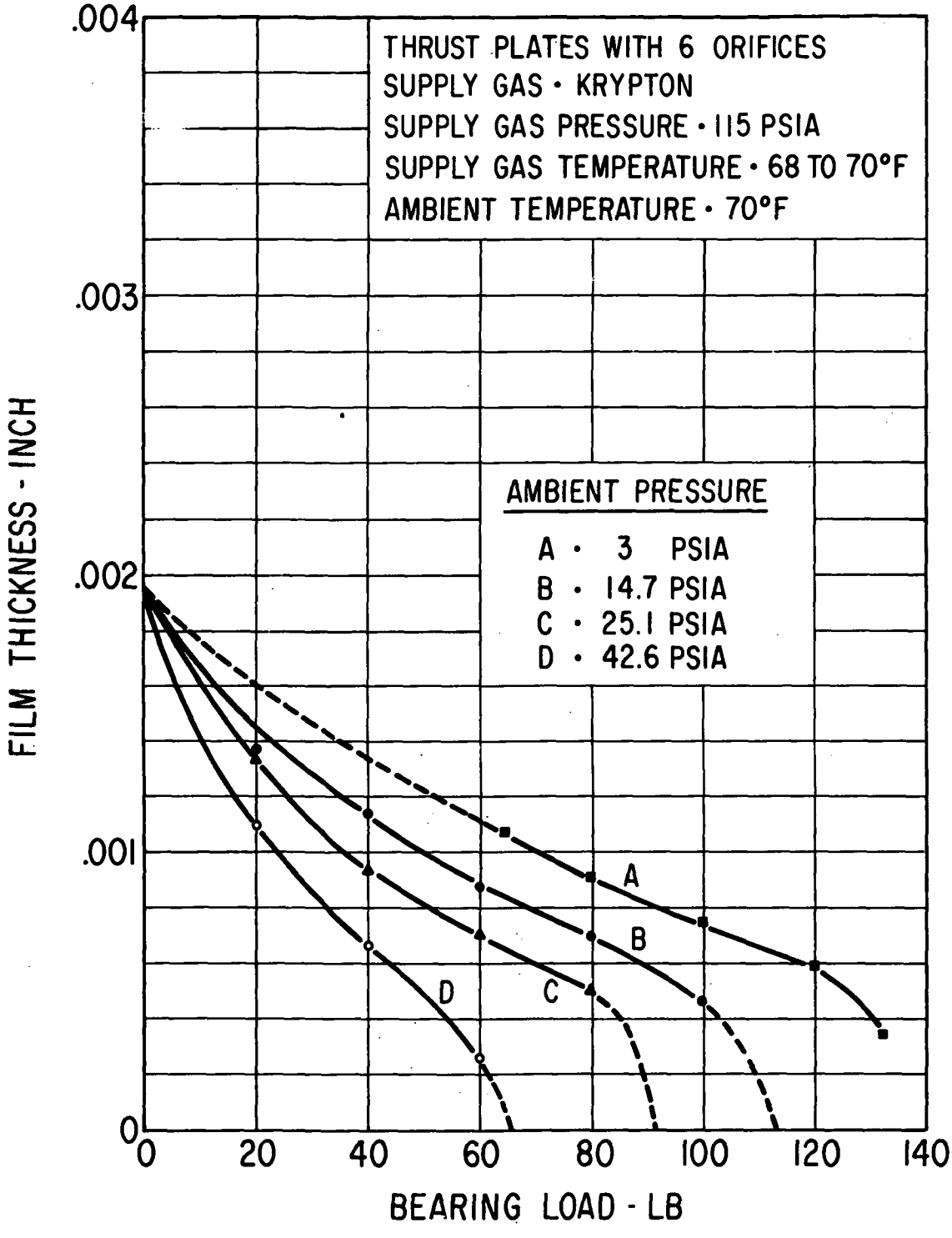

Fig. 46 Measured Hydrostatic Film Thickness for Double-Acting Spiral-Groove Thrust Bearing With 6 Orifices at 115 psia Supply Pressure in Krypton

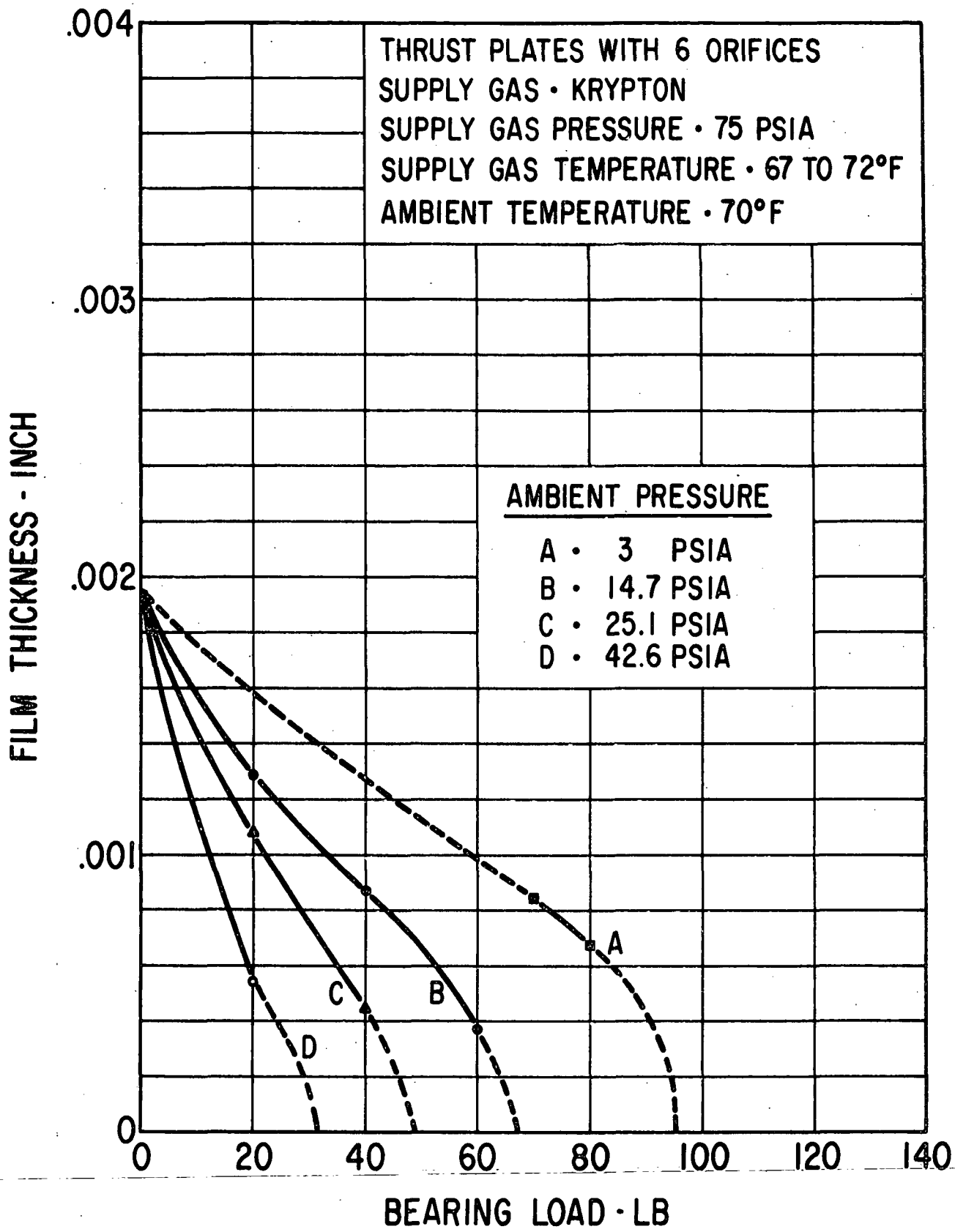

Fig. 47 Measured Hydrostatic Film Thickness for Double-Acting Spiral-Groove Thrust Bearing With 6 Orifices at 75 psia Supply Pressure in Krypton

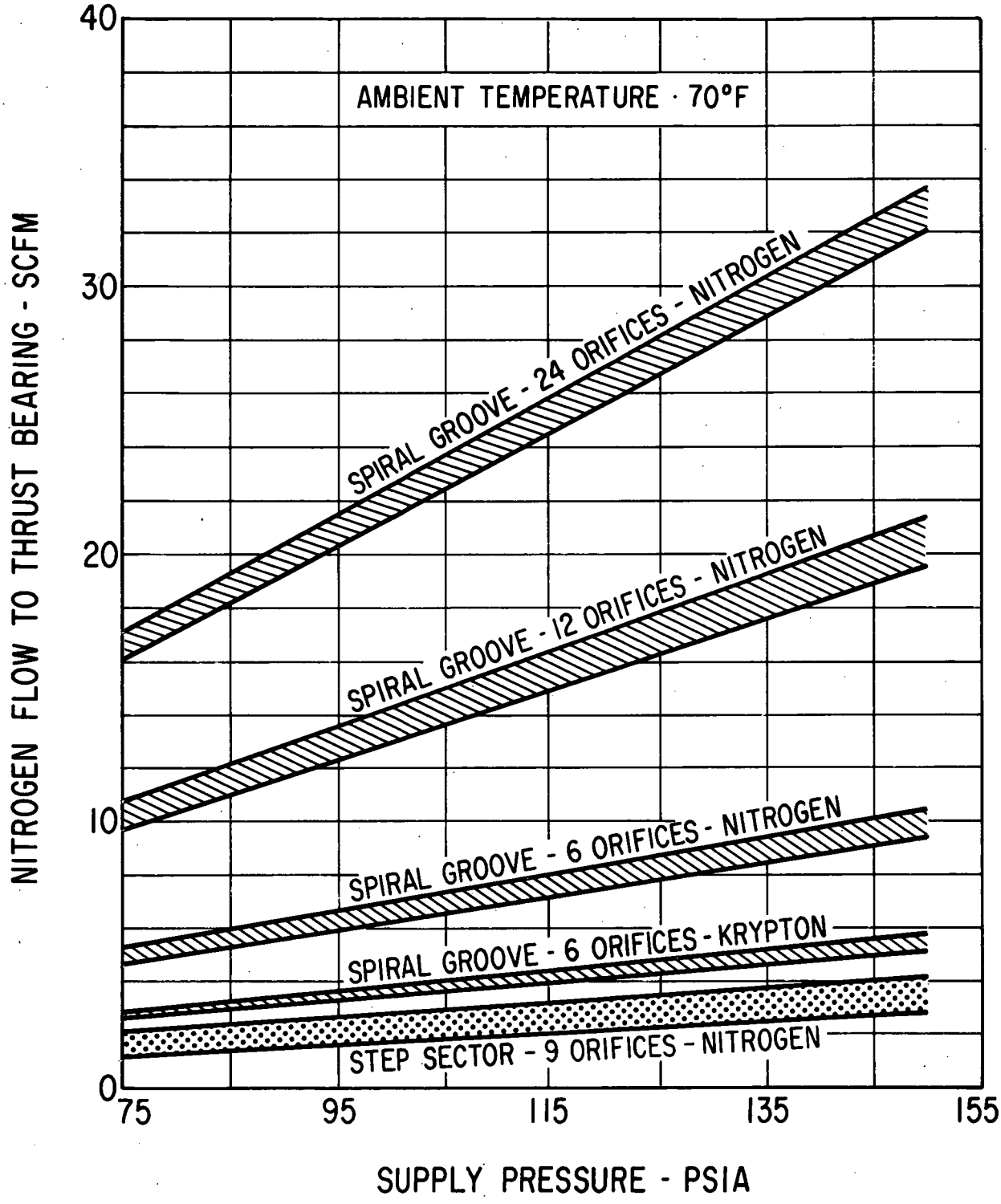

Fig. 48 Measured Hydrostatic Flow For Double-Acting Thrust Bearings

film thickness measurements. Within the band of flow measurement readings, no clear trend could be associated with either bearing loads or ambient pressure, although some correlation between low load and higher flow was noted, especially for the six orifice bearing. Also shown in Figure 48 is the krypton supply flow with the six orifice bearing. The flow difference between the measured krypton and nitrogen flow agrees with theoretical predictions.

Stability Investigation for the Spiral-Groove Thrust Bearing

A frequently encountered limitation in hydrostatic gas thrust bearing operation is the occurrence of pneumatic hammer, which is an axial rotor vibration induced by the bearing. Pneumatic hammer occurs with various intensities and may lead to gas film breakdown and equipment damage. The basic parameters for pneumatic hammering are well understood, however, an exact prediction for the onset of hammer in the thrust bearing geometry with its large spiral-grooved section was not available. Therefore, the experimental program was planned to establish pneumatic hammer thresholds for bearing geometry (number of orifice holes) bearing loads, supply and ambient pressure. In addition to the regular operating tests in conjunction with the measurement of the gas film thickness as described above, the soft mounted test fixture was subjected to low level vertical vibrations over the frequency range 5 to 2000 cycles per second, while the thrust bearing was operated over the identical range of test parameters as covered for the film thickness measurements.

Pneumatic hammer was not observed for the spiral-groove thrust bearing under any of these conditions, including the tests conducted in krypton.

Calculated Hydrostatic Performance of the Spiral-Groove Thrust Bearing

The calculated hydrostatic thrust bearing performance shown in Figure 9 and discussed in the section entitled "Thrust Bearing Analysis" was made by using a hydrostatic thrust bearing analysis available at that time and making approximate corrections for the effect of the hydrodynamic spiral grooves. More recently, MTI has developed a computer program to calculate hydrostatic bearing performance for a spiral groove thrust bearing equipped with gas supply orifices. The program which is adaptable to many different bearing surface geometries, was set up to calculate load versus gas film data for the exact BRU spiral-groove bearing geometry.

Newly calculated values of bearing film thickness versus load are shown in Figure 49 for the six orifice bearing with krypton at 150 psia as supply gas. Comparison with experimentally measured values obtained under test conditions identical to those assumed for the calculations, indicates good agreement up to eccentricity values around $\epsilon^* = 0.7$ where the previously noted drop in experimentally obtained film thicknesses occur.

In Figures 50 and 51, two more plots of calculated and experimentally obtained gas film thicknesses are shown. The test and operating conditions which are represented in Figures 50 and 51 span the two extremes of very low load carrying capacity of a six orifice bearing at 75 psia gas supply

*ϵ = total play - 2 x film thickness/total play.

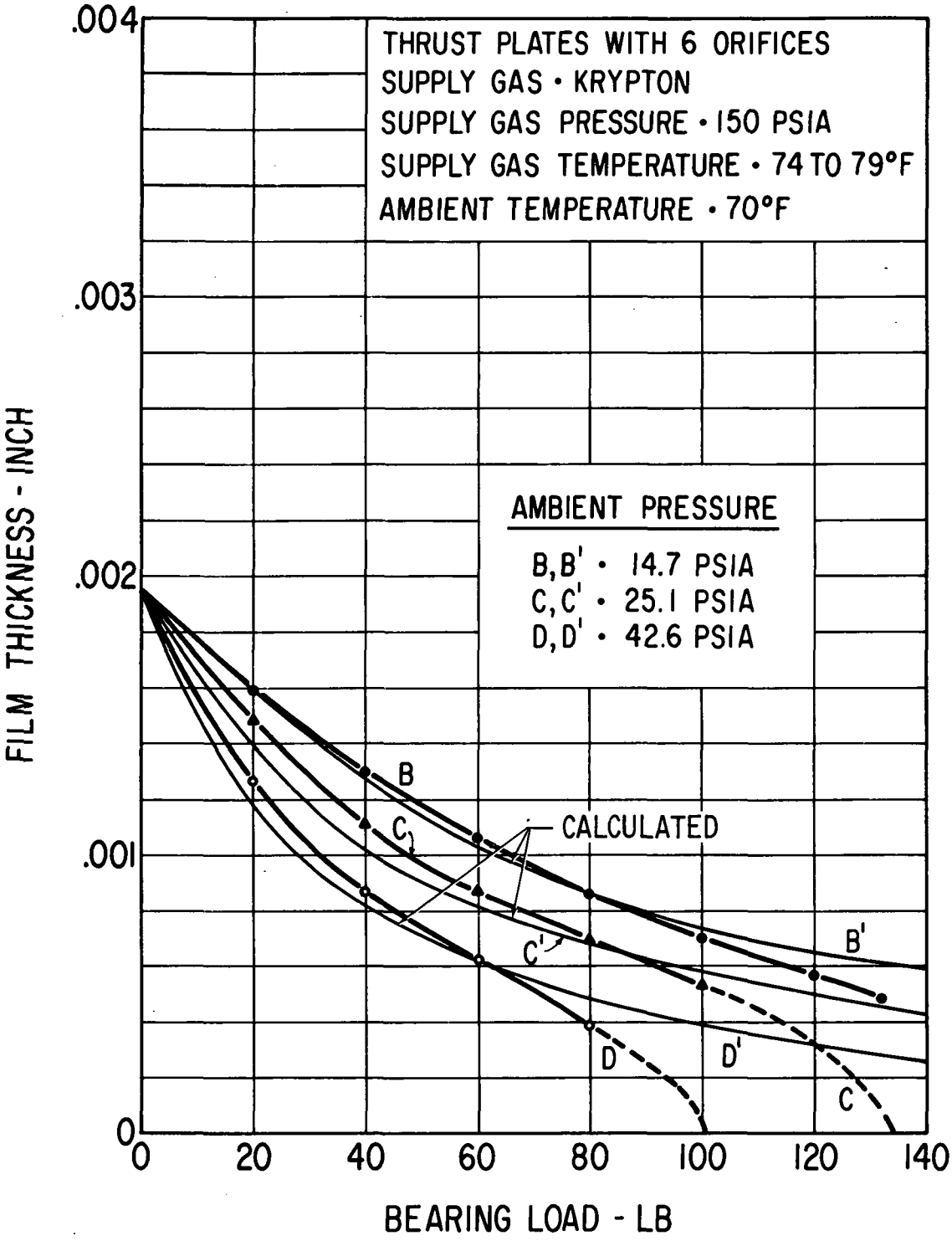

Fig. 49 Calculated and Measured Hydrostatic Film Thicknesses for Double-Acting Spiral-Groove Thrust Bearing at 150 psia Supply Pressure in Krypton

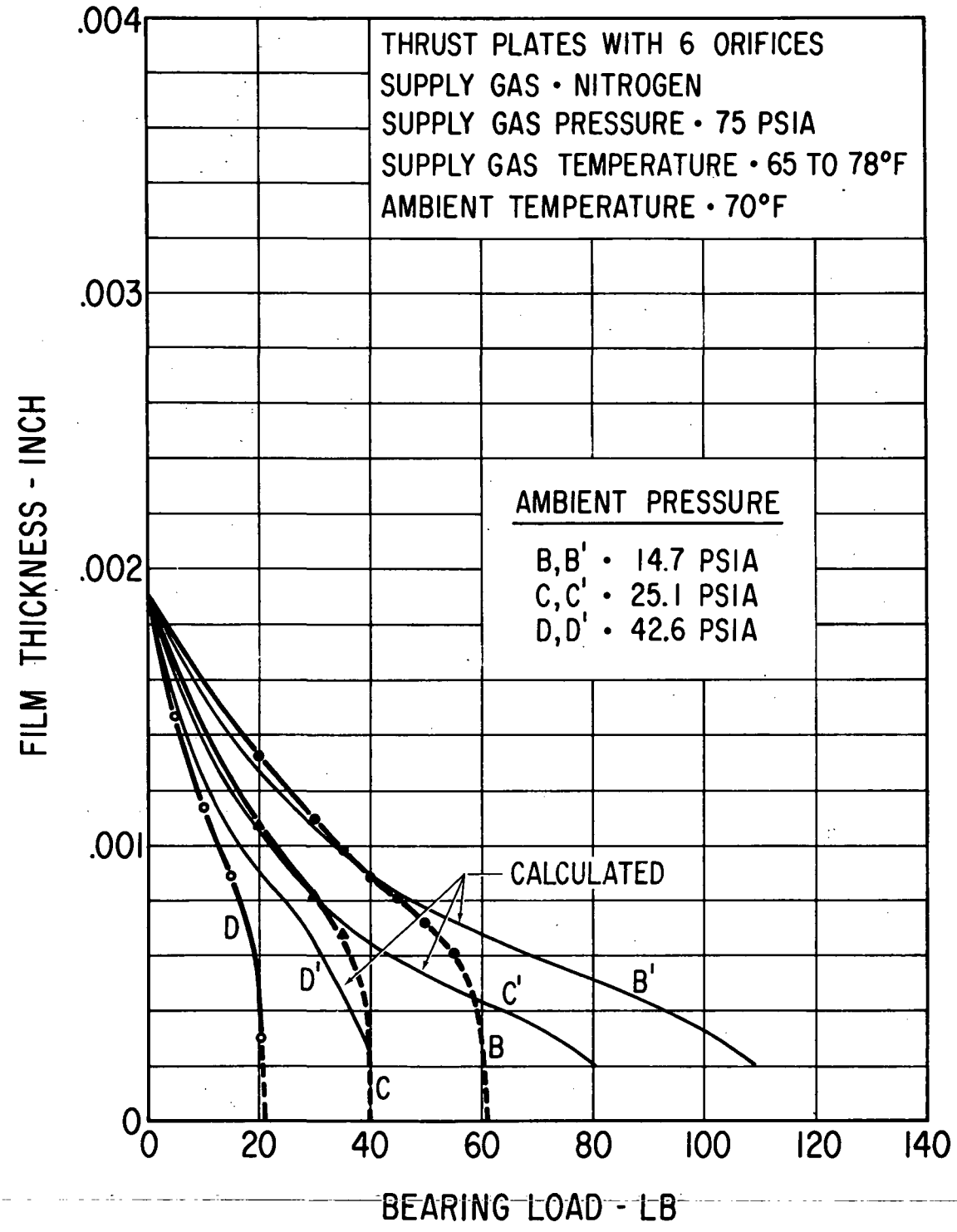

Fig. 50 Calculated and Measured Hydrostatic Film Thicknesses for Double-Acting Spiral-Groove Thrust Bearing at 75 psia Supply Pressure in Nitrogen

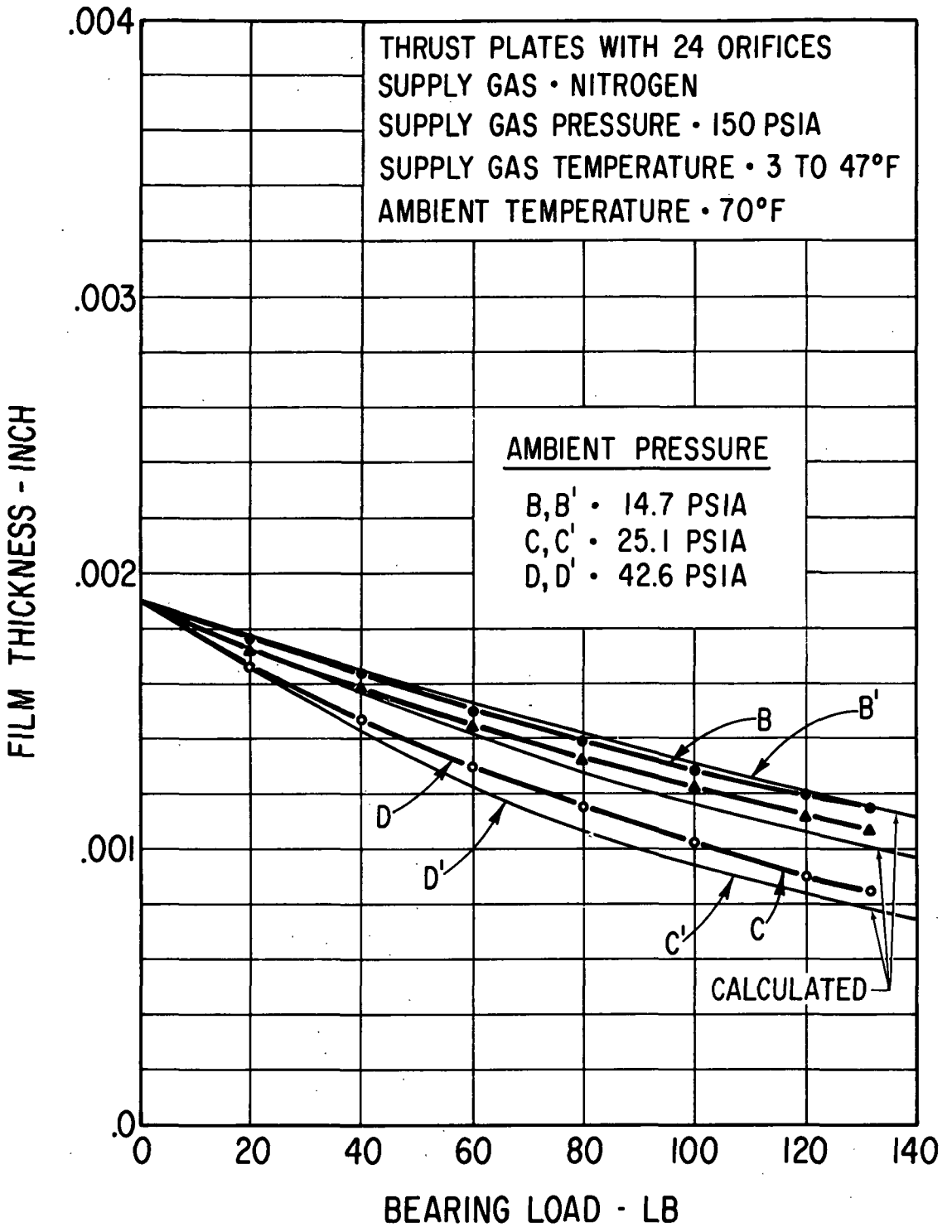

Fig. 51 Calculated and Measured Hydrostatic Film Thicknesses for Double-Acting Spiral-Groove Thrust Bearing at 150 psia Supply Pressure in Nitrogen

pressure and the maximum load carrying capacity obtained with a 24 orifice bearing at 150 psia supply pressure. Agreement between calculation and experiment is equally good in both cases. In Figure 50 there is even a hint of a rapid film thickness drop-off or lockup, though not quite as steep or as early in the load scale as experienced experimentally.

MEASURED HYDROSTATIC PERFORMANCE OF THE STEP-SECTOR THRUST BEARING

Film Thickness Measurements with Nitrogen as Supply Gas

Gas film thicknesses for the NASA-supplied step-sector prototype thrust bearing which incorporated a pinned gimbal (see Figure 27) under nonrotational hydrostatic operating conditions are shown in Figures 52 through 56.

The effective average end-to-end bearing clearance under test conditions was 0.00225 inch, which is considerably less than the 0.003 inch specified nominal clearance. Under pretest set-up conditions a maximum clearance of 0.00245 inch could be achieved when a 20-lb axial load was applied first in one and then in the opposite direction. Under operating conditions with a unidirectional load from zero to 100 pounds, the maximum travel was 0.00122 inch (1/2 total clearance).

Experimentally measured bearing eccentricity ratios for the step-sector thrust bearing are of similar magnitude as those for the six orifice back-up bearing, but actual film thickness values are only approximately half as large because total bearing clearance of the step-sector thrust bearing was also only approximately half as large as for the spiral-groove bearing.

The lockup phenomenon occurs in the step-sector thrust bearing at similar eccentricity ratios as in the spiral-groove bearing.

Stability of the Step-Sector Thrust Bearing

Pneumatic hammer was prevalent in the step-sector thrust bearing at all subatmospheric ambient pressures for all gas supply pressures between 90 and 150 psia. This phenomenon occurred without externally inducing vibration by means of the electric shaker attached to the test rig.

Experimentally observed rotor amplitudes due to pneumatic hammer ranged up to 60 percent of the total thrust bearing clearance. No consistent correlation was found between amplitudes and load or bearing supply and bearing ambient pressures.

"Beating" - a cyclic increase and decrease in rotor vibrational amplitude - also occurred irregularly.

Figure 57 shows two photos representative of large amplitude hammer and large amplitude beating. In both photos one major vertical division represents approximately 0.00050 inch or 0.00025 inch peak-to-peak amplitude for the "plain" pneumatic hammer and approximately 0.0002 inch for the maximum beat amplitude.

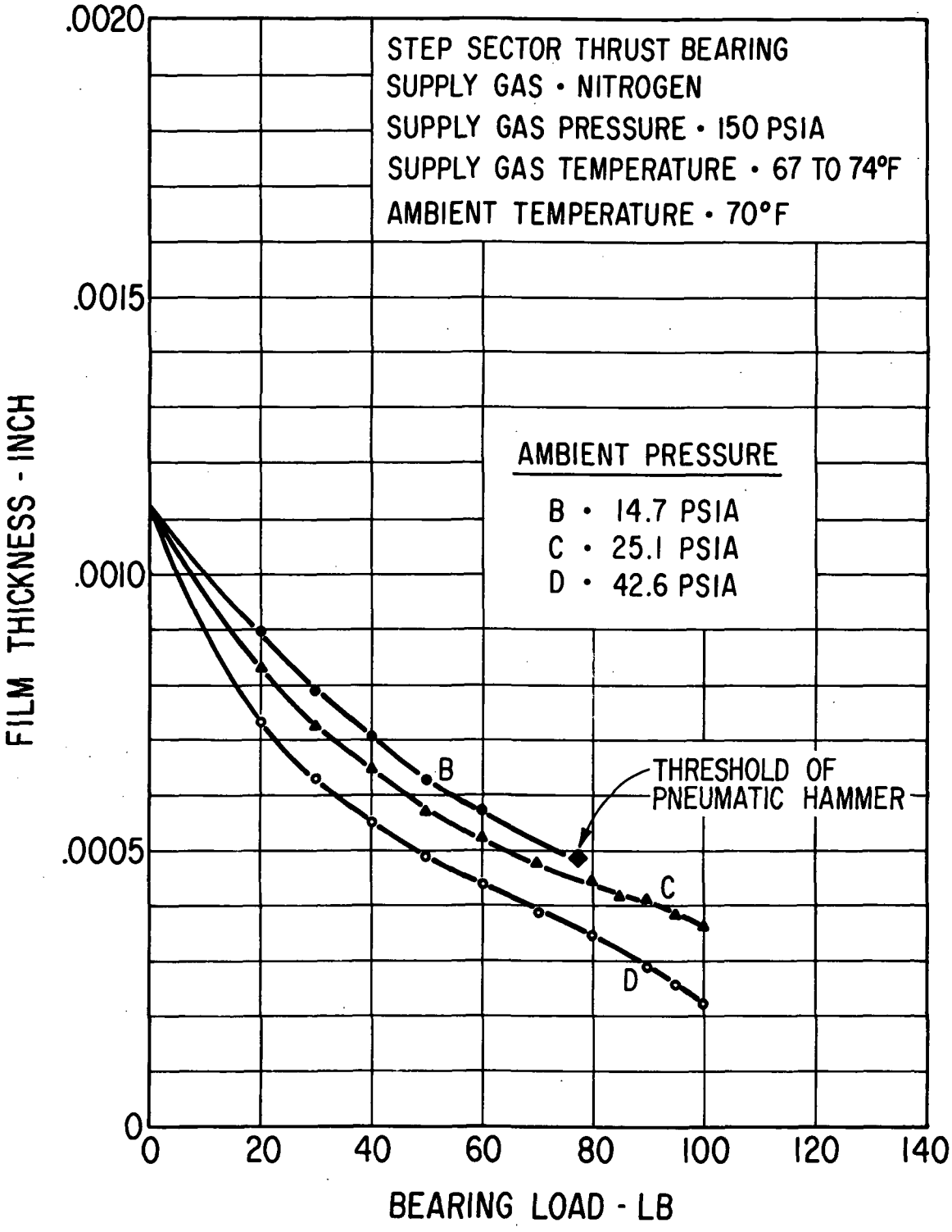

Fig. 52 Measured Hydrostatic Film Thickness for Double-Acting Step-Sector Thrust Bearing at 150 psia Supply Pressure

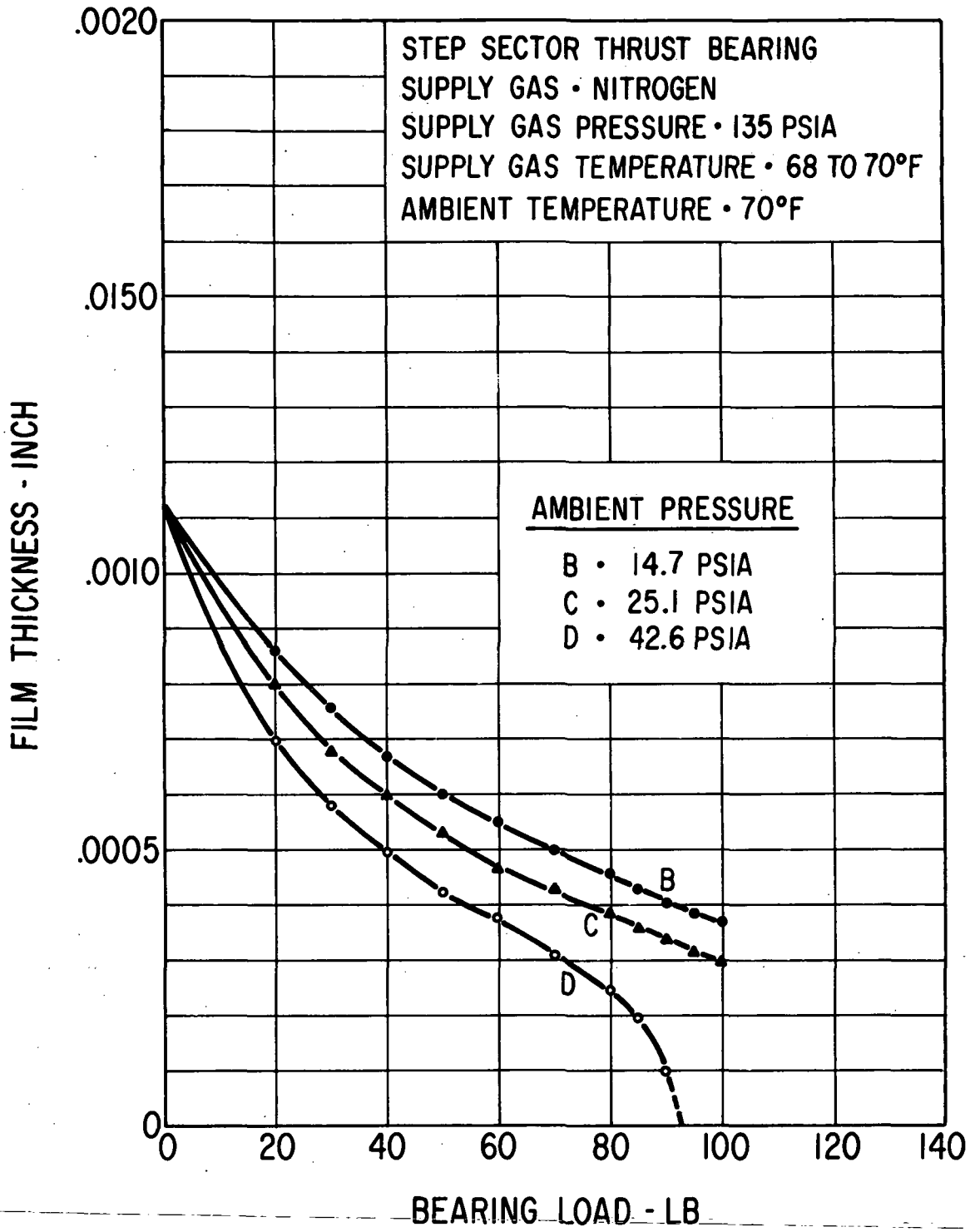

Fig. 53 Measured Hydrostatic Film Thickness for Double-Acting Step-Sector Thrust Bearing at 135 psia Supply Pressure

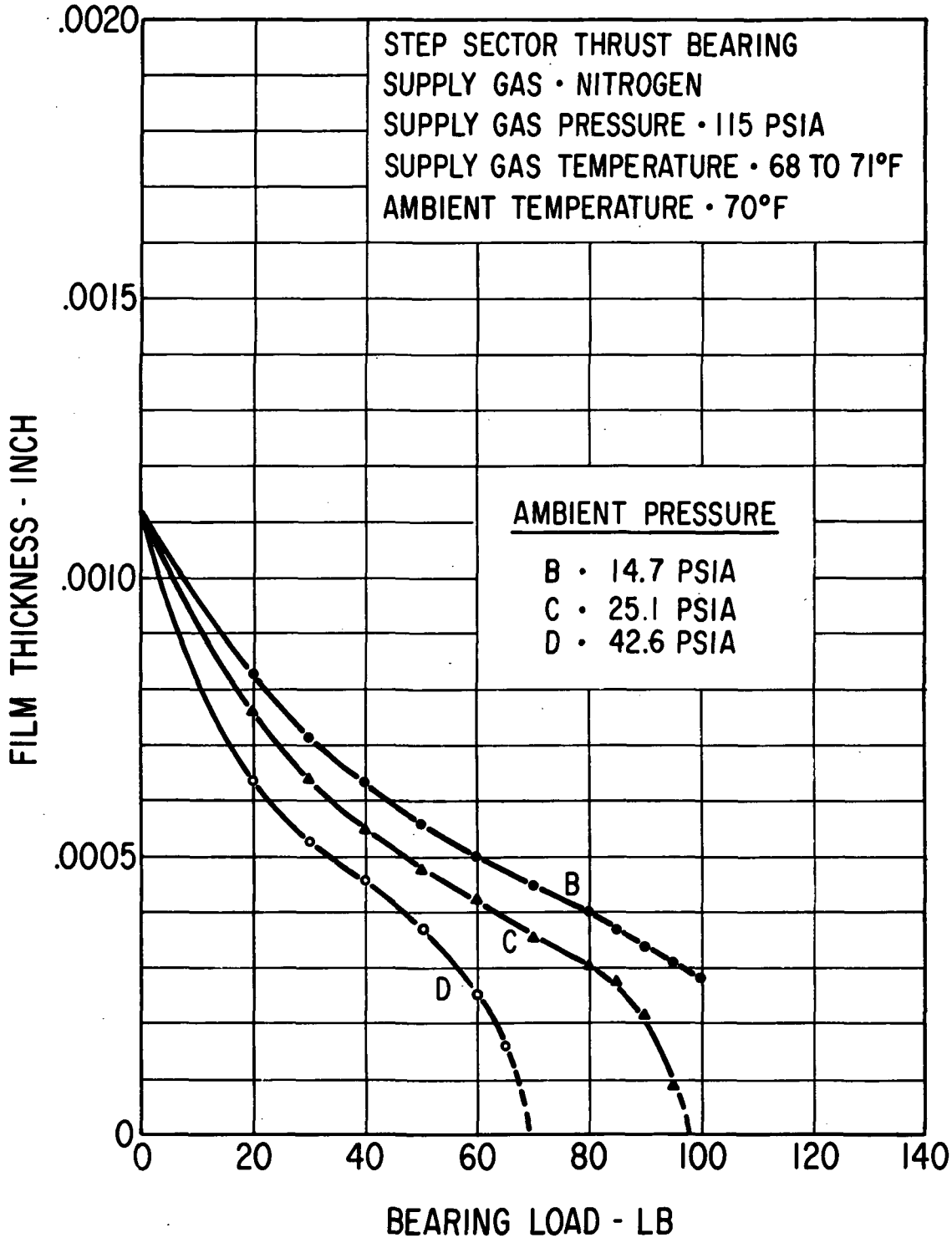

Fig. 54 Measured Hydrostatic Film Thickness for Double-Acting Step-Sector Thrust Bearing at 115 psia Supply Pressure

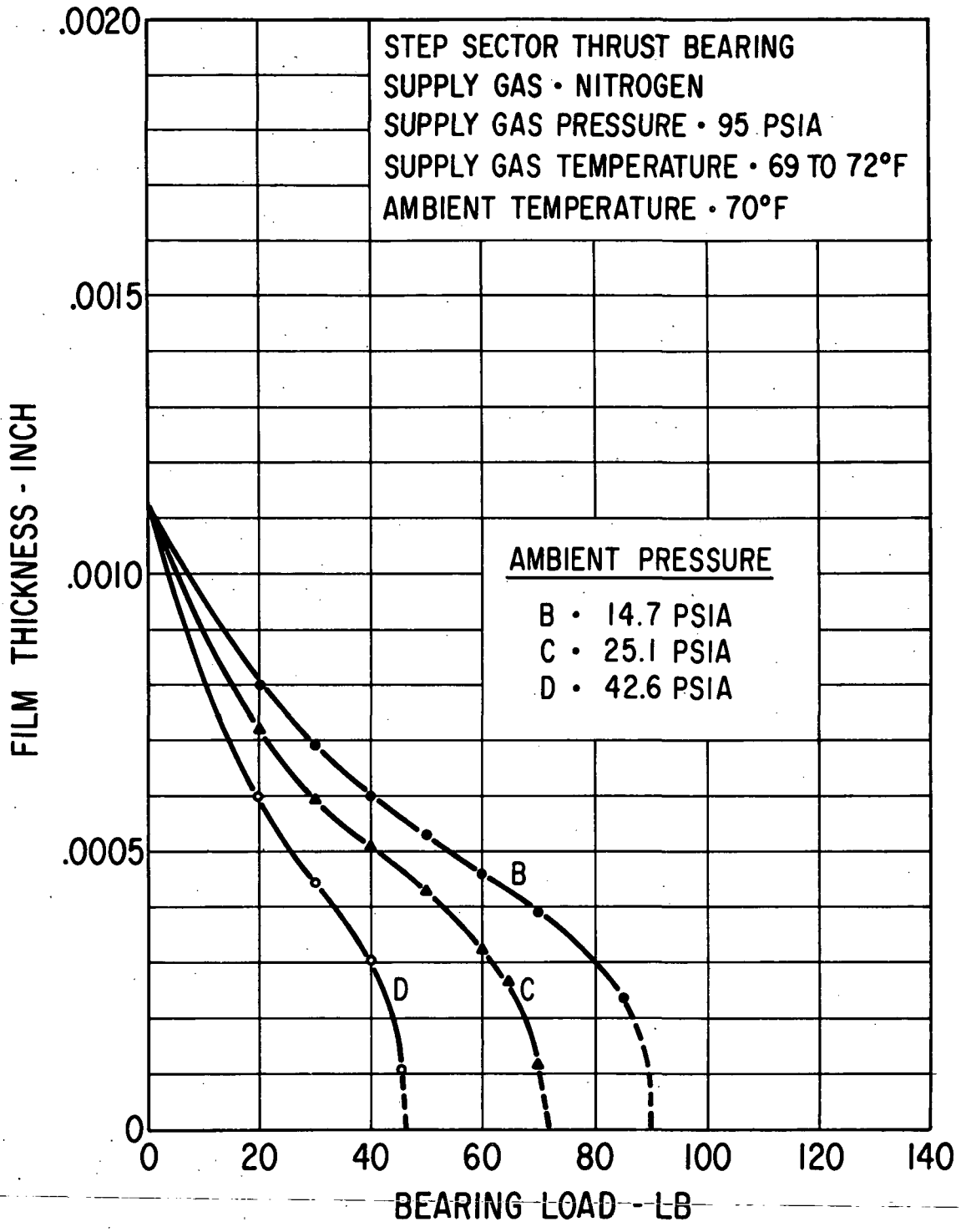

Fig. 55 Measured Hydrostatic Film Thickness for Double-Acting Step-Sector Thrust Bearing at 95 psia Supply Pressure

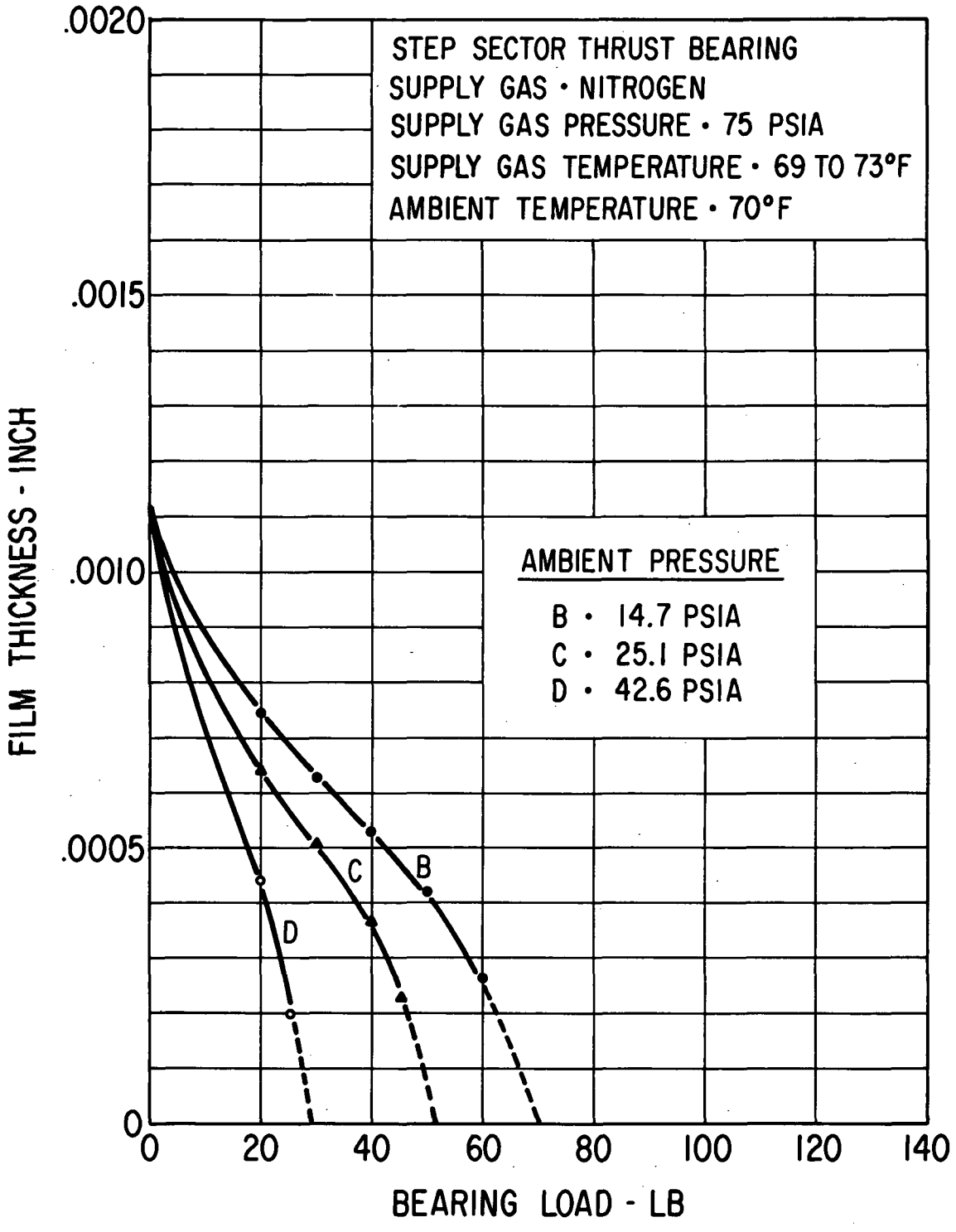

Fig. 56 Measured Hydrostatic Film Thickness for Double-Acting Step-Sector Thrust Bearing at 75 psia Supply Pressure

PLAIN HAMMER

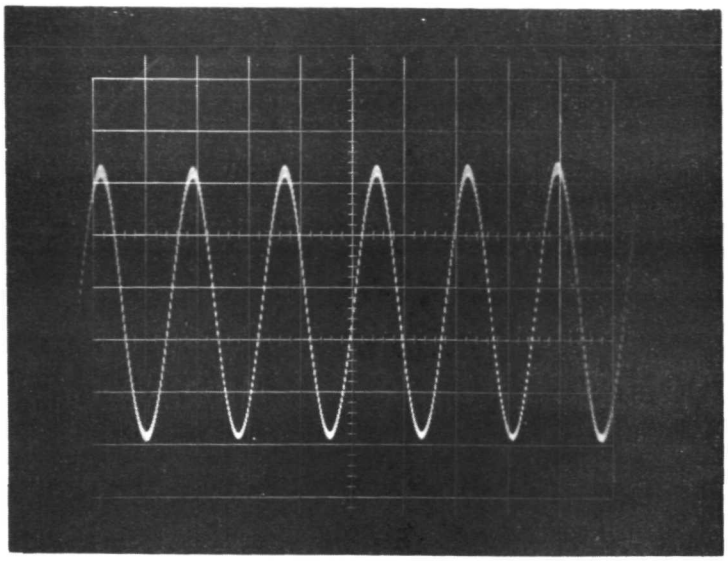

VIBRATION FREQUENCY ≅ 570 HZ

HAMMER WITH
BEAT FREQUENCY

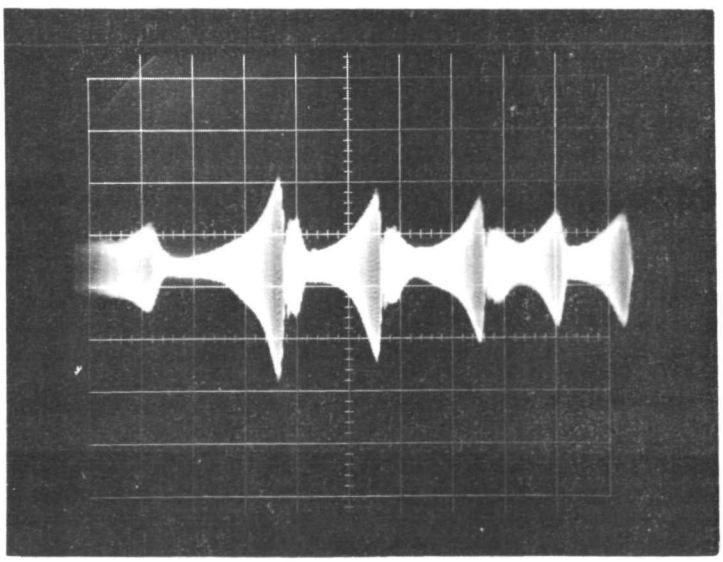

ONE MAJOR HORIZONTAL DIVISION = 0.1 SEC.

BOTH PHOTOS: ONE MAJOR VERTICAL DIVISION ≅ .000050

Fig. 57 Pneumatic Hammer in Step-Sector Thrust Bearing

The frequency of the "plain" hammer vibration is approximately 550 cycles per second. Hammer frequencies ranged between 500 and 750 cycles per second, with the higher frequencies occurring at higher bearing loads. At 14.7 psia ambient bearing pressure, the pneumatic hammer threshold was found at 77 lbs bearing load (Figure 52).

Supply Gas Flow for Step-Sector Thrust Bearing

The total supply gas flow for the step-sector thrust bearing was shown in Figure 48. The range of flow values indicated covers all test conditions of bearing load and bearing ambient pressure, which were represented in the gas film thickness curves shown in Figures 52 through 56. There was a discernable trend for the higher flow values to occur at the no-load condition.

The supply gas flow values for the step-sector thrust bearing are lower than those for the six orifice spiral-groove bearing and are considered to be primarily the result of the smaller axial clearance of the step-sector bearing.

EXPERIMENTAL PERFORMANCE OF SINGLE TILTING PAD JOURNAL BEARING WITH NONCONFORMING PIVOTS

A comprehensive test program was conducted to experimentally determine the performance characteristics of the nonconforming pivoted pad journal bearing and to demonstrate its suitability for the BRU application.

These journal bearings are of the self-acting pivoted-pad type, with three pad segments per bearing. The pads are supported by nonconforming pivots. Included in the journal bearing design is provision for hydrostatic lift-off of each pad during BRU start-up and shutdown. Hydrostatic lift-off is obtained via a single hydrostatic orifice and associated flow-control valves located within each pad. Predicted performance of the journal bearings under BRU operating conditions was previously discussed in the section entitled "Journal Bearing Analysis".

All of the herein reported pad testing was performed at 400°F to closely simulate the steady-state operating temperature of the BRU journal bearing cavities. Pad performance was measured at three ambient pressure levels; 14.7, 25.1 and 42.6 psia. These pressure levels correspond to BRU operation at 3.0, 6.0 and 10.5 KWe, respectively. (The lowest BRU design power level (2.25 KWe) could not be simulated since the test rig was not implimented for subatmospheric testing.)

Because of the high cost of the He-Xe gas mixture, all testing was done using argon gas. Since the viscosity of argon is lower than that of He-Xe the measured values of hydrodynamic film thickness in argon are lower than would be expected in He-Xe. Under ideal pad geometry conditions (i.e., neglecting hydrostatic orifice and orifice recess effects), film thickness values in He-Xe would be 8 to 14 percent higher, depending on pad load and ambient pressure, than those obtained in argon.

The test program was performed using one journal bearing pad. The test pad which was shown in Figure 18 exactly represented the pads designed for the BRU. The pad was instrumented with three capacitance probes to measure film thickness between the pad and test journal, and one thermocouple for measurement of pad temperature. Two capacitance probes were located near the edge of the bearing on the pivot line and one located near the leading edge on the pad axial center line

The following test data were obtained for the single test pad:

a) hydrodynamic performance in argon at 400°F over a range of loads and ambient pressures,

b) effect of pivot valves and pad surface interruptions (orifice and orifice recess) on hydrodynamic performance,

c) hydrostatic performance over a range of loads and ambient pressures for a fixed hydrostatic supply pressure,

d) effect on hydrostatic performance of primary and secondary pivot valves,

e) performance of the flexure-mounted pad when operating in the hybrid mode (hydrostatic gas turned on, the journal rotating),

f) performance of the flexure-mounted pad when operating in the hydrodynamic mode, and

g) threshold of pad stability when operating in each of the hydrodynamic, hydrostatic and hybrid modes.

DESCRIPTION OF TEST APPARATUS

The test rig rotor used for testing the single pivoted pad journal bearing is shown in Figure 58. The test journal is overhung from a turbine driven high-speed spindle assembly. The bearing pad is attached to a dead weight loading mechanism (which is part of the dry box).

The entire assembly is enclosed in a sealed dry box which can be pressurized with any desired ambient gas. For the tests described herein the dry box was supplied with argon at sufficiently high pressures to maintain outflow at the noncontacting seals and at the back-pressure regulator.

Within the dry box is a clam shell heater assembly which was placed around the test bearing assembly to achieve the desired ambient temperature. The heater was operator controlled through rheostats according to the indications of test pad temperature, obtained from the output of a Chromel-Alumel thermocouple welded to the back side of the test pad.

Rotor speed was read out on a Hewlett-Packard counter, model 521 A which converted a six-per-revolution signal from an electro-magnetic pickup into tenths of shaft revolutions. Speed control was maintained by an operator who adjusted a regulator on the supply line to the air turbine driving the rotor.

An overall view of the test set-up is shown in Figure 59. This picture shows the exterior of the dry box (weights for pad loading can be seen at the top of the dry box) and the instrumentation used.

Film Thickness Measurement System

Capacitance type displacement sensors and Wayne Kerr amplifiers were used for film thickness measurements, together with a Fairchild 1100 digital volt meter for amplitude read-out and an oscilloscope for visual monitoring. The capacitance sensors had a linear range of 0.005 inch. They were made of 416 stainless steel so that their thermal expansion coefficient would match that of the test pad in which they were mounted. The capacitance sensors were individually calibrated in a calibration fixture before mounting in the test pad.

To assure best possible accuracy of gas film thickness measurements, additional extensive in-place calibration checks were conducted with the test

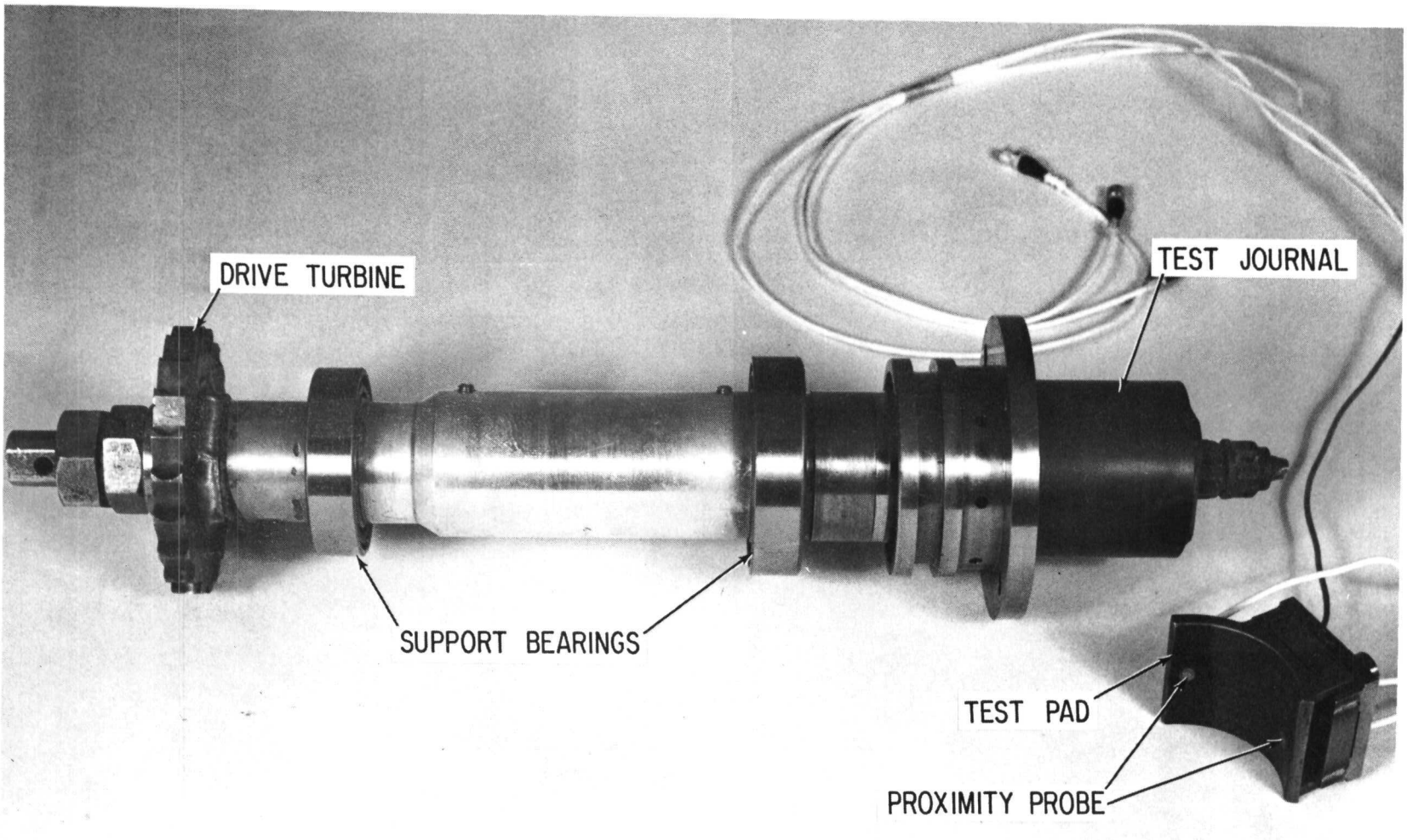

Fig. 58 Single-Pad Bearing Test Rig Rotor and Test Pad

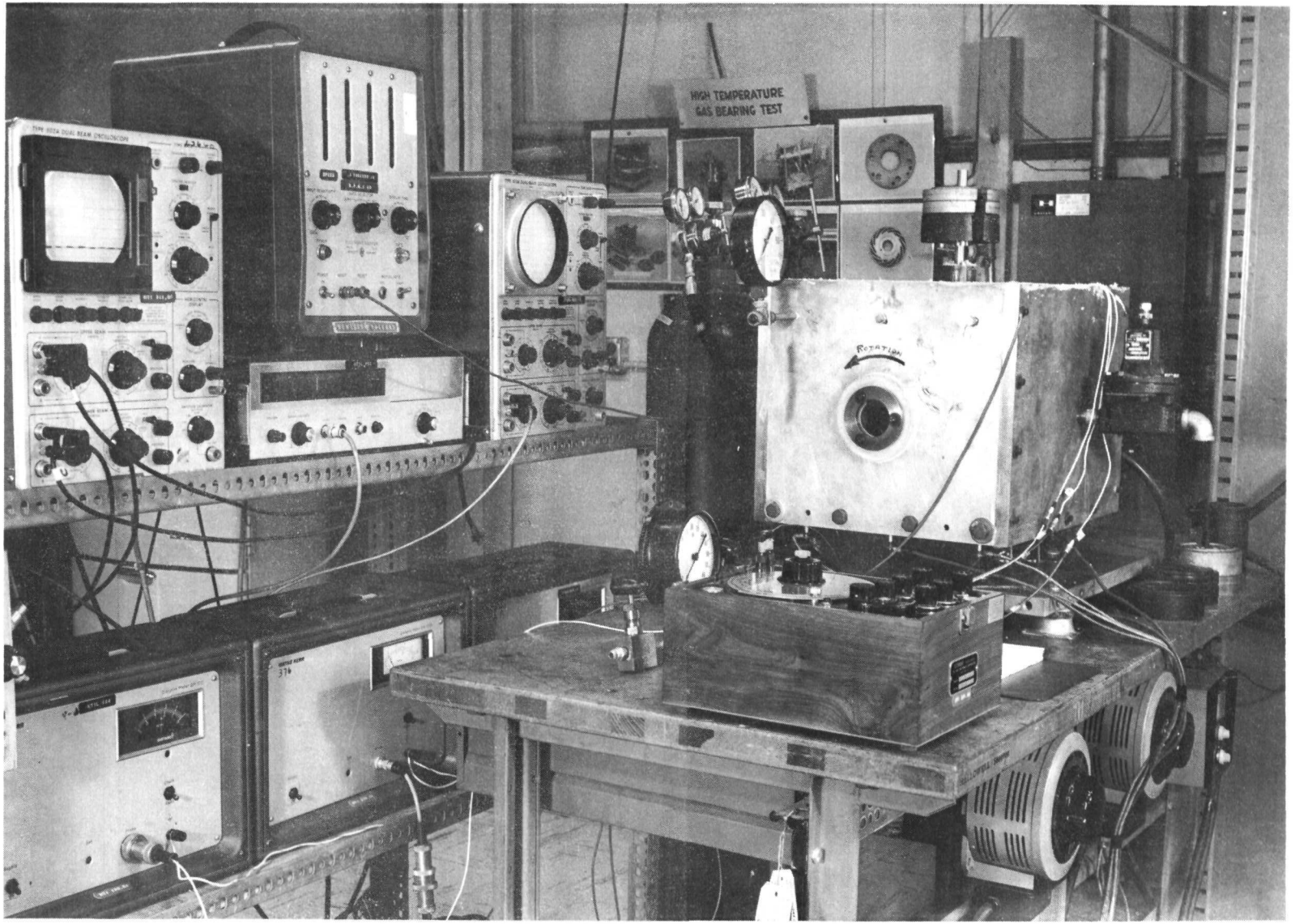

Fig. 59 Overall View of Single-Pad Journal Bearing Test Setup

pad installed against the shaft and all test instrumentation connected. For these checks either a plastic or stainless steel shim was inserted between pad and shaft with cut-outs for the sensors and the resulting change in read-out recorded. Shims of 0.0005 and 0.001 inch thickness were used. Calibration of the capacitance sensors against the chrome oxide coating of the test shaft led to the following observations:

1) The capacitance sensor read through the nonconducting chrome oxide coating that covers the conducting steel test shaft, but with a high level of attenuation. Even though the chrome oxide coating was approximately 10 mils thick, the capacitance sensor reading, with the sensor facing and touching the coating, was only 0.0003 inch.

2) Imperfection in the chrome oxide coating and the substrate surface caused the "zero" reading taken with the pad resting upon the shaft to vary circumferentially around the shaft. For the two pivot line probes in the pivoted pad, the variation was about $\pm$ 0.000060 and 0.000030 inches.

3) There was no noticeable change in the probe sensitivity between room temperature and 400°F, when a 0.001 inch thick stainless steel shim was removed from between pad and shaft after heating of the test vessel. However, there was a relatively large change in the zero reading of the sensor when the temperature of the pad – shaft assembly was increased. To compensate for the temperature sensitive zero shift, a "zero" sensor reading was taken prior to and, usually, immediately after conclusion of each experimental run This was accomplished by turning the rotor by hand in 18° increments and recording the digital volt meter readings. The average was then taken as the zero film thickness starting point prior to commencement of rotor rotation. For all probes, the arithmetic average of all readings came very close to integrated average. Since these two values were also found to be well represented by the mean between high and low readings, the latter was used for determining the zero position prior to each test run.

MEASURED HYDRODYNAMIC PERFORMANCE

Reference Condition

Curves of calculated hydrodynamic film thickness for the single-pivoted pad without hydrostatic orifice or orifice recess are shown in Figures 60 through 62 as a function of pad load. (Pad load was varied by changine the weights on the dead weight loading mechanism.) The film thickness values are those at the pivot location. The condition of a smooth pad surface (i.e., no orifice or orifice recess interruptions) is the optimum load carrying condition for the pad, and hence was chosen as the reference condition for comparison of test results.

The calculated film thickness curves on Figures 60, 61, and 62 pertain to the following pad geometry and operating conditions:

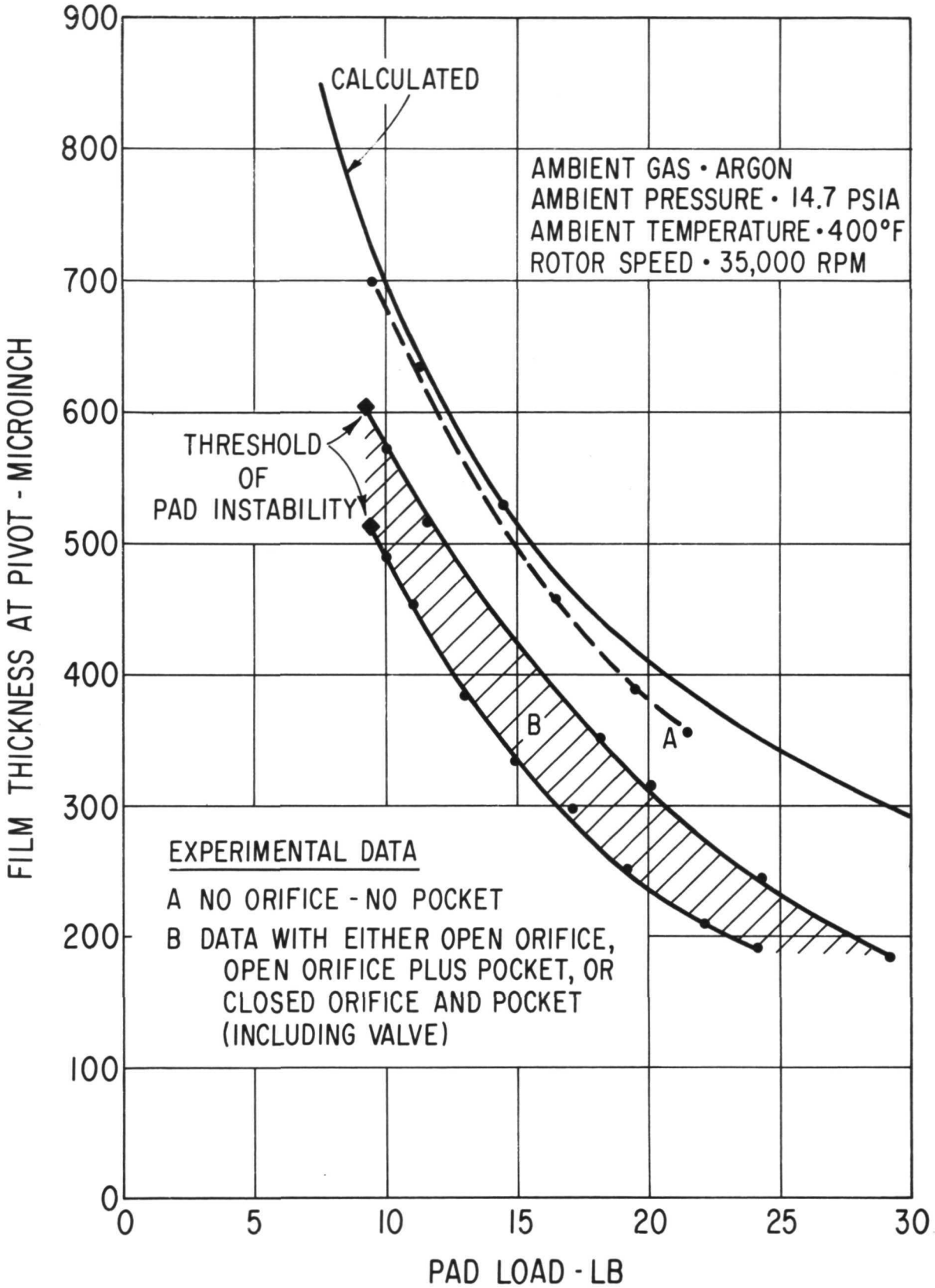

Fig. 60 Calculated and Measured Hydrodynamic Load Capacity of the Single Pivoted Pad at 14.7 psia Ambient Pressure

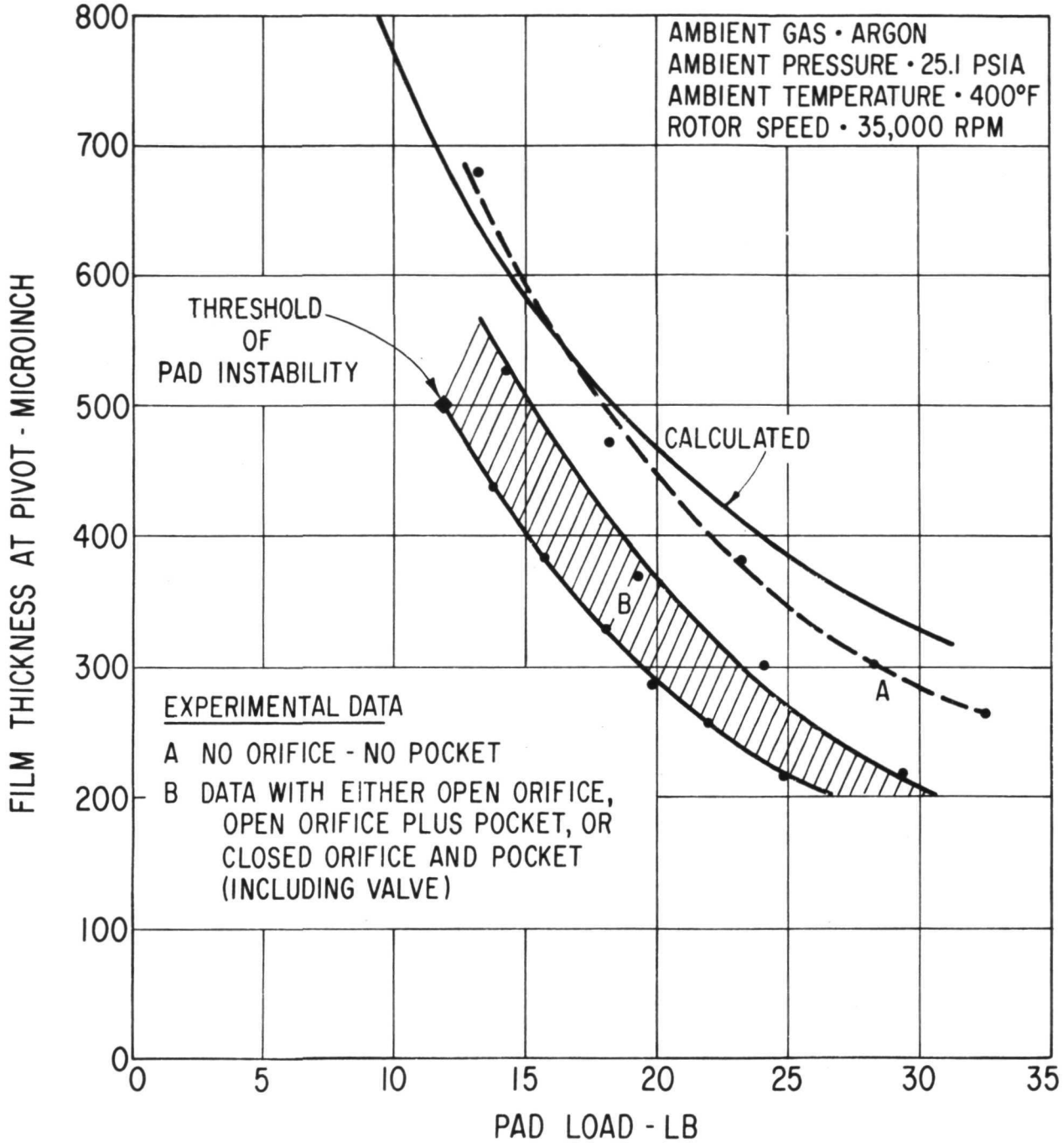

Fig. 61 Calculated and Measured Hydrodynamic Load Capacity of the Single Pivoted Pad at 25.1 psia Ambient Pressure

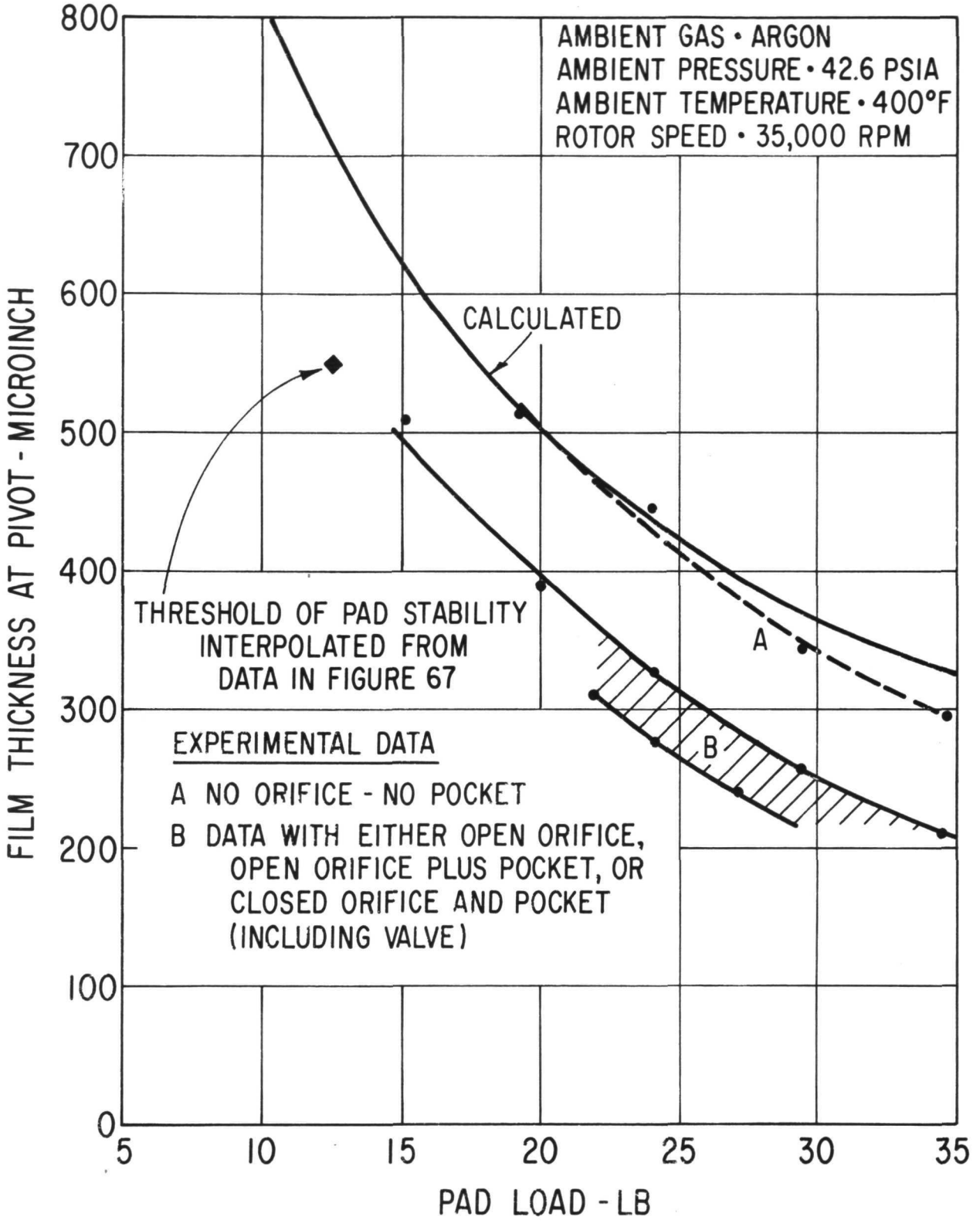

Fig. 62 Calculated and Measured Hydrodynamic Load Capacity of the Single Pivoted Pad at 42.6 psia Ambient Pressure

Pad radius - 0.875 inch
Pad length - 1.31 inch
Pivot location from leading edge - 65 percent
Pad circumferential arc length - 110 degrees
Rotor speed - 35,000 rpm
Ambient gas - argon
Gas viscosity - 0.463×10^{-8} lb-sec/in.^{2} (argon at 400°F)
Ambient pressure - 14.7, 25.1 42.6 psia (Figures 60, 61, 62 respectively)
Ambient temperature - 400°F

The above pad geometry is precisely that used for the MTI-designed BRU back-up journal bearings. The operating conditions are those of the BRU except for the ambient gas and the rotor speed. The BRU journal bearings will actually operate in a helium-xenon gas mixture which has a viscosity of approximately 0.53×10^{-8} lb-sec/in.^{2} at 400°F. Nominal BRU rotor speed is 36,000 rpm.

Measured film thickness values, at the pivot location, for the single dead-weight-loaded test pad without orifice or orifice recess are plotted as experimental curves "A" on Figures 60, 61 and 62. The experimental operating conditions were the same as those listed above for the calculated performance.

It is seen from Figures 60, 61, and 62 that there is quite good agreement between the theoretically calculated and the experimentally measured load capacity curves for ideal pad geometry (i.e., no hydrostatic orifice or orifice recess). Under actual BRU operating conditions (36,000 rpm in He-Xe gas), theory predicts that the film thickness values will be 8 to 14 percent higher, depending on the specific pad load and ambient pressure condition.

Effect of Surface Interruptions on Pad Load Capacity

Measured hydrodynamic film thickness values (at the pivot location) were obtained for the single pivoted pad with the following types of pad surface interruptions:

1. an open, 0.0135-inch diameter orifice hole (no orifice recess or orifice check valve),
2. open orifice hole plus orifice recess* (no orifice check valve),
3. orifice recess only (orifice hole plugged with epoxy),
4. orifice recess plus orifice sealed by orifice check valve.

The above mentioned orifice, orifice recess, and orifice check valve are, of course, elements of the pad hydrostatic lift-off system.

* The orifice recess was a 0.5 x 0.25 inch rectangular pocket, 0.1 to 0.3 mils deep.

All values of measured hydrodynamic film thickness for the above listed pad surface interruptions fell within region "B" shown on Figures 60, 61 and 62.

Generally, the experimental results for each type of surface condition formed smooth curves which were nearly parallel to each other, indicating a minimum amount of data scatter. However, considerations of experimental accuracy and repeatability of the measurements make it advisable not to emphasize the exact ranking of the curves, other than to point out the distinct difference between the pad without surface interruptions (curves "A") and the pad with surface interruptions (region "B").

Data runs with the orifice, the orifice recess, and the orifice check valve (condition 4 listed above) were performed on several different occasions. The load capacity curves from these runs lay, in some cases, in the middle of region B, and in other cases at the lower limit of the region. Although this variation may have been due to limitations of experimental accuracy and/or repeatability, we believe that the orifice check valve (also referred to as the primary valve) may not have been working reliably.

Performance of the Single Pivoted Pad (with orifice, orifice recess, and orifice valve) When Mounted on a Flexure

For these tests the dead weight loading mechanism was removed and the single pivoted pad was supported by a flexure having a measured stiffness of 2500 lb/in. (Figure 63). The pad and flexure were assembled such that the pad was preloaded against the shaft with a 12 pound preload. This value was not changed throughout the course of the tests. Measured hydrodynamic film thickness values for the the three ambient pressure consitions of 14.7, 25.1 and 42.6 psia are shown plotted against rotor speed in Figure 64. At the lower end of the speed range, the starting points were arbitrarily chosen. For the 14.7 psia ambient pressure condition, tests were conducted up to 46,500 rpm. For the 25.1 and 42.6 psia ambient pressure conditions, experimental operation was limited by pad roll instability to speeds less than 44,500 and 38,500 rpm respectively.

When the Figure 64 data was initially recorded, the unequal difference in film thickness between the 14.7, 25.1 and 42.6 psia ambient pressure conditions was noted. As a check on possible experimental error, additional film thickness measurements were made at a constant 35,000 rpm, but for various ambient pressure conditions. The result of this test, shown in Figure 65, Curve "A", confirms that the increase in film thickness resulting from increases in ambient pressure is greater between 25.1 and 42.6 psia than between 14.7 and 25.1 psia. Curve "B" of Figure 65 shows the performance of the pad in air at room temperature.

Pad Stability

Throughout the single pad hydrodynamic tests, a phenomenon was observed that is called here, for simplicity, "pad instability". The observed pad motion was in the roll mode, with one complete roll cycle for every two shaft revolutions. A typical oscilloscope trace of this motion, as depicted

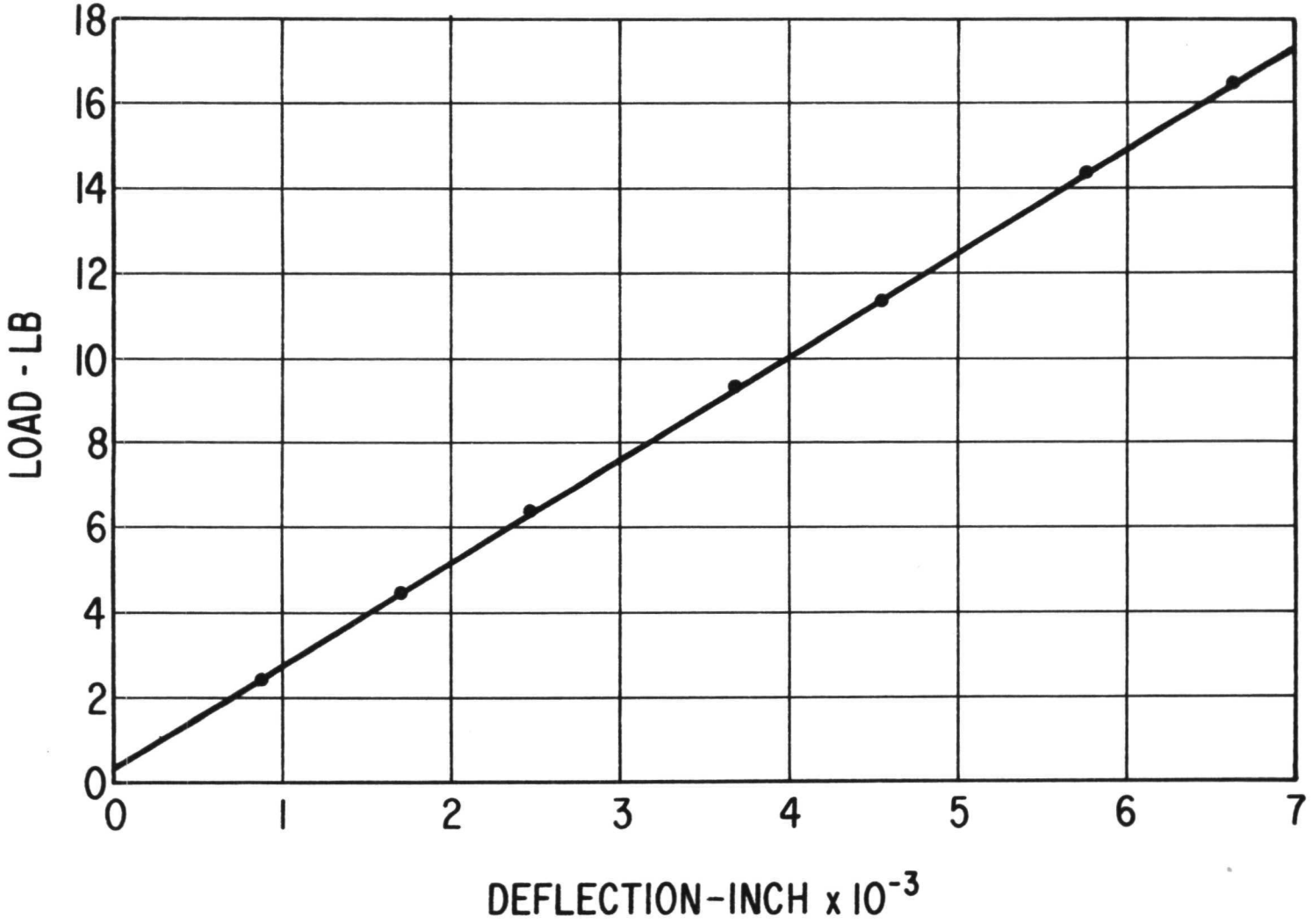

Fig. 63 Measured Load Versus Deflection for the Upper Pad Pivot-Support Flexure

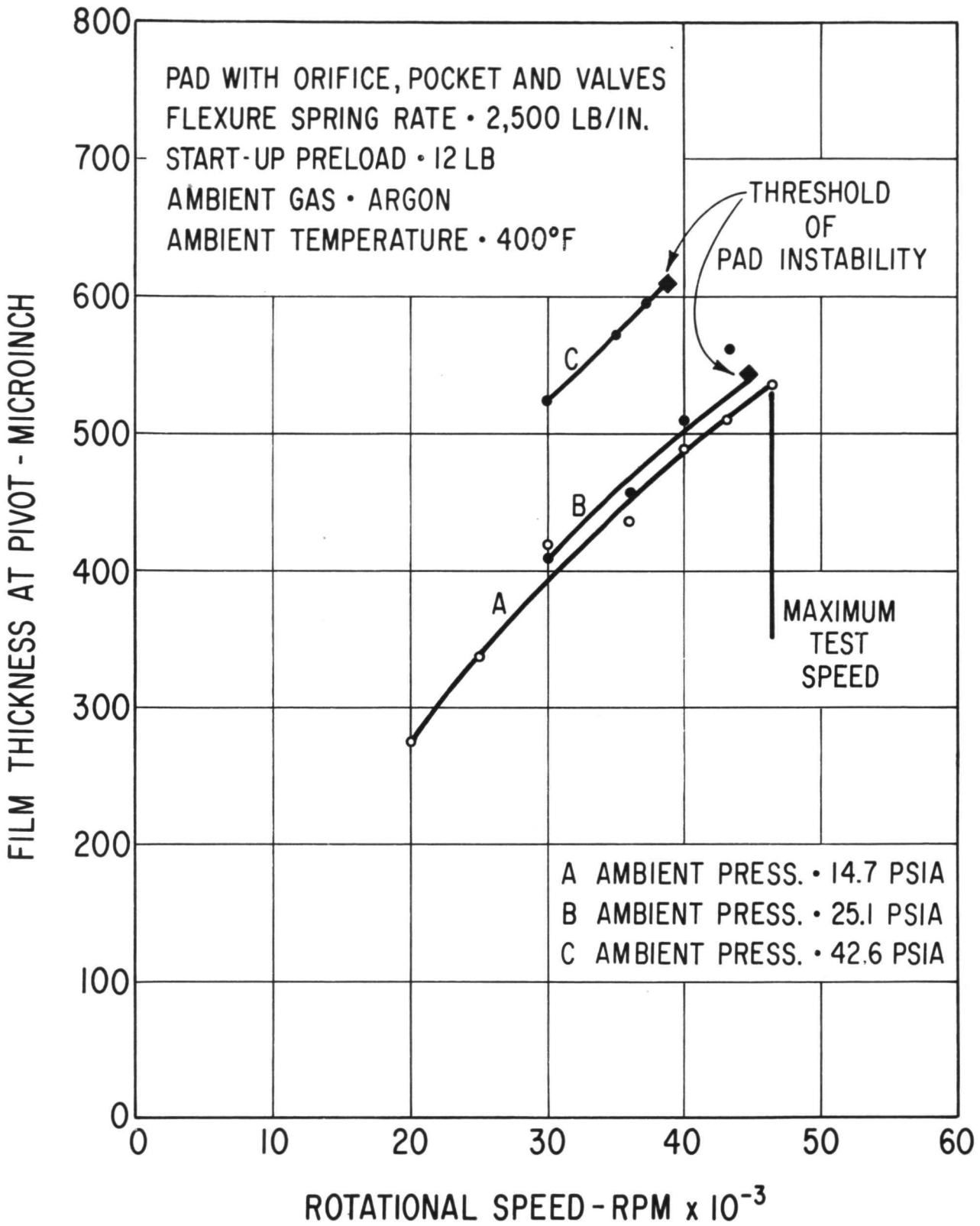

Fig. 64 Measured Hydrodynamic Performance of the Single Pivoted Pad When Mounted on the Pivot-Support Flexure

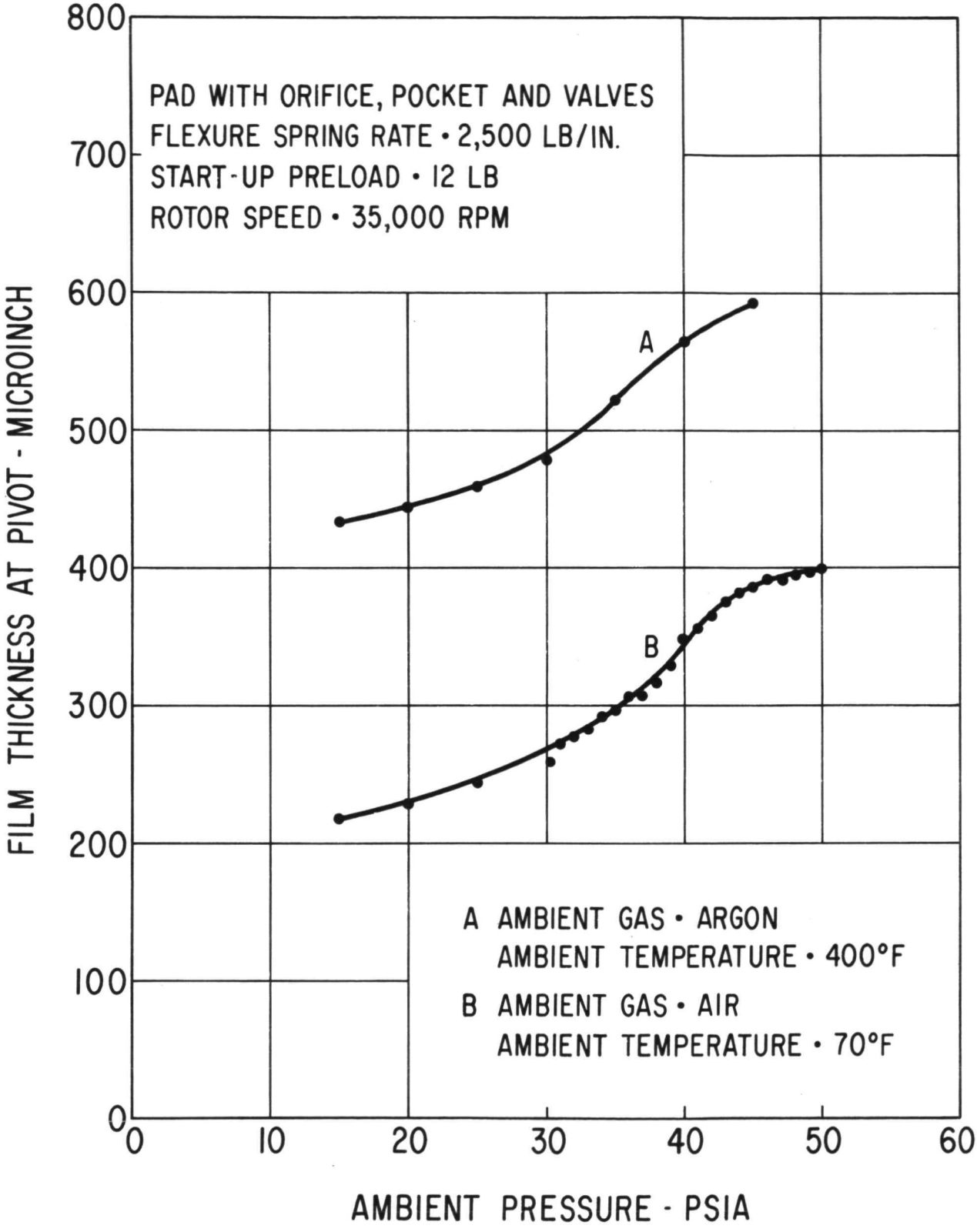

Fig. 65 Measured Hydrodynamic Performance of the Single Pivoted Pad When Mounted on the Pivot-Support Flexure

by the two capacitance sensors placed in the pad surface and axially located on each side of the pivot, is shown in Figure 66. The start of the roll motion of the pad was always preceded by a rapid increase in synchronous pad radial motions. Once started, the pad roll motion increased rapidly with increasing rotor speed, leading quickly to physical contact between the axial pad edges and the saft, as evidenced by wear patterns. No attempts were made during testing to drive the rotor through the frequency range of pad roll motions.

The onset of pad instabilities depended noticeably upon such hydrodynamic operating variables as ambient pressure, rotor speed, and pad load, but could not be directly related to pivot film thickness. Some hysteresis and considerable nonlinearity in the instability threshold as a function of rotor speed was also observed. For example: If, at a constant pad load, instability was induced by increasing the rotor speed beyond the stability limit, subsequent reduction in rotor speed would generally not stabilize the motion until a speed lower than the original instability threshold was reached (hysteresis). On the other hand, with very gradual speed increases, it was sometimes possible to exceed the lowest threshold limit by considerable amounts. In Figure 67, which indicates the stable and unstable operating regions for the dead-weight-loaded pad, only the lowest observed threshold limits are shown for the three ambient pressure conditions investigated.

It should also be noted here that under hydrodynamic with jacking gas (hybrid) operating conditions, no pad roll instabilities were observed in the tested speed region between 15,000 and 40,000 rpm, even though the pivot film thickness exceeded 0.001 inch.

The instability threshold points plotted on Figure 64, for the flexure-supported pad, indicate that stable operation was maintained to higher rotational speeds than would be predicted from the stability threshold curves on Figure 67. However, there is an important difference between the data of Figures 64 and 67. The data on Figure 67 (as well as the instability points plotted on Figures 60, 61 and 62) were obtained during the single-pad load capacity tests. As previously indicated, these tests were conducted by dead-weight (massive) loading of the pad. Furthermore, as previously mentioned, the data on Figure 67 represent the lowest observed instability thresholds. On numberous occasions during the dead-weight-loaded tests, the Figure 67 threshold limits were exceeded by significant amounts. If the lower threshold limits plotted on Figure 67 indeed reflect the influence of the massive pad loading technique, then the instability threshold points plotted on Figure 64 (where the pad is mounted on a flexure in a manner similar to the actual BRU configuration) should more accurately represent the single pad stability limits for the BRU design configuration.

One final test result relative to the roll instability was obtained. A question was raised as to whether the roll instability might be the result of excessive pad restraint due to mechanical interference in the pivot region, or perhaps due to the capacitance probe lead wires. Accordingly, a test run was made with increased clearance between the pivot stem shoulder and the pivot-stem retaining nut. Additionally, two of the three lead wires to

ROTATIONAL SPEED · 35,400 RPM
PAD LOAD · APPROXIMATELY 8 LB
VERTICAL SCALE · ONE MAJOR DIVISION APPROXIMATELY 0.000250 IN.
HORIZONTAL SCALE · ONE MAJOR DIVISION 2 MILLISECONDS
TWO CAPACITANCE SENSORS MOUNTED ON EITHER SIDE OF PIVOT. AXIAL DISTANCE BETWEEN SENSORS 0.88 IN.

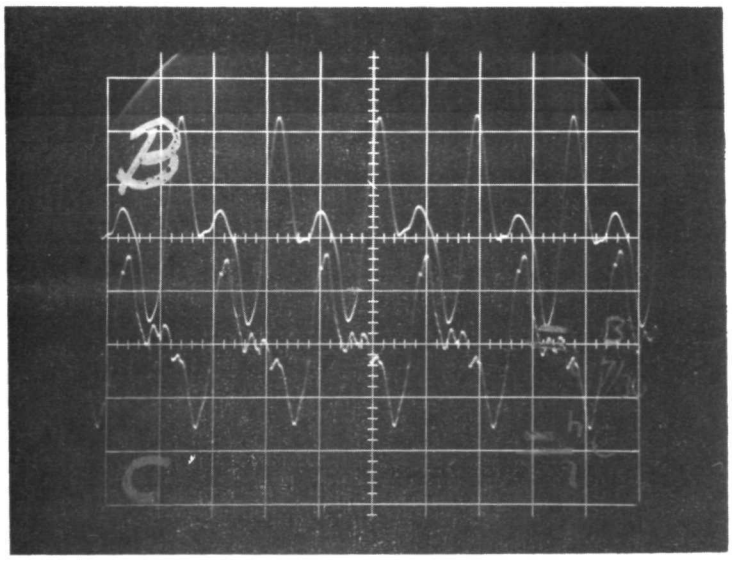

Fig. 66 Oscilloscope Traces Showing Hydrodynamic Instability of the Single Pivoted Pad in the Roll Direction

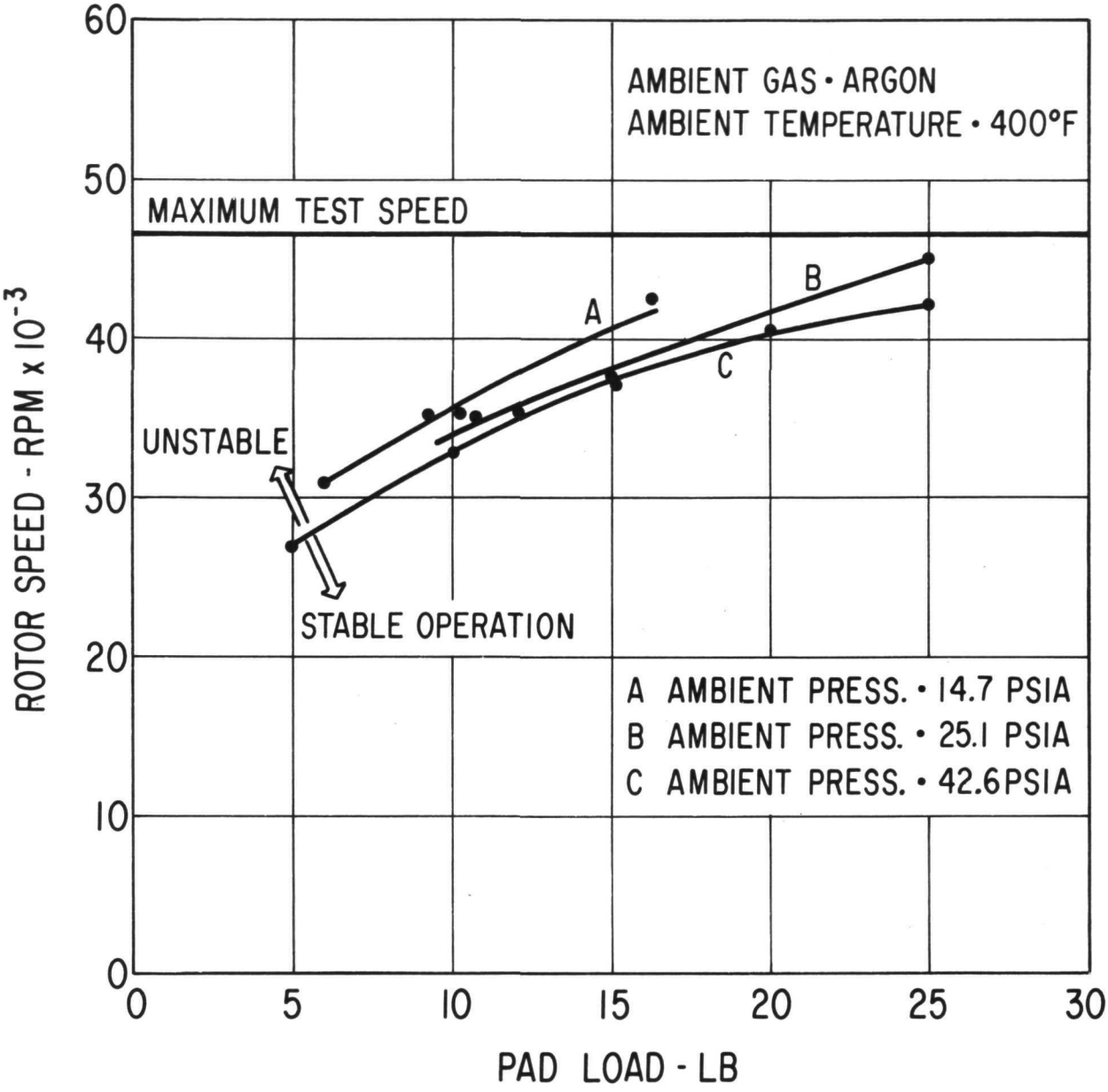

Fig. 67 Measured Hydrodynamic Instability Threshold Curves for the Single Pivoted Pad (Minimum Threshold Values Obtained During Dead-Weight Load Capacity Testing)

the pad capacitance probes were removed. These changes did not result in any detectable shift of the instability threshold points.

MEASURED HYDROSTATIC PERFORMANCE

Film Thickness Measurements for the Single Pivoted Pad with Orifice, Orifice Recess, and Pivot Valve (no shaft rotation)

Measurements of hydrostatic film thickness as a function of pad load and ambient gas pressure are presented in Figure 68. For these tests the pad was supplied with argon at 150 psia pressure and 70°F. The pad was equipped with an orifice of 0.0135-inch diameter, an orifice recess (0.5 x 0.25 inches by 0.1 to 0.3 mils deep), and primary and secondary pivot valves. Tests conducted without the primary valve installed showed the hydrostatic performance to be unaffected. Without the secondary valve, however, the pad did not lift off the test rotor. Instability in the form of pneumatic hammer was encountered at some light pad loads (7 pounds or less) at ambient pressures of 14.7 and 25.1 psia.

Supply Gas Flow and Pressure Requirements for the Single Pivoted Pad at Various Loads and Ambient Pressures

Data was obtained for single-pad hydrostatic gas flow (argon) as a function of pad load at various ambient gas pressures and constant gas supply pressure of 150 psia (Figure 69). There is a distinct increase in flow rate at low pad loads in all three flow curves in Figure 69. This increase is believed to be associated with the effect of pivot/pivot-seat separation on the sealing of the secondary pivot valve. Increased leakage occurs when the dead weight load on the pivot stem is insufficient to balance the gas supply pressure acting against the underside of the pivot stem, thereby allowing pivot/pivot-seat separation.

The supply pressure required to achieve pad lift off is shown in Figure 70. The need for high supply pressures at loads below ten pounds shows the effect of secondary valve leakage resulting from pivot/pivot-seat separation. It is felt that venting the cavity between the secondary valve and the retaining nut might reduce the hydrostatic flow and pressure requirements at low loads.

Film Thickness for the Single Pivoted Pad, Flexure Mounted, During Hybrid Operation

Measurements of film thickness as a function of rotational speed for the single pivoted pad, mounted on the 2500 lb/in. flexure with a preload of 12 pounds (preload established at room temperature), are shown in Figure 71. The pad was hydrostatically supplied with argon at 70°F and 150 psia. The gas surrounding the pad was also argon, but at 400°F and atmospheric pressure (14.7 psia). Data was recorded for a speed range of 15,000 to 40,000 rpm.

The above operating conditions are comparable to a "hot" BRU start-up with hydrostatic "jacking" gas, followed by continued operation with the jacking gas supply left on. No difficulties were encountered, even though the pivot

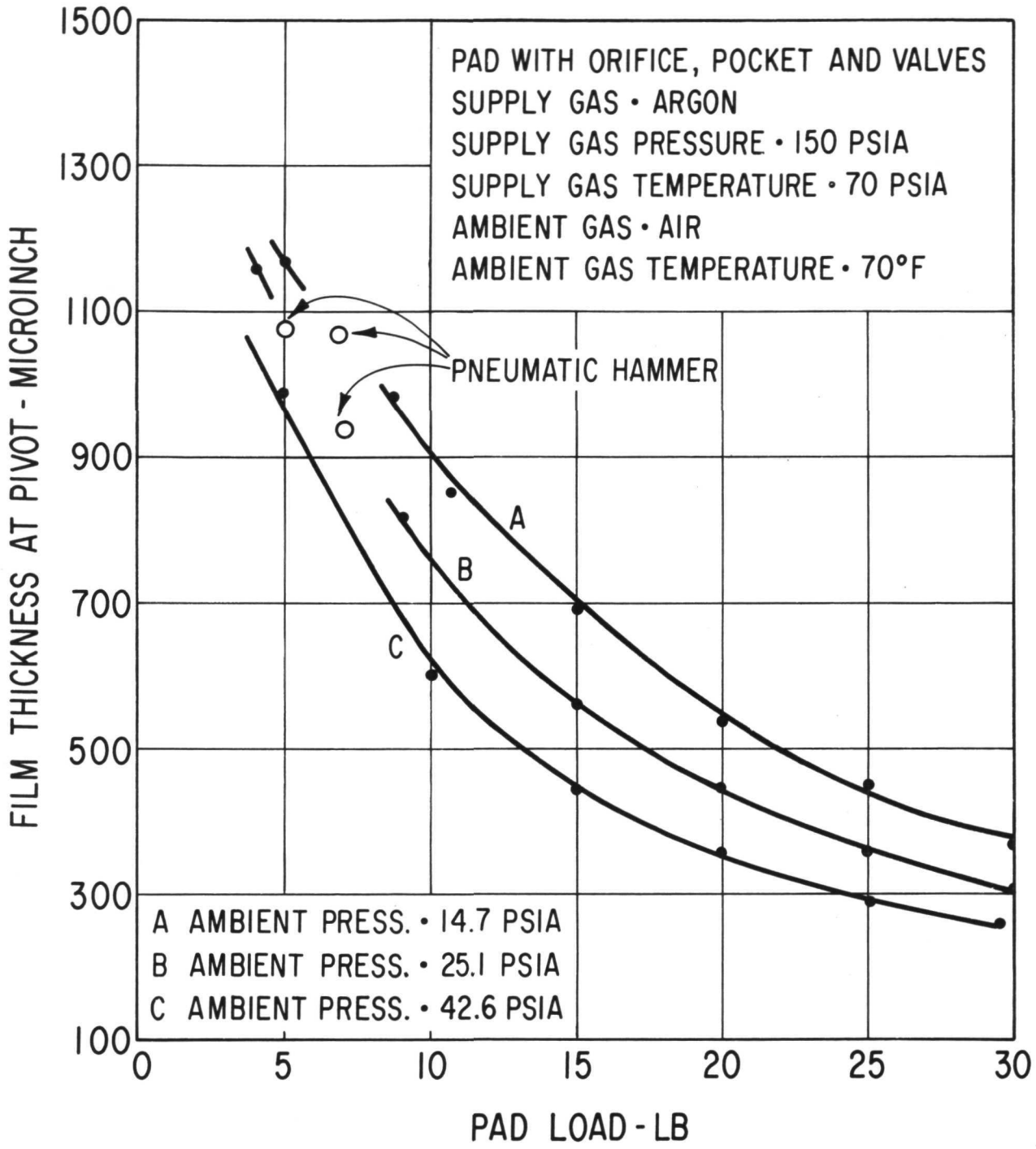

Fig. 68 Measured Hydrostatic Load Capacity of the Single Pivoted Pad

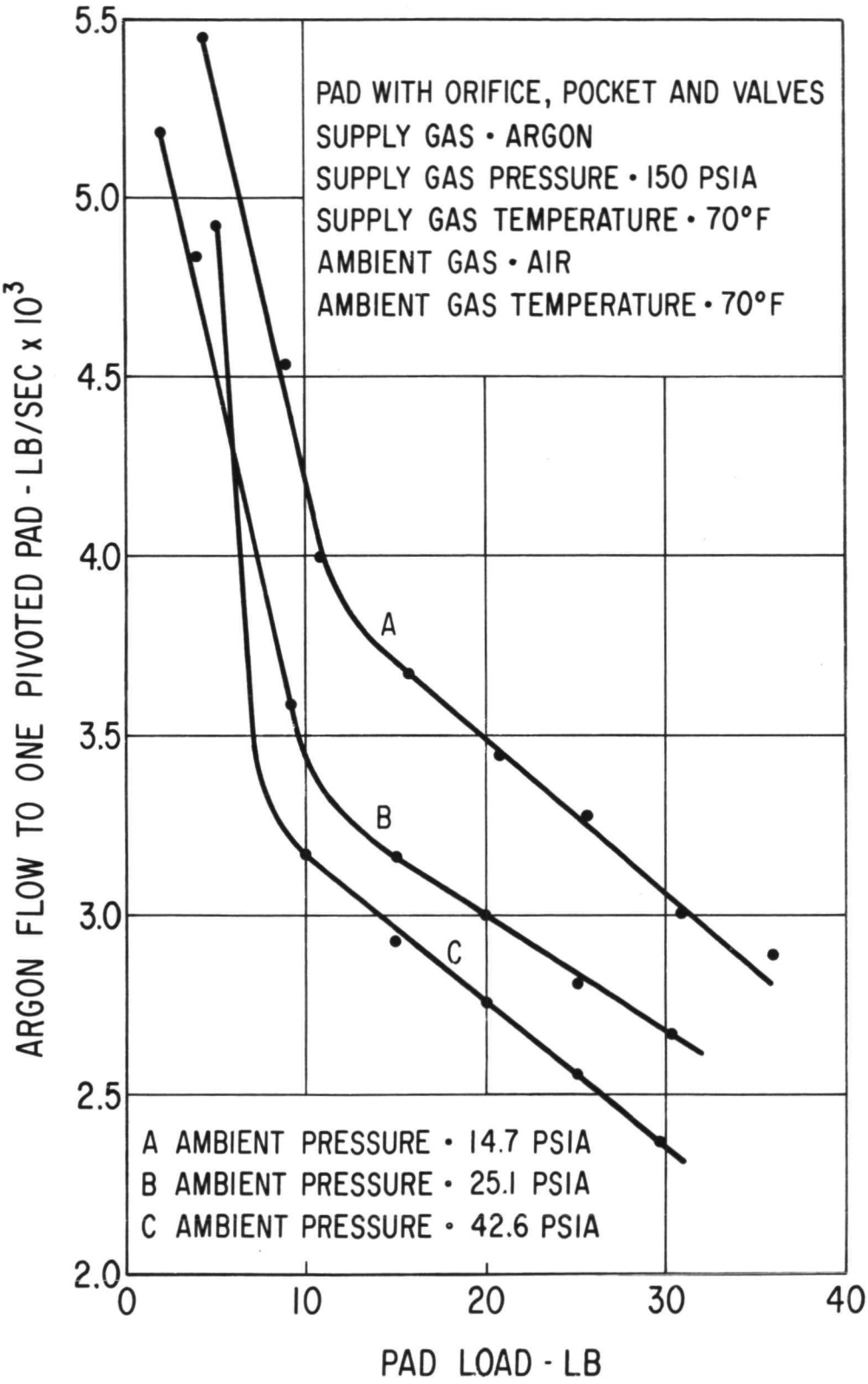

Fig. 69 Measured Hydrostatic Flow Rate for the Single Pivoted Pad

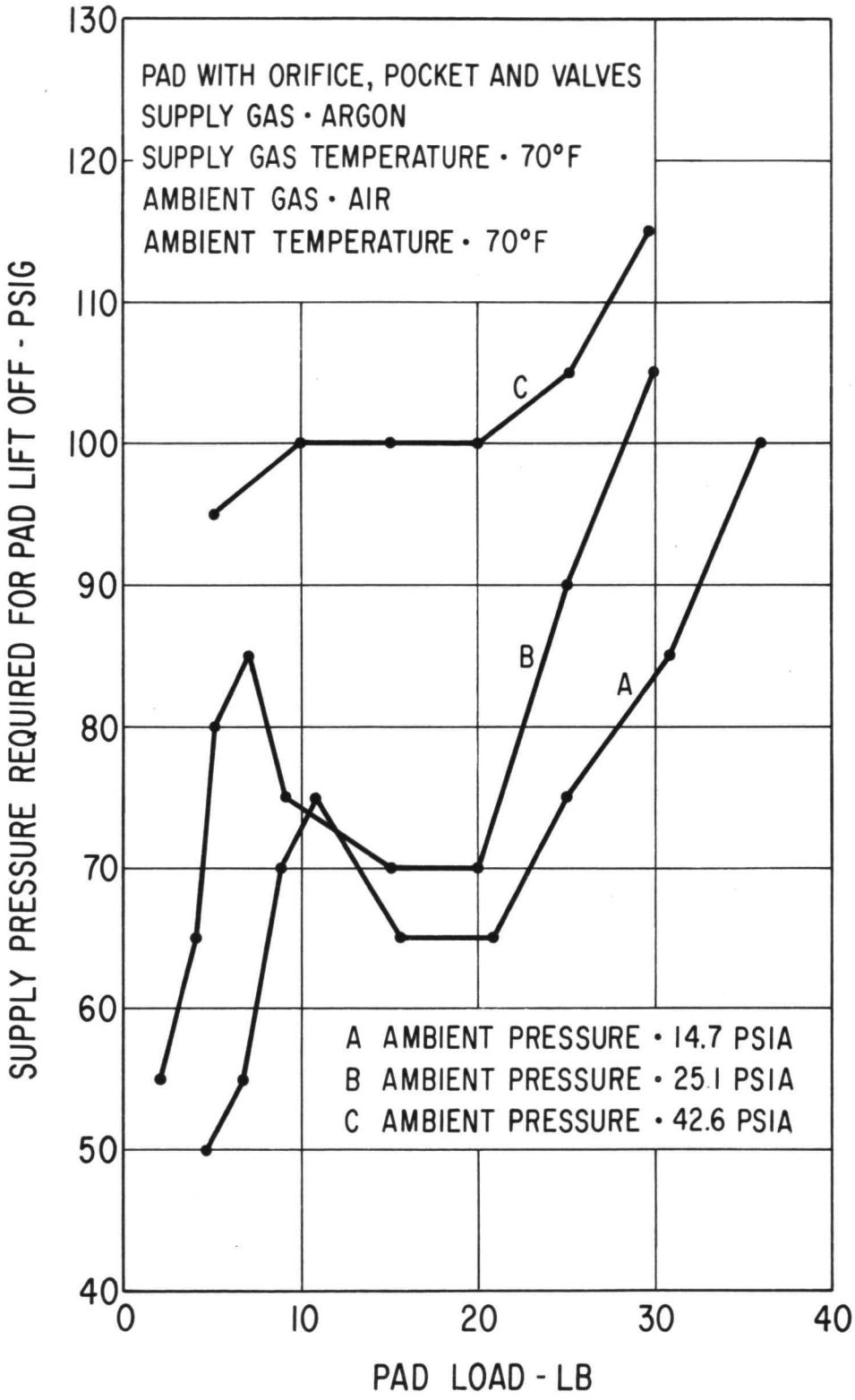

Fig. 70 Measured Supply Pressure Required for Hydrostatic Lift-Off of the Single Pivoted Pad

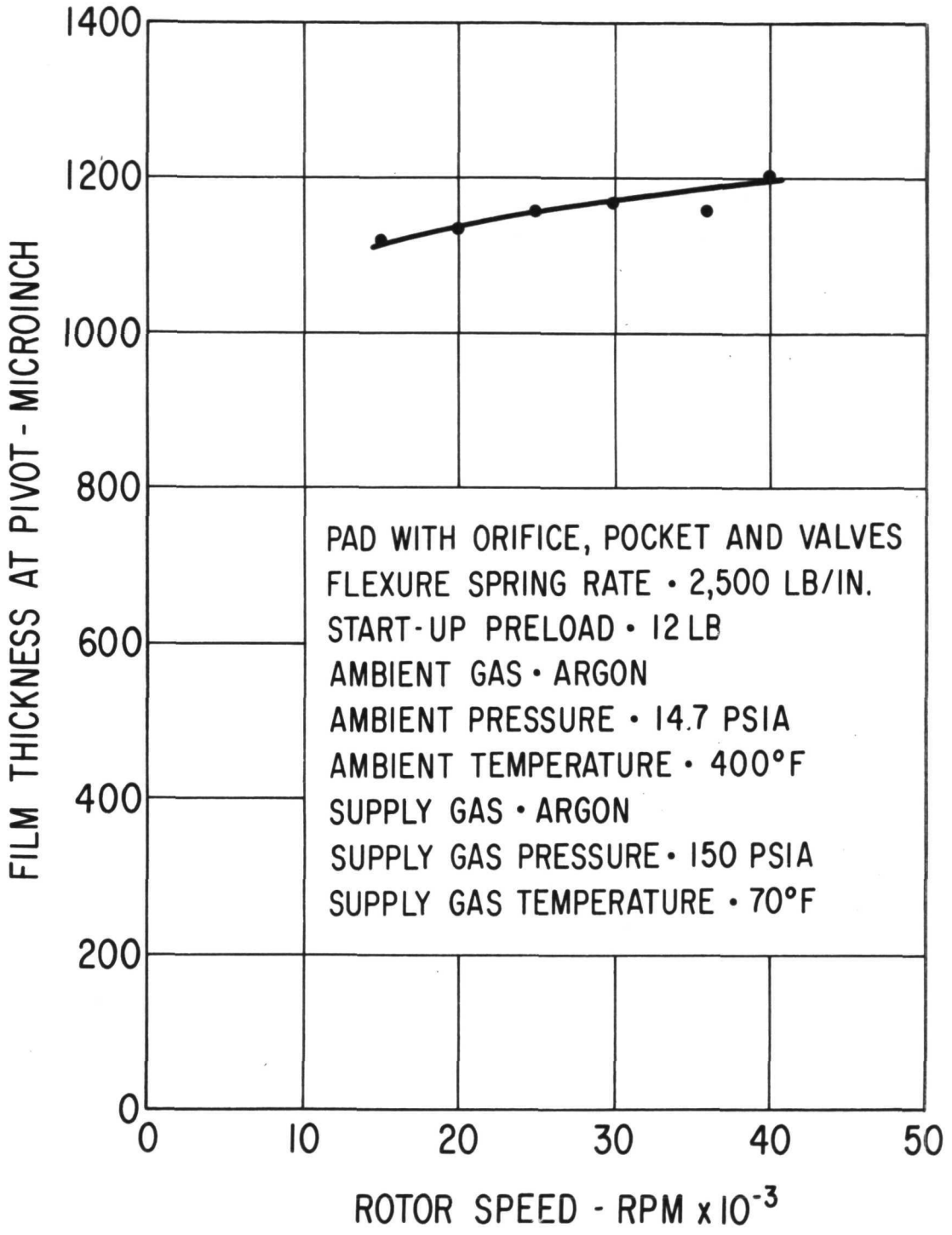

Fig. 71 Measured Hybrid Performance of the Single Pivoted Pad at 14.7 psia Ambient Pressure

film thickness under hybrid operating conditions is approximately equal to the sum of the hydrostatic and hydrodynamic film thickness obtained separately.

EXPERIMENTAL PERFORMANCE OF SINGLE TILTING PAD JOURNAL BEARING WITH "CRUCIFORM" FLEXURE MOUNT

In addition to conducting tests on the pivoted-pad journal bearing with a non-conforming pivot, tests were also conducted on a single-pad journal bearing with a flexure support instead of a pivot.

Although there exists considerable successful experience with the use of pivots in tilting-pad journal bearings, there still remains several inherent characteristics of pivots which give rise to questions about the long-term reliability of this type of bearing. The question of pivot reliability is further compounded for the BRU because of the present requirement for hydrostatic lift-off of each pad during BRU start-up and shutdown. The hydrostatic requirement adds mechanical complexity to the nonconforming pivot assembly in the form of a secondary valve. For the conforming pivot, the hydrostatic capability requires (1) attainment and maintainment of precision-lapped surfaces between matched pairs of pivot and pivot seats, and (2) interruption of these precision surfaces with a hydrostatic feed hole.

Recognizing the inherent and the particular uncertainties of the BRU pivot designs (as mentioned above and in the previous sections of this report), MTI conceived a novel flexure arrangement which eliminates the pivot elements, but still permits the necessary roll, pitch and yaw degrees of freedom of the tilting pad. The flexure arrangement is herein called the "cruciform" support. A photograph of the individual cruciform and pad parts (excluding the gas supply line for the hydrostatic lift-off bearing) is shown in Figure 72. Figure 73 is a photograph of the assembled cruciform-supported test pad.

The cruciform support consists of two orthogonal flexures with low stiffness in the pitch, roll and yaw directions of the individual tilting pad and high stiffness in the radial direction. The pad/cruciform assembly can, be mounted on a radial flexure in the same manner currently used in the BRU for the pivot-supported pads.

The cruciform-supported test pad was subjected to both hydrodynamic and hydrostatic tests in argon at ambient pressure and temperature conditions representative of 3.0, 6.0 and 10.5 KW (e) BRU power generating levels. The intrinsic feasibility of the cruciform as a replacement for the pivot/pivot-seat arrangement was determined by comparing the above test results to test results obtained from the pivot-supported single-pad tests discussed in the preceding section.

Because of the high cost of the He-Xe gas mixture, all testing was done using argon gas. Since the viscosity of argon is lower than that of He-Xe, the measured values of hydrodynamic film thickness in argon are lower than would be expected in He-Xe. Under ideal pad geometry conditions (i.e., neglecting hydrostatic orfice and orifice recess effects), film thickness values in He-Xe would be 8 to 14 percent higher, depending on pad load and ambient pressure, than those obtained in argon.

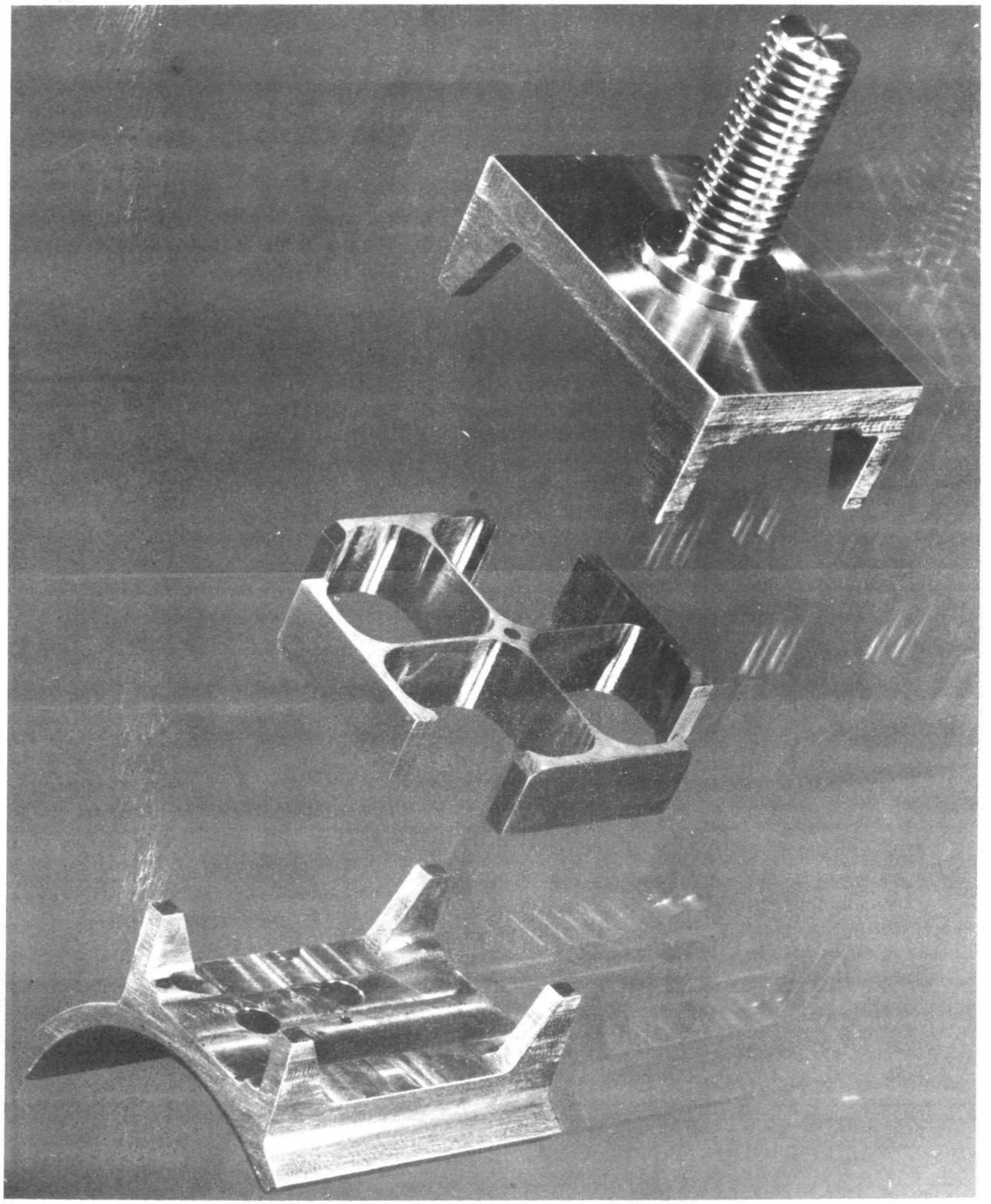

Fig. 72 Major Parts for Cruciform-Supported Test Pad

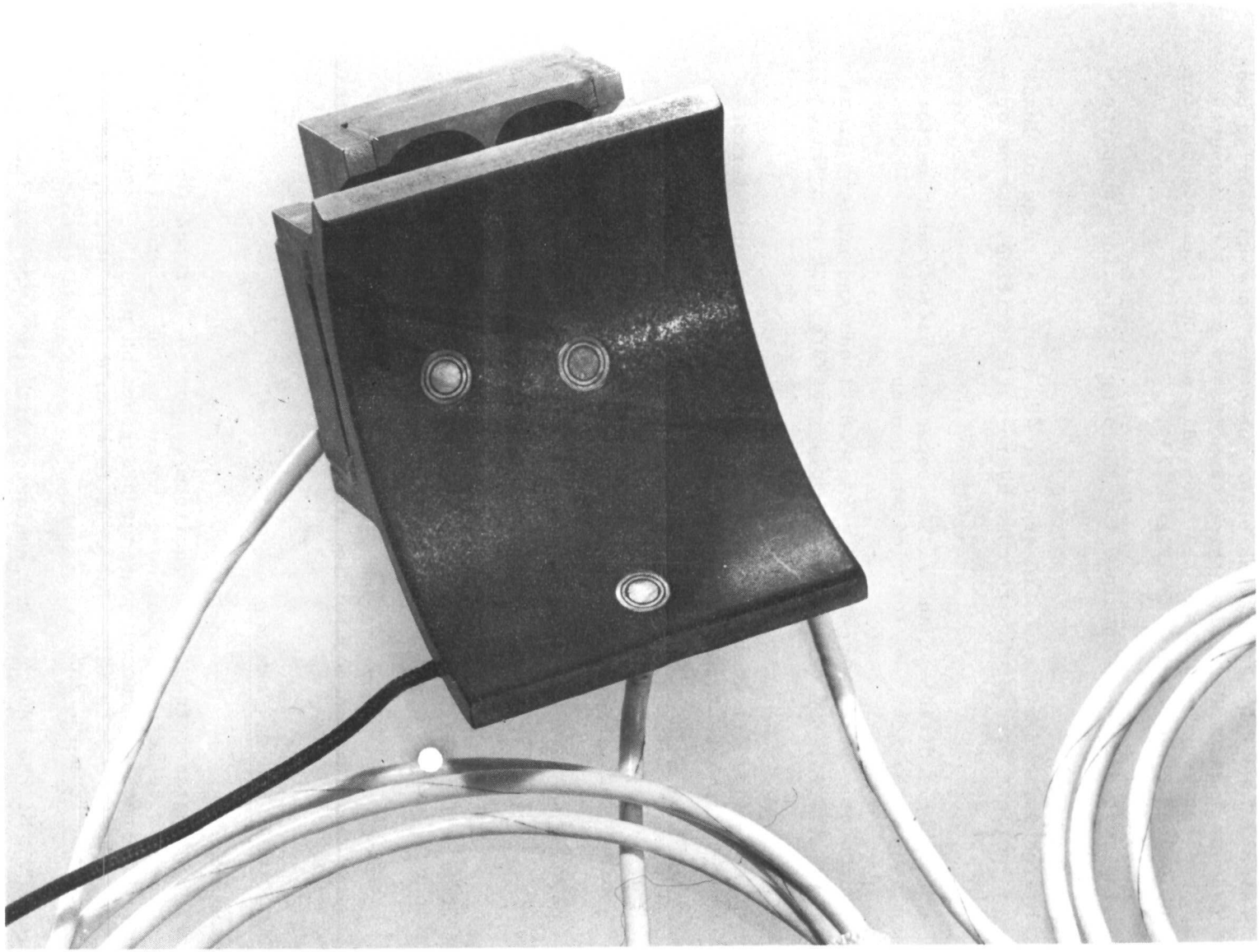

Fig. 73 View of Cruciform-Supported Test Pad in Assembled Configuration

The test program was performed using one cruciform-supported journal bearing pad. The geometry and dimensions of the bearing surface remained the same as designed (and tested) for the pivot-supported back-up bearing pads. The test pad was instrumented with three capacitance probes to measure film thickness between the pad and test journal, and one thermocouple for measurement of pad temperature (see Figure 73).

The following test data were obtained for the single cruciform-supported test pad:

a) hydrodynamic performance in argon at 400°F over a range of loads and ambient pressures with open hydrostatic orifice, but no orifice recess

b) effect of addition of an orifice recess on hydrodynamic performance of the test pad (orifice still open)

c) hydrostatic performance over a range of loads and ambient pressures for a fixed hydrostatic supply pressure, but no orifice recess

d) effect of addition of an orifice recess on hydrostatic performance of the test pad

e) performance of the pad when mounted on a radial flexure and operating in the hybrid mode (hydrostatic gas turned on and journal rotating)

f) performance of the pad when mounted on a radial flexure and operating in the hydrodynamic mode with open orifice.

The term "open orifice", as used above, means that the inlet side of the hydrostatic orifice was open to pad ambient pressure.

The test was performed using the same test equipment that was used to test the single-pad with nonconforming pivot and described earlier in this report.

MEASURED HYDRODYNAMIC PERFORMANCE

Test Pad Geometry

The geometrical parameters of the cruciform-supported test pad (excluding orifice recess) were identical to those chosen for the reference MTI design of the BRU back-up journal bearings described on page 48, except for the pad substrate material. The cruciform, cruciform holder, and pad were constructed from IN-736X.

The performance of the test pad was evaluated with two types of interruptions in the surface of the pad:

1. An open, 0.0135-inch diameter orifice hold (no orifice recess or orifice check valve);

2. Open orifice hold plus orifice recess* (no check valve).

The above mentioned orifice and orifice recess are required elements of the hydrostatic lift-off system.

Hydrodynamic Load Capacity Tests

The hydrodynamic dead-weight load capacity tests were performed at the following conditions:

Rotor Speed	:	36,000 rpm
Ambient Gas	:	Argon
Gas Viscosity	:	0.463×10^{-8} lb-sec/in^2 (argon at 400°F)
Ambient Pressure	:	14.7, 25.1, 42.6 psia
Ambient Temperature	:	400°F

The preceding operating conditions are those of the BRU except for the ambient gas. The BRU journal bearings will actually operate in a helium-xenon gas mixture which has a viscosity of approximately 0.53×10^{-8} lb-sec/in.^{2} at 400°F. When operating in the He-Xe mixture, theory predicts that the bearing film thickness values will be 8 to 14 percent greater, depending on the particular values of pad load and ambient pressure, than would be obtained in argon.

Figure 74 shows measured hydrodynamic film thickness values at the pivot point of the dead-weight-loaded test pad for the surface conditions of open hydrostatic orifice, but no orifice recess. The three curves shown in Figure 74 are for 14.7, 25.1 and 42.6 psia ambient pressure conditions, corresponding to BRU operation at 3.0, 6.0, and 10.5KWe, respectively.

Figure 75 shows similar hydrodynamic dead-weight load capacity results for the test pad with both open orifice and orifice recess interruptions in the pad surface.

The test results shown in Figures 74 and 75 are comparable to those previously reported for the single pivot-supported pad with open orifice only and with open orifice plus orifice recess. However, at high pad loads (15 to 25 pounds), the measured pivot-point film thickness for the cruciform-supported pad appears to be slightly smaller than for the pivot-support pad. This is illustrated by the comparison of load capacity results at 25.1 psia shown in Figure 76.

Contrary to our experience with the pivot-supported pad, experimental operation of the single cruciform-supported pad was not curtailed at low pad loads by pad instabilities. Larger than average pad vibrations were observed in two narrow speed regions, around 34,000 and 41,000 rpm. However, the test instrumentation indicated that the pad was following the

* The orifice recess was approximately 0.030-inches wide by 0.20-inches long (the 0.20-inch dimension being in the direction of shaft rotation) by 0.0001 to 0.0003 inches deep.

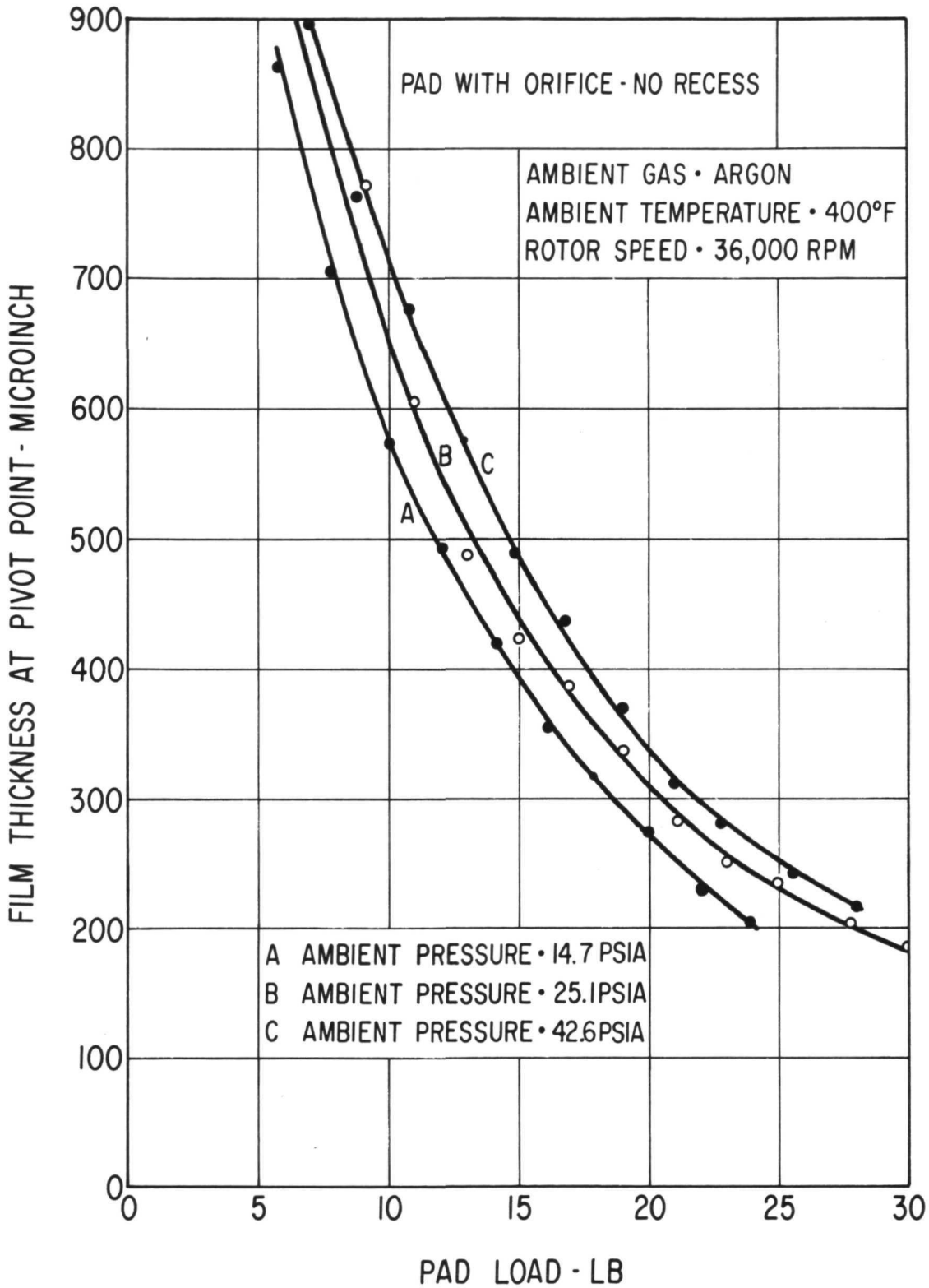

Fig. 74 Measured Hydrodynamic Film Thickness Versus Load for the Cruciform-Supported Pad With Open Hydrostatic Orifice, But No Orifice Recess

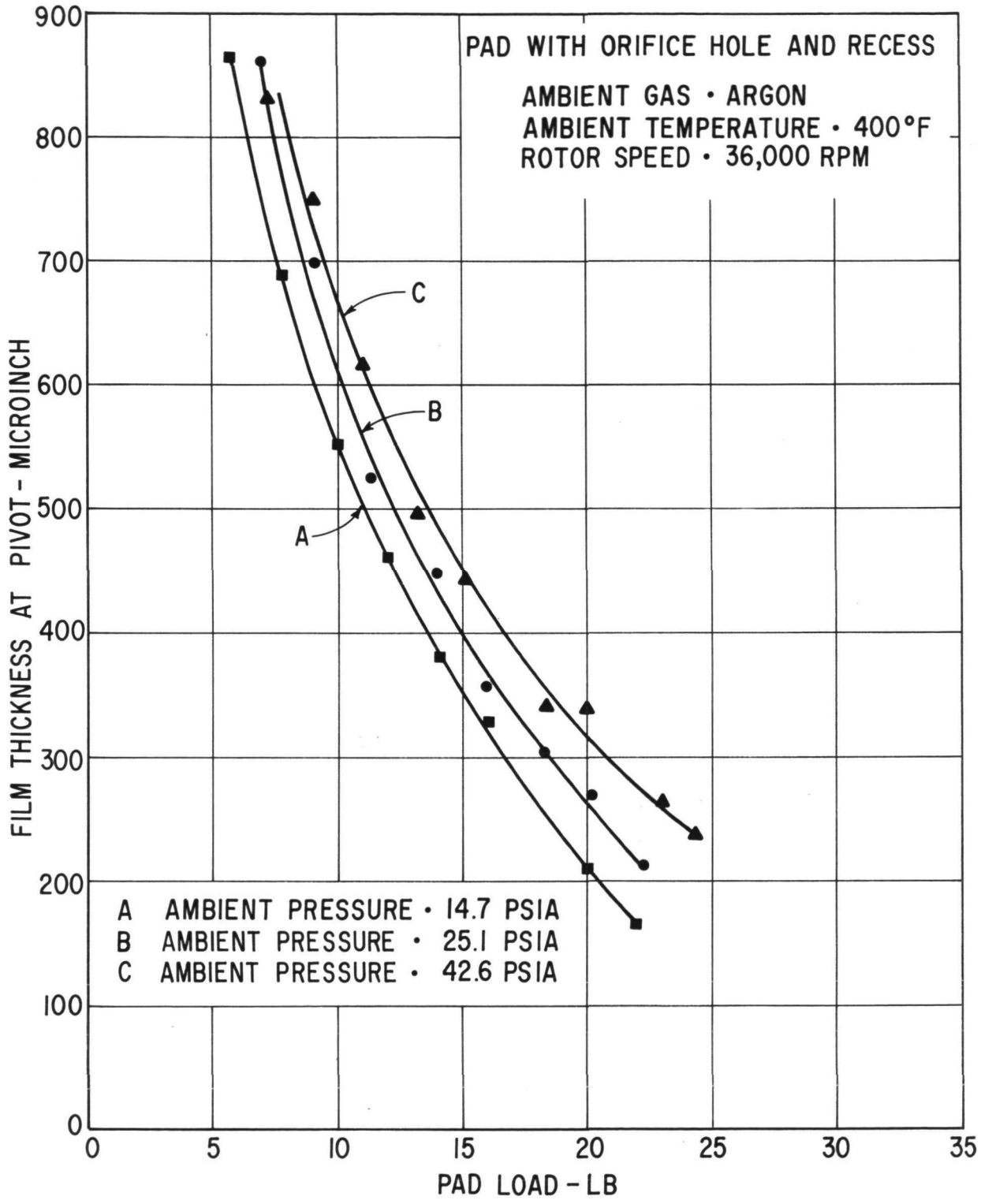

Fig. 75 Measured Hydrodynamic Film Thickness Versus Load for the Cruciform-Supported Pad With Open Hydrostatic Orifice and Orifice Recess

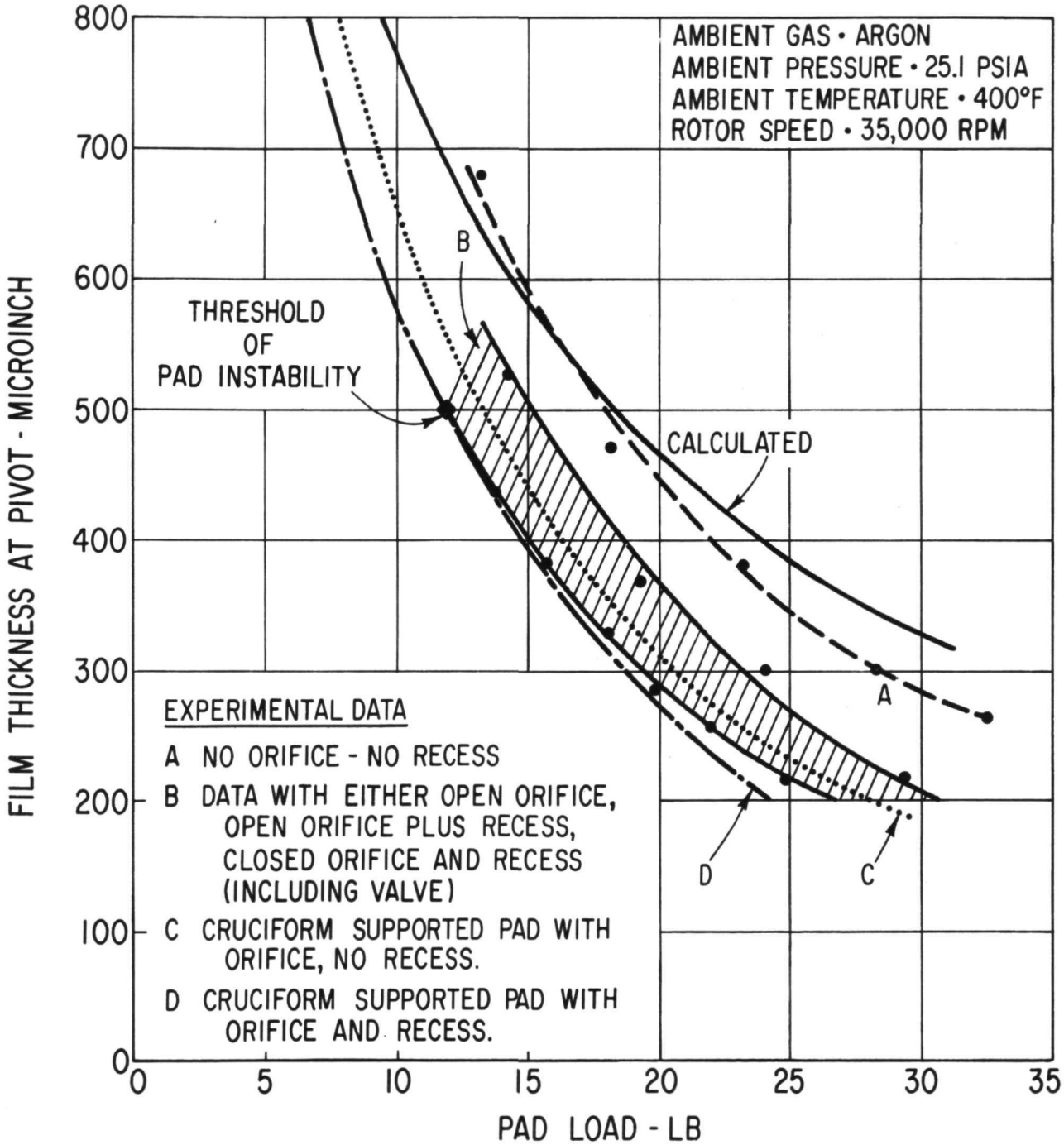

Fig. 76 Comparison of Measured Hydrodynamic Load Capacity of the Cruciform-Supported and the Pivot-Supported Test Pads at 25.1 psia Ambient Pressure

dynamic behavior of the ball-bearing-supported test shaft. Without the test pad in place, it was observed that the test shaft would whirl with even larger amplitudes at these particular speeds.

Hydrodynamic Performance of the Cruciform-Supported Pad Mounted on Radial Flexure

For these tests the single cruciform-supported pad was mounted on a radial flexure having a stiffness of 2,500 pounds per inch (the same flexure as was used for the nonconforming pivoted-pad tests). The pad and flexure were assembled such that the pad was preloaded against the shaft with a 12-pound preload at room temperature conditions. This value was not changed or adjusted throughout the course of the tests. Measured hydrodynamic film thickness values for the ambient pressure conditions of 14.7, 25.1 and 42.6 psia are shown plotted against rotor speed in Figure 77. Tests were conducted over the full test speed range up 46,500 rpm. No pad instabilities were observed at any time.

Comparison of the data in Figures 75 and 77 appears to suggest that the actual flexure preload at running conditions (400°F ambient) was reduced to approximately 10 pounds. Such a preload reduction could have been caused by a differential thermal expansion of 0.0008 inch between the flexure support structure in the test rig and the cruciform-supported test pad. The existence of differential thermal expansion is plausible, considering the size of the support structure and the method of heating (radiant heat).

A possible unloading effect produced by the stainless steel tubing used to supply hydrostatic gas from the bulkhead fitting in the test chamber wall to the bearing pad can be discounted. Tests performed with the tubing completely disconnected gave very nearly identical results to those shown in Figure 77.

MEASURED HYDROSTATIC PERFORMANCE

Hydrostatic Load Capacity Tests (No Rotation)

The first series of hydrostatic load capacity tests were conducted without any recess around the hydrostatic orifice. Measurements of pivot-point film thickness as a function of pad load and ambient pressure for this pad configuration are shown in Figure 78. For these tests the pad was supplied with argon at 150 psia pressure at 70°F. The pad was equipped with a single gas-supply orifice of 0.0135-inch diameter.

In this configuration it was found that the pad would suddenly lose its load carrying capacity (i.e., film collapse would suddenly occur) at high values of pad load whenever shaft rotation was started under load. Without rotation the pad could support higher loads, as indicated by the data points to the right of the lock-up threshold shown in Figure 78.

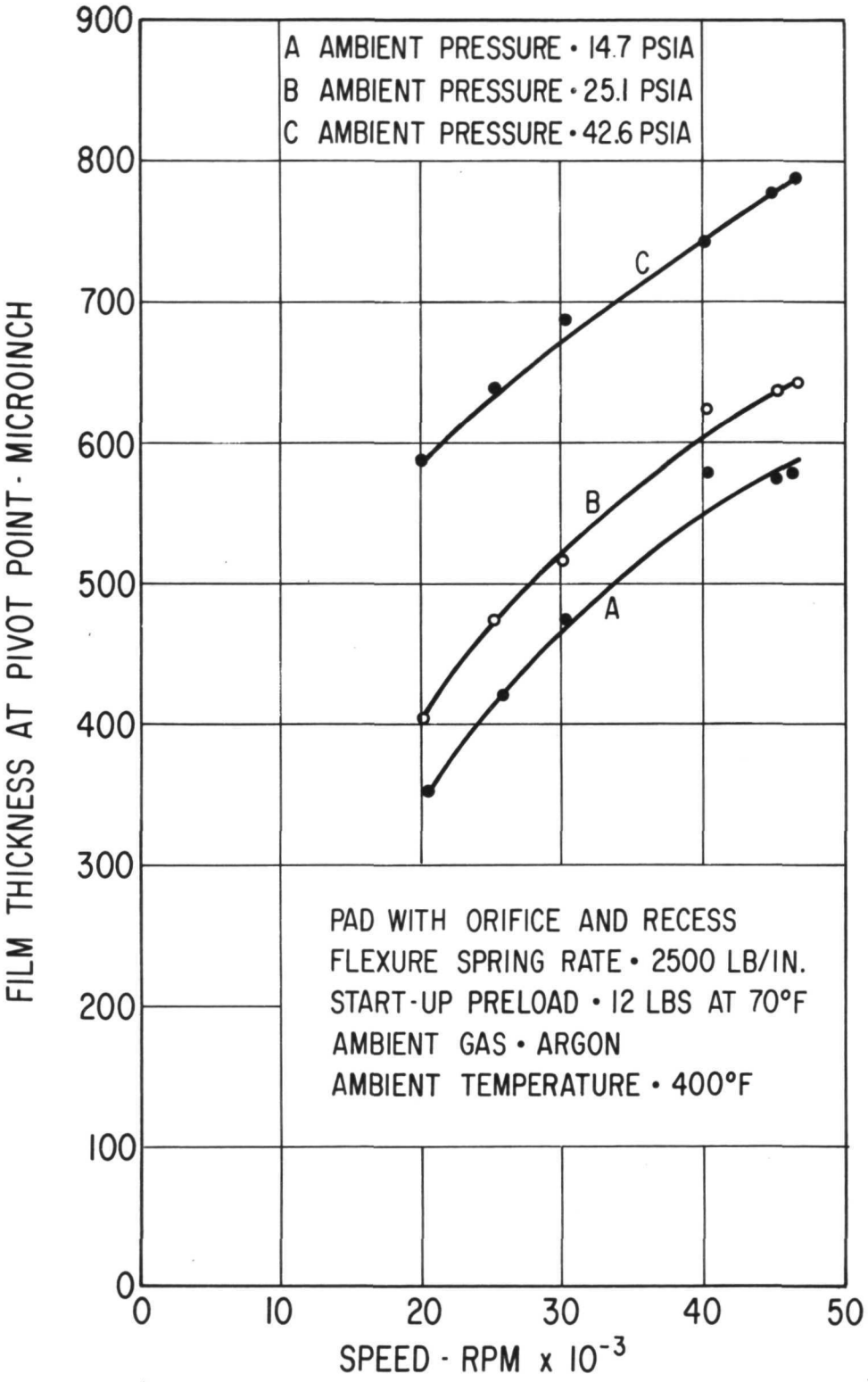

Fig. 77 Measured Hydrodynamic Film Thickness Versus Speed for the Cruciform-Supported Pad (With Open Orifice and Orifice Recess) When Mounted on a 2500 Lb/In Radial Flexure

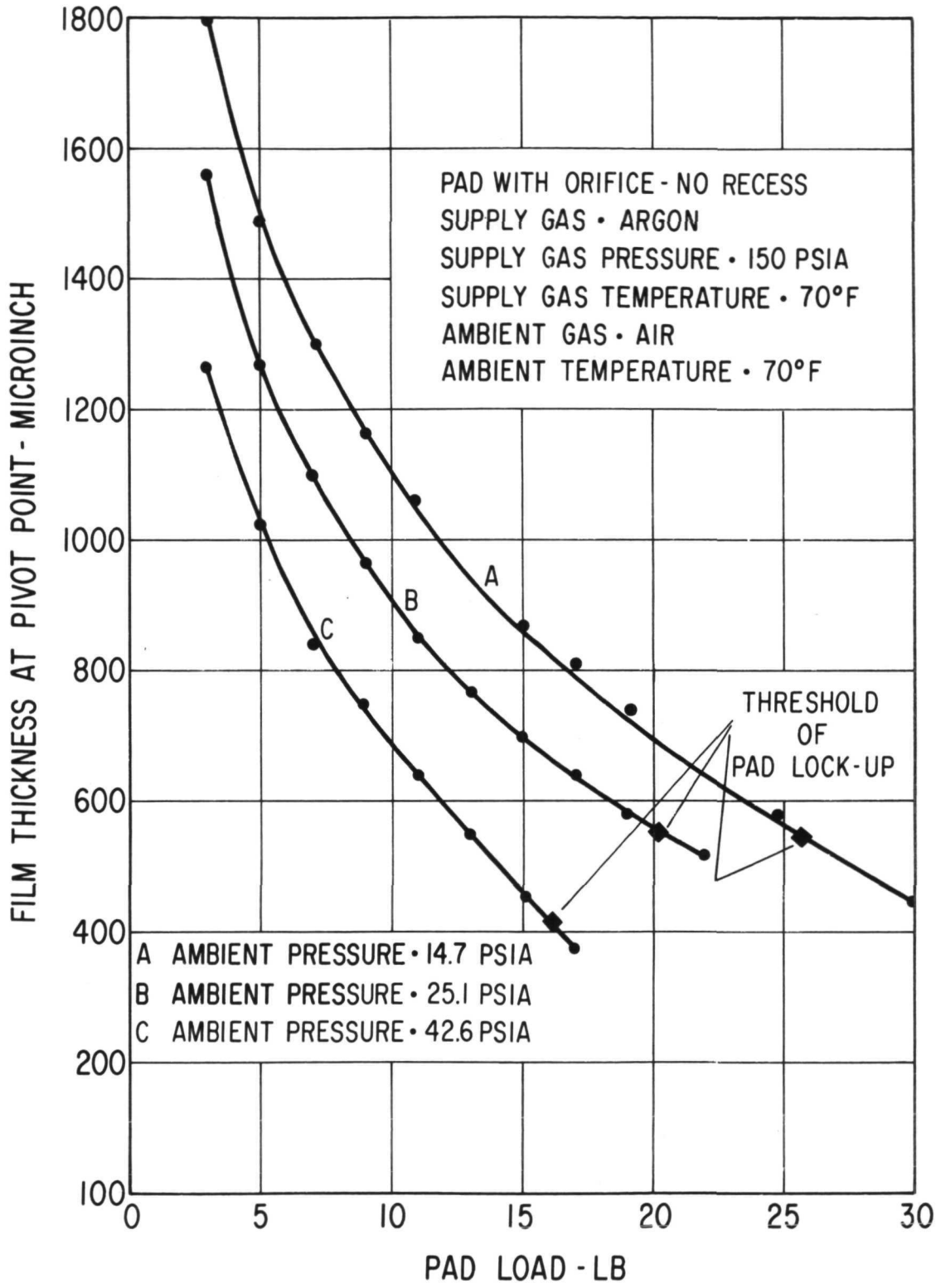

Fig. 78 Measured Hydrostatic Film Thickness Versus Load for the Cruciform-Supported Pad Without Orifice Recess

The second series of hydrostatic load capacity tests were conducted with a recess around the hydrostatic orifice. Measurements of pivot-point film thickness as a function of pad load and ambient pressure for this configuration are shown in Figure 79. Test conditions were identical to those described for the test of the pad without orifice recess. No instabilities - either pneumatic hammer or pad lock-up - were observed for this pad configuration.

Hydrostatic Flow and Pressure Requirements as a Function of Pad Load and Ambient Pressure

Gas flow data as a function of load and ambient pressure for the cruciform-supported test pad, without and with orifice recess, is shown in Figures 80 and 81, respectively. The hydrostatic supply pressure was a constant 150 psia, at a nominal temperature of 70°F.

The supply pressure required to achieve pad lift-off is shown in Figure 82 for the pad without orifice recess and in Figure 83 for the pad equipped with an orifice recess. The addition of the orifice recess has the expected effect of increasing the required supply flow for a given pad load and of decreasing the supply pressure required for lift-off under identical load conditions.

Hybrid Performance of the Cruciform-Supported Pad Mounted on a Radial Flexure

Measurements of film thickness as a function of rotational speed for the cruciform-supported test pad, mounted on a 2,500 pound per inch radial flexure at a preload value of 12 pounds (preload established at room temperature), are shown in Figure 84. The pad was hydrostatically supplied with argon at 70°F and 150 psia. The gas surrounding the pad was also argon, but at 400°F. Data was recorded for a speed range of 15,000 to 47,500 rpm and for ambient pressures of 14.7, 25.1, and 42.6 psia.

The data in Figure 84 appear to follow the hypothesis previously stated in this report, that flexure preload decreased from the original setting of 12 pounds at room temperature to approximately 10 pounds at 400° ambient. The data obtained for the flexure mounted, cruciform-supported pad is consistent in magnitude with the data obtained for the same pad with dead-weight loading, and also with all previously reported data for the single pivot-supported test pad if the assumption of reduced pad loading (10 pounds) is allowed to stand. Conversely, there is no apparent reason to expect a sharp increase in film thickness solely because the cruciform- supported pad was mounted on a radial flexure.

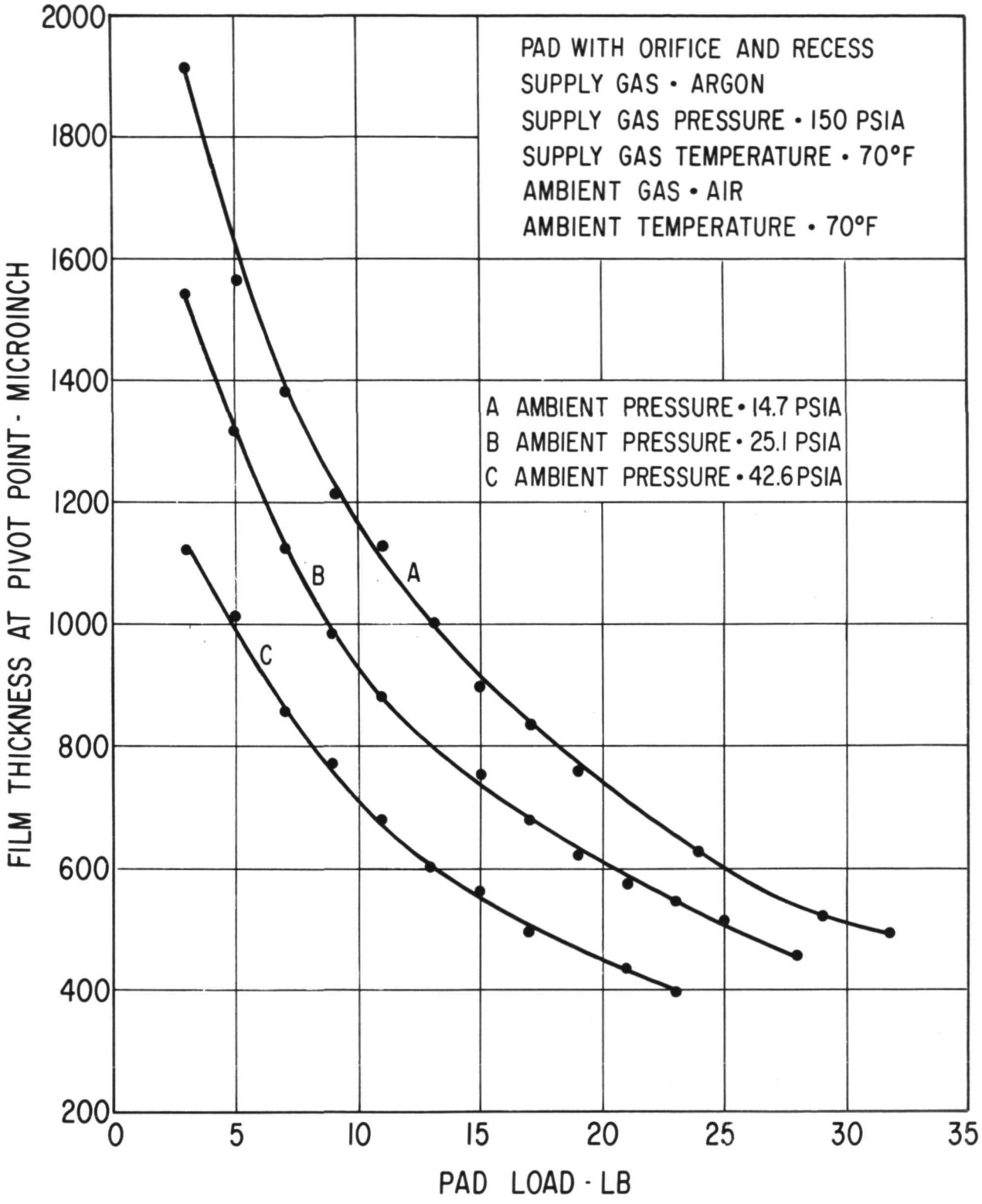

Fig. 79 Measured Hydrostatic Film Thickness Versus Load for the Cruciform-Supported Pad With Orifice Recess

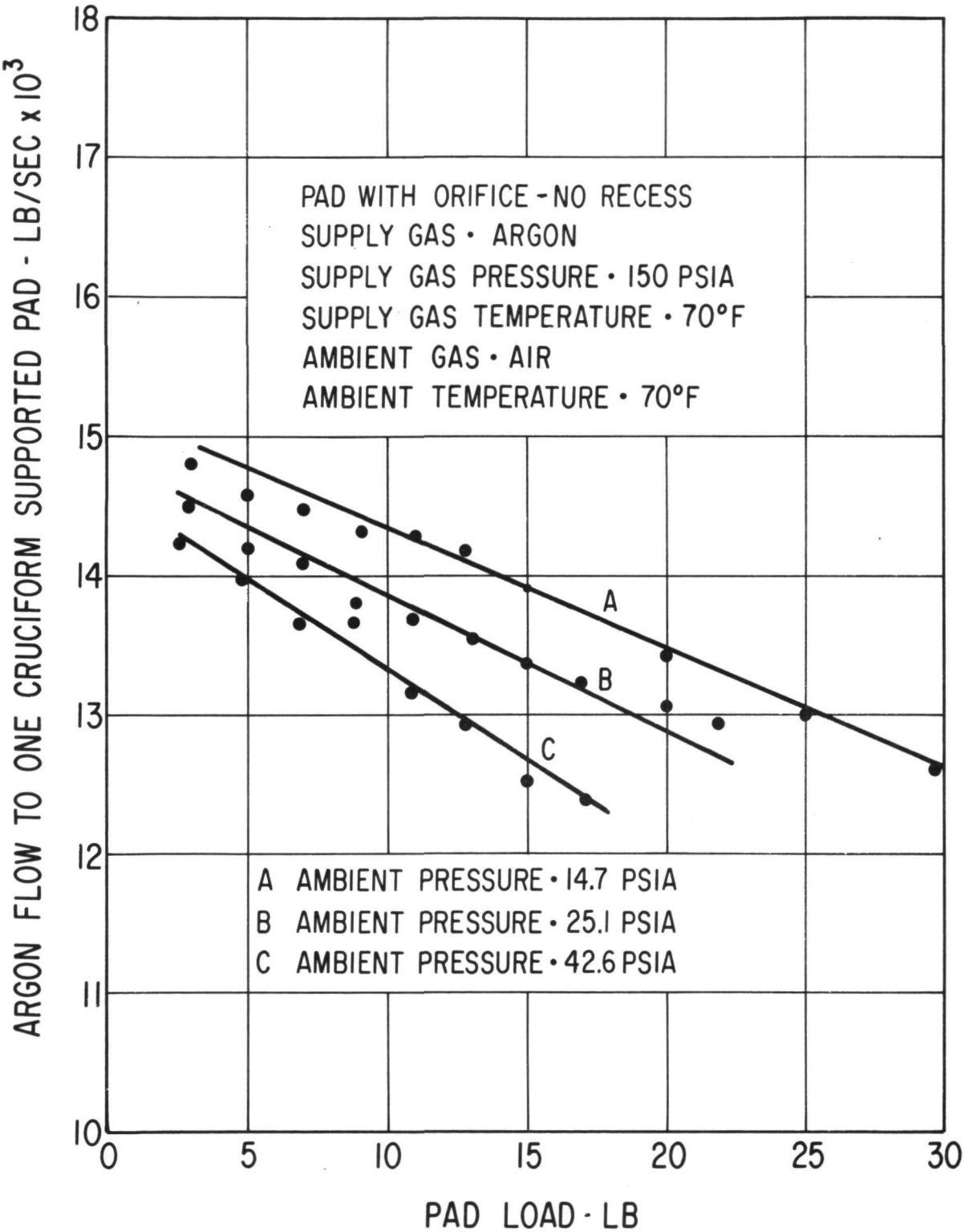

Fig. 80 Measured Hydrostatic Flow Versus Pad Load for the Cruciform-Supported Pad Without Orifice Recess

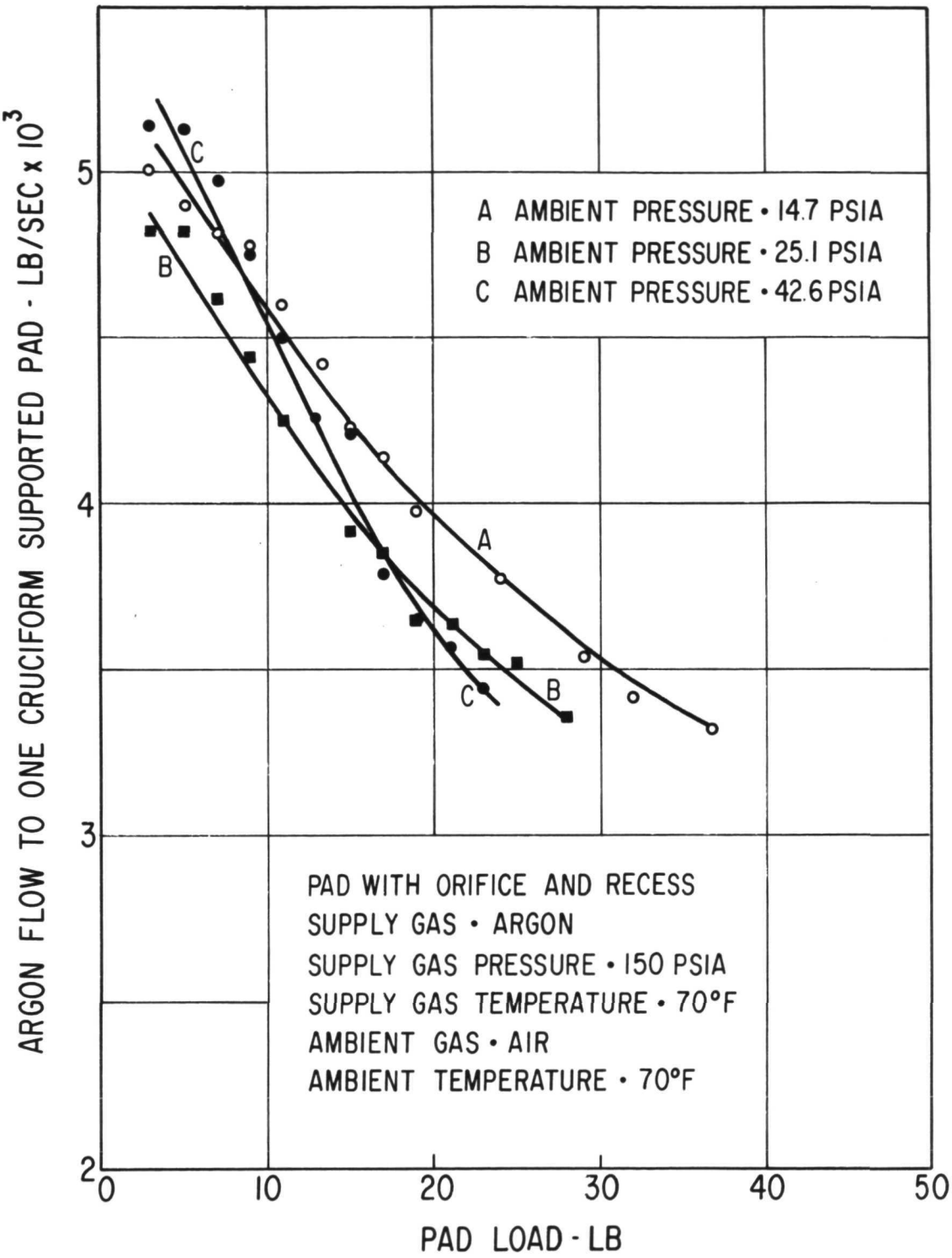

Fig. 81 Measured Hydrostatic Flow Versus Pad Load for the Cruciform-Supported Pad With Orifice Recess

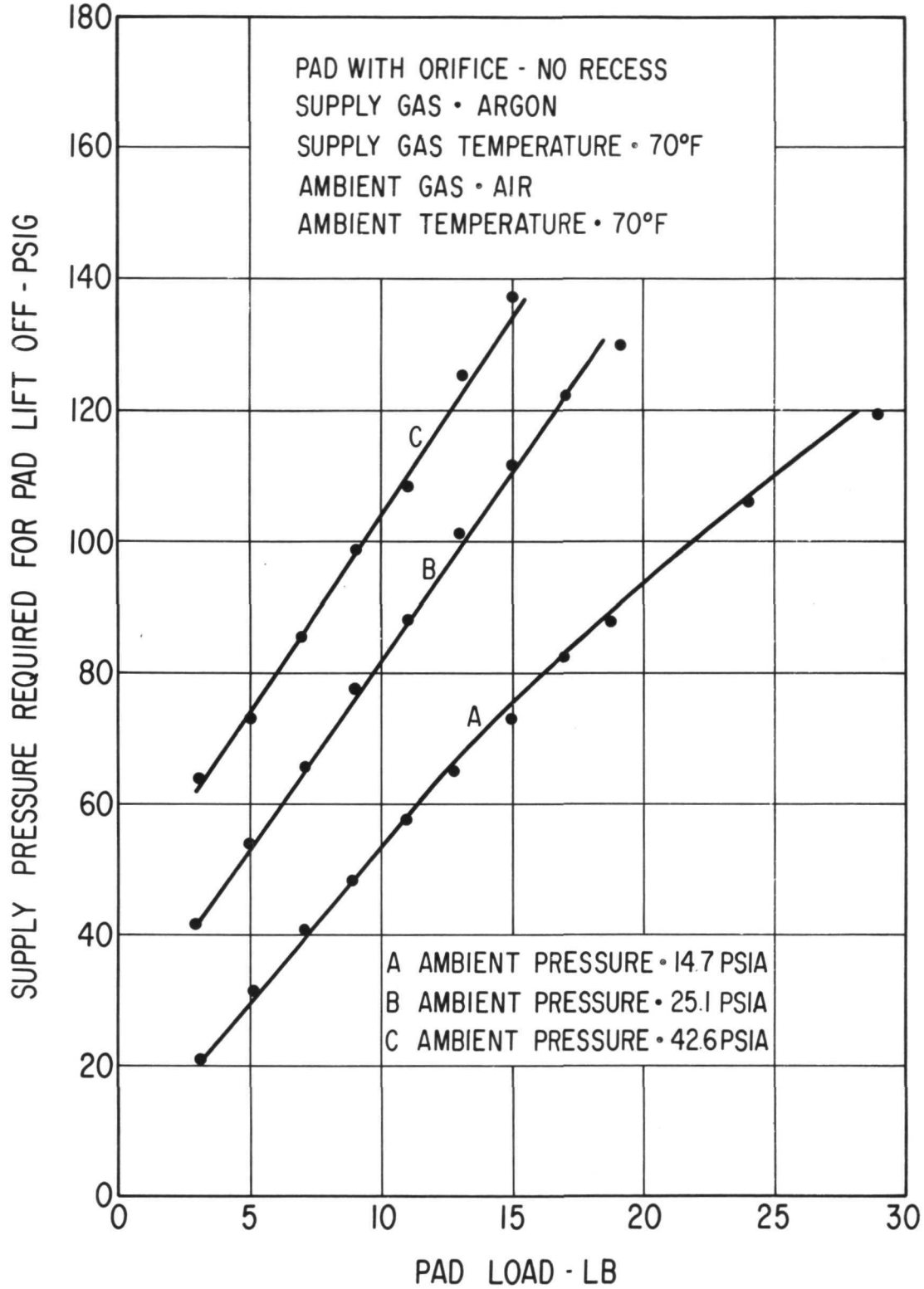

Fig. 82 Measured Supply Pressure Versus Load For Hydrostatic Lift-Off of the Cruciform-Supported Pad Without Orifice Recess

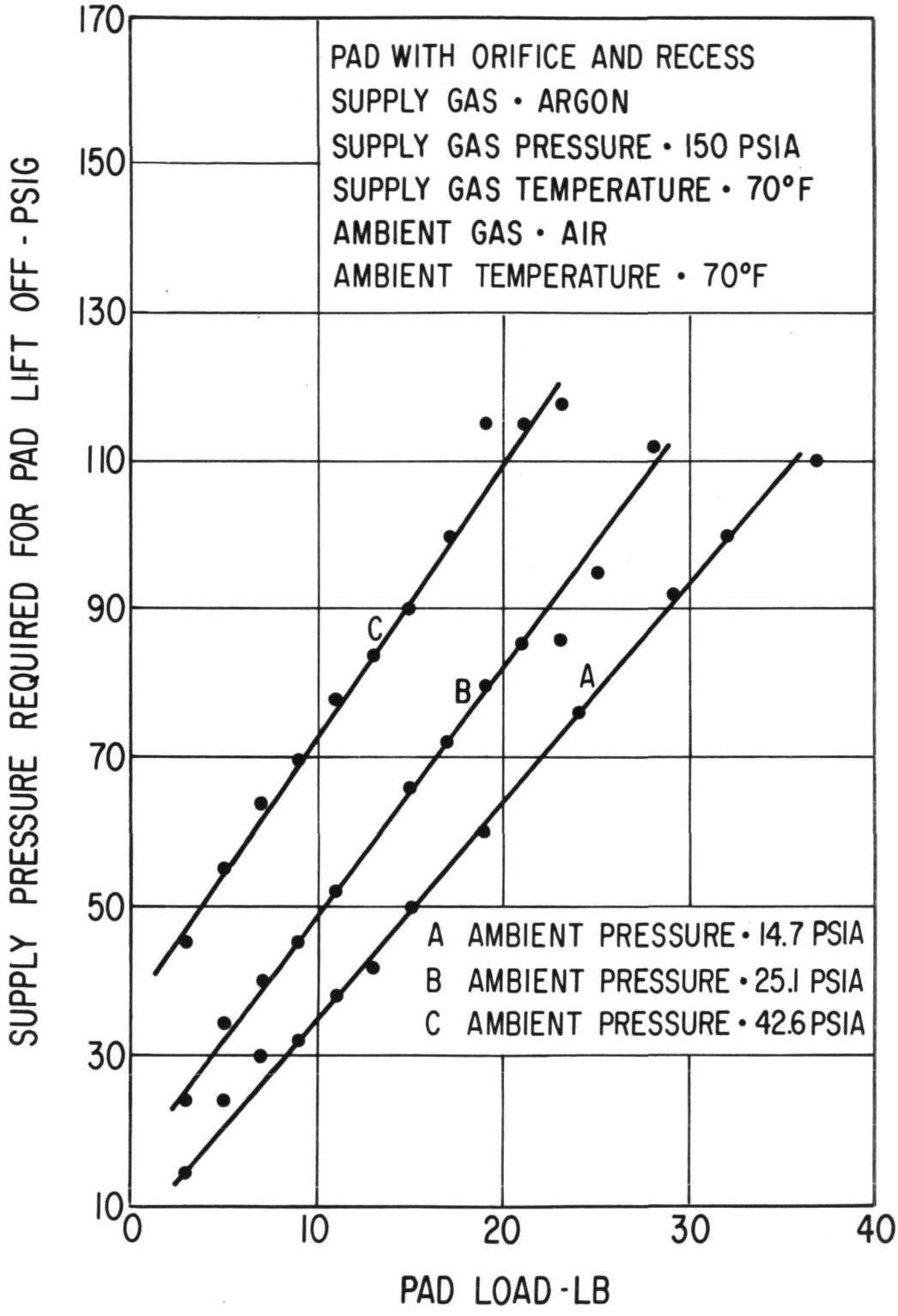

Fig. 83 Measured Supply Pressure Versus Load For Hydrostatic Lift-Off of the Cruciform-Supported Pad With Orifice Recess

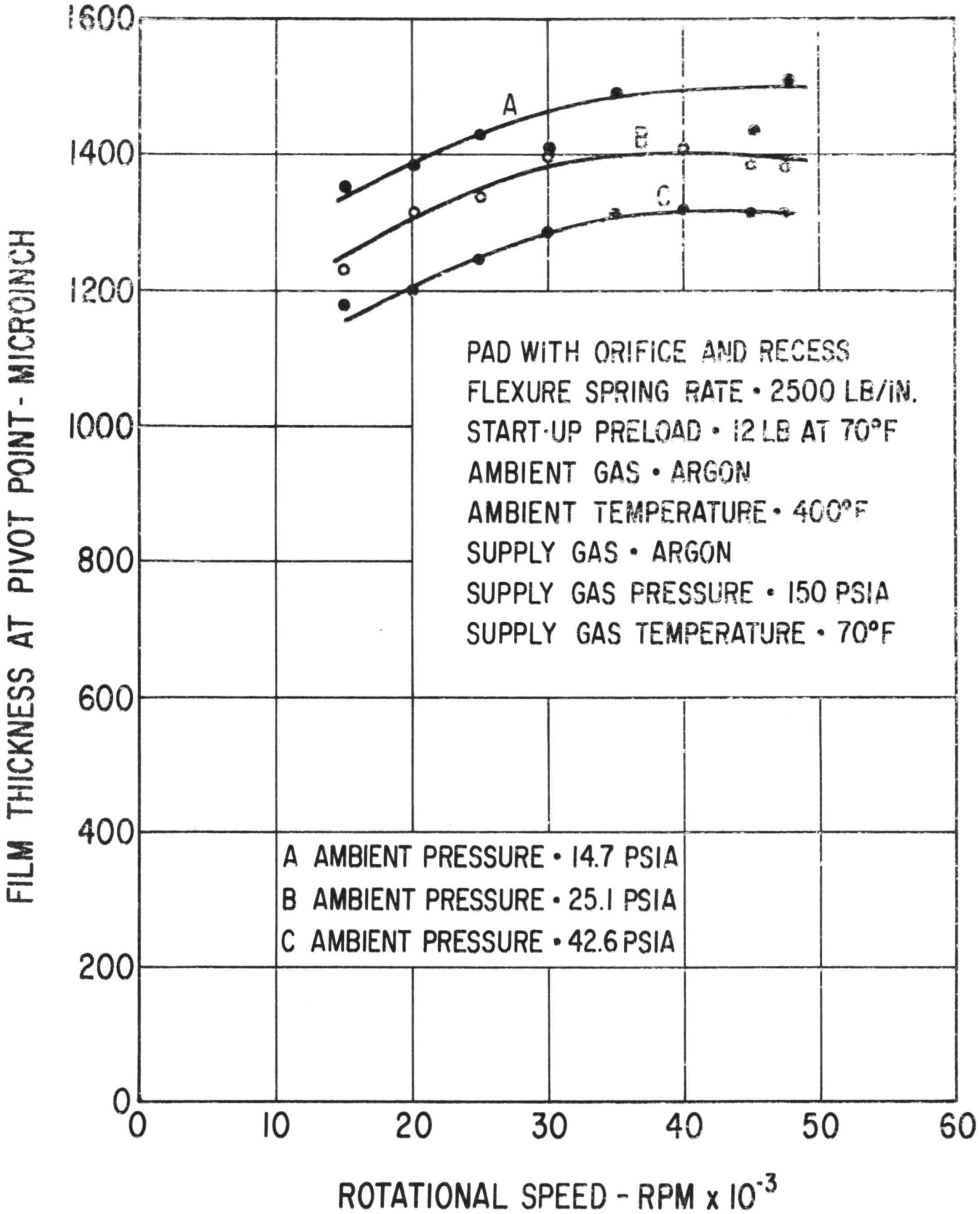

Fig. 84 Measured Hybrid Film Thickness Versus Load for the Cruciform-Supported Pad (With Orifice Recess) When Mounted on a 2500 Lb/In Radial Flexure

EXPERIMENTAL PERFORMANCE OF SINGLE TILTING PAD JOURNAL BEARING WITH MODIFIED "CRUCIFORM" FLEXURE MOUNT

As a result of the successful test experience with the single prototype "cruciform" tilting pad bearing, a modified "cruciform" mount was prepared which was suitable for testing in the BRU or BRU Dynamic Simulator. The journal bearing with the modified "cruciform" flexure mount is shown in Figures 85, 86, and 87.

The principal differences between the modified "cruciform" and the prototype "cruciform" (shown previously in Figures 72 and 73) were as follows:

1. The cruciform was electron beam welded to the pad and holder instead of using epoxy cement as had been done with the prototype bearing.

2. The stiffness of the cruciform was reduced by increasing the length and decreasing the thickness of the end beams. The calculated elastic properties of the modified cruciform are:

Radial Stiffness	$K_R = 9.1 \times 10^4$ lb/in
Pitch & Roll Stiffness	$K_p = K_r = 9.2$ in-lb/rad
Yaw Stiffness	$K_{yaw} = 21.1$ in-lb/rad

as compared to the following elastic properties of the prototype of the prototype cruciform:

Radial Stiffness	$K_R = 9.7 \times 15^4$ lb/in
Pitch & Roll Stiffness	$K_p = K_r = 24.8$ in-lb/rad
Yaw Stiffness	$K_{yaw} = 26.0$ in-lb/rad

3. The jacking gas tube was attached to the pad in a position slightly displaced from the pivot point so as to avoid bringing the tube through the center of the cruciform assembly. To avoid imposing a moment upon the pad during hydrostatic operation, a shallow pocket was placed in the pad surface directly under the pivot point. The displaced jacking gas supply was introduced near the corner of the pocket.

4. Access holes were added to the cruciform holder to allow assembly of the proximity probes and jacking gas supply tube after welding of the assembly.

5. The deflection of the cruciform flexure is limited by stops integral with the cruciform components. The stops limit the motion so that the maximum fiber stress induced due to the motion is less than 50 percent of the yield strength of the material.

6. The method of attaching the flexure beam to the cruciform holder allows for relative rotation (in yaw direction) between

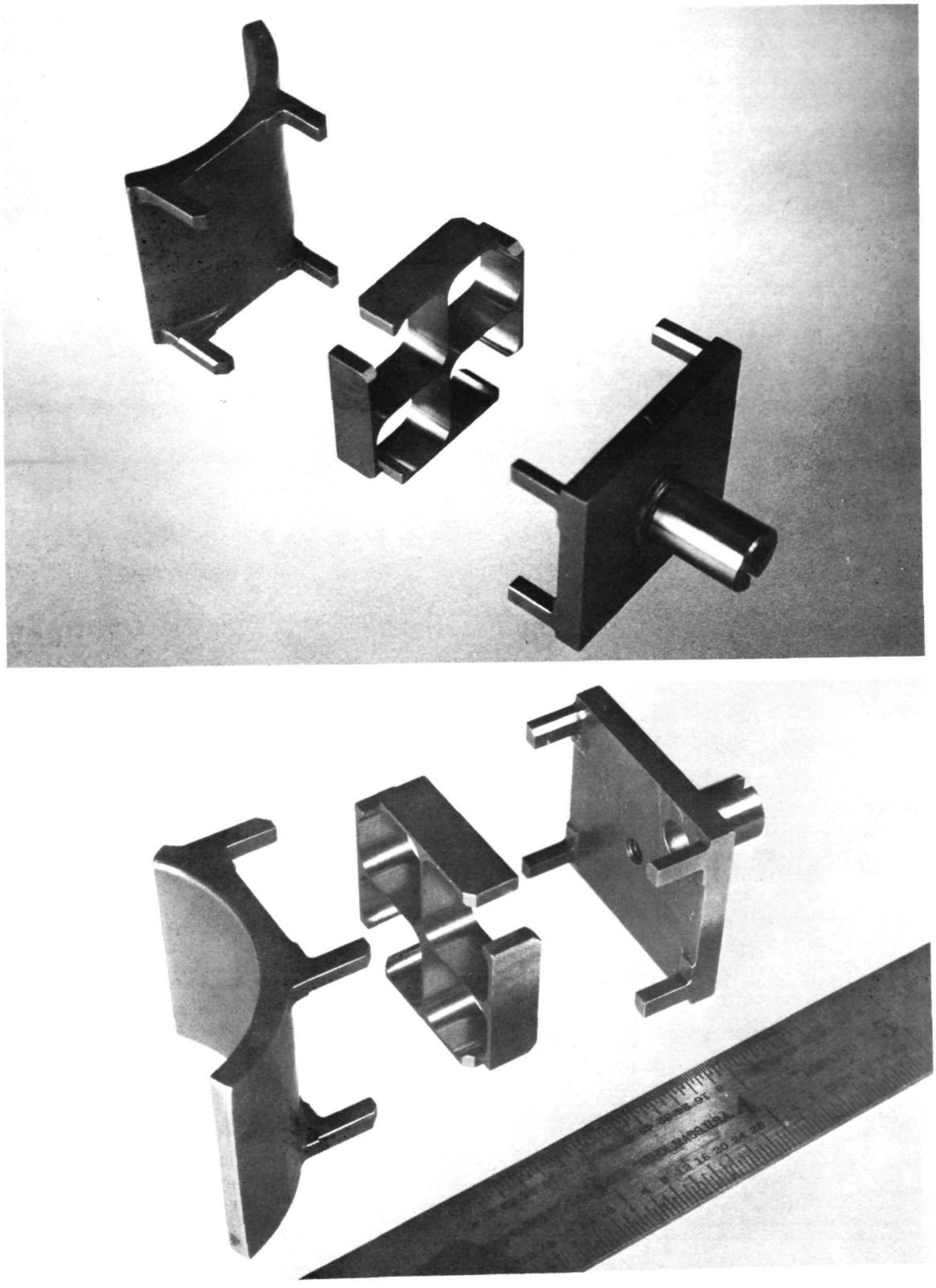

Fig. 85 Modified, Cruciform-Supported, Tilting-Pad Bearing
Bearing Components

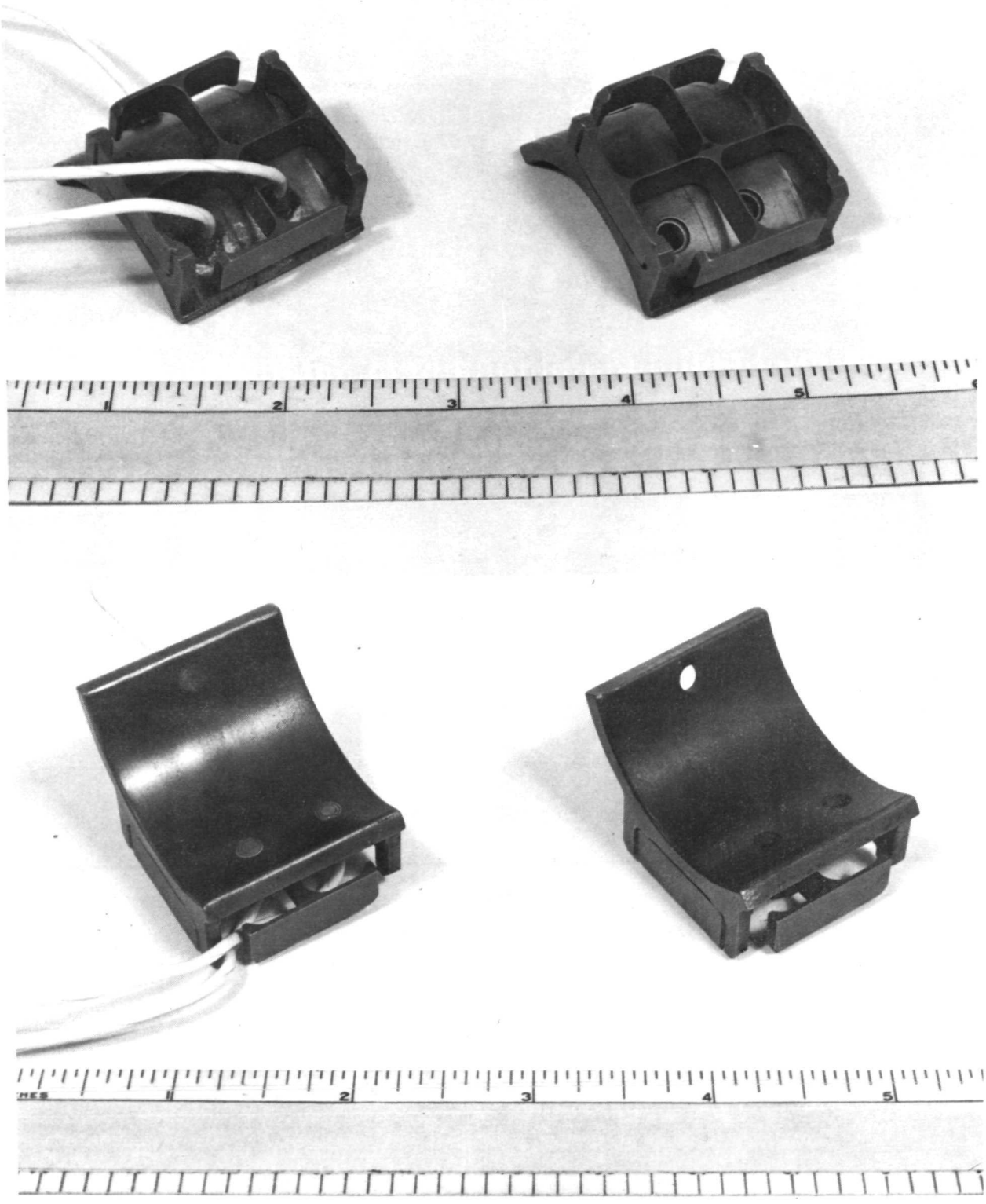

Fig. 86 Modified, Cruciform-Supported, Tilting-Pad Bearing Before and After Installing Proximity Probes

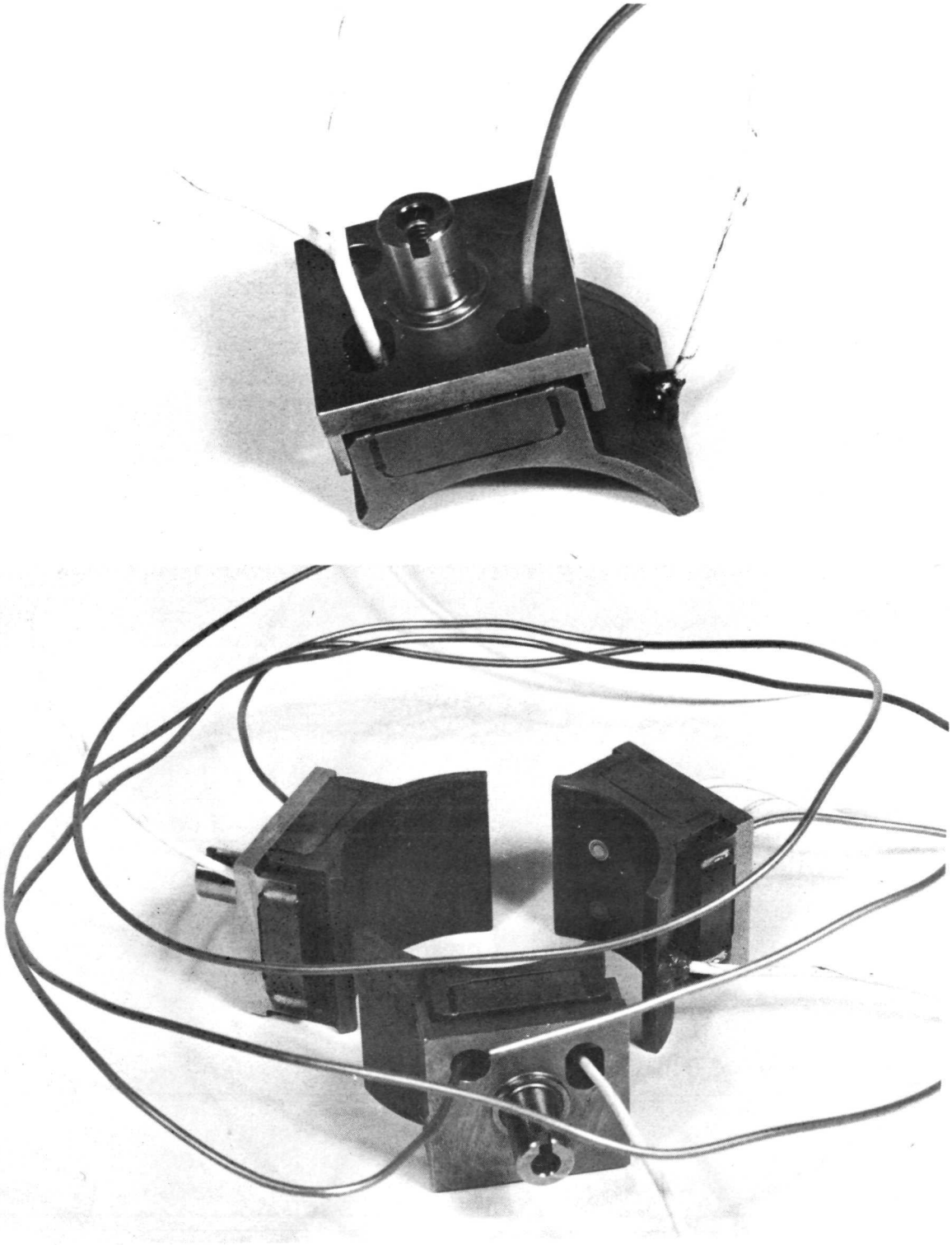

Fig. 87 Instrumented, Modified, Cruciform-Supported, Tilting-Pad Pad and Bearing Assembly

the parts. This feature was introduced to simplify the alignment requirement during assembly.

MEASURED HYDROSTATIC PERFORMANCE

Test Pad Geometry

The geometrical parameters of the modified cruciform-supported test pad were identical to those chosen for the reference MTI design of the BRU back-up journal bearings (including the prototype cruciform pad) described on pages 48 and 49.

Hydrostatic Load Capacity Tests (of Rotation)

One of the pads was subjected to a load vs film thickness test under room ambient pressure and temperature conditions while being supplied with 150 psia argon jacking gas. The primary purpose of this test was to determine whether the modifications to the cruciform design or the method of inducing the jack gas to the pad described earlier had any detrumental effect on the hydrostatic bearing performance.

The results of the load vs film thickness test is shown in Figure 88.

The data shown in Figure 88 has been compared with the results of the tests conducted on the prototype cruciform pad built earlier in the program and described in the preceeding section. This comparison is shown in Figure 89 where it can be seen that the data from Figure 88 falls near the lower end of the test band of the prototype pad.

In testing of hydrostatic bearings on self-aligning mounts (flexures of pivots), it is difficult to achieve a high degree of experimental repeatability. This is because the bearing tends to cock under the influence of extraneous forces such as those resulting from the jacking gas line, probe leads, and misalignment of the load direction relative to the bearing center of pressure. These misaligning or cocking forces are small compared to the stiffness of the bearing film under normal hydrodynamic operation. Thus under normal hydrodynamic (high speed) operation, the pad is well aligned with the journal.

However, at zero speed, the bearing stiffness is derived entirely from the hydrostatic component provided for jacking or zero speed lift-off. The hydrostatic stiffness is typically very small because the orifice and recess characteristics are designed in such a manner as to minimize the deterioration in hydrodynamic performance caused by the presence of the orifice and recess in the critical area of the pad (area of peak hydrodynamic pressure). Because of the low hydrostatic stiffness, the effects of the aforementioned cocking forces are significant which, of course, led to the problems of poor repeatability and an expectancy of a wide range of test data.

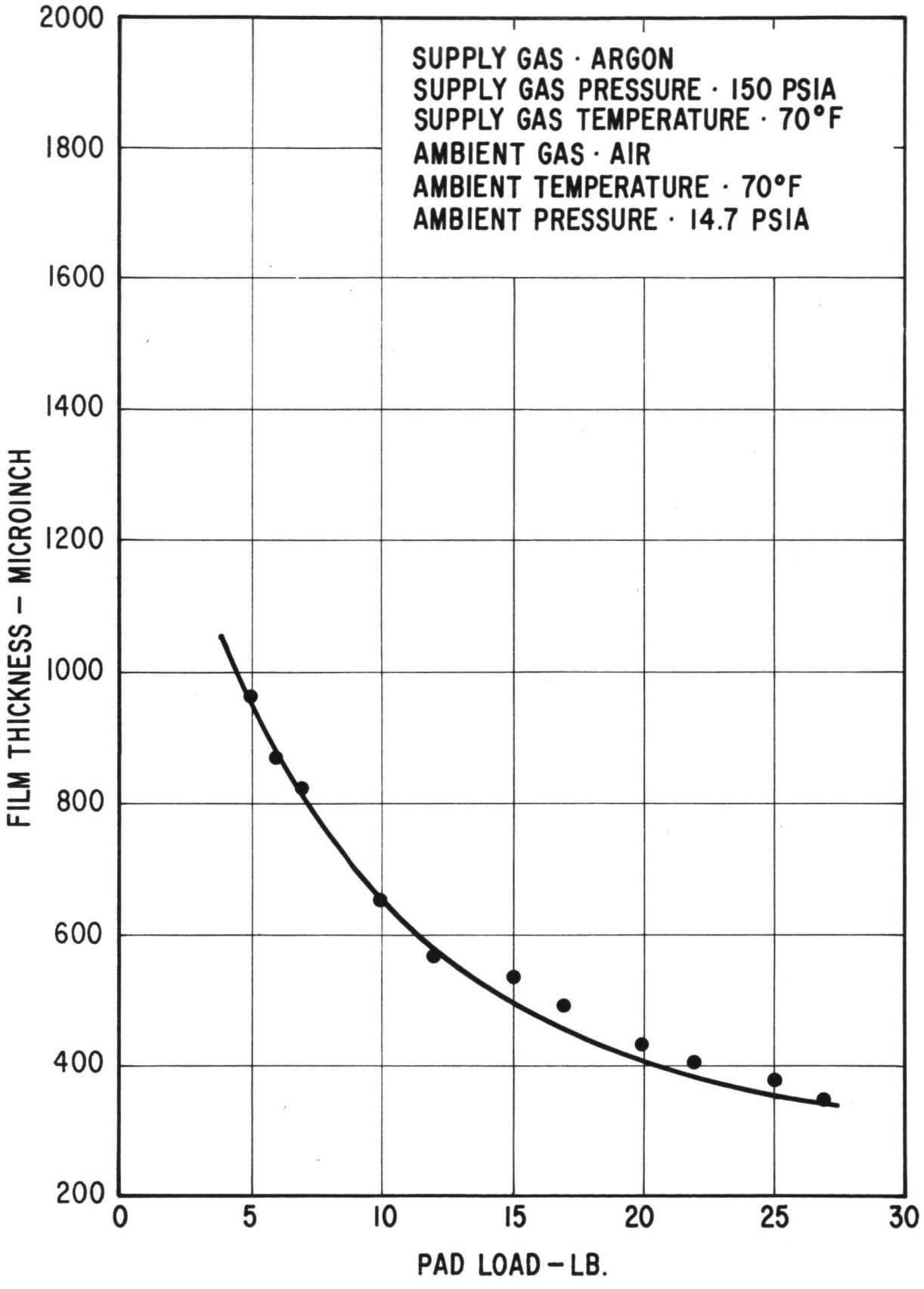

Fig. 88 Measured Hydrostatic Film Thickness Versus Load for the Modified, Cruciform-Supported Pad

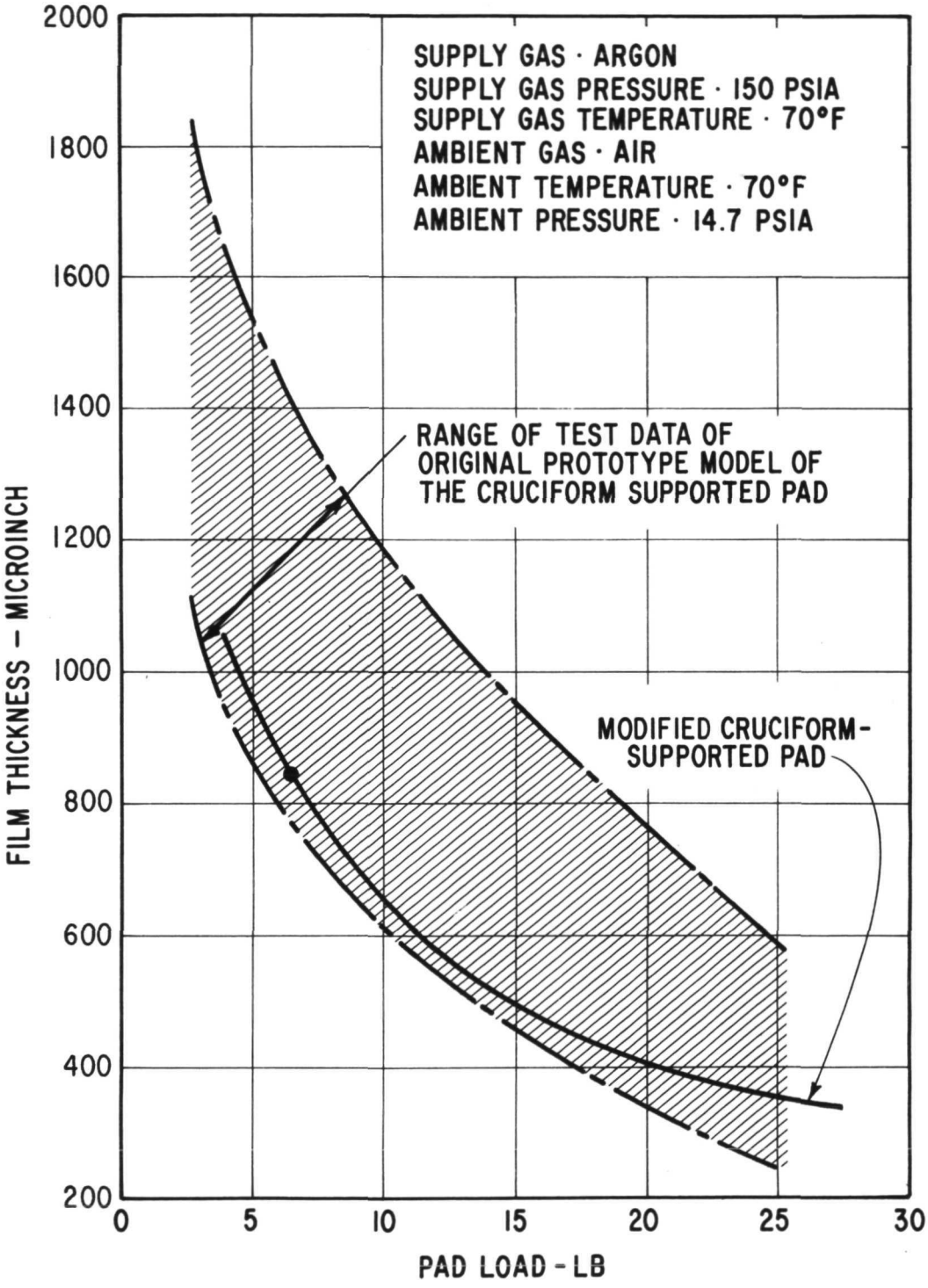

Fig. 89 Hydrostatic Film Thickness Versus Load for Cruciform-Supported Pads

Since jacking is provided only to lift the bearing during start-up and shutdown operations, a small amount of misalignment of the pad relative to the journal and relatively small film thickness at zero speed are quite tolerable. This is because, at higher speeds where the potential for bearing surface damage is higher, the film thickness and degree of alignment is also increased due to the speed dependant hydrodynamic load capacity component.

In the case of the modified cruciform supported pad, film thickness lying on the lower end of the previously established test band is not unexpected. This is because of the differences in location of the film thickness probes between the two test pads. The prototype cruciform pad probe was located nearer the pivot line and nearer the axial centerline of the pad than the probe in the modified cruciform pad. Thus the effects of pad misalignment would be more evident in the later tests. Furthermore, it was determined that the pad did cock in a direction to indicate smaller films at the location of the monitor probe.

It was thus concluded that the modified cruciform bearing will perform substantially the same as the prototype cruciform bearing previously described.

SUMMARY OF RESULTS AND CONCLUSIONS

The objective of this program was to design, fabricate, test, and deliver to the NASA Lewis Research Center journal and thrust bearing assemblies capable of being installed into the NASA 2 to 15 KW Brayton cycle rotating unit (BRU). The BRU was developed under contract NAS 3-9427. The bearings developed on the subject contract (sometimes referred to as "back-up" bearings) were designed in such a way that they could be installed directly into the BRU without modification to the BRU bearing mounting flanges or other components.

An initial design study was undertaken to optimize the bearing designs with respect to geometric configuration and size. With regard to the journal bearings, the NASA specified the tilting pad type. Two methods of supporting the tilting pads were to be considered. One was to utilize a nonconforming pivot (relative motion accommodated by elastic deformation and rolling within Hertzian contact zone). The other pad support method was to utilize a flexible member ("cruciform") which eliminated the possibility of relative sliding at the joint between the pad and housing members. The thrust bearing configuration was not specified.

Following the design phase, bearing components were fabricated and tested at MTI to verify performance predictions and to identify problem areas not uncovered in the design phase. Finally, one complete set of each nonconforming pivot and modified cruciform journal bearings and helical groove thrust bearings evolved in the design phase was fabricated and supplied to the NASA Lewis Research Center for further testing.

The observations and conclusions resulting from the design and component test phases are presented in the following paragraphs.

CONCLUSIONS DRAWN FROM THRUST BEARING DESIGN ANALYSIS

To ensure reliable operation of the BRU over the specified range of operation conditions, the following conclusions relating to the thrust bearing have been drawn.

1. The spiral-grooved thrust plate design is preferable to the step-sector design principally because of the higher "ultimate" load carrying capacity which is attainable from the spiral-grooved design.

2. The thrust bearing should be increased in size from the current 3.5 inches O.D to 4.25 inches O.D. The present inside diameter of 2.1 inches should be retained. The principal benefits to be derived from this increase in size are:

   a) approximately 0.0005 inch increase in film thickness at the maximum load condition,

   b) approximately three-fold increase in "ultimate" load carrying capacity, and

c) approximately three-fold increase in angular stiffness of the gas film.

The principal penalty resulting from this change will be an increase in the friction power losses as follows:

Horizontal or Space Hydrodynamic

Alternator Power Level (KW)	Friction Loss For Original 3.5 Inch Diameter Double-Acting Bearing (watts)	Friction Loss For Recommended 4.25" Diameter Double-Acting Bearing (watts)	Increase In Friction Loss (watts)
10.5	182	240	58
6.0	148	220	72
2.25	130	215	85
Vertical Operation - Hydrodynamic (Terrestrial)			
10.5	127	205	78
6.0	110	197	87
2.25	140	205	65

3. Increase the axial play between the thrust runner and thrust stators from 0.003 inch to 0.004 inch for the purpose of minimizing the power loss.
4. Retain the method presently used for the dissipation of thrust bearing friction generated heat. That is, the radial inflow of heat through the thrust-runner into a shrunk-fit copper shunt, then axial heat flow, across a further shrink fit, to the compressor wheel and into the system process fluid.
5. Utilize a flexure-type self-sligning mechanism to support the thrust bearing assembly.

CONCLUSIONS DRAWN FROM JOURNAL BEARING DESIGN ANALYSIS

To ensure reliable operation of the BRU over the specified range of operating conditions, the following conclusions relative to the journal bearings have been drawn.

1. The present three pad journal bearing configuration with one flexure mounted pad should be retained.
2. The present bearing size should be retained.
3. Primary and secondary valves need to be introduced into the nonconforming pivoted pad design to prevent loss of hydrodynamic film pressure and loss of hydrostatic supply gas to the bearing cavity.

4. The present 2000 lb/in flexure provides for a high tolerance of radial thermal gradients. However, it results in clamping of the shaft at start-up making hydrostatic jacking mandatory. Thus, a stiffer flexure (6,250 lb/in) should be tested in the BRU to assess its flexibility relative to elimination of jacking and to assess its limitations relative to actual radial thermal gradients.

The dimensions of the recommended bearings are given as follows:

Journal diameter at 70^{o}F and zero RPM (inches)	1.7496
Pad diameter at 70^{o}F (inches)	1.7544
Pad length (inches)	1.312
Pad arc length (degrees)	110
Pivot position (ratio)	0.65
Pivot diameter (inches)	0.375
Pivot seat diameter (inches)	0.3937
Coating	Cr_2O_3

The operating characteristics of the journal bearing at the 6.0 KW power level design point are as follows:

	Space operation	Horizontal operation in a 1g environment
Clearance ratio C/R	2.5×10^{-3}	2.5×10^{-3}
Pivot point film thickness (inches)	0.66×10^{-3} (all pads)	0.54×10^{-3} (loaded pads)
Friction loss/bearing (watts)	51.0	52.0
Pivot/seat contact zone stress (psi)	3.6×10^{4} (all pivots)	4.0×10^{4} (loaded pivots)

CONCLUSIONS DRAWN FROM HYDROSTATIC PERFORMANCE TESTING OF THE SPIRAL GROOVE AND THE STEP-SECTOR THRUST BEARINGS

The nonrotational hydrostatic tests of the spiral groove thrust bearing designed and built on the subject contract indicated:

1. The spiral groove thrust bearing operating with nitrogen or krypton was free of pneumatic hammer or other instabilities over the bearing ambient pressure range of the BRU, for all tested bearing gas supply pressures between 75 and 150 psia and for all three bearing configurations with 6, 12 or 24 orifices in each bearing plate.

2. The ultimate hydrostatic load capacity increases with the number of supply orifices, as does the gas flow. As no instabilities were encountered (up to the maximum number of orifices tested), any suitable combination of desired load carrying capacity and

permissible bearing gas flow may be selected. (Maximum bearing load carrying capacity is limited to 132 pounds, due to stress considerations for the flexural support of the thrust bearing.)

3. Bearing operating clearance (film thickness) should exceed 0.0005 inch at all selected operating conditions to avoid bearing "lock-up", a sudden collapse of the gas film due to overload. The "lock-up" phenomenon was found to occur under all operating conditions and bearing geometries when the bearing eccentricity ratio (film thickness/end play) exceed approximately $\epsilon = 0.7$.

The nonrotational hydrostatic tests of the NASA supplied prototype BRU step-sector thrust bearing indicated:

1. Pneumatic hammer was prevalent in the step-sector thrust bearing at all sub-atmospheric ambient pressures for all gas supply pressures between 90 and 150 psia. Experimentally observed rotor amplitudes due to pneumatic hammer ranged up to 60 percent of the total thrust bearing clearance.

2. Experimentally measured bearing eccentricity ratios for the step-sector thrust bearing were of similar magnitude as those for the six orifice spiral groove thrust bearing. Actual film thickness, however, were only about half as large because the total bearing clearance of the step-sector thrust bearing was also only approximately half as large as for the spiral-groove bearing.

3. The lockup phenomenon occurs in the step-sector thrust bearing at similar eccentricity ratio, as in the spiral-groove bearing.

CONCLUSIONS DRAWN FROM EXPERIMENTAL PERFORMANCE TESTING OF SINGLE TILTING PAD JOURNAL BEARING WITH NONCONFORMING PIVOTS

1. The minimum film thickness of the currently designed* nonconforming pivoted pad journal bearing under hydrodynamic operation is in excess of 0.0002 inches for all BRU operating conditions. This is considered an acceptable minimum film thickness.

2. If the need for hydrostatic pad lift-off could be eliminated, the currently designed back-up journal bearings (with orifice and orifice recess deleted) would have a minimum film thickness under hydrodynamic operation in excess of 0.0003 inches for all BRU operating conditions.

3. For the currently designed back-up journal bearings, the secondary pivot valve is essential to proper hydrostatic operation of the bearings.

4. For the currently designed back-up journal bearings, adequate hydrostatic performance can be obtained with or without the primary pivot valve (i.e., the check valve for hydrodynamic operation).

* The term 'currently designed' implies 'with orifice and orifice recess for hydrostatic lift-off'

5. The sealing capability of the primary pivot valve is highly sensitive to surface scratches in the valve seat. For this, and perhaps other unidentified reasons, the sealing reliability of the primary pivot valve must be questioned.

6. The following two instability modes were observed during the single pad tests:

   a) Pad instability in the roll direction during hydrodynamic operation. The frequency of the roll instability was one-half rotational speed. The instability mode resulted in contact between the ends of the pad and the test journal. This instability fell within the BRU operating range (in terms of pad load and speed).

   b) Pneumatic hammer during hydrostatic operation. This resulted in large radial pad motions, with pad contact occurring under some, but not all, of the hammer conditions. This instability fell outside the operating speed range.

7. The hydrodynamic stability of the presently designed back-up journal bearing should be further studied under actual BRU design and operating conditions. The single pad test data shows that the threshold of pad roll instability lies above BRU design-point speed (36,000 rpm), but below the required overspeed condition (46,500 rpm). Since the instability threshold points for the single pad lie within the BRU operating envelope, the following question must be raised: Is the instability threshold data obtained from the single pad tests in argon indicative of inadequate journal bearing stability margin in the actual BRU operating mode? The answer to this question is not immediately obvious because of the following differences between the single pad tests and the BRU operating conditions:

   a) The BRU helium-xenon gas has a slightly higher viscosity and a considerably lower gas constant than does argon;

   b) The BRU operates as a complete rotor-bearing-system assembly rather than a single pad.

   For these reasons, definite conclusions relative to hydrodynamic stability margin for the BRU back-up journal bearings cannot be inferred from the herein reported data.

8. The hydrostatic stability of the presently designed back-up journal bearing should likewise be further studied. Although the single pad test data shows that the threshold of pneumatic hammer lies outside the range of expected pad loads, final determination of stability margin should be based on the actual BRU configuration operating in helium-xenon gas.

CONCLUSIONS DRAWN FROM EXPERIMENTAL PERFORMANCE TESTING OF SINGLE TILTING-PAD JOURNAL BEARING WITH "CRUCIFORM" FLEXURE MOUNT

Based on consideration of the herein presented test data for a cruciform-supported pad (both the prototype and modified designs), together with the test data presented for a pivot-supported pad, it is concluded that the hydrodynamic/hydrostatic load capacity of the cruciform-supported pad is essentially the same as that of the pivot-supported pad. From a hydrodynamic/hydrostatic stability standpoint, the cruciform-supported pad is better than the pivot-supported pad. Consequently, from the standpoint of pad performance, the cruciform supported appears to be a completely acceptable alternative to the pivot support for the BRU tilting-pad journal bearings.

Following is a somewhat more specific listing of conclusions for the cruciform-supported pad:

1. The hydrodynamic load capacity of the cruciform-supported pad, as currently configured for hydrostatic lift-off (that is, with hydrostatic orifice and orifice recess in the pad surface), is essentially the same as that of the pivot-supported pad. There is some suggestion in the data that the load capacity of the cruciform-supported pad may actually be slightly lower (particularly at high pad loads) than that of the pivot-supported pad. However, this suggestion would have to be investigated by more precise testing since we are talking about possible differences of less than 50 microinches in film thickness. Valid distinction of such small differences between two absolute measurements of film thickness is beyond the accuracy of the present test set-up.
2. The cruciform-supported pad was not tested with the hydrostatic orifice plugged (i.e., with a completely smooth pad surface). Consequently, we do not know how much additional film thickness might be achieved from the cruciform-supported pad if the requirement for hydrostatic lift-off could be eliminated.
3. The test data shows that some orifice recess must be provided around the hydrostatic orifice to prevent bearing lock-up at high pad loads.
4. The problem of pivot-pivot-seat separation cannot, of course, occur in the cruciform-supported design.
5. At no time during testing of the cruciform-supported pad was any instability of pneumatic hammer observed. With recess around the hydrostatic orifice, there is no hydrostatic lock-up.

LIST OF SYMBOLS

C_P	Specific heat (constant pressure) BTU/lb-^oF
C_P	Machined bearing clearance - inches
C_P	Assembled Bearing clearance - inches
CPS	Frequency - cycles per second
g	Gravitational constant
h	Heat transfer coefficient - BRU/hr-ft^2-^oF
h	Film thickness - inches or mils
h_m	Minimum film thickness - inches or mils
ID	Inside diameter - inches
k	Thermal conductivity - BTU/hr-ft-^oF
K	Stiffness - lb/in
m	Preload factor - dimensionless
OD	Outside diameter - inches
P_a	Ambient pressure - psia
R	Radius - inches
R_1	Inside radius - inches
R_o	Outside radius - inches
R_p	Pad Radius - inches
R_s	Shaft radius - inches
SCFM	Volume flow - standard cubic feet per minute
T	Temperature - ^oF
ΔT	Temperature differance - ^oF
w	Land or seal width - inches

LIST OF SYMBOLS (Cont'd)

δ	Step depth - inches or mils
ϵ	Eccentricity ratio - dimensionless
θ_g	Groove angle - degrees
θ_{tot}	Pad angle - degrees
μ	Absolute viscosity - lb/ft-sec or lb-sec/in^2 (Reyns)